ENHANCEMENTS OF SHEAR TESTS FOR ASPHALT CONCRETE

By

YAZEED SULEIMAN JWEIHAN

DISSERTATION

Submitted in partial fulfillment of the requirements
for the degree of Doctor of Philosophy in Civil Engineering at
The University of Texas at Arlington
December 2019

Arlington, Texas

Supervising Committee:

Dr. Stefan Romanoschi, Supervising Professor
Dr. Sahadat Hossain,
Dr. Xinbao Yu,
Dr. Stefan Dancila.

Acknowledgements

First of all, I would like to express my sincere gratitude and appreciation to my advisor, Prof. Stefan Romanoschi, for his passion for teaching, kind guidance, motivation, and continuous advice throughout my time as his student. His patience and guidance helped me to complete this research at the University of Texas at Arlington (UTA) properly and successfully. He cared so much about my research and responded to my queries so promptly. Indeed, it has been extremely great learning and experience to work under his supervision.

I would also like to thank my committee members: Dr. Sahadat Hossain, Dr. Xinbao Yu, and Dr. Stefan Dancila for their effort and interest in reviewing this dissertation. Their insightful comments made this research much better. I also extend my thanks to the technical staff at the machine shop in the UTA: Mr. Kermit Beird, and Mr. Sam Williams for their technical support and help to fabricate all designed laboratory parts for this research. Also, special thanks to Mr. Mitchell Page, a QC technician at Austin bridge and road company, for his help while collecting the asphalt mixes.

Very special recognition and respect go to my sponsor, Mutah University, Jordan, for supporting me financially to pursue my graduate studies in Civil Engineering. I look ahead to fulfil my obligation to it by joining its research and teaching members. I am also thankful for all the staff of the Civil Engineering department in the UTA for giving me the best education and knowledge in the Infrastructure System Engineering and Management field. This accomplishment would not have been possible without them.

My profound thanks to my lovely parents, Mr. Suleiman Jweihan and Mrs. Manal Jweihan, who have taught me to be persistent and independent through their moral and emotional supports in my life. I would also like to express my most heartfelt thanks to my beloved, my wife Marwa

Jweihan, for her love, patience, and understanding along the way of my study. I also would like to thank my brothers, Sultan, Saif, Eyad, and Tamer for their overwhelming motivation and encouragement in all my endeavors. The support they have given has been extensive in my pursuit of higher education.

Not enough thankfulness can be given to my friends who I met during the past few years of this journey. Special thanks go to my friends Mr. Mladjan John and his wife Mrs. Svjetlana Grujicic for their endless love and inspiration in my everyday life, away from my home country. Also, it has been my pleasure to study and work with my sweet friends: Constantin Popescu, Mohsen Talebsafa, and Ana-Maria Coca, who made the doctoral pursuit a very enjoyable experience in my life.

November 13, 2019

Abstract

ENHANCEMENTS OF SHEAR TESTS FOR ASPHALT CONCRETE

YAZEED SULEIMAN JWEIHAN, Ph.D.

The University of Texas at Arlington, 2019

Supervising Professor: Stefan A. Romanoschi

The measurement of the fundamental shear properties of asphalt mixes is imperative to the improvement of modelling of rutting development in asphalt concrete. The Duplicate Shear Tester (DST) is a recent device developed at the University of Texas at Arlington as a replacement to the Superpave Shear Tester (SST). It measures the average shear properties of two asphalt concrete specimens at the same time. It has ability to perform the two common SST tests: the FSCH and RSCH in according to the standard test method AASHTO T-320. Although the DST has successfully satisfied the objectives of being a reliable, inexpensive and simple test device, further modifications were required to simplify and improve the testing procedure. Therefore, this study aimed mainly to enhance the shear testing for asphalt mixes through modifying the DST device and developing a new shear tester device that is able to measure the shear properties of asphalt mixes under controlled normal stress. The new device is called the "Shear Tester with Normal Stress (STNS)".

The DST device was modified to be lighter in weight and to accommodate other shapes of asphalt mix specimens of circular diameter with two sizes, and rectangular specimens cut from horizontal and vertical slices. The STNS device was developed successfully with only simple and inexpensive testing attachments for the purpose to simulate the state of stresses within the rutting

zone of asphalt pavements. Two shear tests were performed by this new device: the Frequency Shear Test at Normal Stress (FSNS), and the Repeated Shear Test at Normal Stress (RSNS).

To study the accuracy of the shear test devices, three asphalt mixes of Superpave (types D and C) and dense graded type B were tested. Three shear parameters were obtained from each device: the shear dynamic modulus |G*| and shear phase angle (δ) from the FSCH & FSNS tests, and the total permanent deformation (PD) from the RSCH & RSNS tests. Both STNS tests were performed by applying a normal stress of 113 kPa (16.35 Psi). The test results proved the ability of the DST device to provide repeatable measurements with relatively low coefficient of variations (COV). At high load frequencies of 10 Hz and 5.0 Hz, the |G*| of all DST groups yielded COV values of less than 8% for mixes D and B, and less than 11% for mix C. The phase angle of all DST groups had COV values of less than 8.0% for mixes D and B, and less than 10% for mix C at all loading frequencies. The (PD) measurements of all DST groups had COV values of less than 13% for asphalt mixes D and C, and less than 8% for mix B except that for some groups of mix B as they had a COV values of about 17%.

The test results of STNS testing groups showed generally high variabilities for the measured |G*| and phase angle, whereas they had low variabilities for the (PD) measurements. At high load frequencies, the COV values of the |G*| were less than 24%, 35%, and 38% for mixes D, C, and B, respectively. The COV values of the phase angles showed comparable values to that of the |G*| at high load frequencies. They had COV values of less than 30%, 35%, and 26% for mixes D, C, and B, respectively. The maximum COV value of the (PD) at 5,000 load cycles were about 14%, 12%, and 17% for mixes D, C and B, respectively. For each asphalt mix, however, there is at least one STNS group had COV value of less than 8.0% for the measured PD.

An analysis of variance (ANOVA) technique was conducted to compare the tests results from both devices. The comparison includes testing the influence of four different test factors on the mean values of the G*@10Hz frequency and the accumulated (PD) at 5,000 load cycles by using the calculated "*P-value*" at 95% level of confidence. It was found that the daily times production affects the values of both parameters for mix D only and affects the G*@10Hz value for mix B tested with the DST device. Also, it affects both parameters for mixes D and C and the accumulated PD for mix B tested with the STNS device. Using the DST device, different diameter for circular specimens affects the G*@10Hz and accumulated PD values for mix D only. Also, different cut directions for the rectangular specimens affect the G*@10Hz for mix C, and the accumulated PD for mix B. It was shown that varying the testing device would sometimes affect the value of both G*@10Hz and accumulated PD. The DST device usually provided higher values for the G*@10Hz than the STNS device for samples collected at all daily time of production. Testing asphalt mixes with the two devices, however, provided unclear trends for the accumulated PD values.

Table of Contents

Acknowledgements iii

Abstract v

Table of Contents viii

List of Figures xii

List of Tables xvi

Chapter 1: Introduction 1

1.1 Background 1

1.2 Research Rationale 6

1.3 Research Objectives 6

1.4 Dissertation Outline 7

Chapter 2: Background of Asphalt Concrete Permanent Deformation 8

2.1 Introduction 8

2.2 Rutting Types 9

2.3 Rutting Mechanisms 11

2.4 Rut Depth Measurements 13

2.5 Factors Affecting Rutting 17

2.5.1 Aggregate 19

2.5.2 Binder 19

2.5.3 Mixes 20

2.5.4 Test field conditions 21
2.6 Rutting Prediction Approaches 21
2.6.1 Layer Strain Approach 22
2.6.2 Viscoelastic Approach 23
2.7 Permanent Deformation Laboratory Tests 24
2.7.1 The Fundamental Tests 29
2.7.2 The Empirical Tests 34
2.7.3 The Simulative Tests 37
Chapter 3: Background of Asphalt Concrete Shear Tests 39
3.1 Superpave Shear Tester (SST) 39
3.1.1 Background 39
3.1.2 SST System 41
3.1.3 SST Tests 44
3.1.4 SST Test Procedure 60
3.1.5 Evaluation of the SST tests 64
3.1.6 Using SST data for rutting prediction and asphalt mix analysis 68
3.2 Duplicate Shear Tester (DST) 81
3.2.1 Background 81
3.2.2 DST System 84
3.2.3 DST Components and Description 89

3.2.4 DST Evaluations 95

Chapter 4: DST Modifications and STNS Development 102

4.1 Modifications to the DST device 102

4.2 Development of the STNS device 108

4.2.1 The Concept and Loading Condition of the STNS device 112

Chapter 5: Materials and Testing Methods 117

5.1 Selecting Asphalt Mixes 118

5.2 Tests Plan 125

5.3 Asphalt Mixes Sampling 127

5.4 Specimen Preparations 131

5.4.1 Cutting Procedure of (C6) Specimens. 132

5.4.2 Cutting Procedure of (C4) Specimens 137

5.4.3 Cutting Procedure for the Rectangular Specimens 139

5.5 Volumetric Measurements 151

5.6 Assembling Samples 154

5.7 Testing Temperatures and Conditions 157

5.8 Executing of the Shear Tests and Collecting the Data 157

5.8.1 Execution of the FSCH tests 162

5.8.2 Execution of the FSNS tests 166

5.8.3 Execution of the RSCH tests 170

5.8.4 Execution of the RSNS tests 172
5.9 Cleaning Samples 173
Chapter 6: Tests Results and Discussion 174
6.1 Introduction 174
6.1.1 Discussion on the DST device Results. 175
6.1.2 Discussion on the STNS Results 185
6.2 Statistical Comparison of Test Results Using ANOVA 194
Chapter 7: Conclusions and Recommendations 202
7.1 Conclusions 202
7.2 Recommendations 206
References 207
Biographical Information 214
Appendix A: Duplicate Shear Tester (DST), Parts Drawings 215
Appendix B: Shear Tester with Normal Stress (STNS), Parts Drawings 223
Appendix C: Specimens Cut Preparations, Detailed Drawings 231
Appendix D: Sample Holders, Detailed Drawings 235
Appendix E: Mix Design Data 249
Appendix F: Asphalt Concrete Gyratory Samples & Volumetric Measurements 253
Appendix G: Tests results summaries (Raw data) 275

List of Figures

Figure 2-1. Shear Deformation Rutting Schematic 9
Figure 2-2. Rutting Cause Principles 13
Figure 2-3. Rut Depth measurement using a Straightedge 14
Figure 2-4. Five-points Rut depth measurements 15
Figure 2-5. Rut Depth versus Air Voids for GPS Pavement Studies 21
Figure 2-6. Layer Strain Approach 22
Figure 2-7. Creep Testing 30
Figure 2-8. Typical Creep Stress and Strain Relationships 30
Figure 2-9. Schematic of Repeated Load Triaxial Test 31
Figure 2-10. Schematic of Indirect Tensile Test 33
Figure 2-11. Illustration of the Marshall test applied load and recorded data 35
Figure 2-12. Diagrammatic Sketch of the Hveem Stabilometer 36
Figure 3-1. Superpave Shear Tester (SST) 40
Figure 3-2. SST Specimen Loading Conditions 43
Figure 3-3. Schematic View of an SST Device 44
Figure 3-4. Conceptual view of the Volumetric Test 44
Figure 3-5. Ramping of Confining Pressure, Volumetric Test at 20 °C 45
Figure 3-6. Conceptual View of the Uniaxial test 46
Figure 3-7. Axial Stress and Confining Stress versus Time, Uniaxial Test at 20°C 47
..... 49
Figure 3-8. RSCH Shear and Axial Stresses versus Time 49
..... 50
Figure 3-9. Typical relationship between permanent strain and loading cycles 50
Figure 3-10. Regression Constants when plotted on log-log scale 51
Figure 3-11. Conceptual View of the FSCH test 53
Figure 3-12. Shear Strain and Axial Stress Pulses - FSCH Test 54
Figure 3-13. Conceptual View of the SSCH test 56
Figure 3-14. Shear and Axial Stresses versus Time of SSCH Test at 20°C 56
Figure 3-15. typical graph of Shear strain versus time of SSCH test at 40 °C 57
Figure 3-16. RSCSR Shear and Axial Stresses versus Time 59

Figure 3-17. Typical Plot from a failing RSCSR test 60
Figure 3-18. Conceptual View of the SST Plate Gluing Device 62
Figure 3-19. Set-Up of Confined SST Specimens 63
Figure 3-20. Diagram of the Abridged Procedure for Permanent Deformation 71
Figure 3-21. The original DST device inside the UTM-25 testing machine 82
Figure 3-22. The main components of the UTM-25 testing machine 83
Figure 3-23. Change in volume of compacted HMA due to shear stresses application 85
Figure 3-24. Illustration of the Superpave Shear Test Loads 85
Figure 3-25. Simplifying drawings to the DST load condition 86
Figure 3-26. Mini-Rail Miniature Linear Guides System 87
Figure 3-27. The Modified DST Supporting Plate 88
Figure 3-28. Steel and Aluminum Plates of the DST 90
Figure 3-29. A DST Steel Plate with the new holes at bottom 91
Figure 3-30. The Modified DST Aluminum Plate 92
Figure 3-31. Loading Attachments for the DST 93
Figure 3-32. DST Coupling Attachment Details 94
Figure 3-33. LVDT's Mount Components 94
Figure 3-34. Position of the LVDT mount assembly on the DST 95
Figure 4-1. Diagram of the DST device. 103
Figure 4-2. The difference between the DST samples. 104
Figure 4-3. The RSCH and FSCH loading attachments. 106
Figure 4-4. The LVDT mount with the new holder- DST device. 108
Figure 4-5. Diagram of the STNS device. 109
Figure 4-6. Diagram of the side plate (B) with the Air cylinders setup. 110
Figure 4-7. The LVDT Mount - SNTS Device. 112
Figure 4-9. Illustration to the loading concept of the STNS device. 115
Figure 5-1. Testing Methods of This Study. 117
..... 120
Figure 5-2. Asphalt concrete specimens of the three selected mixes. 120
Figure 5-3. Gradation chart of asphalt mix D. 124
Figure 5-4. Gradation chart of asphalt mix C. 124

Figure 5-5. Gradation chart of asphalt mix B. 125
Figure 5-6. The first part of testing groups 126
Figure 5-7. The second part of testing groups 127
Figure 5-8. Sampling Methods of Asphalt Mixes 128
Figure 5-9. Asphalt Concrete Specimens After Cutting. 131
Figure 5-10. Illustration drawing to the Three Saw-cuts preparations of a gyratory sample. 132
Figure 5-11. Sample Holder of C6 Specimens 133
Figure 5-12. Saw Cut Machine 134
Figure 5-14. Illustration drawings to the Step 2. 136
..... 136
Figure 5-15. Illustration drawings to the Step 3. 136
..... 136
Figure 5-16. Illustration drawings to the Step 4. 136
Figure 5-17. Illustration drawings to the Step 5. 137
Figure 5-18. Vertical holder of gyratory samples 138
Figure 5-19. Coring Machine of the C4 Specimens. 139
Figure 5-20. Sample Holder of cutting Rectangular Specimens 140
Figure 5-21. Steel Blocks associated to the Rectangular Holder 140
Figure 5-22. Illustration drawings to the first trimming of RH specimens. 142
Figure 5-23. Illustration drawings to the second trimming of RH specimens. 143
Figure 5-26. Illustration drawing to the “two saw-cuts” preparations. 146
Figure 5-27. Illustration drawings to the 4.92″ height sample preparations. 147
..... 149
Figure 5-29. Illustration drawings to the second trim of RV specimens. 149
..... 149
Figure 5-30. Illustration drawings to the third trim of RV specimens. 149
Figure 5-31. Illustration drawings to the fourth trim of RV specimens. 150
Figure 5-32. Illustration drawings to the fifth trim of RV specimens. 151
Figure 5-33. Curing of Asphalt Concrete Specimens 152
Figure 5-34. Procedure of Gluing a DST Sample. 156
Figure 5-35. Procedure of Gluing an STNS Sample 156

Figure 5-36. An assembled DST Sample. 157
Figure 5-37. Installation of the DST Supporting Plate on the UTM-25 Loading table. 158
Figure 5-38. DST Device inside the UTM-25 chamber. 159
Figure 5-39. Initial Setup of the STNS device frame. 160
Figure 5-40. STNS Device inside the UTM-25 chamber. 161
Figure 5-41. A screenshot of a performed FSCH test. 166
Figure 5-42. A screenshot of a performed FSNS test. 170
Figure 5-43. A screenshot of a performed RSCH test. 171
Figure 5-44. A screenshot of a performed RSNS test. 173
Figure 6-1. Average Shear Dynamic Modulus of DST testing groups- Asphalt Mix D 176
Figure 6-2. Average Shear Dynamic Modulus of DST testing groups- Asphalt Mix C 177
Figure 6-3. Average Shear Dynamic Modulus of DST testing groups- Asphalt Mix B 178
Figure 6-4. Average Shear Phase Angle of DST testing groups- Asphalt Mix D 180
Figure 6-5. Average Shear Phase Angle of DST testing groups- Asphalt Mix C 181
Figure 6-6. Average Shear Phase Angle of DST testing groups- Asphalt Mix B 182
Figure 6-7. Average Permanent Deformation of all DST groups- Mixes D, C& B 184
Figure 6-8. Average Shear Dynamic Modulus of asphalt Mix D- STNS device 186
Figure 6-9. Average Shear Dynamic Modulus of asphalt Mix C- STNS device 186
Figure 6-10. Average Shear Dynamic Modulus of asphalt Mix B- STNS device 187
Figure 6-11. Average Shear Phase Angle of asphalt Mix D- STNS device 189
Figure 6-12. Average Shear Phase Angle of asphalt Mix C- STNS device 189
Figure 6-13. Average Shear Phase Angle of asphalt Mix B- STNS device 190
Figure 6-27. Average Permanent Deformation of all asphalt mixes-STNS device. 193
Figure 6-28. G*@10Hz for samples collected at Morning. 199
Figure 6-29. G*@10Hz for samples collected at Noon 199
Figure 6-30. G*@10Hz for samples collected at Afternoon. 200
Figure 6-31. PD for samples collected at Morning. 200
Figure 6-32. PD for samples collected at Noon. 201
Figure 6-33. PD for samples collected at Afternoon. 201

List of Tables

Table 2-1. Rutting Severity Levels 16
Table 2-2. Factors affecting rutting of asphalt-concrete mixtures 18
Table 2-3. Comparative Assessment of Permanent Deformation Test Methods 25
Table 2-3. Comparative Assessment of Permanent Deformation Test Methods 26
Table 3-1. Volumetric Test Pressure 45
Table 3-2. Uniaxial Test Parameters 47
Table 3-3. Criteria for Evaluating Rut Resistance Using RSCH Permanent Shear Strain 49
Table 3-4. FSCH Test Parameters 54
Table 3-5. SSCH Test Parameters 56
Table 3-6. Suggested Stress Values for the RSCSR test 58
Table 3-7. Appropriate Air Void Percentage for Compacted SST Specimens 61
Table 3-8. COV of Mixtures Properties Determined by different SST tests 74
Table 3-9. FSCH Test Results of the original DST, Shear Dynamic Modulus and Phase Angle 97
Table 3-10. RSCH Test Results of the original DST, Shear Permanent Deformation 98
Table 3-11. FSCH Test Results of the Modified DST, Shear Dynamic Modulus and Phase Angle 100
Table 3-12. RSCH test results of the Modified DST, Shear Permanent Deformation 100
Table 5-1. Master Gradation Limits (% passing by weight or volume) of the Dense Graded (DG) Asphalt Mixes 118
Table 5-2. Master Gradation Limits (% passing by weight or volume) of the Superpave (SP) Asphalt Mixes 119
Table 5-3. Mix design summary of asphalt mix D 121
Table 5-4. Mix design summary of asphalt mix C 122
Table 5-5. Mix design summary of asphalt mix B 123
Table 5-6. Sampling details of Asphalt Mixes 128
Table 5-7. Theoretical Maximum Specific Gravity of Asphalt Mixes 129
Table 5-8. Compaction Temperatures of Asphalt Mixes 130
Table 5-9. Appropriate Air Void Percentage for Compacted SST Specimens 131
Table 5-10. DST input diameters in the UTS-023 software 162
Table 5-11. Shear stress levels of the FSCH tests. 164

Table 5-12. Shear stress levels of the FSNS tests. 167
Table 6-1. COV of Shear Dynamic Modulus (G*) of DST groups- Mixes D, C& B. 179
Table 6-2. COV of Shear Phase Angle (δ) of DST groups- Mixes D, C& B. 183
Table 6-3. COV of Permanent Deformation of all DST groups- Mixes D, C& B 184
Table 6-4. COV of Shear Dynamic Modulus (G*) of STNS groups- Mixes D, C& B. 188
Table 6-5. COV of Shear Phase Angle 191
Table 6-6. COV of Permanent Deformation of all STNS groups- Mixes D, C& B. 193
Table 6-7. "*P-value*" results from the ANOVA analysis 196
Table 6-8. Hypotheses results at 95% level of confidence 197

Chapter 1: Introduction

1.1 Background

Rutting or permanent deformation is one of the most common distresses in flexible pavements. It exhibits as a permanent longitudinal depression in the wheel paths, sometimes with small upheavals to the sides. Rutting is developed due to the action of repetitive heavy loads traffic. Since most of the rutting occurs predominantly in the wheel paths and within the top 3 to 4 inches of the surface layer of asphalt pavements, a high-quality mixture is required in this layer. Rutting appears more often on asphalt pavements in hot climates and under slow moving traffic. Rutting not only develops in the surface layer of asphalt pavement, it may also develop in the other sub-layers of the pavement structure (Sousa, et al., 1991; Brown & Cross, 1992; Witczak, 2007).

Rutting represents a major safety and comfort issues for road users. When vehicles pass over rutted portion of pavement, steering may become difficult. Also, water accumulated in the ruts during the rain may cause vehicles to slide. Further, rutting causes a reduction in pavement thickness in the wheel paths that accelerates development of fatigue cracking (Sousa, et al., 1991; Bahuguna, 2003).

Densification and shear deformation of asphalt mixes are the main reasons for rutting in flexible pavements (Sousa, et al., 1991). The vertical down-ward densification of asphalt material induced by the repeated traffic loads on asphalt pavements is mainly caused by insufficient compaction effort after placing the HMA layer. The lateral shear movements of asphalt mixes, on the other hand, is usually caused by a lack of shear strength or insufficient amount of air-voids content of the asphalt mix (Witczak, 2007). The shear deformation is the dominant mechanism of rutting in flexible pavements (Sousa, et al., 1991).

Several factors affect rutting susceptibility of asphalt mixes. Among them, the properties of asphalt mixes have the most influence on the rutting development. Dense graded mixes with low air voids mitigate the permanent deformation by enhancing the interlock between aggregates better than the open or gap graded mixes. Rutting potential also reduces when aggregates with high angularity rather than round aggregates are used. High binder viscosity increases rutting resistance. Some other factors like binder content, air void content, compaction, temperature, surface layer thickness and moduli play an important role in rutting resistance. The ability of asphalt mixture to resist rutting is altered by varying any of these factors. Therefore, all of these factors should be considered at the design stage in order to reduce the rutting potential of asphalt mixes (Sousa, et al., 1991).

Although the asphalt mix components and properties have a major influence on rutting potential, no single parameter can be used individually for rut predication with a high level of confidence (Brown & Cross, 1992). Therefore, appropriate laboratory test methods are needed to determine the susceptibility of asphalt mixes to permanent deformation. Several laboratory test methods were performed to characterize the elastic, plastic, viscoelastic, and shear strength responses of asphalt mixtures (Sousa, et al., 1991). Those methods include fundamental, empirical, and simulative tests. Hveem and Marshall tests were the most empirical design methods that have been developed over the years for asphalt mixes design. The Hveem design method was developed in California in the 1930's and has been extensively applied in the western states. The Marshall method was developed later in Mississippi in the 1940s. These two methods were widely used in the United states and around the world because they used density/void analysis and stability/flow tests for asphalt design. Later, in 1993, the Strategic Highway Research Program (SHRP) developed a new method as a last product of its research called the Superpave design method,

which is an acronym for Superior Performing Asphalt Pavements. This method is considered a comprehensive design method. It replaced the previous design because it includes an improved system for selecting asphalts, aggregates, mix design, and pavement performance analysis (NHI, 2000).

Although the Superpave is a comprehensive design method, the method is based solely on volumetric analysis with no mechanical tests like in the Marshall and Hveem methods where the flow and stability tests are used. Therefore, the development of laboratory simple performance tests (SPT) for evaluating rutting and fatigue performance was imperative to address this issue. The Simple Performance Tests (SPT) are a group of test methods that measure the asphalt mixture responses and characteristics caused by traffic and climate actions. Their results Support the superpave volumetric analysis procedure and allow to evaluate the asphalt mixes ability to resist fracture and permanent deformation (Witczak, et al., 2002).

Simulative tests attempt to simulate in the laboratory the stress conditions in field for rutting performance evaluation. The French Rut Tester, Hamburg wheel tracking device, and Georgia Loaded Wheel Test are the most common simulative tests. Generally, these tests asses the rutting susceptibility of HMA through repeated rolling of a rubber or steel wheel over asphalt concrete specimens.

Fundamental tests like the Supperpave Shear Tester (SST) and Field Shear test (FST) evaluate rutting susceptibility by measuring the shear strength and shear modulus of asphalt mixes (Goodman, 2000; Brown, et al., 2001). The (SST) was developed under the SHRP program to measure the asphalt mixture properties and predict the permanent deformation. It measures the shear dynamic modulus of a laboratory asphalt specimen compacted with the Superpave gyratory compactor (SGC). In the SST, the specimen is subjected to horizontal shear force along with a

vertical axial force to maintain the specimen height during the shear test. Out of the six tests that can be performed by the SST device, only two tests are effectively used to characterize asphalt performance against rutting. The Frequency Sweep Test at Constant Height (FSCH) and the Repeated Shear Test at Constant Height (RSCH). The FSCH test is used to measure the complex shear modulus and phase angle of asphalt mixes, whereas the RSCH test is used to measure the cumulative permanent shear deformation under repeated shear cycles (Pavement Interactive, 2008). Although the SST tests is efficient to predict rutting potential of asphalt pavements, it is not used widely due it's complexity and high cost of approximately $250,000 USD (Goodman, 2000).

An attempt to replace the SST device with other simple and less expensive device was attained during the NCHRP Project 9-7 where the first FST device was developed. The Field shear tester (FST) measures the dynamic shear modulus of a compacted asphalt specimen by shearing the specimen along its diameter axis, which means along different planes to the aggregate orientation (Witczak, et al., 2002). The FST device was modified during the NCHRP Project 9-18 to be compact and user friendly. However, it was found that this device could be used only for QC/QA applications due to the complexity of stress and strain distributions near the specimen grips (Christensen, Bonaquist, & Handojo, 2002). Later, the FST was dropped from any further experimental or evaluation tests because it was found that the correlation between the rut depth and stiffness parameters measured with the FST was very poor comparing to the correlations obtained by the SST device (Witczak, et al., 2002).

Since neither of the SST or the FST devices was suitable for widespread use and implementation, and there is an imperative need for a simple and inexpensive test device for measuring the fundamental shear properties of asphalt mixes, Khajeh-Hosseini, (2015) has developed a new device at the University of Texas at Arlington to replicate the loading conditions

and constraints of the SST. The device was named the “Duplicate Shear Tester (DST)” because it measures the average mechanical shear properties of two cylindrical specimens loaded at the same time. The main advantages of the DST device were its low cost and simplicity comparing that with the SST.

The DST was used to perform the two common SST tests: the FSCH and RSCH in accordance to the standard test method AASHTO-T 320. The tests were performed by utilizing a universal testing machine. This brings a major advantage to the DST device as it can be adopted in many laboratories having a universal test machine. The device proved to provides reliable measurements for the dynamic shear modulus and phase angle of asphalt mixes at load frequencies ranged from 0.5 to 10 Hz (Khajeh-Hosseini, 2015; Jweihan, 2018).

A recent study in the University of Texas at Arlington was performed by Jweihan, (2018) to improve the DST and to assess the variability of the results obtained with the modified device through conducting the FSCH and RSCH tests. The main modification of the DST device included an additional mini linear rail system to assure a vertical motion for the DST middle plate. The results obtained with the modified DST device had relatively low coefficient of variations. 7% to 23% for the dynamic shear modulus, 3% to 11% for the phase angle, and about 20% for the permanent shear deformation at 5,000 shear load cycles. Even though the modified DST has successfully satisfied the objectives of a new reliable, inexpensive and simple test device, further modifications are required to simplify and improve the testing procedure by making the device lighter and able to accommodate specimens of other shapes (Jweihan, 2018).

1.2 Research Rationale

Since 90% of rutting in asphalt mixes occurs due to the shear deformation and it is limited to the upper 3 to 4 inches of the HMA layer, better laboratory test method for evaluating the resistance of asphalt mixes to rutting is needed. Therefore, the DST device needs to be further modified to be lighter and capable to accommodate rectangular and smaller circular asphalt concrete specimens. Also, a new shear tester needs to be developed to investigate the shear responses of asphalt mixes when normal stresses are applied at the same time with the shear stresses.

This is needed because when the asphalt mix moves laterally under the action of shear stress, the asphalt mix is also subjected to normal stresses. These normal stresses are developed due to the wheel loads passing over the pavement surface. It is desirable that the new device would subject the asphalt samples to similar loading conditions as in the standard test method AASHTO T-320, but with an additional normal stress applied at the same time with the shear stress. The device is called the "Shear Tester with Normal Stress (STNS)".

1.3 Research Objectives

The objectives of this research study are:

1- To assess the variability of the DST during a typical daily production of HMA by performing the FSCH and RECH tests in accordance to the standard test method AASHTO-T 320.

2- To investigate if rectangular or smaller diameter circular specimens provide the same results.

3- To develop the "Shear Tester with Normal Stress (STNS)" device to perform the Frequency Shear Test at Normal Stress (FSNS) and the Repeated Shear Test at Normal Stress (RSNS) and assess the repeatability of results obtained from the two tests.

4- To compare the tests results by using a statistical analysis of variation (ANOVA).

1.4 Dissertation Outline

This dissertation is divided into seven chapters. Chapter 1 provides a brief statement of permanent deformation problem in asphalt pavements, including research rationale, and objectives of the study. Chapter 2 summarizes a literature review of permanent deformation in flexible pavements including rutting mechanisms, common methods of prediction, and existing rutting tests. Chapter 3 focuses on previous shear tests devices that have been developed to predict permanent deformation in asphalt concrete. It covers a full description of the Superpave Shear Tester (SST) and Duplicate Shear Tester (DST). Chapter 4 describes in detail the approach for modifying the Duplicate Shear Tester (DST) and developing the Shear Tester with Normal Stress (STNS). It contains drawing models, descriptions, and concepts of the two devices. Chapter 5 covers the testing materials and test methods of this study; beginning from the selection of the asphalt mixes until the completion of the tests. Chapter 6 contains the experimental results and discussion. It also includes a statistical analysis of variation (ANOVA) for the measured shear parameters. Finally, the conclusions of this study and recommendations for future studies are presented in Chapter7.

Chapter 2: Background of Asphalt Concrete Permanent Deformation

2.1 Introduction

Poor performance of HMA pavements can be result due to five common distress types including: permanent deformation, thermal cracking, fatigue cracking, stripping, and loss in surface friction. Among these distresses, rutting could result with an unsatisfactory pavement through a sudden failure, while others need couple of years of service to show up (Zhang et al, 2005). Moreover, rutting was rated through a comprehensive survey study as the most significant distress in asphalt pavements that should be considered by the simple performance tests (SPT), followed by fatigue cracking and thermal cracking (Witczak, et al., 2002).

Rutting or permanent deformation is a critical distress mechanism in flexible pavements. This unrecoverable deformation develops due to accumulation of small deformations induced at every load application (NHI, 2000). It occurs as a permanent longitudinal depression in the wheel paths with small upheavals to the sides that mainly induced by the shear deformation of the HMA layer (Sousa, et al., 1991), as shown in Figure 2-1. Many field studies in Texas has been shown that rutting appears typically at 2-4 inches of the upper HMA layer (Zhou, et al., 2010).

Rutting has been attributed to the increase in repetitive heavy loads of traffic passing on asphalt pavements. It is however considered in many parts of the United States as a serious concern that affects road user safety especially when water may accumulate in the ruts and cause definite threat of vehicles hydroplaning as well as difficulty in steering (Sousa, et al., 1991). It also causes bleeding where the asphalt binder rises to the surface resulting in a very slippery pavement causing accidents. Another effect of rutting is a reduction in pavement thickness that accelerates pavement failure under fatigue cracking (Bahuguna, 2003). Therefore, it is important to make efforts to

minimize rutting potential through studying rutting behavior and causes before placing asphalt mixes in service (Sousa, et al., 1991; Scullion, et al., 2004).

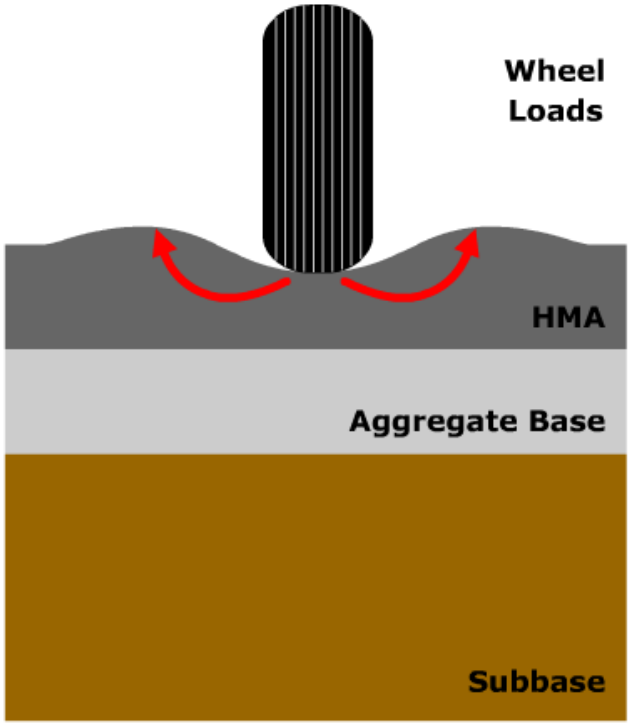

Figure 2-1. Shear Deformation Rutting Schematic (Pavement Interactive, 2018)

This chapter discusses a general background of permanent deformation types, mechanism, and affecting factors. A brief review of both layer strain and viscoelastic approaches for rutting prediction are also discussed. Finally, three main test methods categories that characterize rutting response of asphalt material are discussed. The test methods include fundamental, empirical, and simulative tests.

2.2 Rutting Types

Rutting can be categorized into two main types based on its' causes and pavement layers in which the rutting occurs as the follows:

1- One-dimension densification or vertical compression.

2- Lateral Flow or shear permanent movement.

The one-dimension densification is mainly caused by densifying asphalt materials in the vertical direction near to the wheel path's center and without humps to the side of the depression. This densification is caused due to either excessive air voids content in the asphalt mixes or insufficient compaction effort after placing the HMA layer. A low to moderate sever rutting is usually the results of this type of rutting (Witczak, 2007).

The shear permanent movement creates a depression near the center of the wheel path with humps to the side that is caused by a lateral flow of asphalt materials. The lateral displacement is usually induced due to a lack of shear strength or insufficient amount of air-voids content of the surface mix. Low voids content of 3% or less in asphalt layer after the compaction allow the asphalt to act more like a lubricant instead of a binder in the mixes especially during hot weather. Bleeding and flushing, however, can occur on the pavement surface as a result of over-densification in the HMA layer due to heavy traffic loads. In this type of rutting, a moderate to severe rutting level well usually result (Witczak, 2007).

Rutting can also associate with the base, subbase, and/or subgrade layers' deformation. This type of rutting is mainly developed by either consolidation or densification with or without a lateral movement of unbound material underneath the HMA layer. Longitudinal cracking at the center and outside edges of ruts on the pavement surface usually results when asphalt mixes is too stiff (Witczak, 2007).

2.3 Rutting Mechanisms

Surface distortion is caused by inelastic or permanent deformation that is induced by the action of repeated wheel loads in one or more layers of pavements. Applying a wheel load to the pavement surface deforms the HMA and pavement's sublayers in proportional to the stiffness and thickness of each layer at the temperature and speed of loading. A residual amount of deformation remains after releasing every wheel load. Rutting occurs due to the action of a repeated wheel load when the residual deformations accumulate and increase the permanent deformation. Since asphalt is a thermo viscoelastic material and its behavior depends on the temperature and rate of loading, the length of loading time affects rutting. Therefore, the amount of deformation on highway at higher speeds will be less than that at slower speeds, given the same load magnitude and temperature (Witczak, 2007).

Rutting is mainly caused by the combination of asphalt mix densification and shear deformation. The densification is a gradual reduction of air voids in pavement layers due to repeated traffic loads application on pavement surface after the initial compaction. Densification is sometimes revealed when underneath layers containing fine-grained materials and high levels of moisture. However, HMA layer is more susceptible to densification due to higher compressive stresses and temperatures near the surface. The shear deformation, on the other hand, means a permanent sher flow with or without a change in volume of asphalt mixes. It develops as a result of lateral movements of asphalt mixes under shear stresses of repeated traffic loads causing depressions in the loaded area. This type of rutting usually happens when the shear strength of asphalt mixes is relatively low (Witczak, 2007; Moghadas, et al., 2015).

Rutting can develop not only in the surface wearing layer but also in other sub-layers of the pavement structure including the subgrade (Sousa, et al., 1991). Small permanent deformations

of any or all pavement layers accumulate in asphalt pavements forming eventually rutting. In general, rutting happens when there is a problem in construction or asphalt mixes design. The construction or structural problem happens due to under-designed or under-compacted pavement layers. It could also happen due to water intrusion as it weakens the unbound base or subgrade layer. The asphalt mix design problem is a result of inappropriate shear strength to resist the subjected repeated heavy traffic loads (Zhou, et al., 2010).

Rutting occurs gradually over different times of pavement service life. As mentioned previously, there are two mechanisms of rutting: densification and shear deformation. The densification mechanism, that usually induced by repeated heavy loads application, is responsible to "initial rutting" in the early years of pavement life, whereas the shear deformation mechanism is responsible to "secondary rutting" that develops anytime throughout pavements life. At this stage of rutting, permanent shear flow of asphalt material is moved from underneath the wheel path to the sides causing upheavals (Pradhan, 1995). However, it is indicated that the shear deformation is the dominant mechanism of about 90 % of the rutting in asphalt mixes (Sousa, et al., 1991).

Asphalt pavement rutting has two main causes: rutting from weak subgrade or base layer and from weak asphalt mixtures, as illustrated in Figure 2-2. The weak subgrade or base rutting type is often referred to as a structural problem that occurs when a high stress is applied to the underlying layers of pavement and there is insufficient pavement strength or thickness to reduce this stress to an acceptable level.

The rutting due to weak asphalt concrete, on the other hand, is caused by a material problem that results when the shear strength of asphalt mixes is not enough to resist the repeated heavy loads. In this case, permanent deformations are produced by a downward and lateral movement of

asphalt mix. This type of rutting is susceptible to high temperatures as it occurs usually during summer. While this type of rutting is related to asphalt mix problem, it can be addressed by considering binder and aggregate properties to provide sufficient shear strength. This can be satisfied by selecting an asphalt binder that is stiff and elastic enough at high temperatures to be able to return to its original shape without permanent deformation after the load is released. Selecting an angular aggregate that has a high degree of internal friction is another way to minimize this type of rutting (McGennis, et al., 1994; NHI, 2000). Brown and Cross, (1992) have concluded also that high quality asphalt mixes are required in the upper layers of pavements since it has been observed through pavements' trench-cuts that rutting usually occurs in the top 3-4 inches of the HMA.

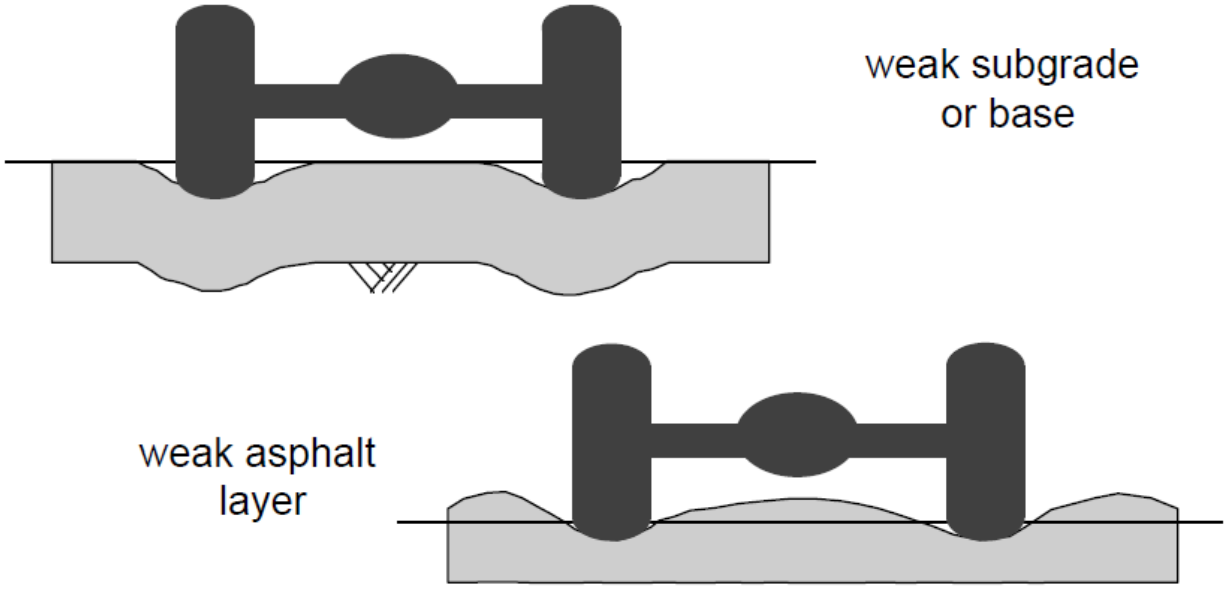

Figure 2-2. Rutting Cause Principles (NHI, 2000)

2.4 Rut Depth Measurements

Rut depth is defined as "the maximum measured perpendicular distance between the bottom surface of the straightedge and the contact area of the gauge with the pavement surface at

a specific location" (ASTM-E1703/E1703M, 2015). The rut depth can be measured either manually or automatically. The manual measurement of rut depth is simply performed by placing a straightedge on the pavement surface across the rut and perpendicular to the traffic flow and measuring the greatest vertical distance between the bottom of the straightedge and the pavement surface with a measuring gauge, as shown in Figure 2-3. The ASTM specification for this method requires that a minimum length of the straightedge to be 1.73m (5.67ft) in order to ensure that it spans the entire rut width (ASTM-E1703/E1703M, 2015).

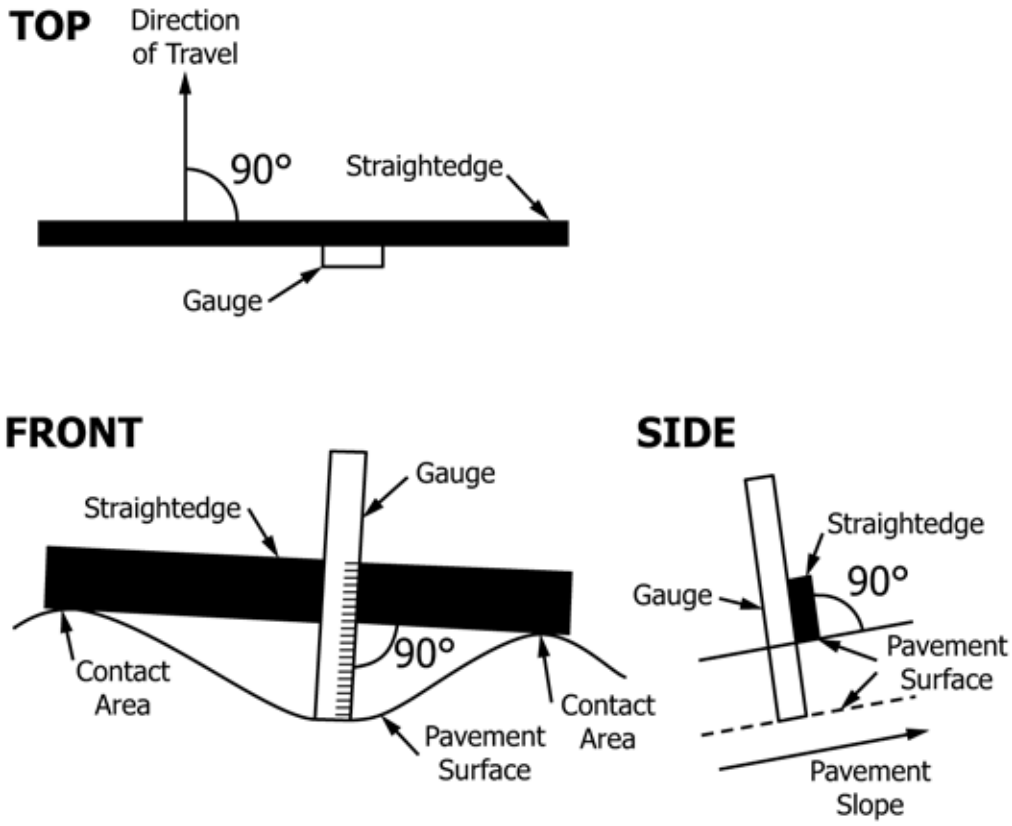

Figure 2-3. Rut Depth measurement using a Straightedge (ASTM-E1703/E1703M, 2015).

The automated measurements of the rut depth, on the other hand, is performed by using lasers or ultrasonic transducer sensors mounted in a vehicle travelling over pavements at highway speeds to measure the transverse profile of a pavement section. They are generally referred as "Profilometers". This method allows numerous rut measurements, accurate measurements and can

obtain data in very short time interval comparing to the manual method. The safety risk of this method is also reduced since the measuring crew can obtain the data from inside the vehicle and without conflicting with traffic flow (Mallela & Wang, 2006; Hoffman & Sargand, 2011).

The AASHTO provisional standard on rut-depth measurements provides a method for measuring rut depth at pavement surface. The method requires five transverse profile points across both wheel-paths as a minimum number of points to determine the rut depth at a transverse profile, as shown in Figure 2-4. In this method, the transverse profile should be measured at maximum spacing of 10m (33ft) over a summary interval in the longitudinal direction of the survey lanes. The summary interval is usually defined by the agency and it is generally for 0.1 km (0.1 mile). The maximum and average rut depth measured from each wheel-path within the selected interval should be recorded in the measurement report (AASHTO R48-10, 2013).

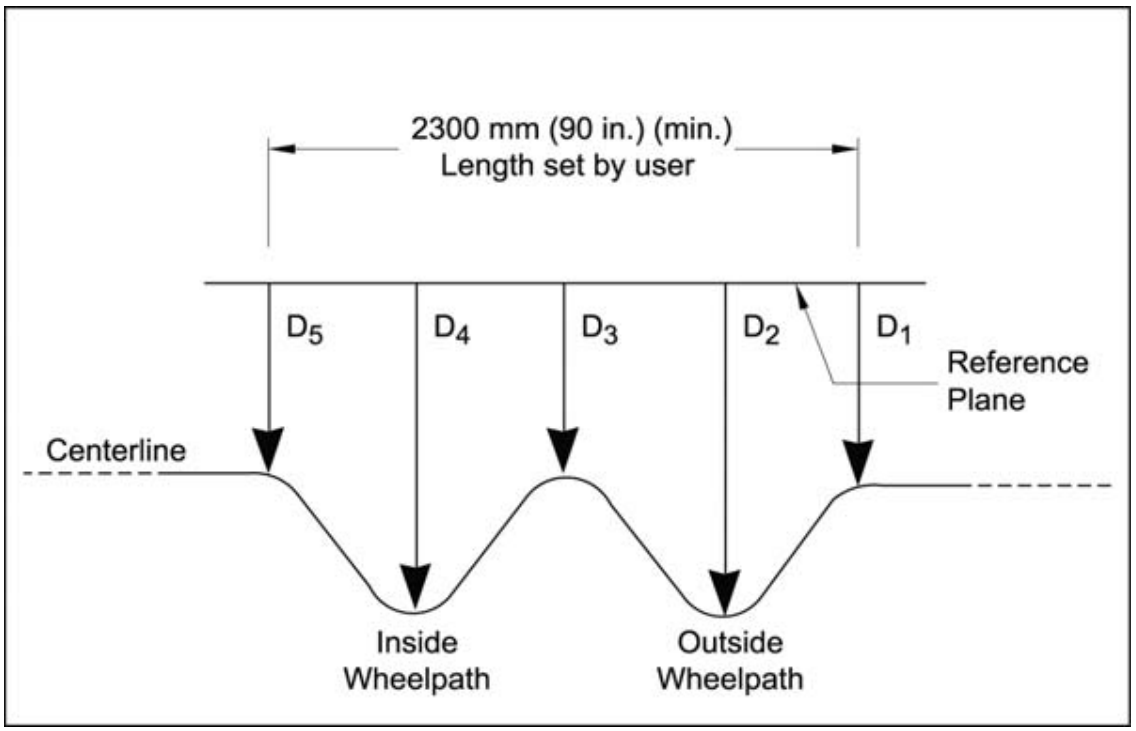

Figure 2-4. Five-points Rut depth measurements (AASHTO R48-10, 2013).

The five-points rut depth calculations are shown below in Equations 2-1 and 2-2:

$$R_o = D_2 - \frac{D_1 + M}{2} \qquad (2\text{-}1)$$

$$R_i = D_4 - \frac{D_5 + M}{2} \qquad (2\text{-}2)$$

Where:

$M = \frac{D_1 + D_5}{2}$ or D_3, whichever is less;

R_o = rut depth outside wheel path estimate (mm);

R_i = rut depth inside wheel path estimate (mm);

$D_1, D_2 \ldots . D_{15}$ = height measured as shown in Figure 1 (mm).

This standard is intended to measure the rut depth with a vehicle traveling on the survey lanes at highway speeds. However, it can be performed manually as illustrated previously. The transverse profile is determined through vertical distances between an imaginary string line and the pavement surface. The string line is placed across the traffic lane from the shoulder to the lane line. For the manual measurements, the string line may bend at the hump between the wheel paths where the hump is higher than the edges. Therefore, the distances D1, D3, and D5 are required to be zero (AASHTO R48-10, 2013). Rutting distress, however, is measured in surface area (square meters or square feet) and its severity level is determined in according to the mean depth of rut. The severity levels of rutting are specified in Table 2-1 (ASTM D6433, 2016).

Table 2-1. Rutting Severity Levels (ASTM D6433, 2016)

Severity Levels	Mean Rut Depths
Low	6 to 13 mm (0.25 to 0.5 in)
Medium	13 to 25 mm (> 0.5 to 1 in)
High	>25 mm (>1 in)

2.5 Factors Affecting Rutting

Permanent deformation of asphalt mixes is a complex phenomenon that is influenced by many factors including asphalt mix's properties and other test or field conditions. Moreover, the properties of asphalt mixes that influence permanent deformation change over time till useful pavement life is achieved. When asphalt ages, the viscosity of asphalt mixes reduces making the potential of permanent deformation increases. Moisture damage may also enhance rutting potential in some mixes (Witczak, 2007). Different factors that may influence permanent deformation development are shown in Table 2-2. A brief discussion on their influences are discussed below.

Table 2-2. Factors affecting rutting of asphalt-concrete mixtures (Sousa, et al., 1991).

	Factor	Change in Factor	Effect of Change in Factor on Rutting Resistance
Aggregate	Surface Texture	Smooth to rough	Increase
	Gradation	Gap to continuous	Increase
	Shape	Rounded to angular	Increase
	Size	Increase in maximum size	Increase
Binder	Stiffness ***a**	Increase	Increase
Mixture	Binder content	Increase	Decrease
	Air void content ***b**	Increase	Decrease
	VMA	Increase	Decrease ***c**
	Method of compaction	***d**	***d**
Test field conditions	Temperature	Increase	Decrease
	State of stress /strain	Increase in tire contact pressure	Decrease
	Load repetitions	Increase	Decrease
	Water	Dry to wet	Decrease if mix is water sensitive

***a -** Refers to stiffness at temperature at which rutting propensity is being determined. Modifiers may be utilized to increase stiffness at critical temperatures, thereby reducing rutting potential.
***b -** When air void contents are less than about 3 percent, the rutting potential of mixes increases.
***c -** It is argued that very low VMA's (e.g., less than 10 percent) should be avoided.
***d -** The method of compaction, either laboratory or field, may influence the structure of the system and therefore the propensity for rutting.

2.5.1 Aggregate

Aggregates play an important role in rutting resistance. Rough texture aggregates with high angularity reduce the potential of rutting much better than round and smooth aggregates. Dense graded mixes with low air voids mitigate rutting by enhancing the interlock between aggregates more efficiently than the open or gap graded mixes (Sousa, et al., 1991). Also, well compacted mixtures with a strong aggregate structure provide rutting resistance much better than poorly compacted mixtures since they can withstand high axial forces at small amount of shear strain levels (Witczak, et al., 2002).

A study performed by National Center for Asphalt Technology, NCAT, to evaluate rutting performance in the United States under different conditions of climate, aggregate angularity, and construction practice has concluded that "Rutting on high volume roadways can be prevented if angular coarse and fine aggregates are used and if the air voids in the mixture do not fall below approximately 3.0%" (Brown and Cross, 1992).

2.5.2 Binder

Since asphalt binder is a viscoelastic material, asphalt viscosity affects rutting performance. Low viscosity binder is more susceptible to rutting since it has low stiffness against shear deformation. Asphalt binders modified with polymers increase rutting resistance due to their high viscosity comparing to that of conventional binders (Sousa, et al., 1991). Witczak, et al., (2002) also state that a stiffer binder increases rutting resistance ability through minimizing shear strains in the aggregate skeleton.

2.5.3 Mixes

Proportion of binder and air void contents in asphalt mixes affects mixtures' stability. A high asphalt content increases rutting potential through decreasing air voids content and increasing the separation between aggregate's particles in a very tight air void structure, whereas a low content of asphalt binders ends up with low workability for asphalt mixes by increasing the required high compaction energy in the field (Sousa, et al., 1991).

High air voids content in asphalt mixes, on the other hand, resulting in a more stable state of densification and less shear resistance because asphalt binder can move easily into the entrapped air voids (Long, F. M, 2001). Sousa, (1994) states that a data obtained from general pavement studies (GPS), by SHRP, have showed a large rut depth for dense-graded mixes, which was observed in sites where the air void content was below 3%, as shown in Figure 2-5. That's justified due to the reduction in air void content that resulting in low bearing capacity (low stability) in aggregate skeleton of asphalt mixes, when binder acts as lubricant between aggregates and reduces the interlock pressures between particles. Moreover, Brown and Cross, (1992) have concluded that in-place air void of HMA should be at least 3% to decrease rutting potential over pavement's life span. Thus, it would be required to place asphalt mixes with an air void content of around 5-7% in order to obtain the minimum content of 3% air voids after the compaction. Generally, preferable asphalt mixtures for rut resistance should be designed with a low binder content and compacted to a low air void content of at least 3% so that it does not compromise asphalt mix's workability, durability and fatigue cracking resistance (Long, F. M, 2001).

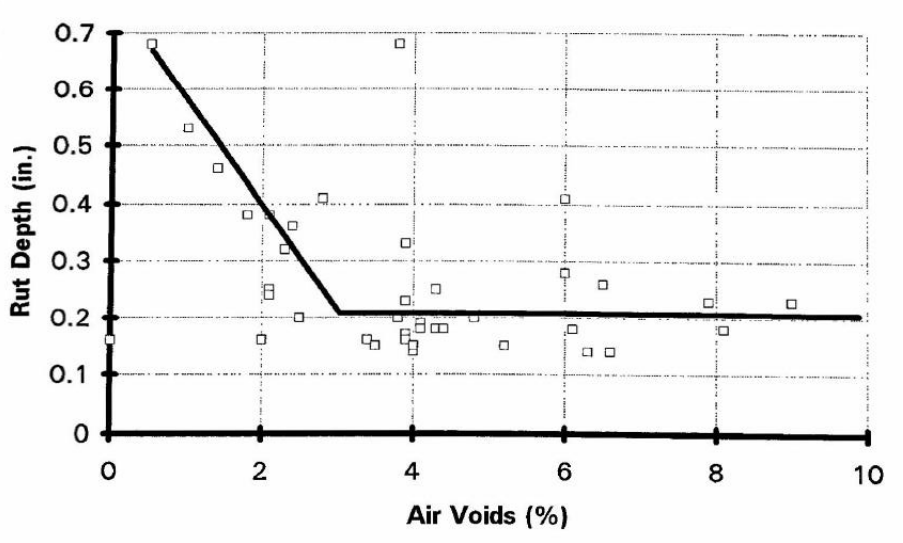

Figure 2-5. Rut Depth versus Air Voids for GPS Pavement Studies (Sousa,1994)

2.5.4 Test field conditions

Other factors including field conditions would also affect rutting resistance of asphalt mixes. These factors including field temperature, tire pressures developed by traffic loading, and heavy traffic proportions. Increasing any of these factors will significantly accelerates rutting potential (Sousa, et al., 1991).

2.6 Rutting Prediction Approaches

Asphalt concrete is a viscoelastic material and its' behavior depends on environmental and loading conditions. It may exhibit as a viscous liquid with unrecoverable deformation after releasing the load and other times exhibit as an elastic solid material with a recoverable deformation (NHI,2000). Many procedures, however, attempt to estimate the amount of permanent deformation occurring in the asphalt pavements based on the viscoelastic behavior. Layer Strain and Viscoelastic Approaches are the two common analytical procedures of rutting analysis and prediction. They are discussed below.

2.6.1 Layer Strain Approach

The layer-strain approach typically uses either linear or nonlinear elastic theory to predict rut depth. Although nonlinear elastic theory provides more accurate prediction, it has been limited due to its complexity. This theory predicts the total rut depth by dividing each layer of pavement structure into sublayers. An elastic analysis is used to calculate the stress state at the center of each sublayer, as illustrated in Figure 2-6. The corresponding axial permanent strain, ϵ_i^p, of each sublayer of thickness, Δz_i, can be determined by using some compression laboratory tests including either creep or repeated loading tests; usually from triaxial tests. The total predicted rut depth, Δp , of total number of sublayers, *n*, is calculated using Equation 2-3 (Sousa, et al., 1991).

$$\Delta p = \sum_{i=1}^{n}\left[\left(\epsilon_i^p\right)(\Delta z_i)\right] \qquad (2\text{-}3)$$

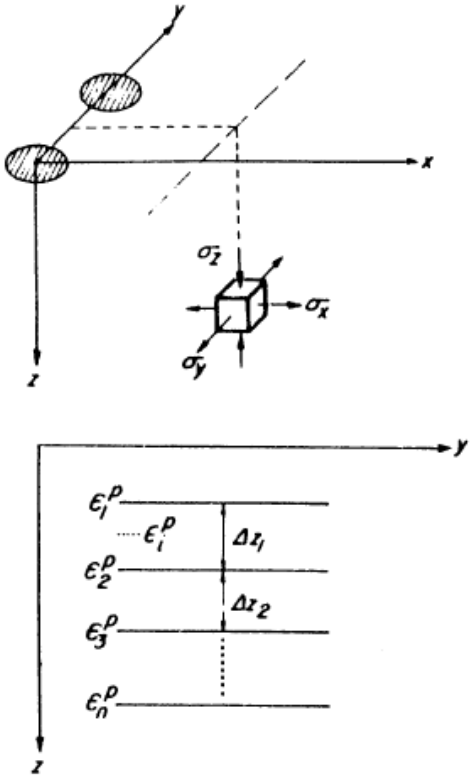

Figure 2-6. Layer Strain Approach (Sousa, et al., 1991).

Although this method is considered as a simple approach to predict rut depth, it does not include the shear components of pavements. This approach only considers the center of the loaded area under tires and ignores the shear responses of pavement within the entire rutting zone such as the “humps” that occur along the sides of the tire edge (Sousa, et al., 1991). Also, some other behaviors corresponding to rutting like shear flow at the edge of tire and permanent deformation after removing the loads are not accounted in this method. Therefore, modeling asphalt concrete as a linear elastic material is unable to predict rutting (Long, F. M, 2001).

2.6.2 Viscoelastic Approach

This approach attempts to predict rutting performance based on viscoelastic behavior of asphalt concrete. Unlike the layer strain approach, rutting is assumed to be formed as a result of asphalt material shear flow and it is independent to the elastic properties of asphalt mixes (Collop, et al., 1995). In this approach, both moving wheel loads and the time-dependent nature of asphalt concrete are considered in purpose to identify the states of stress and strain within the pavement layers through utilizing either Maxwell and /or Kelvin elements of deferent configurations or other generalized compliance relationships (Sousa, et al., 1991).

Determining the viscosity of pavement layer over a wide range of environmental conditions is essential to the successful application of the linear viscoelasticity model. This model, however, has some advantages for rutting prediction. They include the exact accounting of permanent deformation distribution of all layers. Also, the effects of vehicle speed (loading time) and pavement temperature are taken in consideration (Collop, et al., 1995). Nonlinear viscoelastic model, on the other hand, is more realistic than the linear viscoelastic model. Yet it seems to be prohibited since it is mathematically complex and difficult to use, which makes the latter to be a

common approach for rutting prediction. Although the viscoelastic approach is sounder for rutting prediction than the layer strain method, its complexity and the poor relation between the predicted and measured values have limited its advantages for rutting prediction (Sousa, et al., 1991).

2.7 Permanent Deformation Laboratory Tests

Developing simple and accurate procedures for the purpose of evaluating permanent deformation susceptibility of asphalt mixes is an imperative issue, yet it still to be developed. Khosla and Omer (1985) state that "the choice of test method for the characterization of asphaltic mixtures has a pronounced effect on predicted performance". Thus, several laboratory tests were performed to characterize asphalt concrete parameters of permanent deformation response including the elastic, plastic, viscoelastic, and shear strength of asphalt mixtures (Sousa, et al., 1991). Permanent deformation tests can be classified generally as:

1- Fundamental tests, that include: Uniaxial and Triaxial Tests, Diametral Test, and Shear Loading Tests.
2- Empirical tests, that include: Marshall Test, Hveem Test, Gyratory Testing Machine (GTM), and Lateral Pressure Indicator (LPI).
3- Simulative tests, that include: Asphalt Pavement Analyzer, Hamburg Wheel-Tracking Device, French Rutting Tester, Purdue University Laboratory Wheel Tracking Device, Model Mobile Load Simulator, Dry Wheel Tracker, and Rotary Loaded Wheel Tester.

The advantages and disadvantages of each of these tests are summarized in Table 2-3 (Brown, et al., 2001).

Table 2-3. Comparative Assessment of Permanent Deformation Test Methods (Brown, et al., 2001).

Test Methods		Advantages	Disadvantages
Fundamental: Uniaxial Tests	Uniaxial Static (Creep)	Easy to perform.	Ability to predict performance is questionable.
		Test equipment is simple and generally available.	Restricted test temperature and load levels does not simulate field conditions.
		Well known.	Does not simulate field dynamic phenomena.
		More technical information.	Difficult to obtain 2:1 ratio specimen in lab.
	Uniaxial Repeated Load	Better simulates traffic conditions.	Equipment is more complex.
			Restricted test temperature and load levels does not simulate field conditions.
			Difficult to obtain 2:1 ratio specimen in lab.
	Uniaxial Dynamic Modulus	Nondestructive tests.	Equipment is more complex.
			Difficult to obtain 2:1 ratio specimen in lab.
	Uniaxial Strength Test	Easy to perform.	Questionable ability to predict permanent deformation.
		Test equipment is simple and generally available.	
		Minimum test time.	
Fundamental: Triaxial Tests	Triaxial Static (Creep Confined)	Relatively simple test and equipment.	Requires a triaxial chamber
		Test temperature and load levels better simulate field conditions than unconfined.	Confinement increases complexity of the test.
		Potentially inexpensive.	
	Triaxial Repeated Load	Test temperature and load levels better simulate field conditions than unconfined.	Equipment is relatively complex and expensive.
		Better expresses traffic conditions.	
		Can accommodate varied specimen sizes.	Requires a triaxial chamber.
		Criteria available.	

Table 2-3. Comparative Assessment of Permanent Deformation Test Methods (Cont.)
(Brown, et al., 2001).

Test Methods		Advantages	Disadvantages
Fundamental: Triaxial Tests	Triaxial Dynamic Modulus	Provides necessary input for structural analysis.	At high temperature it is a complex test system (small deformation measurement sensitivity is needed at high temperature).
			Some possible minor problem due to stud, LVDT arrangement.
		Nondestructive test.	Equipment is more complex and expensive.
			Requires a triaxial chamber.
	Triaxial Strength	Relatively simple test and equipment.	Ability to predict permanent deformation is questionable.
		Minimum test time.	Requires a triaxial chamber.
Fundamental: Diametral Tests	Diametral Static (Creep)	Test is easy to perform.	•State of stress is nonuniform and strongly dependent on the shape of the specimen. •May be inappropriate for estimating permanent deformation. •High temperature (load) changes in the specimen shape affect the state of stress and the test measurement significantly. •Were found to overestimate rutting. •For the dynamic test, the equipment is complex.
		Equipment is generally available in most labs.	
		Specimen is easy to fabricate.	
	Diametral Repeated Load	Test is easy to perform.	
		Specimen is easy to fabricate.	
	Diametral Dynamic Modulus	Specimen is easy to fabricate.	
		Nondestructive test.	
	Diametral Strength Test	Test is easy to perform.	
		Equipment is generally available in most labs.	
		Specimen is easy to fabricate.	
		Minimum test time.	
Fundamental: Shear Tests	SST Frequency Sweep Test - Shear Dynamic Modulus	The applied shear strain simulates the effect of road traffic.	Equipment is extremely expensive and rarely available.
		AASHTO standardized procedure available.	Test is complex and difficult to run, usually need special training.
		Specimen is prepared with SGC samples.	
		Master curve could be drawn from different temperatures and frequencies.	SGC samples need to be cut and glued before testing.
		Non-destructive test	

Table 2-3. Comparative Assessment of Permanent Deformation Test Methods (Cont.) (Brown, et al., 2001).

Test Methods		Advantages	Disadvantages
Fundamental: Shear Tests	SST Repeated Shear at Constant Height	The applied shear strains simulate the effect of road traffic.	Equipment is extremely expensive and rarely available.
			Test is complex and difficult to run, usually need special training.
		AASHTO standardized procedure available.	SGC samples need to be cut and glued before testing
		Specimen is prepared with SGC samples.	High COV of test results.
			More than three replicates are needed.
	Triaxial Shear Strength Test	Short test time.	Much less used.
			Confined specimen requirements add complexity.
Empirical Tests	Marshall Test	Wide spread, well known, standardized for mix design.	Not able to correctly rank mixes for permanent deformation.
		Test procedure standardized.	
		Easiest to implement and short test time.	Little data to indicate it is related to performance.
		Equipment available in all labs.	
	Hveem Test	Developed with a good basic philosophy.	Not used as widely as Marshall in the past.
		Short test time.	California kneading compacter needed.
		Triaxial load applied.	Not able to correctly rank mixes for permanent deformation.
	GTM	Simulate the action of rollers during construction.	Equipment not widely available.
		Parameters are generated during compaction.	Not able to correctly rank mixes for permanent deformation.
		Criteria available.	
	Lateral Pressure Indicator	Test during compaction.	Problems to interpret test results.
			Not much data available.

Table 2-3. Comparative Assessment of Permanent Deformation Test Methods (Cont.) (Brown, et al., 2001).

Test Methods		Advantages	Disadvantages
Simulative Tests	Asphalt Pavement Analyzer	Simulates field traffic and temperature conditions.	Relatively expensive except for new table top version.
		Modified and improved from GLWT.	
		Simple to perform.	
		3-6 samples can be tested at the same time.	
		Most widely used LWT in the US.	
		Guidelines (criteria) are available.	
		Cylindrical specimens use SGC.	
	Hamburg Wheel-Tracking Device	Widely used in Germany.	Less potential to be accepted widely in the United States.
		Capable of evaluating moisture-induced damage.	
		2 samples tested at same time.	
	French Rutting Tester	Successfully used in France.	Not widely available in U.S.
		Two HMA slabs can be tested at one time.	
	PURWheel	Specimen can be from field as well as lab prepared.	Linear compactor needed.
			Not widely available.
	Model Mobile Load Simulator	Specimen is scaled to full-scaled load simulator.	Extra materials needed.
			Not suitable for routine use.
			Standard for lab specimen fabrication needs to be developed.
	RLWT	Use SGC sample.	Not widely used in the United States.
		Some relationship with APA rut depth.	Very little data available.
	Wessex Device	Two specimens could be tested at one time.	Not widely used in the United States.
		Use SGC samples.	Very little data available.

The most popular tests of the three tests categories are discussed below. They include: The Uniaxial and Triaxial tests, and Diametrical tests as for the fundamental tests; The Marshall and Hveem tests as for the empirical tests; The Asphalt Pavement Analyzer, Hamburg Wheel-Tracking Device, and French Rutting tester as for the simulative tests. In chapter three, the Superpave Shear Tests (SST) along with other shear test systems will be discussed.

2.7.1 The Fundamental Tests

2.7.1.1 Uniaxial and Triaxial Tests

These tests mainly include testing confined and unconfined cylindrical sample of asphalt concrete under different loading conditions of creep, repeated or dynamic. In the creep test, a concrete sample is placed between two steel plates and fixed at one of those platens, as shown in Figure 2-7. The confined creep test is performed by applying a confining pressure of 138 kPa along with a vertical pressure of at least 828 kPa at temperature 60°C, whereas the unconfined creep test is performed by applying only a constant axial load of 100 kPa on the movable platen for a period of one hour at constant temperature of 40°C. The specimen deformation (strain), in this test, is measured as a function of loading time, as shown in Figure 2-8 (Brown, et al., 2001). It was found that the results of this test are unconstrained to the sample size proportions providing the sample should have flat and parallel ends with a lubrication to minimize the friction effect at contact between the platens ends and the specimen (Sousa, et al., 1991).

Although the creep test is relatively easy and inexpensive test, a friction will be developed between the platen ends and specimen resulting in a localized state of stress near the platen ends that affects the accuracy of the measured Young's modulus (E) especially at elevated temperatures

(Weissman, et al., 1999). In addition, the ability of the unconfined creep test to predict rutting is doubtable since its' conditions do not closely simulate the field condition (Brown, et al., 2001).

Figure 2-7. Creep Testing (Brown, et al., 2001)

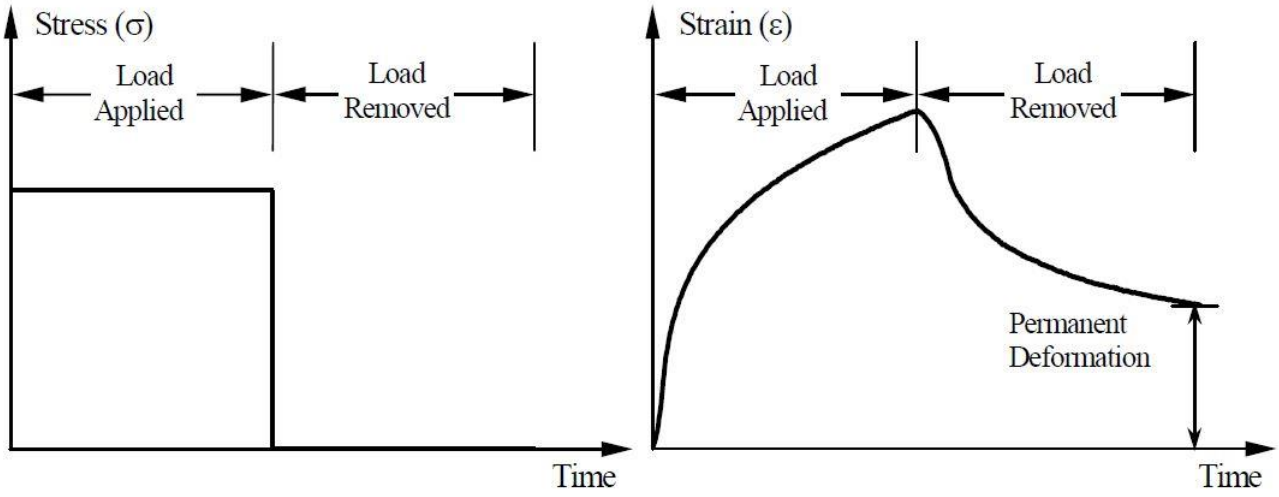

Figure 2-8. Typical Creep Stress and Strain Relationships (Brown, et al., 2001)

The repeated load uniaxial and triaxial tests are generally performed to measure permanent deformation of asphalt mixes through applying several thousand repetition load cycles at a certain

frequency. The cumulative permanent deformation is typically measured as a function of the load repetitions number. Similar to the advantage of confined creep tests, the vertical and horizontal stresses can be applied at the same time to simulate field conditions (Brown, et al., 2001). In the repeated tests, a cylindrical sample is subjected to repeated tension and compression axial loads along with confining stress in a controlled temperature chamber, as shown in Figure 2-9. The pulses are applied typically within time period ranges from 0.1 to 1.0 second. The horizontal and vertical strains of the specimen will be measured by fixed axial LVDTs and lateral gauges, respectively. However, it has been indicated in several studies that repeated load triaxial tests are more efficient tests to characterize asphalt pavement rutting than the creep tests (Sousa, et al., 1991).

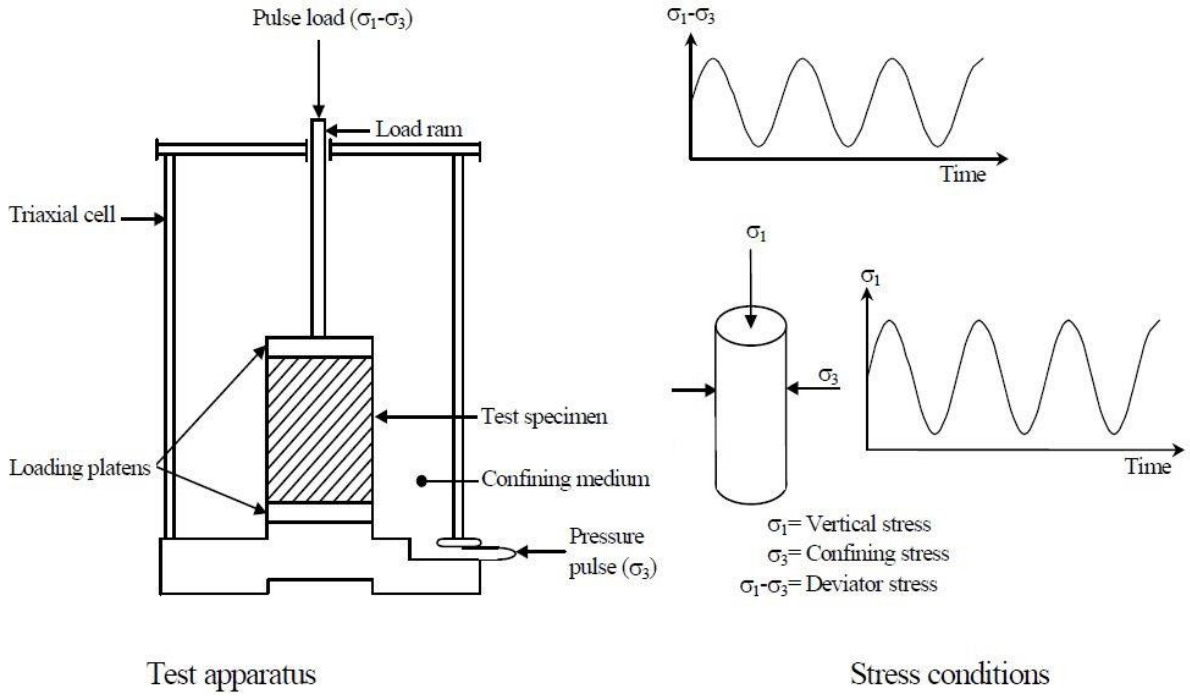

Figure 2-9. Schematic of Repeated Load Triaxial Test (Brown, et al., 2001)

The uniaxial and triaxial dynamic modulus tests are more advanced tests that used to determine additional properties for linear viscoelastic materials characterization. These tests measure

dynamic modulus and phase angle of asphalt concrete as functions of load frequencies, cycles, and temperature. The dynamic modulus is defined as the ratio of peak stress to the peak strain, whereas the phase angle is the time lag between the applied stress and corresponding strain (Sousa, et al., 1994a). In the dynamic tests, a 4-inch diameter by 8-inch height HMA sample is subjected to sinusoidal compressive stress over various range of frequencies of 1,4, and 16 Hz for 30 to 45 seconds. A constant lateral pressure is applied in the triaxial dynamic test along with the sinusoidal compressive stress. The dynamic tests are more difficult than the repeated tests due to the requirement of more accurate system to measure the deformation. Thus, these tests are no longer used for purpose of quality control (Brown, et al., 2001).

In general, the uniaxial and triaxial tests have advantages due to their non-complexity in implementation as well as the wide range of stress state including shear components that can be obtained by varying the applied pressures. However, it has been reported that should not rely only on the triaxle tests for rutting prediction since the produced shear stress components do not correlate properly with the results from the field (Sousa, et al., 1994a).

2.7.1.2 Diametral Test

The diametrical compression test or “Indirect-tension” device is also known as Brazilian test. This test is used to measure the resilient modulus (stiffness) of asphalt concrete by applying repeated diametric loads of a haversine or other appropriate waveforms (Zhang, et al.,2005). In this test, a cylindrical sample of HMA is placed between two flat platens and subjected to a compressive force along its’ diameter, as shown in Figure 2-10. The specimen fails due to the induced tensile stresses at the center of the compact and along its diameter. The horizontal

deformation of the specimen is then measured to calculate the resilient modulus with an assumed Poisson's ratio (Brown, et al., 2001).

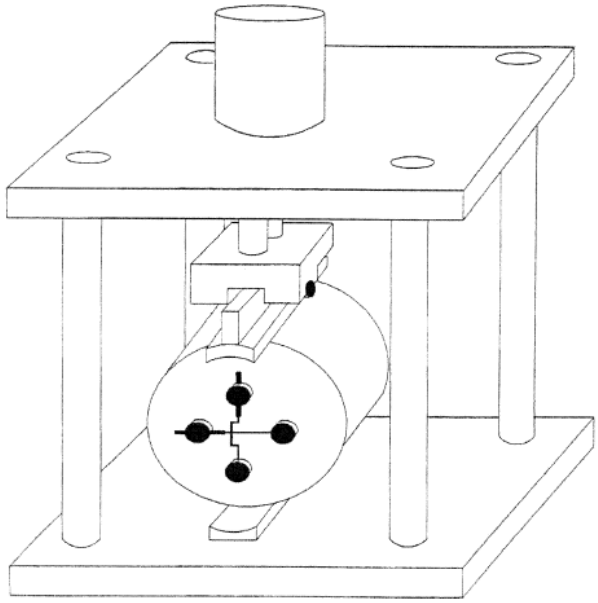

Figure 2-10. Schematic of Indirect Tensile Test (Witczak, et al., 2002)

Sousa, et al., (1991) have suggested that the diametral test is better for the repeated load testing to measure the modulus comparing with diametral creep measurements, which takes longer time of testing. However, diametrical test has been considered inappropriate tool for rutting prediction because the state of stress is non-uniform and depends on the specimen shape, except of the tension stress along the vertical diameter of the specimen (Sousa, et al., 1991). Khosla and Omer (1985) have found also that rut depth predictions using diametral test always give overestimated results by comparing with the results determined by the direct compression tests (uniaxial creep tests). In addition, Brown, et al., (2001) have mentioned that this test is not good for rutting prediction purpose since it is a tensile test type and its' results are apparently influenced significantly by binder properties.

2.7.2 The Empirical Tests

2.7.2.1 The Marshall Test

The Marshall mix design method was developed originally by Bruce Marshall of the Mississippi Highway Department around 1939 and then revised by the U.S. Army around 1943 due to the increasing of aircraft wheel loads during the second world war (Roberts, et al., 2009). The aim of this test to measure the strength of asphalt mixes compacted to a standard laboratory compaction effort. Also, it is used to optimize the design asphalt content and quality control (Brown, et al., 2001).

In this test, two asphalt properties are determined: Marshall stability and Marshall flow. The Marshall stability is the maximum load that specimen can hold before failure, whereas the Marshall flow is the measured deformation of the specimen before failure. Marshall stiffness index, on the other hand, is another property that can be used to characterize asphalt mixes. It is an empirical value of the asphalt mix's stiffness that is determined by dividing the asphalt stability over the asphalt flow. A Higher stiffness index value indicates a stiffer mix and hence less susceptible to permanent deformation (Brown, et al., 2001).

A compacted HMA test specimen of 4 inches' diameter and 2.5 inches in height is prepared according to the standard AASHTO R68-15: "Preparation of Asphalt Mixtures by Means of the Marshall Apparatus" and placed in the Marshall apparatus. The test is performed by applying a load at constant rate of movement of 50.8 mm (20 in.) per minutes until the specimen failure is reached, and then the maximum load is recorded (Stability value). An attached dial gauge measures the specimen's deformation (Flow value) at 0.25 mm (0.01 inch) increments during the loading process (AASHTO T 245, 2015). Figure 2-11 illustrates schematically the applied load and the

recorded data of Marshall test. Although the Marshall test is simple, relatively inexpensive, and widely used, it is believed that impact compaction used in this method does not simulate mixes densification in fields and that the Marshall stability does not estimate the HMA shear strength effectively (NHI, 2000). Furthermore, sever studies have been showed that this test is unable to measure effectively mixes performance against permanent deformation or even to rank mixes in accordance to their rutting resistance (Brown, et al., 2001).

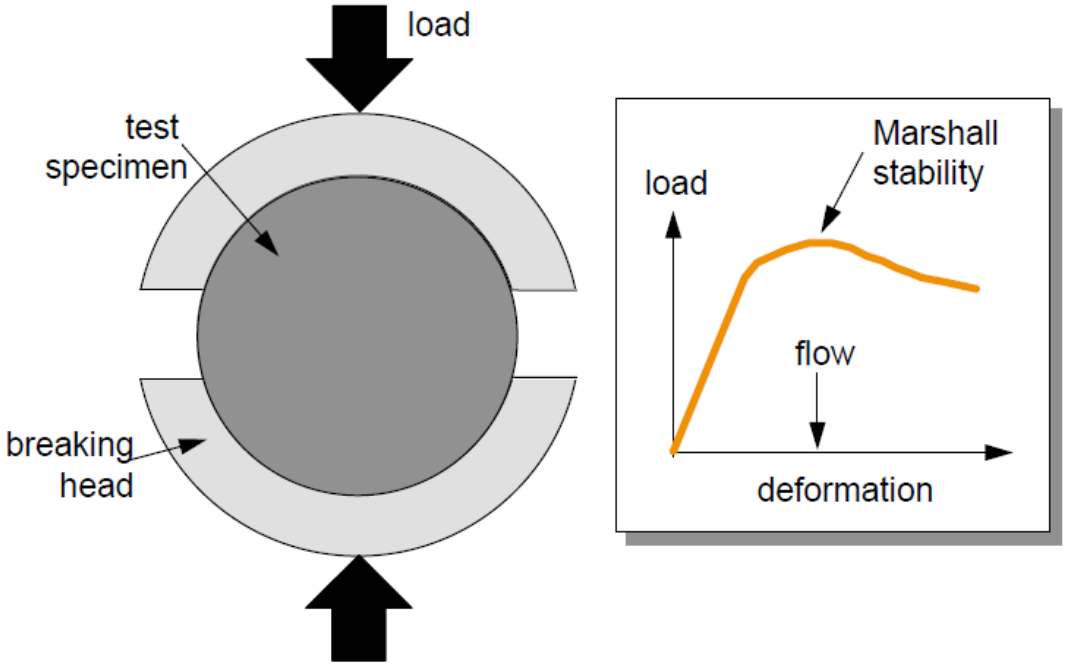

Figure 2-11. Illustration of the Marshall test applied load and recorded data (NHI, 2000)

2.7.2.2 The Hveem Test

The Hveem mix design method was developed in California by Francis Hveem in the late 1920s and 1930s. The test was invented after realizing that a good performance asphalt mix in relation to rutting is not guaranteed to achieve with a proper content of oil in the mixes. Therefore, a proper test for evaluating the ability of asphalt mixes to resist shear forces applied by wheel loads was needed. This concern led eventually to develop the device called the Hveem Stabilometer, as

shown in Figure 2-12 (Roberts, et al., 2009). The Hveem Stabilometer is a triaxial testing device consisting of a rubber sleeve inside a cylindrical metallic container that surrounds with oil to register the horizontal pressure generated as a result of applying a vertical load to a compacted HMA specimen (AASHTO T 246, 2015).

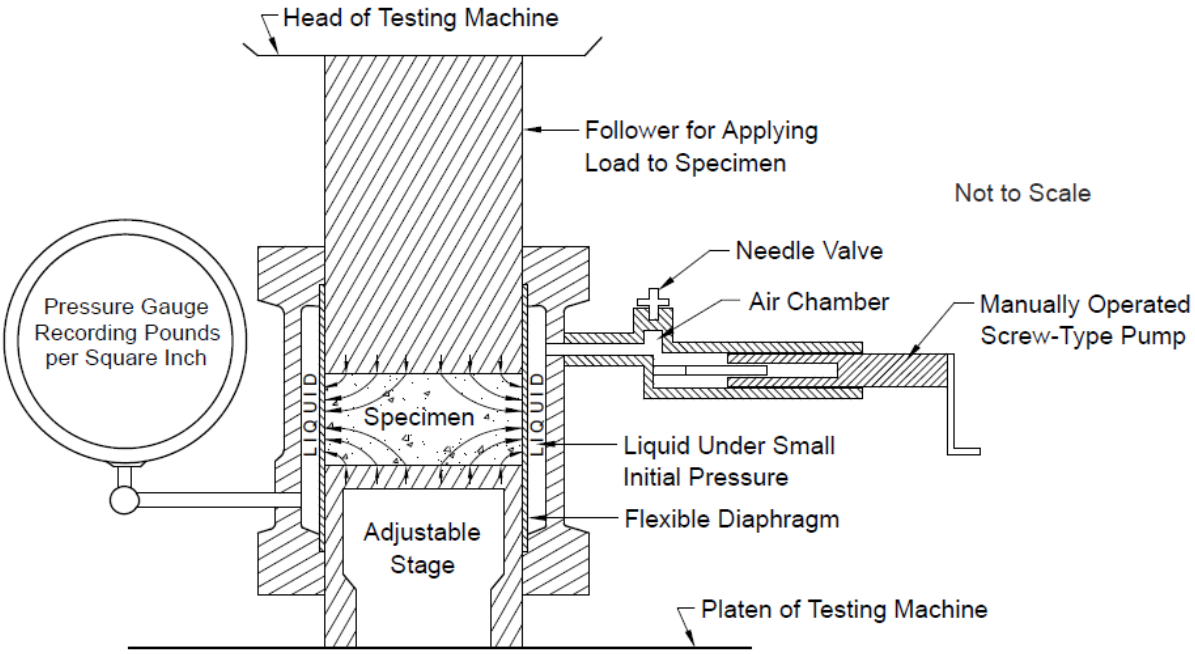

Figure 2-12. Diagrammatic Sketch of the Hveem Stabilometer (AASHTO T 246, 2015)

The concept of the Hveem Stabilometer is an empirical measurement of the internal friction component of shear strength within a mixture. The test is performed by applying a vertical axial load to a standard compacted HMA specimen of 2.5 in. height and 4 in. in diameter at 60 ± 1 °C temperature. The transmitted lateral pressure is then measured by a pressure gauge. The specimen is compacted in the California Kneading Compactor in accordance to the standard test method AASHTO T 247. This test, like with the Marshall test, gives an indication when a mix is too rich in binder by measuring a low stability value (AASHTO T 246, 2015; Guide, S. M. D, 2001).

The Hveem Stabilometer device, however, is relatively expensive and not portable. It also measures the internal friction of mixes which is more an aggregate property than a property of the binder. Another concern, on the other hand, was related to selecting asphalt content based on Hveem procedure since it may cause a durability problem to asphalt mixes (NHI, 2000; Guide, S. M. D, 2001). Therefore, this test was replaced by the Superpave design method because it was an inappropriate performance testing procedure due to the lack of test results that were related to the mix performance in the field (Brown, et al., 2001).

2.7.3 The Simulative Tests

2.7.3.1 Wheel Track Tests

Wheel track tests are categorized as simulative tests of evaluate permanent deformation performance. These tests attempt to simulate stress conditions caused in fields by testing in laboratories. In these tests, an asphalt concrete specimen is subjected to repeated wheel loads and the rutting depth is then evaluated in relation with the number of repeated loads before failure. Several wheel track tests were used to predict rutting, but the Asphalt Pavement Analyzer, Hamburg Wheel-Tracking Device, and French Rutting tester are the most common tests (Zhang, et al.,2005 & Brown, et al., 2001).

The Asphalt Pavement Analyzer (APA) is a revised device of the Georgia Loaded Wheel Tester (GLWT). This test typically simulates rutting by applying 8,000 load cycles on specimens through an aluminum wheel. A 445 N load is applied back and forth onto a pressurized pneumatic hose of 690 kPa placed on HMA specimens. The procedure of this test is similar to the GLWT, but it has an advantage that the specimens can be tested either in dry or submerged condition (Zhang, et al.,2005 & Brown, et al., 2001).

The Hamburg Wheel-Tracking Device (HWTD) is used widely in Germany to evaluate rutting and stripping of asphalt mixes. In this test, a steel wheel of 47 mm wide and 705 N force is applied for 20,000 passes back and forth over two HMA slap samples or till 20 mm of deformation is achieved. This test is performed under water at temperature ranging from 25 °C to 70°C (Zhang, et al.,2005 & Brown, et al., 2001).

The French Rutting Tester (FRT) or LCPC wheel tracker is successfully used in France as it is able to simulate rutting on two HMA slab samples at the same time. A load of 5,000 N is applied onto a pneumatic tire pressurized to 600 kPa. The desired condition of this test is to get a rutting depth of at most 10% of the sample thickness after 30,000 cycles (Zhang, et al.,2005 & Brown, et al., 2001).

In general, wheel tracking tests are not mechanistic tests that closely simulate rutting in the field. However, the recommended criteria of these tests cannot be adopted for different asphalt mixes. They were limited to specific mixes that only expected for high traffic volume. Thus, these tests need to be further evaluated by using other local materials to get a comprehensive understanding of the expected results (Zhang, et al.,2005 & Brown, et al., 2001). A main drawback of these tests inherently lies in “the confounding nature of uncontrollable elements that may affect the experiment and complicate its interpretation” (Sousa, et al., 1991).

Chapter 3: Background of Asphalt Concrete Shear Tests

The development of a simple, inexpensive, and accurate shear test device for measuring the fundamental shear properties of asphalt mixes is imperative. Since rutting is a major distress in asphalt pavement that affect directly the user's safety and comfort, researchers tried to measure the shear properties and responses to improve the asphalt pavement performance. Several shear test systems were developed in the past to measure the fundamental shear properties and responses of asphalt mixes tested under shear loads. The Field Shear Test (FST), In-Situ Shear Stiffness Tester (InSiSST™), and Dynamic Shear Rheometer (DSR) are examples of these devices. The details about these shear test devices can be found in Jweihan, (2018). In this chapter, the Superpave Shear Tester (SST) and Duplicate Shear Tester (DST) are discussed in detail.

3.1 Superpave Shear Tester (SST)

3.1.1 Background

The USA Congress established the Strategic Highway Research Program (SHRP) in 1987 to improve the USA roads performance, safety and durability. The Superpave mix design method was developed later in the 1990s as a last product of the SHRP program. It is a comprehensive method for asphalt mix design and analysis process that provides several test protocols for various test conditions. The method includes three major components: asphalt binder specification, asphalt mix design, and volumetric analysis system. Superpave Shear Tester (SST) was developed by SHRP for quantifying the HMA mix performance (Chowdhury & Button, 2002).

The Superpave Shear Tester, shown in Figure 3-1, is an associated device to the Superpave design method. It is designed to perform all load-related performance tests on asphalt concrete including static and dynamic loading in confined and unconfined conditions. SST device is also

capable to measure some basic properties of asphalt mix that are related to the permanent deformation such as nonlinear elastic property, viscoelastic and tertiary creep properties (Chowdhury & Button, 2002).

SHRP researches proposed six deferent SST tests that able to determine the permanent deformation and fatigue resistance of asphalt mixes. These tests are the following:

- Volumetric Test
- Uniaxial Test
- Repeated Shear at Constant Height Test (RSCH)
- Frequency Sweep at Constant Height Test (FSCH)
- Simple Shear at Constant Height Test (SSCH)
- Repeated Shear at Constant Stress Ratio Test (RSCSR).

Figure 3-1. Superpave Shear Tester (SST) (Chowdhury & Button, 2002)

3.1.2 SST System

The SST is a servo hydraulic with closed-loop feedback systems. It able to determine all load related performance parameters for asphalt materials. It capable to apply various waveforms of static, ramping (increasing or decreasing), and repetitive loads (Harrigan. et al., 1994). Figure 3-2 illustrates a typical loading condition of the SST. This system can be maintained in either by a stress or strain control. The SST device mainly consists of four components, as shown in Figure 3-3:

- Testing apparatus
- Control unit
- Environmental control unit
- Hydraulic system.

The testing apparatus is the main part of the SST. It applies vertical, shearing and confinement loads to the test sample. The applied loads can be static, increased, decreased, or repetitive loads with different waves. The SST device includes temperature and pressure controls and hydraulic actuator. The testing apparatus composed of a reaction frame and a shear table. The reaction frame is a very rigid part that assures the accuracy of the displacement measurements of a tested specimen. The shear table holds the test specimen during the test. It can also be actuated to generate a shear stress to the specimen. The applied loads are transferred to the specimen through loading plates glued the specimen ends. Based on the applied test, different linear variable different transducers (LVDTs) are used to measure the specimen responses during the test by sending a signal to the SST closed-loop feedback system.

The control and data acquisition system is used to record and control some parameters automatically during the test. It records the time, applied loads, specimen deformations and the test chamber temperature. It is a combination of software and hardware systems. The hardware system includes the input and output transducers, the device computer and, the controllers. The software system represents the algorithms that are required to control the apparatus and collect the test data.

The environmental unit maintains the temperature and pressure constants inside the test chamber. The temperature can be controlled to be within a wide range from 1 to 80 °C and an accuracy of ± 0.5°C. The air pressure is supplied from a compressed air stored in a storage tank. The environmental unit controls the air pressure precisely to be applied at a rate of 69 kPa per second up to the maximum pressure of 840 kPa.

The hydraulic system provides the force required to the test specimen in different testing conditions. It consists of horizontal and vertical actuators attached to the specimen. Each actuator has a capacity of almost 32 KN force and a 2 N of resolution. The vertical actuator applies a normal force to the specimen while the horizontal actuator develops a shear force to the specimen by actuating the shear table. This system can also apply a confinement pressure of 1,000 kPa capacity (Chowdhury & Button, 2002; NHI, 2000).

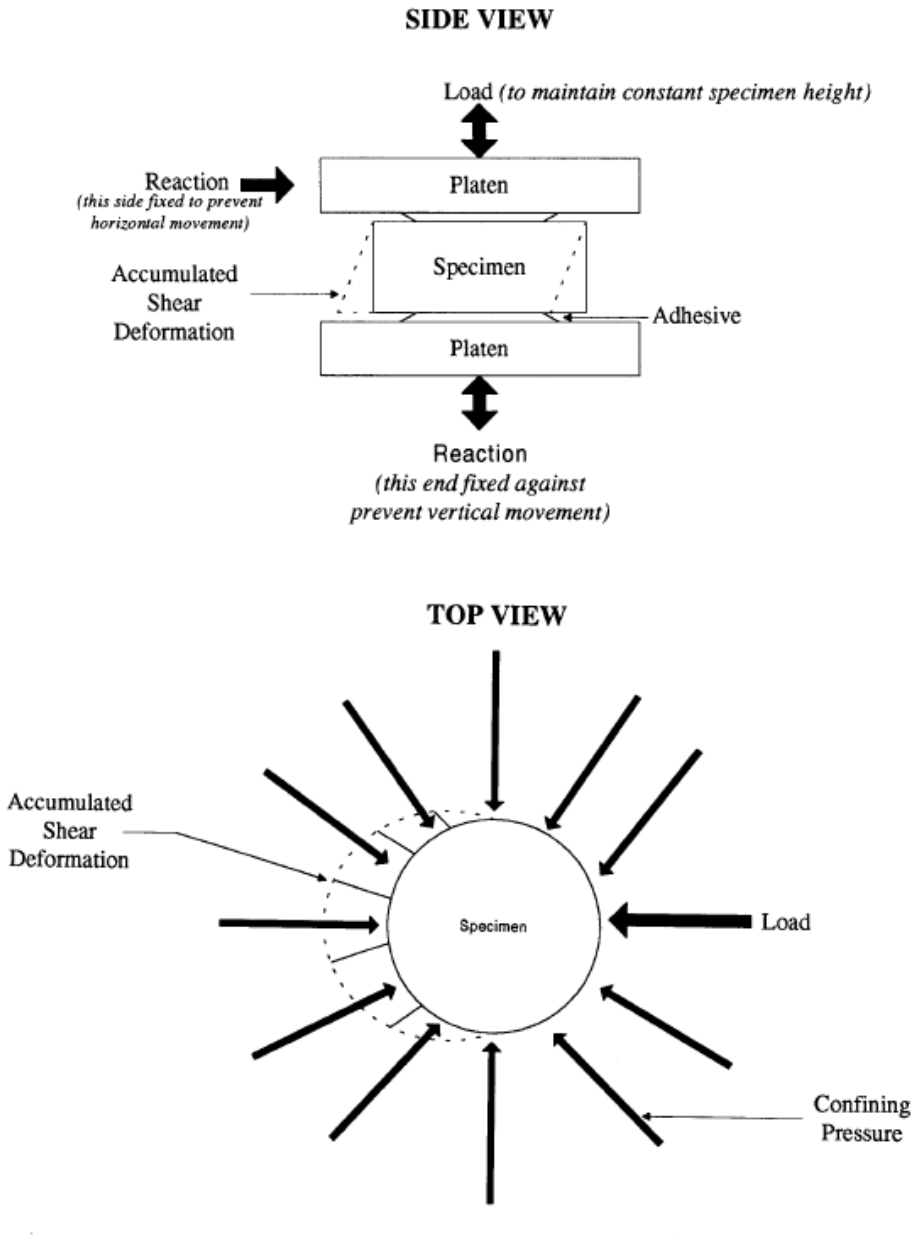

Figure 3-2. SST Specimen Loading Conditions (Harrigan. et al., 1994)

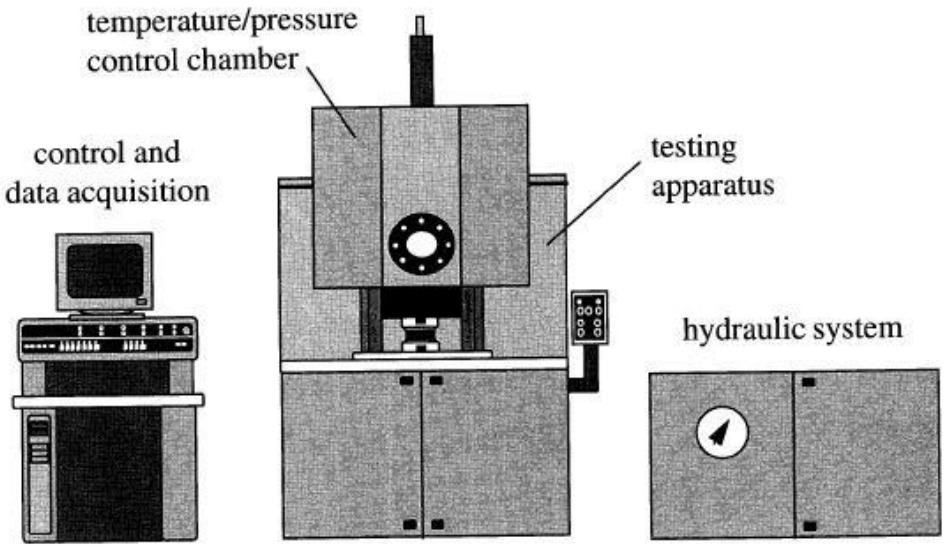

Figure 3-3. Schematic View of an SST Device (Kennedy, et al., 1994)

3.1.3 SST Tests

3.1.3.1 Volumetric Test

In the volumetric test, a confining pressure only is applied to the test specimen. It is referred as a "hydrostatic" test because the specimen volume is subjected to change due to the applied hydrostatic stress around the test specimen. In this test, the specimen perimeter or circumferential strain changes during the test since the specimen is not attached (glued) to loading plates. Figure 3-4. illustrates schematically the test concept.

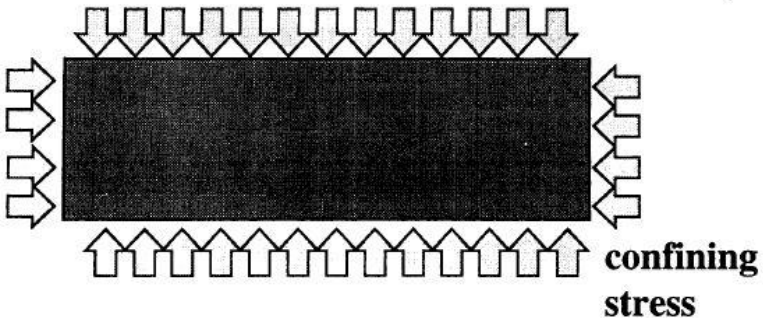

Figure 3-4. Conceptual view of the Volumetric Test (Kennedy, et al., 1994)

The volumetric test is applied at three different temperatures and pressures, as specified in Table 3-1. The test is performed by increasing a confining stress steadily at a rate of 70 kPa per second up to the certain level of a specified pressure depending on the test temperature, followed by keeping the pressure constant for a period of 10 seconds. Then the pressure decreases slowly to zero, as shown in Figure 3-5. A radial LVDT is used to measure the circumferential strain of the test specimen during the test. The significance of performing this test is to determine the permanent deformation and fatigue cracking characteristics (Chowdhury & Button, 2002) (NHI, 2000) (Kennedy, et al., 1994).

Table 3-1. Volumetric Test Pressure (NHI, 2000)

Temperature, °C	Pressure, kPa
4	830
20	690
40	550

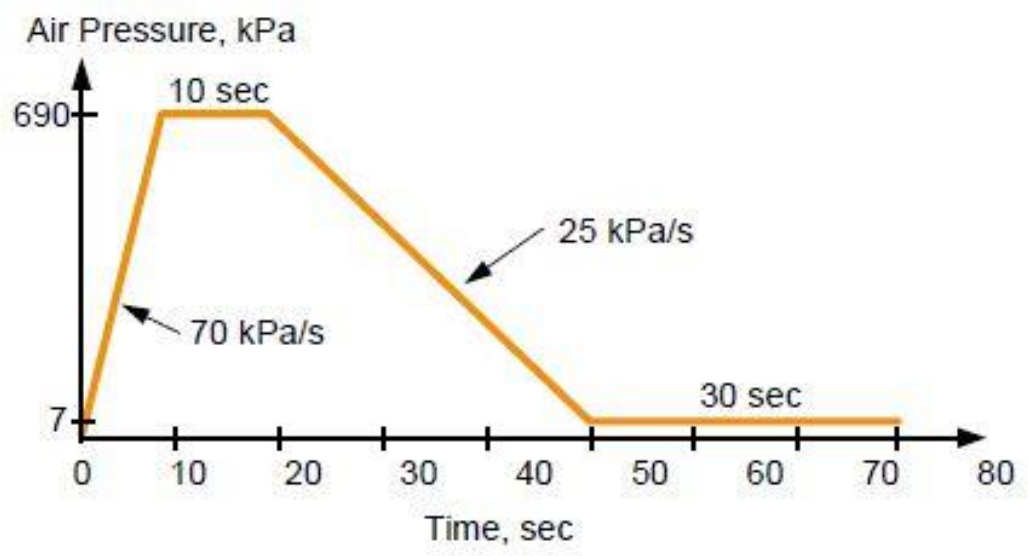

Figure 3-5. Ramping of Confining Pressure, Volumetric Test at 20 °C (NHI, 2000).

3.1.3.2 Uniaxial Test

In the uniaxial test, a test specimen is subjected to an axial compressive load and confining pressure. When the axial load is applied to the specimen, its diameter tries to increase. Meanwhile, radial LVDTs attached to the specimen sense this increase and send a signal to the feedback system to apply a confining air pressure surround the specimen. This action maintains the specimen diameter constant with no radial deformation. Figure 3-6 illustrates schematically the test concept. (Kennedy, et al., 1994) (NHI, 2000)

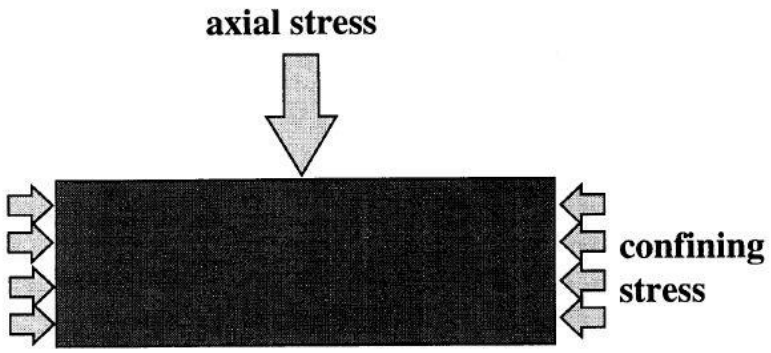

Figure 3-6. Conceptual View of the Uniaxial test (Kennedy, et al., 1994)

The uniaxial test is performed by increasing the axial load at constant rate of 70 kPa per second up to a certain stress level. Table 3-2 shows the desired axial stress depending on the test temperature. The axial stress then remains constant for a period of 10 seconds before it decreases slowly to zero. A variable confining air pressure is applied while applying the axial load in order to prevent any radial deformation. Figure 3-7 illustrates the application of the axial and confining stresses during the test. Axial deformation is a main output of this test that is used for rutting and fatigue cracking analysis (Chowdhury & Button, 2002) (NHI, 2000).

Table 3-2. Uniaxial Test Parameters (NHI, 2000)

Temperature, °C	Axial Stress, kPa
4	655
20	550
40	345

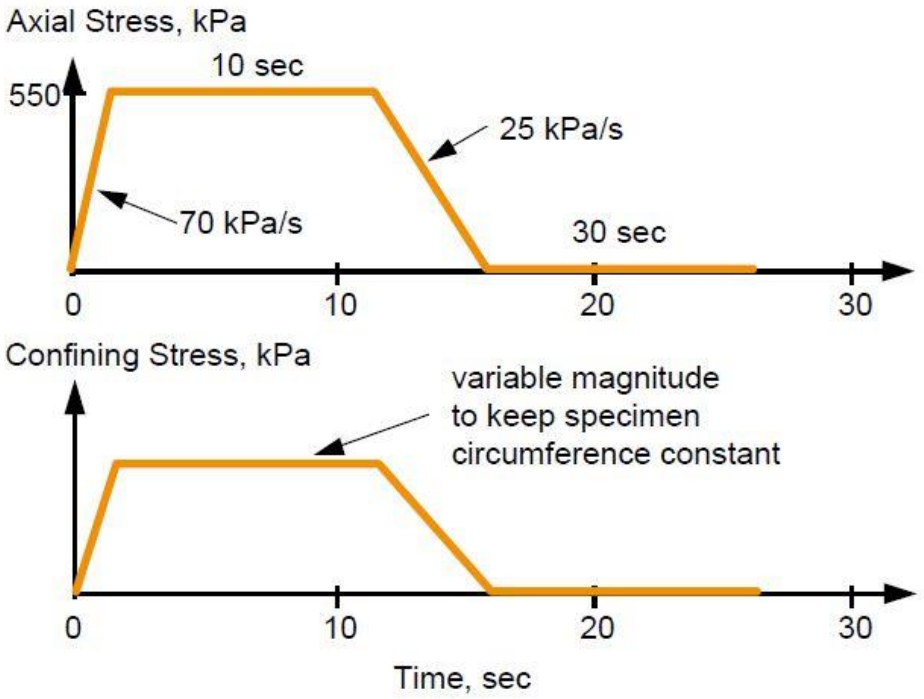

Figure 3-7. Axial Stress and Confining Stress versus Time, Uniaxial Test at 20°C (NHI, 2000)

3.1.3.3 Repeated Shear Test at Constant Height (RSCH)

The RSCH is a stress-controlled test that consists of applying axial and haversine shear loads simultaneously to a compacted HMA specimen. This test is called as “unconfined” test because there is no air confining pressure like in the volumetric and uniaxial tests (Pavement Interactive, 2008). In this test, the variable axial load is necessary to maintain a constant height for the test specimen during the test, while the haversine cyclic shear load is applied to achieve a shear stress of 69kPa. Sousa, (1994) states that at this level of shear stress good mixtures would reveal

some permanent deformation while weak mixtures would not fail rapidly. That's because the critical shear stress level in the fields is found within the range of 140 to 175kPa.

In the RSCH test, the shear stress is applied for a period of 0.1 second followed by 0.6 second of rest. The total period of 0.7 second represents one load cycle, as illustrated in Figure 3-8. The test is performed by applying 5,000 shear load cycles or till the specimen achieves 5% of permeant shear strain, whichever comes first. Sousa, (1994) states that the desired 5% shear strain has been found in several finite element studies that represents to a rut depth of 0.5 in (13 mm). For a specific pavement project, the RSCH test temperature is selected based on the maximum 7-days daily temperature recorded at 2-inch depth in site location. This test is performed to interpret the rut depth (rutting susceptibility), as shown in Table 3-3, based on the measured accumulative permanent shear deformation (Chowdhury & Button, 2002; NHI, 2000; Brown, et al., 2001). At the end of the test, the permanent shear deformation is calculated by using Equation 3-1 (AASHTO T-320, 2004).

The concept of RSCH test, however, is that the specimen dilates when the repeated shear loads are applied. Meanwhile, axial LVDTs sense this expanding in height and send a signal as a feedback to the vertical actuator to apply a sufficient axial force to cancel the dilation (NHI, 2000).

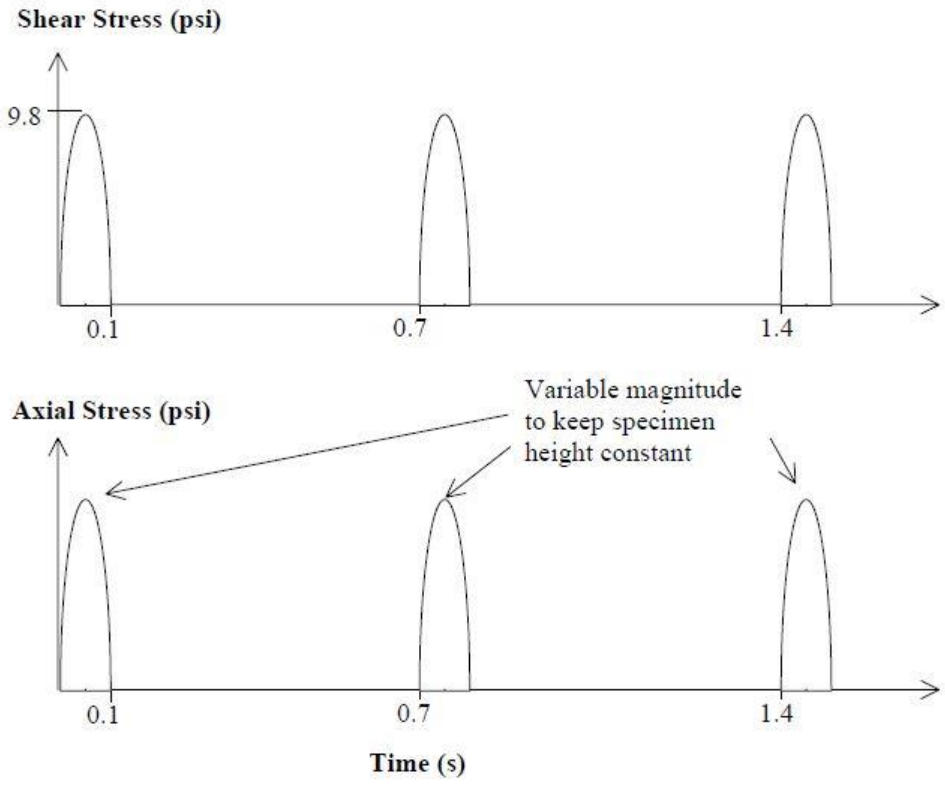

Figure 3-8. RSCH Shear and Axial Stresses versus Time (Chowdhury & Button, 2002)

Table 3-3. Criteria for Evaluating Rut Resistance Using RSCH Permanent Shear Strain (Brown, et al., 2001)

RSCH Maximum Permanent Shear Strain (%)	Rut Resistance
< 1.0	Excellent
1.0 to < 2.0	Good
2.0 to < 3.0	Fair
3.0	Poor

$$\gamma_p = \frac{(\delta \text{ shear,final} - \delta \text{ shear,initial})}{h} \qquad (3\text{-}1)$$

γp= permanent shear strain.

δ shear, final= final recorded deformation by the LVDT at the end of the test.

δ shear, initial= initial shear deformation at the start of the test (nominally zero).

h= specimen height (plate-to-plate height).

In RSCH test, the permanent shear strain is measured and recorded by LVDTs and an acquisition data system. Typically, the result obtained from repeated load tests is a curve of the cumulative permanent deformation versus the number of loading cycles. The curve includes three distinct zones: primary, secondary, and tertiary, as illustrated in Figure 3-9.

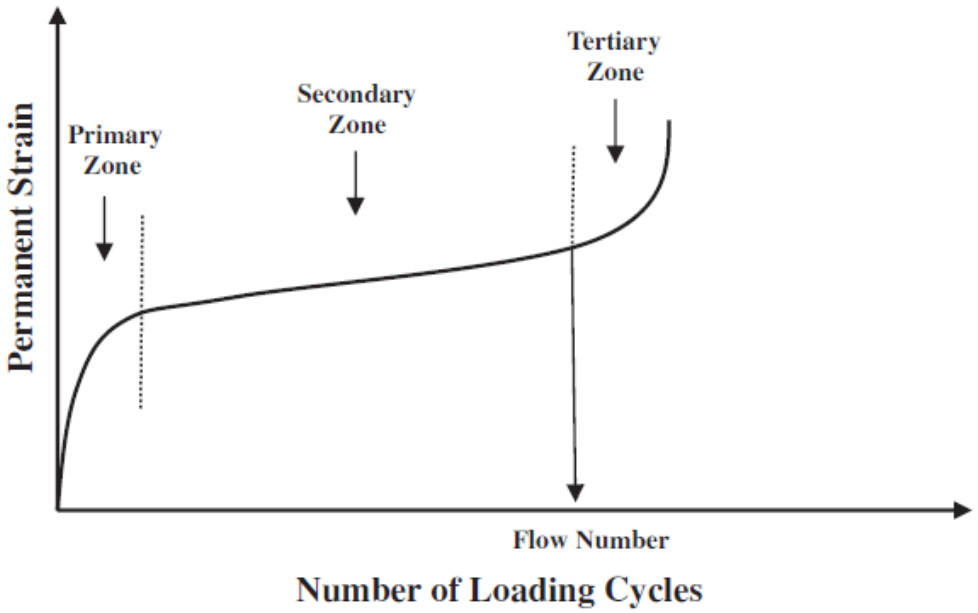

Figure 3-9. Typical relationship between permanent strain and loading cycles (Witczak, et al., 2002)

In the primary stage, asphalt mixes densify quite rapidly at few loading cycles due to the initial compaction of asphalt mixes. The accumulated permanent strain per cycle, however, tends to decrease, reaching a constant value that is called the “onset” of the secondary stage. In this stage, asphalt mixes compact gradually for many load cycles and the amount of permeant deformation per cycle decreases and remains steady before the transition to the tertiary zone. The secondary

zone shows a linear deformation when plotting the deformation versus the number of load cycles on log-log scale. This deformation would continue indefinitely if the mixture is stable. However, if the mixture densifies to a very low air voids content of about 2-3%, the mix deforms permanently and becomes unstable. At this point of instability, the tertiary zone starts where the permanent strain accumulates rapidly again and starts accelerates toward failure. (NHI, 2000; Brown, et al., 2001; Chowdhury & Button, 2002; Scullion, et al., 2004). According to Witczak, et al., (2002), the tertiary zone begins at a cycle number defines as the "flow number". This number is considered as a significant indicator of an asphalt mixture's rutting resistance (Witczak, et al., 2002; Scullion, et al., 2004).

A standard power model represents permanent deformation of RSCH test's specimen is derived from the linear portion of the secondary zone of the permanent shear strain versus load cycles curve. Figure 3-10 illustrates the linear relationship between the permanent stain and loading cycles when they are plotted on log-log scale. The model expressed mathematically in Equation 3-2 (Witczak, et al., 2002).

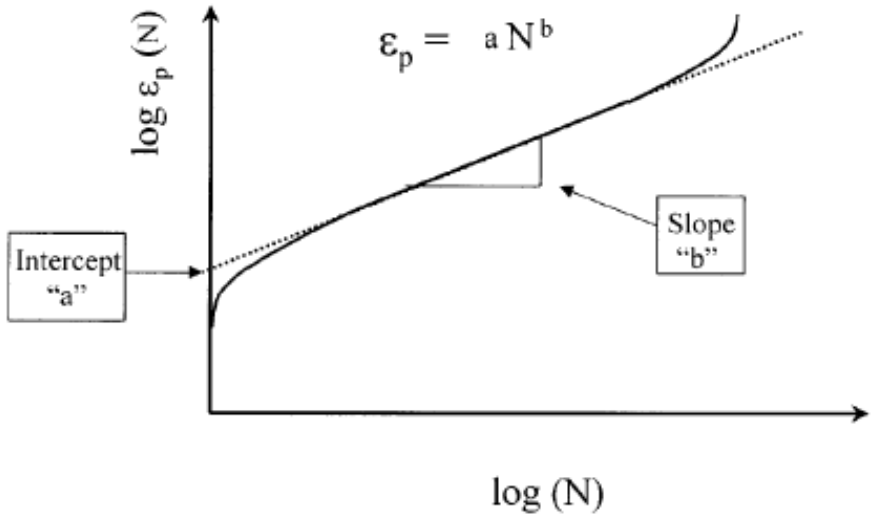

Figure 3-10. Regression Constants when plotted on log-log scale (Witczak, et al., 2002).

$$\varepsilon_p = aN^b \qquad (3\text{-}2)$$

Where,

ε_p: accumulated permanent strain,

N: number of load applications,

a: intercept coefficient,

b: slope coefficient.

3.1.3.4 Frequency Sweep Test at Constant Height (FSCH)

The FSCH test is an unconfined test that applies a strain controlled dynamic shear load and an axial load to an asphalt specimen. The shear load is applied at different frequencies and temperatures while the axial load is applied only to keep the specimen height constant during the test. Figure 3-11 illustrates schematically the test concept. According to AASHTO T-320 (2004), the testing temperature should be "no higher than 12ºC below the high-temperature grade of the asphalt binder". This test is performed to determine the mixture stiffness by measuring the asphalt complex shear modulus (G*) and phase angle (Φ) (AASHTO T-320, 2004) (Chowdhury & Button, 2002) (Kennedy, et al., 1994). The shear dynamic modulus and phase angle can be calculated by using these equations: (Witczak, et al.,2002)

$$|G^*| = \tau 0 / \gamma 0 \qquad (3\text{-}3)$$

$$\Phi = ti / tp \qquad (3\text{-}4)$$

$$G^* = |G^*| \cos\phi + i\,|G^*| \sin\phi \qquad (3\text{-}5)$$

Where:

|G*| = Shear Dynamic Modulus

G* = Complex Shear Modulus

$\tau 0$ = Peak Dynamic Shear Stress

$\gamma 0$ = Peak Recoverable Shear Strain

ti = Time Lag between Stress and Strain Cycles

tp = Time for a Stress Cycle

The FSCH is performed by applying a repeated sinusoidal shear load till the specimen achieves a maximum controlled shear strain of 0.01%. This shear load is applied at several frequencies and cycles, as specified in Table 3-4. The load is applied beginning from the higher to the lower frequency. As for the RSCH test, the specimen tends to dilate while applying the shear force. Consequently, a vertical actuator applies an axial force to maintain the specimen height. The axial force is induced by a close-loop feedback signal received from axial LVDTs attached to the test specimen (Chowdhury & Button, 2002) & (NHI, 2000). Figure 3-12 illustrates the application of shear strain and axial stress during the FSCH test.

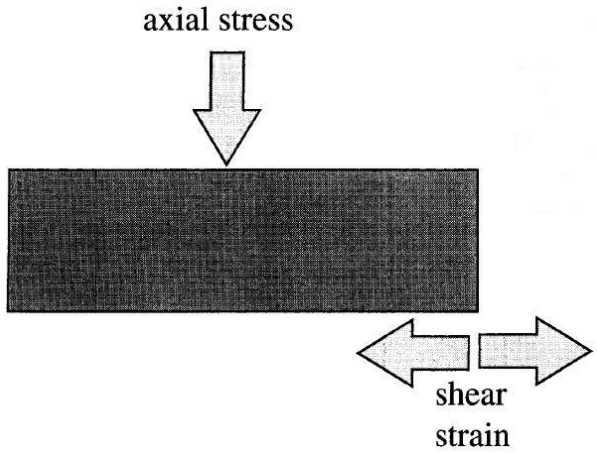

Figure 3-11. Conceptual View of the FSCH test (Kennedy, et al., 1994)

Table 3-4. FSCH Test Parameters (AASHTO T-320, 2004)

Frequency, Hz	Number of load cycles
10	50
5	50
2	20
1	20
0.5	7
0.2	7
0.1	7
0.05	4
0.02	4
0.01	4

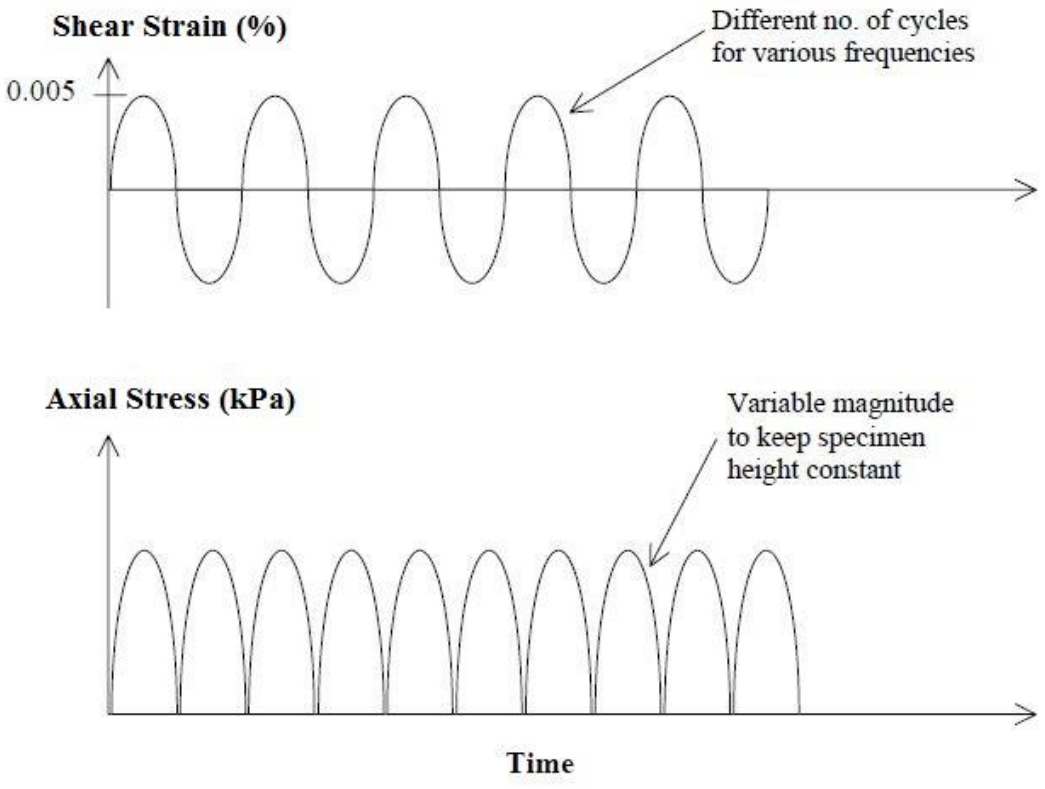

Figure 3-12. Shear Strain and Axial Stress Pulses - FSCH Test (Chowdhury & Button, 2002)

3.1.3.5 Simple Shear at Constant Height (SSCH)

The SSCH is a shear creep test that is performed by applying a controlled shear load along with a static axial load to a tested SST specimen. Figure 3-13 illustrates schematically the test concept. The test is used to determine the elastic and plastic properties of asphalt mixes through measuring the specimen's maximum shear strain that occurs during the test and the permanent shear strain at the end of the test. The test can predict the permanent deformation susceptibility of asphalt mixtures. Lower shear strains (creep strains) at higher temperature indicates for asphalt mixes of good performance whereas higher creep strains at low test temperature indicates the opposite. Same specimens that have been tested in the FSCH can be used in this test (Chowdhury & Button, 2002; NHI, 2000; Pavement Interactive, 2018).

Similar to the FSCH test, the specimen height tends to expand while applying the shear force. However, the specimen height is maintained by applied a static axial force to the specimen. The axial force is induced by the closed-loop feedback system using axial LVDTs. The shear stress is applied at a rate of 70 kPa per second till it achieves a certain level of stress depending on the test temperature, as recommended in Table 3-5. The stress is then kept constant for 10 ± 1 second before it is decreased steady to zero at a rate of 25 ± 1 kPa per second. Afterwards, the stress continues for a period of other 10 ± 1 second at zero stress (AASHTO T-320, 2004; Chowdhury & Button, 2002; NHI, 2000). Schematic illustrations to the applied SSCH test's stresses and shear strain are shown in Figure 3-14 and 3-15, receptively.

Table 3-5. SSCH Test Parameters (AASHTO T-320, 2004)

Temperature, °C	Shear Stress, kPa
4	345± 5
20	105± 5
40	35± 1

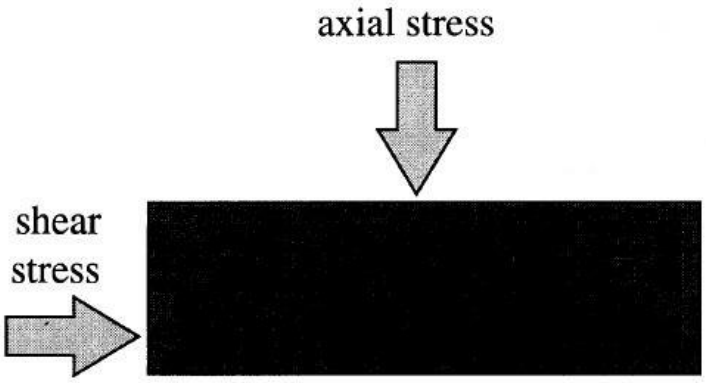

Figure 3-13. Conceptual View of the SSCH test (Kennedy, et al., 1994)

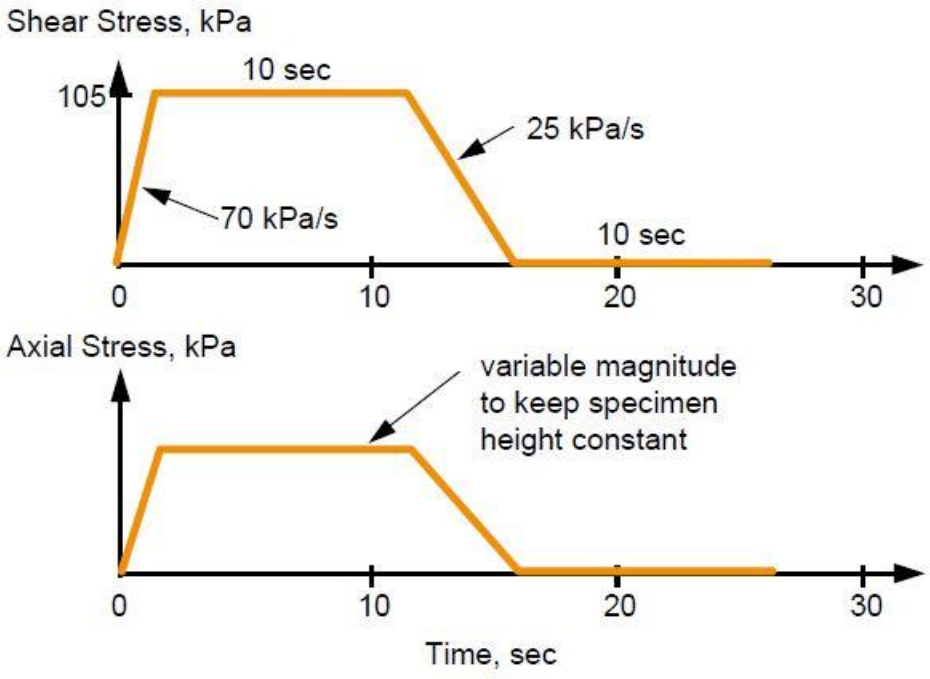

Figure 3-14. Shear and Axial Stresses versus Time of SSCH Test at 20°C (NHI, 2000)

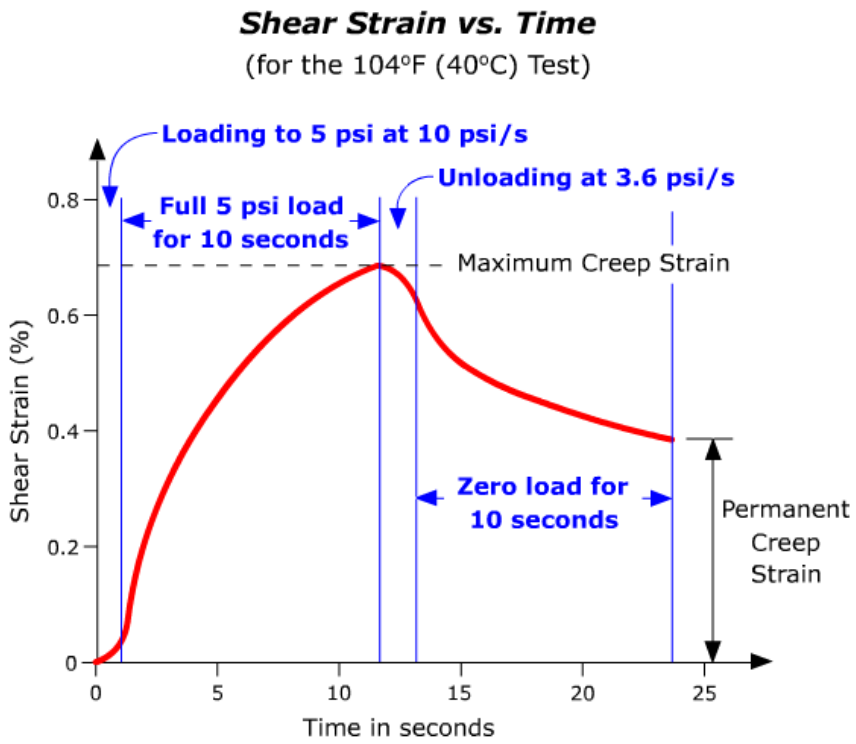

Figure 3-15. typical graph of Shear strain versus time of SSCH test at 40 °C (Pavement Interactive, 2018)

Maximum shear strain, permanent shear strain, and elastic recovery are three material properties of asphalt mixes that can be calculated in the SSCH test. The maximum shear strain and permanent shear strain indicate the permanent deformation susceptibility of the mixes. The elastic recovery indicates the ability of mixes to return to its original shape after releasing the load effect. Therefore, higher maximum and permanent shear strains indicates of more rut susceptibility of asphalt mixes while higher elastic recovery indicates the opposite. The permanent shear deformation can be calculated similar to that in the RSCH test using equation 3-1. The maximum shear strain and elastic recovery for the tested specimen can be calculated using the following equations (AASHTO T-320, 2004; Chowdhury & Button, 2002).

$$\gamma_{max} = \frac{(\delta \text{ shear,max} - \delta \text{ shear,initial})}{h} \quad (3\text{-}6)$$

$$Recovery = \frac{(\delta \text{ shear,max} - \delta \text{ shear,final})}{\delta \text{ shear,max}} \quad (3\text{-}7)$$

Where:

γ max = Maximum Shear Strain.

δ shear, max = Maximum Recorded Deformation by the Shear LVDT.

δ shear, initial = Initial Shear Deformation at the Start of the Test (Normally Zero).

δ shear, final = Final Shear Deformation at the end of the Test.

h = Specimen Height (Plate-to-Plate Measure only).

Recovery = Calculated Recovery of the Specimen.

3.1.3.6 Repeated Shear at Constant Stress Ratio Test (RSCSR)

The RSCSR test consists of applying repeated synchronized haversine shear and axial load pluses to a compacted HMA specimen. Similar to the RSCH test, the total shear load cycle of 0.7 seconds consists of 0.1 second load application followed by 0.6 second of rest, as illustrated in Figure 3-16. During the test, the ratio of the axial to the shear load is maintained constant within a range of 1.2 to 1.5. The stresses values are selected to simulate the real in-place stresses of pavements based on the asphalt content in the HMA layer and the base layer conditions, as suggested in Table 3-6. In the table, the weak base represents any unstabilized granular layer, whereas the strong base represents any stabilized base layer (McGennis, et al., 1994).

Table 3-6. Suggested Stress Values for the RSCSR test (McGennis, et al., 1994).

Base Condition	Asphalt Content					
	High		Medium		Low	
	Shear Stress, kPa	Axial Stress, kPa	Shear Stress, kPa	Axial Stress, kPa	Shear Stress, kPa	Axial Stress, kPa
Weak	84	119	63	98	49	56
Strong	98	175	84	105	56	91

The test is performed, according to AASHTO, by applying 5,000 shear load cycles or till the specimen achieves 5% of the permeant shear strain, whichever comes first. However, the researchers have found that some mixes may not show a tertiary rutting at the 5,000 cycles. Thus, the researchers adopted 10,000 cycles for performing the test and decided to conduct this test at temperature 55°C similar to the RSCH test. The permanent shear strain can be calculated as in the RSCH by using Equation 3-1 (Chowdhury & Button, 2002). The RSCSR test is performed to identify the susceptibility of asphalt mixes to the tertiary rutting. Therefore, the test is typically performed at the extreme condition of the tertiary rutting: at high asphalt contents corresponding to three percent air voids (NHI, 2000). The result of this test is measuring the accumulated permanent shear deformation, as shown in Figure 3-17.

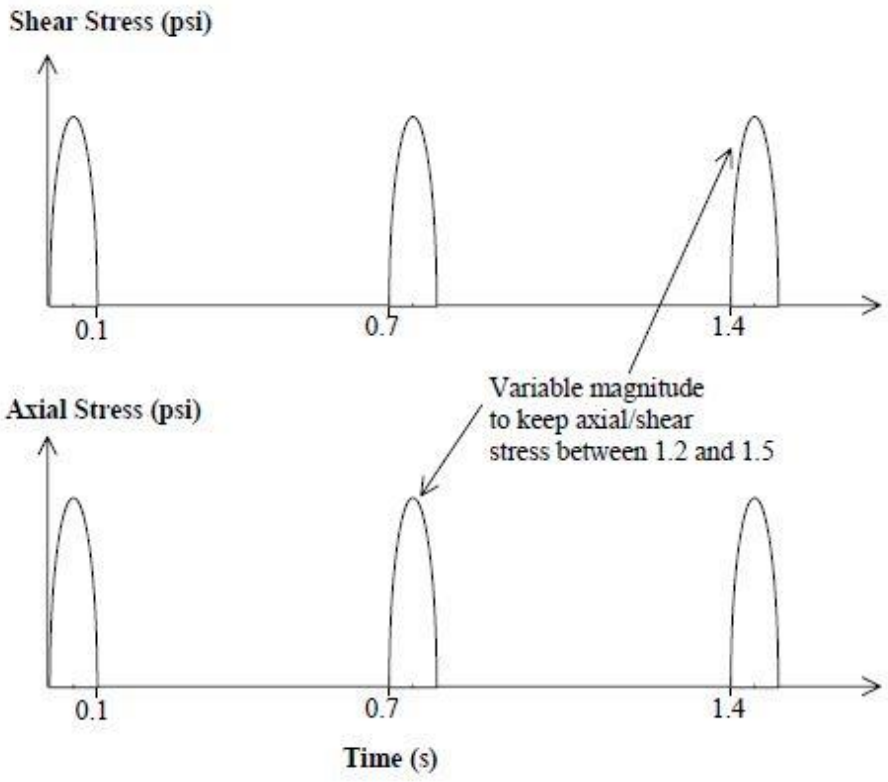

Figure 3-16. RSCSR Shear and Axial Stresses versus Time (Chowdhury & Button, 2002)

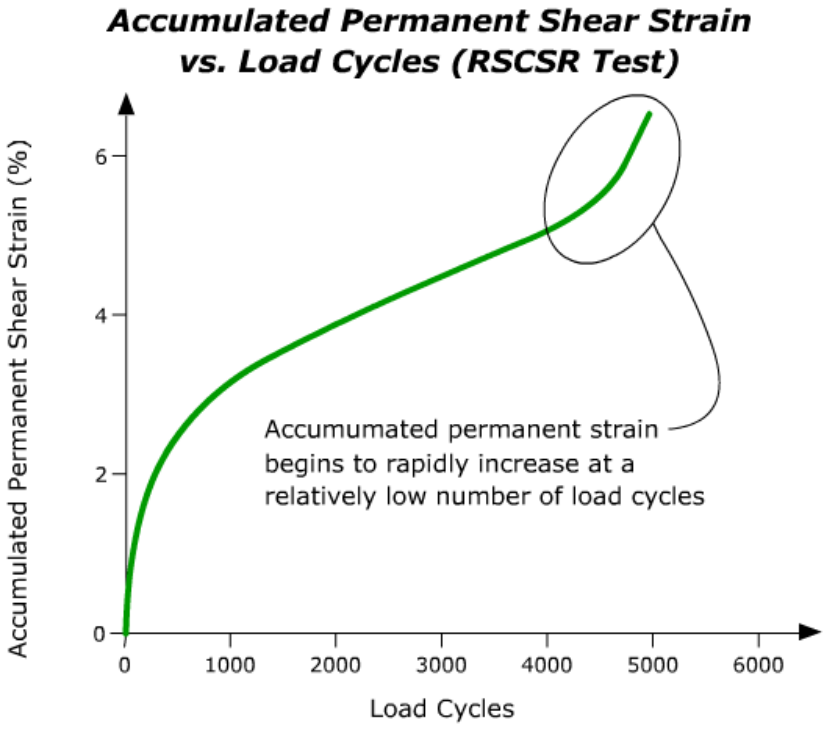

Figure 3-17. Typical Plot from a failing RSCSR test (Pavement Interactive, 2018)

3.1.4 SST Test Procedure

The SST specimen can be prepared in a laboratory or cored from a pavement surface layer. It is a cylindrical asphalt specimen with 150 mm diameter and 50 mm maximum height. The height varies depending on the nominal maximum aggregate size (NMAS) of mixes. The NMAS is defined as one sieve bigger than the first sieve having at least 10% retained of total aggregates. The specimen height should be 50 mm for asphalt mixes with a 19 mm NMAS while a 38 mm height should be for mixes with 12.5, 9.5, and 4.75 mm NMAS (AASHTO T-320, 2004). However, researchers recommend the 50 mm as a standard height for the test specimens regardless the NMAS of asphalt mixes. This height represents the final height of the test specimen after the saw cutting process (Chowdhury & Button, 2002).

Typically, a gyratory compacted specimen should have a diameter of 150 mm and 75mm height after compaction. After the specimen is left to cool at room temperature, the top and bottom ends of the compacted specimen should be cut to achieve the 50 mm height. After sawing, the specimen height and cut faces should be inspected. Both faces must be smooth and parallel to each other. The specimen height variation must not exceed 2 mm. Otherwise; the specimen should be discarded. Based on the intended SST test type, the number of specimens is determined. For example, five test specimens are preferred to perform the RSCH test while three specimens are sufficient for both the FSCH and SSCH tests (AASHTO T-320, 2004).

Specimens are often compacted in a laboratory with a higher air void percentage than the expected percent in the cut specimens. Those percentages depend on the SST tests type as specified in Table 3-7. The aim of increasing the air voids content in the specimen is that the specimen density will increase (lowering the air voids) after sawing the top and bottom ends.

Table 3-7. Appropriate Air Void Percentage for Compacted SST Specimens (AASHTO T-320, 2004)

Test	Air Voids, %
Repeated Shear Test	3.0 ± 0.5
Simple Shear Test	7.0 ± 0.5
Shear Frequency Sweep Test	7.0 ± 0.5

For the unconfined SST tests, two loading plates are glued at top and bottom of the test specimen. These plates are made of aluminum with thickness of at least 20 mm and diameter greater than the specimen diameter by at least 6.35 mm. They should be parallel to avoid any stress concentration while testing. An adhesive material of epoxy cement is used to bond the plates to the specimen ends. The epoxy should have at least 2,000 Mpa modulus. A thin layer of the epoxy is coated on the top of the specimen and on the bottom plate. Then the cylindrical specimen is

centered on the bottom plate. The top plate piece is then lowered onto the top of the specimen at center. A light pressure of 35 kPa is applied for five minutes to assure sufficient bonding between the specimen ends and plates. A plate-specimen assembly device could be used to facilitate the bonding process by squeezing the specimen between the plates firmly as well as keeping the plates parallel. Figure 3-18 illustrates the concept of this device. Excess epoxy at the specimen sides should be removed once the specimen is compressed. Finally, the epoxy should be allowed to cure as recommended by the manufacturer (AASHTO T-320, 2004).

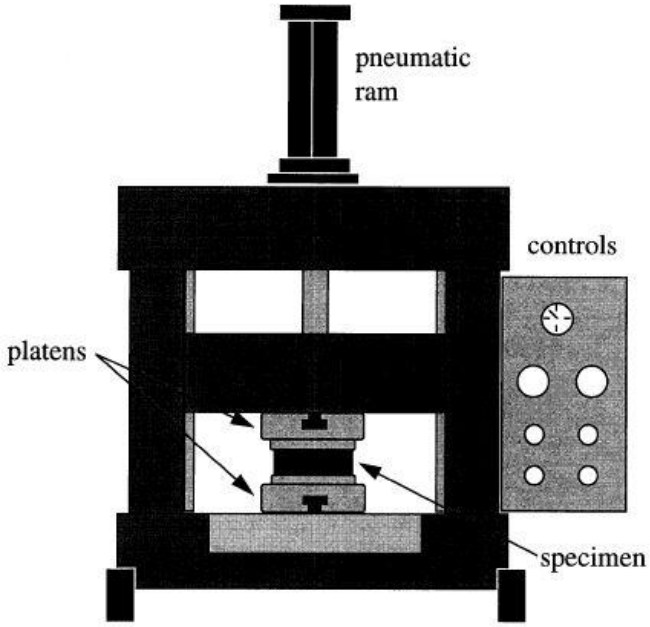

Figure 3-18. Conceptual View of the SST Plate Gluing Device (Kennedy, et al., 1994)

For the confined SST tests, on the other hand, same preparation procedure of the specimens should be followed as in the unconfined tests. However, the plates are placed at top and bottom of the specimen without the gluing process. Also, a rubber membrane underneath the attached radial LVDTs is placed around the specimen, as shown in Figure 3-19 (Kennedy, et al., 1994).

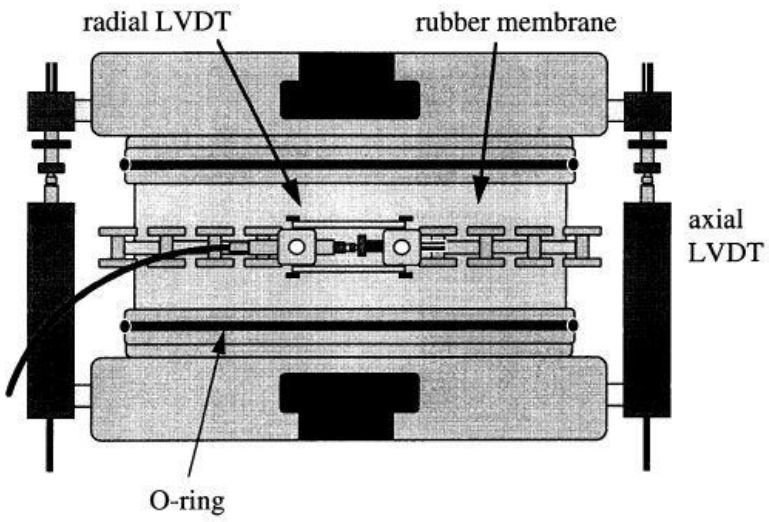

Figure 3-19. Set-Up of Confined SST Specimens (Kennedy, et al., 1994)

The SST hydraulic system should be warmed up at least one hour before launching the test. The specimen should be preconditioned also in the conditioning chamber from 2 to 4 hours followed that by the removing of the specimen from the chamber and the placing it on the shear table. Depending on the test procedure, appropriate axial, horizontal, and radial LVDTs should be attached to the specimen or specimen-plate assembly to measure the load and deformation responses. Only axial LVDTs are used for the confined SST tests (Volumetric and Uniaxial). The specimen is then centered between the vertical heads to be secured before closing the environmental chamber. The test after that can be launched (Chowdhury & Button, 2002) & (AASHTO T-320, 2004).

Once the test has been executed, the specimen should be cleaned from the plates. The specimen-plates assembly is placed in an oven for one hour at 135 °C so that the specimen can be removed. Then a scraper can be used to get rid of adhesive materials stuck on the plates. Any remained adhesive materials can be cleaned by using acetone, kerosene, or any other solvents (AASHTO T-320, 2004).

3.1.5 Evaluation of the SST tests

Chowdhury & Button, (2002) stated that three SST tests protocols were recommended in the AASHTO provisional standard, Interim Guide for April 2001, to be used for asphalt mixtures performance measurements. The tests include: the Simple Shear at Constant Height (SSCH), Frequency Sweep at Constant Height (FSCH) and Repeated Shear at Constant Height (RSCH) tests. Simply, the Volumetric and Uniaxial tests were eliminated from the SST protocols because of the complexity of the test setup procedure and the lack of the test results accuracy. Although the RSCSR test was used as a screening test to evaluate tertiary rutting of asphalt mixtures, it was eliminated also since it provides similar properties like those provided by the RSCH.

According to the creep test nature as the Simple Shear at Constant Height (SSCH) test does, Sousa, et al., (1994b) observed that testing an asphalt specimen under repetitive load tests can predict permanent deformation better than the creep loading tests. This is because the creep loading tests tends to interlock the HMA aggregate and making the mix able to resist any further deformation while testing. The repeated load tests, however, simulate the nature of repetitive wheel loads in the field rather than a single continuous load of application as in the creep tests. The repeated cyclic loads generally do not allow interlocking to occur (Sousa, et al., 1994b).

In a study to verify the best candidate tests satisfying the simple performance test's (SPT) requirements for permanent deformation and fracture distress performances, Witczak, et al., (2002) reported that the data measured by the RSCH and FSCH tests have a good correlation to the field measured rut depth.

Chowdhury & Button, (2002) conducted a study to define the best SST protocol for predicting asphalt pavement performance among the four unconfined SST tests. In that study,

rutting performance of four different asphalt mixes was measured using the FSCH, SSCH, RSCH, and RSCSR tests. The results obtained from the SST tests were compared with results obtained from other three laboratory scale accelerated wheel loaded tests: the Asphalt Pavement Analyzer (APA), 1/3-Scale Model Mobile Load Simulator (MMLS3), and Hamburg Wheel Tracking Device. The results of the study indicate that both RSCH and FSCH tests lead the SST tests for determining rutting performances of asphalt mixes as they ranked the mixtures generally in the same order as the three loaded wheel tests. Also, sensitivity tests using Duncan's multiple range tests indicate that both RSCH and FSCH tests able to provide good sensitivity in their measurements. However, it was concluded that "both the FSCH and RSCH tests were good candidates for the "best" SST protocol", yet the FSCH test is selected as the best SST protocol for rutting susceptibility prediction (Chowdhury & Button, 2002).

The reasons behind selecting the FSCH test as the "best" SST protocol are that the FSCH test is able to measure two fundamental properties of asphalt mixes including the phase angle and complex shear modulus. These parameters can be used for rutting and fatigue predictions. The RSCH test, on the other hand, can only measure the permanent shear strain which is a temperature dependent and not a fundamental material property. FSCH minimizes the specimen damage during the test more than the RSCH test because the FSCH is a strain-controlled test, and not a stress-controlled test, like what RSCH is. In addition, the result of ranking comparison showed that the FSCH ranking result was generally consistent with the MMLS3 test's ranking result. Although the ranking results of the wheel tests were consistent, Chowdhury & Button, (2002) believed that the MMLS3's ranking result is more realistic and can be adopted for the comparison with the SST's ranking results.

The authors conducted another inter-laboratory study to determine a precision and bias for the FSCH test. This was performed by testing three asphalt mixes in six different laboratories across the USA. The idea behind performing that study is to find acceptance values for the responses measured by the FSCH test and to check whether the obtained variation is caused randomly or due to a systematic drawback. It was concluded that the FSCH test has no standard value to be compared with (Chowdhury & Button, 2003).

The ability of the SST tests results to differentiate rutting performance among mixes having same aggregate size and different binder types has been proved by Romero &Mogawer, (1998a). However, the SST tests was unable to discern rutting susceptibility between mixes made with same binders and different nominal maximum aggregate sizes (Romero &Mogawer, 1998b). These findings were obtained through evaluating the performance of different asphalt mixes by conducting the SSCH, FSCH, and RSCH tests and compare the results with other rutting performance results of the same mixes evaluated by FHWA Accelerated Loading Facility (ALF).

On the other hand, Tayebali, et al., (1999) and Martin &Park, (2003) performed studies that proved the ability of the RSCH tests to identify rutting susceptibility of well performing versus poorly performing mixes. This finding was determined through evaluating the RSCH test results and compare it with rutting performance results observed in the fields. The opposite finding was found by Zhang. et al., (2006). They reported a poor relationship between the RSCH test results and field rut depth data measured by the NCAT Test Track. However, the poor relationship was justified due to the good quality of the track construction, thick pavement structure, and moderate weathers which as a result did not produce any sever rutting in the field.

Romero &Mogawer, (1998a) & (1998b) recommended to determine an appropriate sample size for the SST tests and use more than three replicate samples in the tests. Also, they stated that

some of variabilities associated with the SST tests results are attributed to sample preparation, mixture variability, and improper sample size. In addition to the method of analysis which might be a result for a statistical difference. On the other hand, Romero &Masad, (2001) concluded that testing asphalt mixes of NMAS greater than 25 mm in the SST yielded to a considerable variability. However, they found statistically that six replicate samples for the SST tests are appropriate sample size to balance between the accuracy and practicality.

Furthermore, Romero &Anderson, (2001) investigated a proper "trimmed-mean" method of analysis to reduce the RSCH results variability. Asphalt mixes of different properties were used in the study. The mixes include two aggregate gradations of NMAS (12.5 mm and 19 mm), two asphalt binder of PG 70-22 and PG 58-28, and two ranges of air voids: low air voids ($3.5 \pm 0.5\%$) and high air voids ($7 \pm 0.5\%$). Six replicate specimens of each mix were prepared and tested at 50°C to measure the permanent shear strains at 5,000 load cycles. The Coefficient of Variations (COV) analysis were performed for all possible combinations of selecting three, four, five, and six samples from each set of samples. Finally, the "trimmed-mean" method were performed through ranking the results of each set, eliminating the high and low values, and calculating the average COV for the remaining values. To determine the effectiveness of this method, two approaches were analyzed including: six-drop-two and five-drop-two. It was concluded that the most effective way to reduce the RSCH test variability without affecting the mean value is by using the trimmed-mean method of five-drop-two approach. However, if the COV value of a tested set of specimens is more than 20%, the test should be repeated using other samples (Romero &Anderson, 2001).

3.1.6 Using SST data for rutting prediction and asphalt mix analysis

It can be clearly seen from the SST evaluation section that both FSCH and RSCH are the most common and effective SST tests for measuring shear stress responses and evaluating rutting performance of asphalt mixes. Researchers, however, utilized the SST tests' data in general to evaluate rutting performance of asphalt mixes in two approaches by:

- Using the direct relationships between the RSCH's permanent shear strain data and traffic level ESALs in the field.
- Analyzing and ranking the measured parameters from the RSCH and FSCH tests. In this approach, different parameters are analyzed statistically using simple base statistics to rank mixes' performance and compare the results with others measured by accredited laboratories or fields tests under the same conditions and using same mixes.

3.1.6.1 Using direct relationships between the RSCH and ESALs

A quick estimation method of rut depth using RSCH test results is expressed in the SHRP-A-379 Report, Annex A1(1994). The method is applicable for any asphalt mix design over pavements' service life. It follows a simple procedure of calculation using some mathematical equations and an estimated ESALs value. First, the total number of designed ESAL on a given pavement over its effective service life should be estimated. The annual maximum average pavement temperature of the hottest 7-days period is then estimated at a specific pavement depth, usually at 2-inch depth. A software of Superpave mix design can be used to determine the maximum pavement temperature at depth (d) (Harrigan, et al., 1994). An alternative equation, Equation 3-8, was determined by Solaimanian & Kennedy, (1993) can be used also for estimating

the maximum pavement temperature at any depth less than 8-inch. The equation uses the measured maximum pavement temperature at the pavement surface as follows:

$$T_d = T_s(1 - 0.063d + 0.007d^2 - 0.0004d^3) \quad (3\text{-}8)$$

Where:

d= depth in inches,

Ts=maximum pavement temperature (°F) at the surface, and

Td= maximum pavement temperature (°F) at depth (*d*).

The required number of loading cycles in the RSCH test, which is equivalent to the estimated total design ESAL number, is then calculated by using Equation 3-9. The RSCH test is then conducted at the estimated temperature, $T_{\max(d)}$. The resulting maximum permanent shear strain is obtained at the determined shear load cycles. Finally, the estimated rut depth can be determined by using Equation 3-10 (Harrigan, et al., 1994).

It should be mentioned that Equation 1 is considered as a shift factor of the number of RSCH repeated load cycles in the laboratory to the number of ESALs in the field. It is also obtained with a good correlation of $R^2 = 0.8$ for pavements that did not show significant aging (Sousa & Solaimanian, 1994). The relationship of Equation 3-10, on the other hand, was obtained for many loadings and material conditions, and it indicates the linear variation of rut depth with maximum permanent shear strain (Sousa, 1994).

$$\log(cycles) = -4.36 + [1.24 \times \log(ESAL)] \quad (3\text{-}9)$$

$$Rut\ Depth\ (mm) = 279.4 \times [Maximum\ Permanent\ Shear\ Strain] \quad (3\text{-}10)$$

Based on these relationships, an abridged procedure for estimating adequate mixes performance was introduced by Sousa & Solaimanian, (1994) and illustrated in an example by Sousa, (1994). A nomograph of the abridged procedure example is shown in Figure 3-20. The nomograph consists of four quadrants that should be started from Quadrant 1 and followed in clockwise direction. Starting from Quadrant 1, the number of ESALs for pavement design life and maximum allowable rut depth are determined, as shown in the example, a 1,000,000 ESALs and 0.5in rut depth were determined. Moving to Quadrant 2, the maximum allowable permanent shear strain is determined based on the selected maximum rut depth. This can be calculated also by using Equation 3-10. Then, using the relationship "curves" between permanent shear strain and number of cycles obtained from the RSCH tests, the corresponding number of cycles to the maximum allowable permanent shear strain (Calculated from Equation 3-10) is determined for each mix, as shown in Quadrant 3. Moving to Quadrant 4 or using Equation 3-9 to determine the estimated number of ESALs that can be sustained by each mix before achieving the allowable rut depth. Finally, returning to the Quadrant 1 or comparing to the desired ESALs number, adequate mixtures that satisfy the design conditions can be identified as they have ESALs number above the desired number, as shown in the example, mixes C and D are only the adequate mixes (Sousa, 1994).

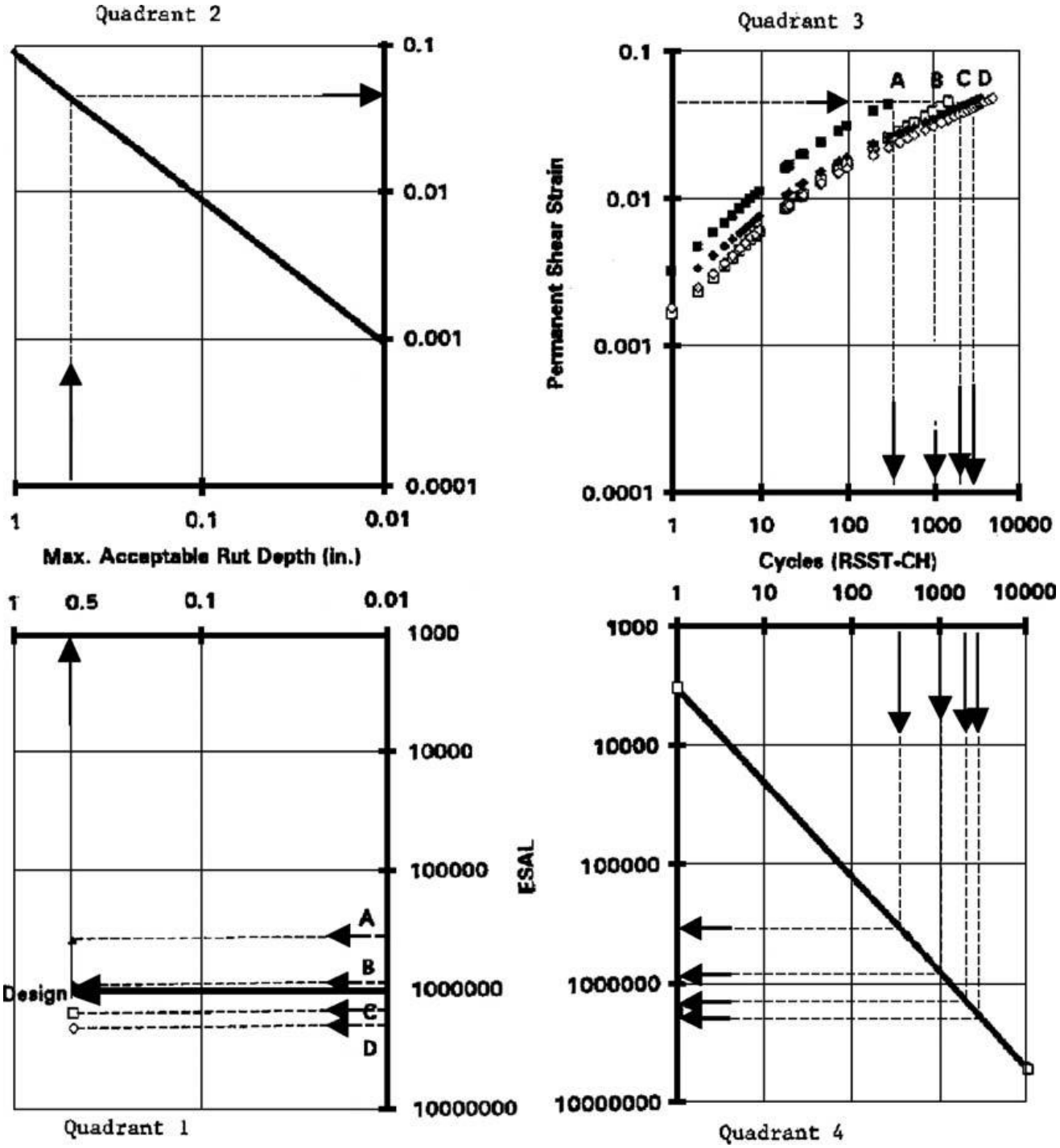

Figure 3-20. Diagram of the Abridged Procedure for Permanent Deformation (Sousa, 1994)

3.1.6.2 Analyzing and Ranking the Measured SST data

Chowdhury & Button, (2002) recommended the FSCH test as the best SST protocol among the four unconfined SST tests for evaluating shear resistance of asphalt mixes. The SST tests data were used to rank four different asphalt mixtures of known rutting performance. The mixtures were tested on the FSCH, SSCH, RSCH, and RSCSR tests. The selected mixes were Type C limestone, Type D rounded river gravel, granite stone mastic asphalt (SMA), and granite Superpave. The FSCH test was performed on three specimens of 7% air voids of each mix and at three different temperatures of 4°C (39°F), 20°C (68°F), and 40°C (104°F). At each temperature, the mean of the mixes values of the measured complex shear modulus (G*) and shear phase angle (δ) were plotted against the logarithm of load frequencies. Using the same specimens of the FSCH test, the SSCH test was performed at three different stress levels and test temperatures to measure three material responses of each mixture: maximum shear strain, permanent shear strain, and elastic recovery. The RSCH and RSCSR tests were performed using other three specimens from each mixture for each test. The specimens were compacted at 3% air voids to enhance tertiary rutting. The RSCH and RSCSR tests were conducted at 55°C (131°F) temperature, and the average accumulated permanent shear strain of each mixture was measured at 10,000 load cycle or 5% accumulated strain, whichever came first.

The ranking process were prepared based on the measured SST parameters. The ranks prepared from the FSCH tests were determined based on the complex shear modulus (G*) and shear phase angle (δ) values. High G* value indicates high performance against rutting while higher δ value indicates the opposite. The G* results were used for determining the ranks in two ways: the value of G* at 10Hz, which simulates highway traffic, and the overall G* versus frequency graphs (position of the plot). The overall δ values versus frequency graphs was used for the ranking

because of the inconsistent trends of the δ values. The three material responses measured by the SSCH tests were also used to rank the mixtures. The SSCH ranks were prepared based on the fact that higher maximum and permanent shear strains indicate more rut susceptibility while higher elastic recovery indicates the opposite. From the RSCH and RSCSR tests, the ranking was prepared based on the measured accumulated permanent shear strain values as a highest value indicates the most rutting susceptibility of asphalt mixtures.

Chowdhury & Button, (2002) also calculated the coefficient of variations (COV) of the obtained SST tests' parameters to evaluate their repeatability. Table 3-8 presents the calculated COV values from the SST tests. The lowest COV values among all SST tests parameters were for the Shear phase angle (δ) followed by the complex shear modulus (G*). The COV values of the SSCH test were relatively very high comparing with the COV values of the FSCH test. The COV results and range values of the RSCH test were relatively low comparing with the high and inconsistence variation values of the RSCSR test. This result supports the suggestion provided by AASHTO provisional standard, Interim Guide (April 2001), that conducting both repeated shear tests is redundant (Chowdhury & Button, 2002).

Table 3-8. COV of Mixtures Properties Determined by different SST tests (Chowdhury & Button, 2002)

Tests	Test Temperature, °F	Test Parameter	Coefficient of Variation, COV			
			Limestone	River Gravel	Granite SMA	Granite Superpave
FSCH	39	Complex shear modulus	26.3	22	11	15.5
		Shear phase angle	10.7	4	5.5	2.6
	68	Complex shear modulus	13.2	12.9	8.4	12.1
		Shear phase angle	8.8	6	2.9	3.5
	104	Complex shear modulus	18	5.4	0.4	13.1
		Shear phase angle	4.7	6.9	0.4	3.7
SSCH	39	Maximum strain	23.1	40.4	18	29
		Permanent strain	37.5	48.6	31.8	42.2
		Elastic recovery	5	11.2	3.5	6.1
	68	Maximum strain	27.6	14.6	72	42.9
		Permanent strain	23.9	16	97	50.2
		Elastic recovery	7.9	4.7	27.7	16.9
	104	Maximum strain	10.7	16.2	18	17
		Permanent strain	7.1	10.1	23	20
		Elastic recovery	4.5	14	10.4	5.1
RSCH	131	Permanent strain	7.3	3.7	9.1	7.6
RSCSR	131	Permanent strain	15.7	2.2	18.8	6.6

Romero &Mogawer, (1998a) conducted a study to evaluate if the SST device can be used to differentiate the properties between asphalt mixes that are prepared from one aggregate source of (19 mm NMAS) and five different binders without need for a model. Three unmodified binders and two modified binders were used as followings: AC-5 (PG 58-34), AC-10 (PG 58-28), AC-20 (PG 64-22), Novophalt (PG 64-22), and Styrelf (PG 82-22), respectively. The asphalt mixes were compacted using the SGC at $7 \pm 0.5\%$ air voids and prepared to be tested on the SSCH and FSCH tests at both 40°C and 58°C. Then the RSCH test was conducted for the same samples at 40°C.

The results obtained from the SST tests were analyzed statistically and compared with performance results of same mixes from the FHWA Accelerated Loading Facility (ALF).

Romero &Mogawer, (1998a) followed a systematic procedure to analyze and compare the data. Since the obtained results from the SST tests showed some variabilities and no known precision and bias existed for the tests procedure, the results were ranked statistically using two methods to determine which averages were significantly different. The first method was prepared through using Fisher's Least Squared Difference (LSD) procedure same as the ALF results were ranked. The second method was used based on the calculated standard deviation ($\mu \pm 2\sigma$). In the second method, groups were given different letters when the means values were statistically different. i.e., if the two standard deviations bands did not overlap. These methods were prepared individually for all parameters obtained from the SSCH, FSCH, and RSCH tests, and compared with ranking results of the FHWA Accelerated Loading Facility. From the SSCH test, four parameters were analyzed: Maximum shear strain, shear modulus, shear strain recovery, and axial stress. Three values were analyzed from the FSCH test: Complex shear Modulus (G*) at 0.1 and 10 Hz, slope of the log G* versus log frequency (Higher slope may indicate less resistance to rutting), and $G^*/Sin\,\delta$ at 0.1 and 10 Hz. Two parameters were evaluated from the RSCH tests: the slope obtained from the permanent deformation model ($\varepsilon_p = aN^b$), and maximum permanent shear strain. Although the slope (b) is a regression parameter and not a material property, it was analyzed because it represents the rate of the deformation.

The results of the study indicated that the average shear modules obtained from the SSCH tests were unable to distinguish between the mixes of modified binders, whereas the axial stresses and recovered strains results were unable at all to differentiate among mixes or even to match the ALF ranks. The obtained complex shear modulus, G*, and $G^*/Sin\,\delta$ parameters from the FSCH tests

at 40 °C were able to discern mixtures similar to each other in accordance with the ALF results. Therefore, using $G^*/Sin\ \delta$ parameter does not add any advantage in performance measurements over the G* parameter. The average values of permanent shear strain in the RSCH tests were able to match the ALF rutting results. However, the RSCH's variabilities made the statistical raking inapplicable. Although the SST tests generally provided high variabilities in measurements, it was concluded that the SST results can be used to differentiate among mixes having same aggregate size and different binder types. Furthermore, the work showed that with some of the SST parameters, it was applicable statistically to rank the mixes so that they match the ALF's performance ranking. However, the obtained high variabilities (coefficient of variation) of about 15% at 40°C and at least 30% at 58°C were justified due to insufficient sample size used in the tests. Therefore, it was recommended to determine an appropriate sample size for the SST tests, as well as more than three replicate samples should be used in the tests (Romero & Mogawer,1998a).

In another study, Romero & Mogawer, (1998b) evaluate the ability of using SST results to discern between mixes with the same binder and different nominal maximum aggregate size (NMAS) on rutting susceptibility without the need of a model. They examine the performance of five different mixes through conducting the SSCH and FSCH tests at both 40°C and 58°C. Then the RSCH test was conducted at 40°C. The asphalt mixes were prepared to include asphalt binders AC-5 (PG58-34) and AC-20 (PG 64-22) with two different aggregate size of (19 and 37.5 mm NMAS). The fifth mix was called "White March" was also prepared as a worst-case scenario. It fully contained river gravel and AC-20 binder. The obtained results from SST tests were analyzed statistically and compared with performance results of the same mixes from the FHWA Accelerated Loading Facility (ALF).

Regarding the analysis approach, Romero & Mogawer, (1998b) calculated individually the mean and standard deviation of all SST parameters followed that by performing a T-test of unequal variance at an α=0.05 (Heteroscedastic test). The T-tests were performed to determine for a measured parameter if it has a significant difference in the means between the fine and course mixes. This approach was applied for all parameters obtained from the SSCH, FSCH, and RSCH tests, and compared with the ALF performance results. From the SSCH test, three parameters were analyzed: shear modulus, shear strain recovery, and axial stress. Three values were analyzed from the FSCH test: Complex shear Modulus (G*) at 10Hz, slope of the log G* versus log frequency, and $G^*/Sin\ \delta$ at 2 Hz. The 2 Hz frequency was selected because it was close to the ALF's loading rate. Two parameters were evaluated from the RSCH tests: the slope obtained from the permanent deformation power model ($\varepsilon_p = aN^b$), and maximum permanent shear strain.

The results indicate that the SST was unable to discern rutting susceptibility between mixes made with same binders and different nominal maximum aggregate size providing that those mixes have shown a significant difference in performance when tested by the ALF. The ALF results indicate that rutting susceptibility decreases with increasing aggregate size, while SST results were unable effectively to separate the mixes' performances due to the obtained high variabilities. It was however recommended to determine statistically an appropriate sample size for the SST tests which might improve the ranking results by given better mean values (Romero & Mogawer, 1998b).

Tayebali, et al., (1999) have evaluated the ability of RSCH test to identify rutting susceptibility of asphalt mixtures in accordance with performing observations from fields. The study evaluates rutting potential measured by the RSCH test of three pavement sections in North Carolina of known field performance. The field observations indicated that the selected sections have a well,

light, and poor performance of rutting after many years in service. Extruded cores were obtained from the wheel-paths and between the wheel-paths in those sections to be evaluated by the RSCH test. Since the properties of the obtained cores vary from section to another, both volumetric and gradation analysis were performed beside the RSCH tests. The results from the volumetric and gradation analysis agreed with the field observations of the well and poor performance sections.

The RSCH tests were conducted to 100,000 cycles or till a maximum 5% accumulated shear strain is obtained, whichever obtained first. The reason of performing the tests at load cycles higher than the specified number of 5,000 load cycles is that to ensure capturing the tertiary flow of asphalt mixes. Two load frequencies of 1.43 Hz and 5 Hz were also used in the RSCH tests to determine the effect of testing time on the results. SHRP superpave binder selecting program (SHRPBIND) was used to calculate the Superpave 50% reliability temperatures for all sections. The calculated temperatures were 53°C for the section of no observed rutting and 55°C for the others. These temperatures were initially used to test the cores obtained from between the wheel-paths. Since the initial results of the RSCH tests indicate a sever rutting for the no observed rutting section, it was believed that the calculated temperatures were too high. Consequently, the second series of cored samples from the wheel-paths were tested at lower temperature of 40°C. Tayebali, et al., (1999) analyzed the results of accumulated permanent shear strain versus shear load cycles curves of all cores. The analysis was performed only by determining rutting susceptibility of cores from through studying the curves and without performing any other statistical calculations. However, the results of the study indicated the ability of the RSCH tests to identify rutting susceptibility of well performing versus poorly performing mixes. Also, it is observed generally that the RSCH results obtained at 5 Hz are similar to that at 1.43 Hz shear load frequency (Tayebali, et al., 1999).

Similarly, the ability of the RSCH test to distinguish the rutting performance between mixes was determined by Martin &Park (2003). They conduct a study to evaluate the ability of APA and RSCH tests to assess rutting performance of asphalt mixes. Both tests were validated through simulating five pavement sections that prematurely failed at *WesTrack* test. Five *WesTrack* sections were simulated through fabricating Superpave gyratory samples in accordance to the *WesTrack's* in-place's air voids and asphalt contents. The replicate specimens were tested in the APA and RSCH tests at approximate 60°C temperature. The results of the tests were used to rank rutting performance of the replaced mixes and compared with the *WesTrack* full-scale ranking results.

The RSCH tests were performed on two replicate specimens of each *WesTrack* section. The average numbers of repeated load-cycles that required to achieve 5% deformation of each mix were used to assess the mixtures performance. The average values of the two replicate specimens of each mix were also fitted with the RSCH power model ($\varepsilon_p = aN^b$) to determine the intercept "a" and slop "b" parameters. The intercept "a" value of each mix was determined at zero load cycles (N=0). These two parameters were used to assess the replicate mixes performance as the initial permanent shear strain affects the overall accumulated deformation while a lower slop indicates better rutting performance. Since two replicate specimens were tested for each mix, a statistical analysis was not developed. However, Martin &Park (2003) followed the same procedure of the previous example illustrated by Sousa (1994) to verify adequate mixtures in rutting performance. The results of the APA and RSCH tests showed an acceptable agreement with the rutting depth measured under full-scale trafficking test, and it was concluded that both tests were able to differentiate between mixes of good and poor rutting performance. Furthermore,

ranking results of the RSCH showed high correlation to asphalt content and air void content of the replicate specimens (Martin &Park, 2003).

In contrast, Zhang. et al., (2006) found a poor relationship between the RSCH test results and field rut depth data measured by the NCAT Test Track. A wide range of 51 asphalt mixes of different properties were tested in the NCAT Test Track of 200-ft long and 10 million ESALs applied in total over a 2-year period to measure rutting depth of asphalt mixes. The RSCH samples were performed from the fresh mixes of the 51 NCAT's mixes during the constriction and compacted to the design density using the SGC. The tests were performed at 64°C to 5,000 load cycles. Permanent shear deformation, shear modulus, slope of RSCH power model, and repetitions to 3% shear strain were determined from the RSCH data of all mixes along with the rut depth results obtained from the NCAT Test Track. Coefficient of correlation "R^2" was determined individually of all RSCH parameters versus the field rut depth from the test track . The R^2 values all RSCH parameters were very low as they ranged from around 0.02% up to 0.17%. This indicated that none of the RSCH parameters has a good relationship with the field rut depths. It was concluded, however, that the poor relationship can be justified by the good quality of the track construction, thick pavement structure, and moderate weather that did not produce any sever rutting in the field.

In addition, Zhang. et al., (2006) evaluated the sensitivity of the RSCH test to asphalt binder type in the NCAT test track asphalt mixes. The sensitivity test was conducted only through examining the effect of different factors on the permanent shear strain values at 5,000 cycles. An analysis of variance tests (ANOVA) including gradation type, PG Grade, and asphalt content factors is performed using three replicate observations of ten sections. It found through performing F-statistics that binder PG grade affects the permanent shear strain ($P<0.05$). Also, t-Tests were

conducted on different combinations of two binder types to evaluate the significance of binder type on mixes containing more aggregate types. The result of the sensitivity tests indicates that using SBR modified PG 76-22 provides better performance (low permanent shear strain on average) than PG 67-22.

3.2 Duplicate Shear Tester (DST)

3.2.1 Background

Although the SST device has proved its ability to measure the fundamental shear properties of asphalt mixes effectively and sufficiently enough for rutting prediction, the high cost and complexity of the device have limited this device to be used widely. According to ASSHTO-T320, the FSCH and RSCH tests are the two common SST tests for measuring the shear stiffness and cumulative permanent shear deformation of asphalt concrete. A Duplicate Shear Tester (DST) has been developed by Khajeh-Hosseini, (2015) and improved by Jweihan, (2018) in the University of Texas at Arlington (UTA) as a replacement test device to the SST. The DST has considered the observed advantages and deficiencies in the SST.

The DST device has replicated the two common SST tests in accordance to the procedures and recommendation of the standard test method AASHTO-T320. The DST is simple, user friendly, and inexpensive test device. It proved its capability to measure the average mechanical shear properties of two specimens at the same time by using a Universal Test Machine (UTM-25) (Khajeh-Hosseini, 2015; Jweihan, 2018). Figure 3-21 shows the original DST device installed inside the UTM testing machine.

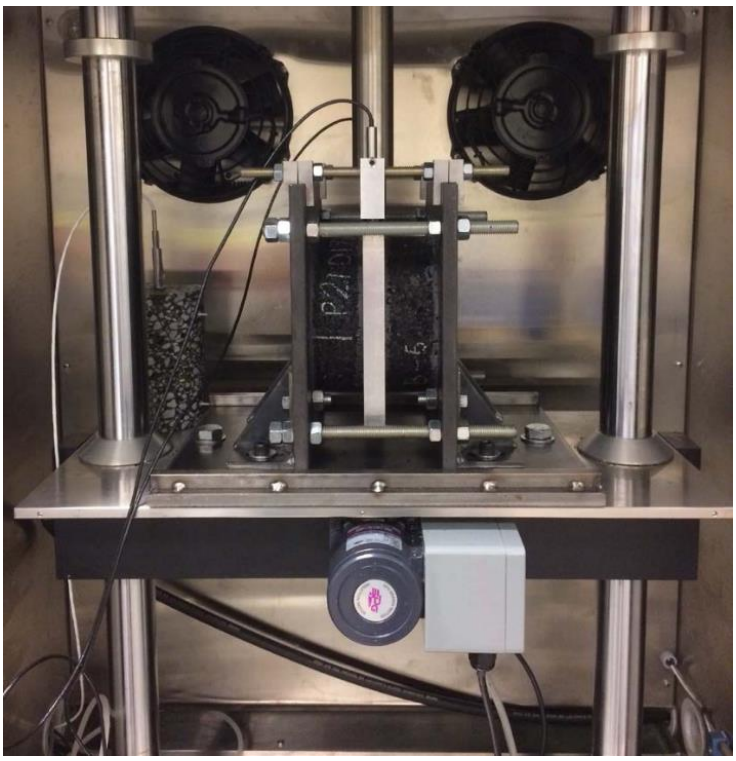

Figure 3-21. The original DST device inside the UTM-25 testing machine (Khajeh-Hosseini, 2015)

The UTM-25 test machine is utilized with five main components that make the machine able to test asphalt concrete under different conditions. Those components include: a loading system, hydraulic system, control and data acquisition system (CDAS), temperature control chamber, and pneumatic system. Figure 3-22 shows the main components of the UTM-25 testing machine.

The UTM-25 loading system includes a vertical actuator and a loading frame. It capable to apply static and dynamic axial loads to the DST specimens. The hydraulic system supplies the loading system with sufficient power to apply the loads. The data acquisition system is needed to control the loading levels, shape, and frequencies as well as record the specimens responses while performing the tests. The temperature chamber is used to perform the test at controlled temperatures based on the test procedure. The pneumatic system is a second actuator connecting

to the UTM-25 testing machine. It is used to apply a controlled confining air pressure depending on the tests' procedure. Utilizing the UTM-25, however, adds two advantages to the DST device:

1- The DST is simple and inexpensive comparing with the SST complexity and high cost.

2- The DST can be adopted universally in laboratories having a universal test machine.

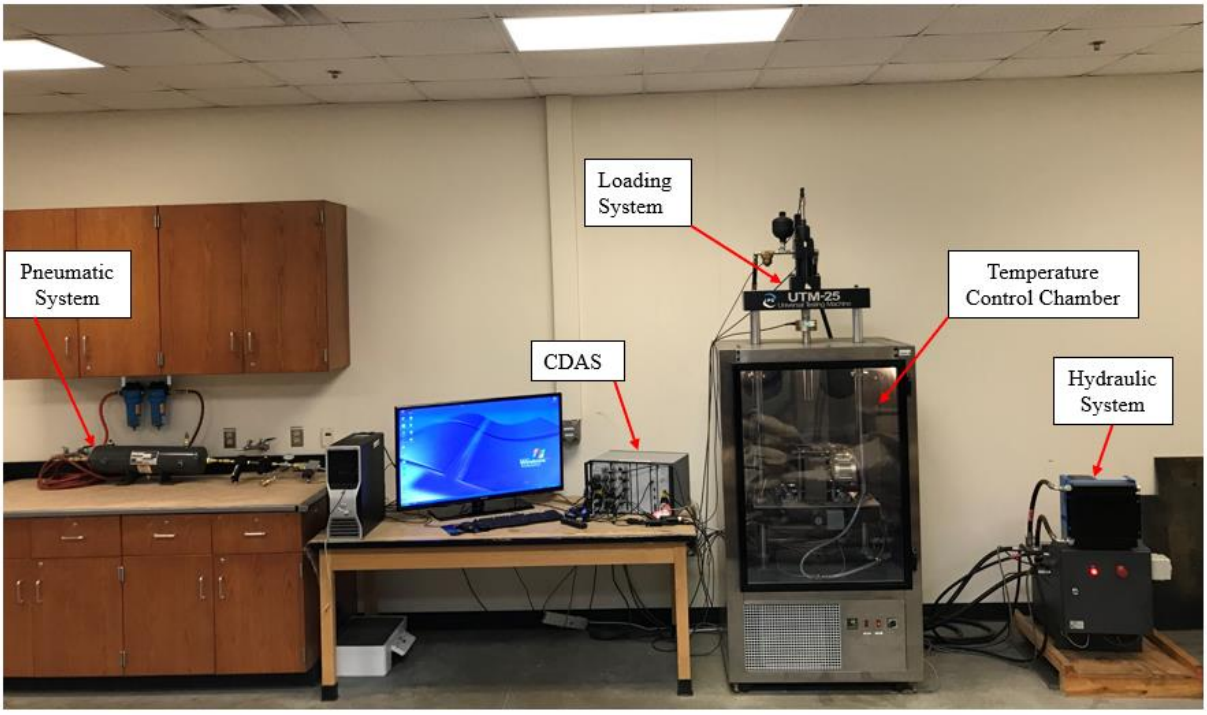

Figure 3-22. The main components of the UTM-25 testing machine.

The DST device is capable to accommodate two specimens of asphalt concrete performed from a gyratory sample compacted on the Superpave Gyratory Compactor (SGC). The specimens should be prepared similar to that for the SST and obtained from a uniform asphalt mix that used for pavement surfaces layers. Each DST sample consists of two identical asphalt concrete specimens that are glued to an aluminum plate in the middle and to two steel plates on the sides. An axial load is applied on the aluminum plate to develop shear forces in the specimens. The procedure of performing the FSCH and RSCH were adopted in the DST to measure the average shear properties of the two asphalt mixes at the same time (Khajeh-Hosseini, 2015; Jweihan, 2018).

3.2.2 DST System

The loading condition and constraints of the SST have been considered in the DST device. As mentioned in the SST section, a static or dynamic shear load is applied in the SST device to an asphalt specimen in a direction normal to the compaction axis. However, this shear load makes the aggregates in the mix to roll over each other causing an expansion in the test specimen in the opposite direction to the shear load application, as shown in Figure 3-23. Since this expansion is resisted in field due to the HMA confinement, the SST simulates this confinement by maintaining the specimen height constant during the test (Pavement Interactive, 2008). A close-loop feedback system represented by LVDTs measures the axial deformation of the SST specimen and applies an axial force to neutralize this deformation and keep the specimen height constant during the tests. Figure 3-24 illustrates the SST loading condition. However, the Duplicate Shear Tester (DST) replicates the SST loading condition and constraints but for two specimens at the same time.

The DST device typically consists of two identical cylindrical specimens of asphalt mixes glued to an aluminum plate in the middle and to steel plates to the sides. The steel plates are fixed and tighten firmly together by four threated rods and adjustable nuts to maintain the test specimens height during the test. This configuration provides a rigid frame set up that keeps specimen height constant during the tests. An axial load is then applied on the aluminum plate between the two specimens to develop shear stresses on the specimens, as illustrated in Figure 3-25 (Khajeh-Hosseini, 2015; Jweihan, 2018)

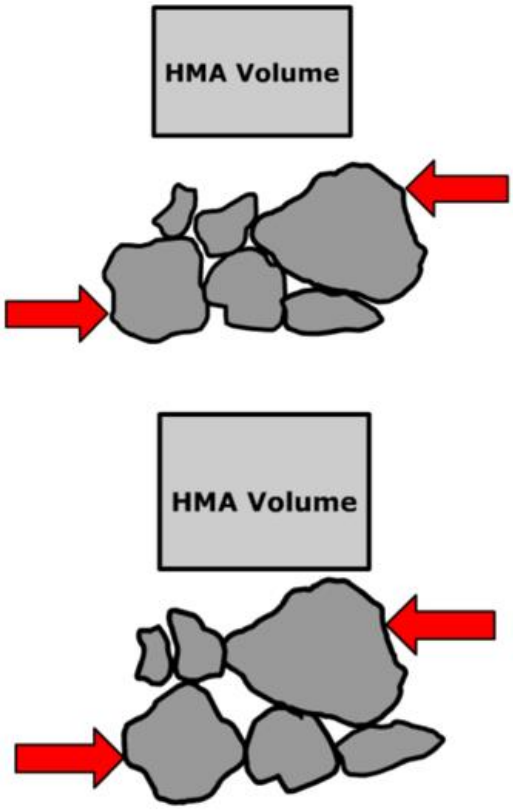

Figure 3-23. Change in volume of compacted HMA due to shear stresses application (Pavement Interactive, 2008)

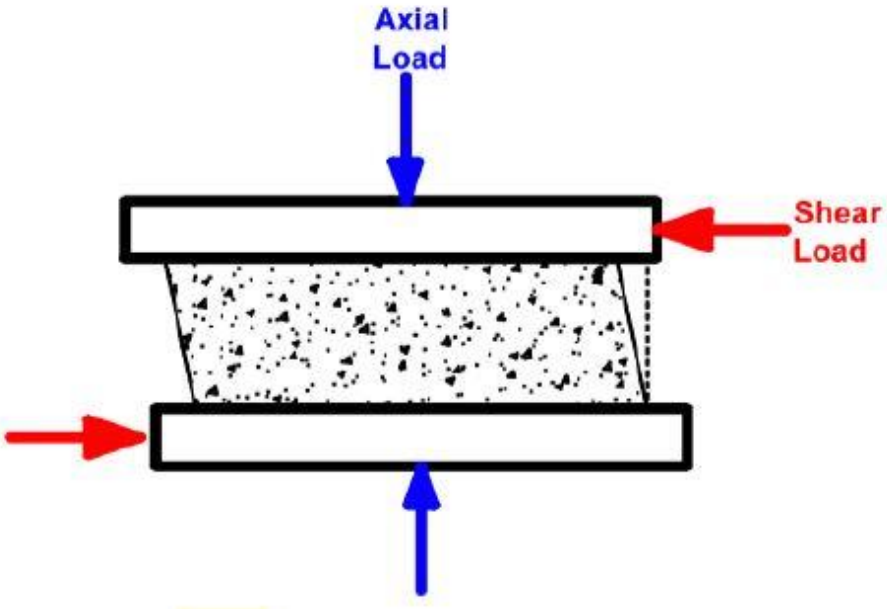

Figure 3-24. Illustration of the Superpave Shear Test Loads (Khajeh-Hosseini, 2015)

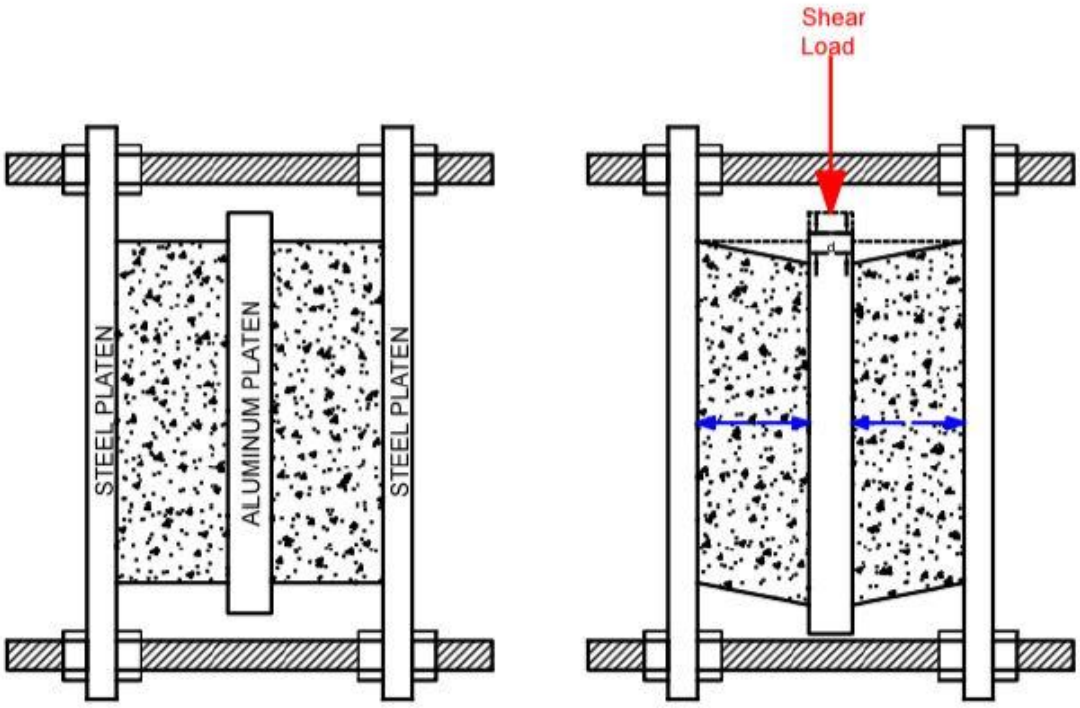

Figure 3-25. Simplifying drawings to the DST load condition (Khajeh-Hosseini, 2015).

Similar to the SST, the DST applies shear forces to the specimens, as well as it maintains their height constant during the test. When the axial load is applied at the top of the middle aluminum plate, the specimens well be subjected to shear stresses. As a result, the specimens try to expand laterally causing normal forces on the middle and side plates. The normal forces are illustrated in the Figure 3-25 by blue arrows within each specimen. It is assumed that the generated normal forces are equal because the specimens are identical in dimensions and made of same asphalt mixes. The dilatancy in the specimens is prevented by mean of the DST rigid frame setup that tights the two plates at sides firmly together using threated rods and adjustable nuts. Therefore, the specimens height will be maintained constant during the DST tests (Khajeh-Hosseini, 2015; Jweihan, 2018).

Recently, the DST device has been improved by Jweihan, (2018) to be included an additional “Mini-Rail Miniature Linear guides” system to assure a completely vertical movements for the DST middle plate. Therefore, the DST system has been required to slide the DST sample inside a special supporting plate with vertical guides. The developed guide system consists of two standard lightweight pieces of aluminum: a 12 mm carriage and 12mm linear rail. These parts were obtained from the “Grainger” Company, and they have part numbers of (2CRP8) for the carriage and (2RLE9) for the linear rail segments.

The carriage is mounted on the linear rail to provide smooth, gliding, and precise motion in a straight line with less vibration, as shown in Figure 3-26. The carriage contains linear sleeve bearings, that are suitable for dirty or corrosive environments. It is also able to withstand relatively high applied loads (Gamut, 2017). Moreover, the Mini-Rail Linear Guides is an economic system that is manufactured at many standard sizes to be suitable for linear movement applications. It has no rolling elements that makes the movements safe against any catastrophic failure during the movements (Pcblinear, 2017).

Figure 3-26. Mini-Rail Miniature Linear Guides System (Gamut, 2017)

Jweihan, (2018) has utilized the linear guides system through modifying the middle aluminum plates and the supporting plate of the DST device. Two 6.0” long segments of the standard 12 mm mini-linear rail were fixed permanently on the lateral sides of the DST middle plate using socket head cap screws (#6-32, 3/8” long). The supporting plate was fabricated to be able to accommodate the whole DST sample. The plate consists of two identical stands of steel that are used to carry two carriages on each side, as shown in Figure 3-27.

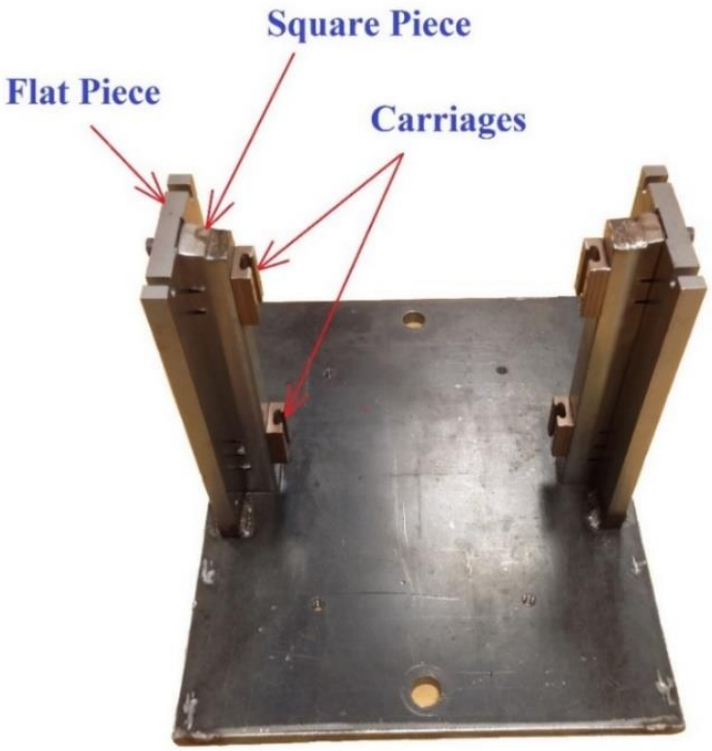

Figure 3-27. The Modified DST Supporting Plate (Jweihan, 2018).

Each stand on the supporting plate consists of two vertical pieces: a flat and a square piece. The flat pieces of 7 in length, 5.5 in width and 0.5 in thickness were welded vertically at sides to the center of the original supporting plate. The square pieces (6.5 in length and 1.0 in width) were fixed vertically on the flat pieces by three screws at each side. On each stand, two carriages of the

linear guides system were fixed on the square piece by screws. The location of the stands along with the carriages were determined precisely so that the DST sample with the attached rails can be slide easily inside the carriages after mounting the DST sample on the supporting plate. The DST supporting plate is fixed on the loading table inside the UTM-25 loading frame by two 5/8”-18, 2.0” long bolts at sides. Follows that by sliding the whole DST sample inside the vertical guides on the supporting plate (Jweihan, 2018).

3.2.3 DST Components and Description

The DST device consists of the following components:

- Two steel plates (10" ×10" × 0.5").
- One aluminum plate (7" × 6.75" × 0.75").
- Two aluminum Mini-Linear Rails (12mm, 6" long).
- Four threaded steel rods (1/2”-13, 8.5" long) and sixteen nuts (1/2”-13).
- Two steel grippers.
- Supporting Plate with the vertical guide system.

The DST steel plates are designed to have a depression at one side with 1/16 inches depth and an average diameter of 5.9 inches. The middle aluminum plate has also the same depressions but at the two sides, as illustrated in Figure 3-28. Those depressions are designed with a 5.875” diameter tapered to 6.0″ at center to accommodate cylindrical specimens of asphalt mixes with a diameter of 150 mm and 50 mm height. The depressions are used to contain an epoxy paste where the specimen should be glued at the center of the steel and aluminum plates, as shown previously in Figure 3-25 (Jweihan, 2018).

The aluminum plate has four holes (1/2 diameter) at corners, whereas the steel plate has eight holes. The inner four holes of the steel plate match the locations of the aluminum plate holes. They

are used only to line up the DST plates to be centered while gluing the DST specimens. The outer four holes of the steel plates are the locations of the four threaded rods and adjustable nuts. The threaded rods, however, have two main functions: to connect the two steel plates together after the epoxy paste is cured, and fix the two grippers at the bottom of the outer sides of the steel plates. Typically, the two grippers, two asphalt specimens, two steel plates, one aluminum plate, four threaded rods, and sixteen adjustable nuts make together a one-unit of DST sample. After assembling the DST sample, it is mounted on the supporting plate inside the UTM-25 chamber for testing (Jweihan, 2018).

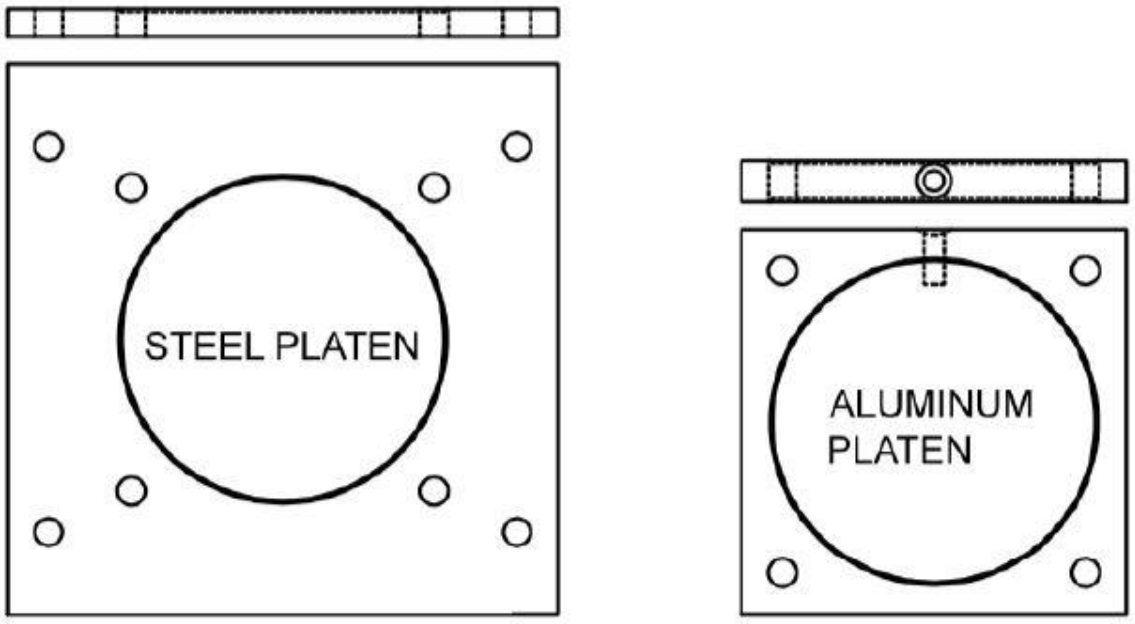

Figure 3-28. Steel and Aluminum Plates of the DST (Khajeh-Hosseini, 2015)

Jweihan, (2018) has modified the steel and aluminum plates at low cost to be used in the modified DST devise instead of fabricating other plates. The locations of the two threated rods at the bottom of the steel plate were changed to avoid the interruption of the threated rods with the vertical stands of the DST supporting plate. The aluminum plate was modified by attaching two standard 12 mm Mini-linear rails segments at its sides. Those rails are used to allow the aluminum

plate to slide inside the “Mini-Carriages” on the vertical stands of the DST supporting plate. The modified steel and aluminum plates are shown in Figure 3-29 and 3-30, respectively.

Due to the change of the threaded rods locations at bottom, it also was necessary to adjust the aluminum plate dimensions so that the plate can be moved vertically while shearing with no interruption with the threated rods at bottom. Therefore, an enough room of 0.25” for the plate movements was considered by shaving a quarter of inch of material along the bottom of the aluminum plate. As a result, the length of the aluminum plate was adjusted to be 6.75 inches instead of the original length of 7.0 inches (Jweihan, 2018).

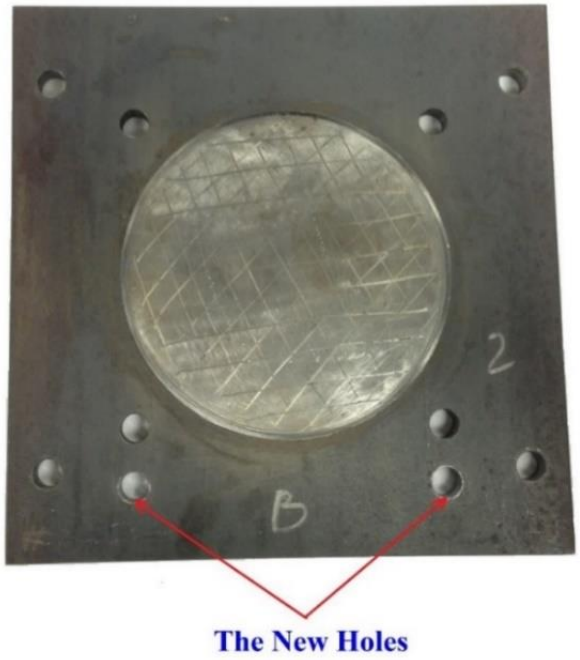

Figure 3-29. A DST Steel Plate with the new holes at bottom (Jweihan, 2018).

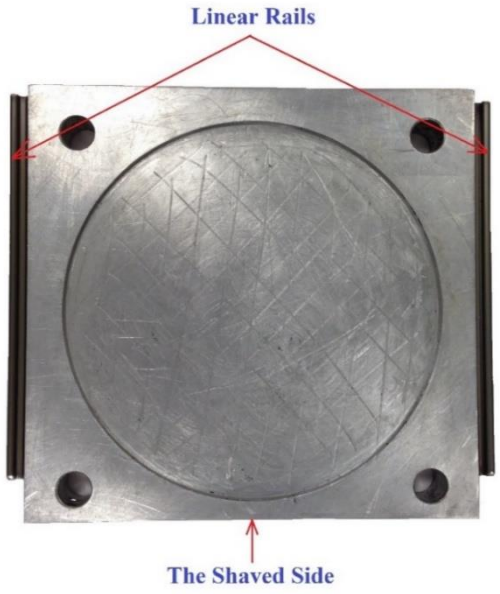

Figure 3-30. The Modified DST Aluminum Plate (Jweihan, 2018).

To facilitate the UTM-25 for performing the DST tests, some accessories have been developed. The accessories are simple, inexpensive, and can be used for other universal testing machines. They include loading attachments, and LVDT mount. The loading attachments, shown in Figure 3-31, provide a capability for the DST to perform the FSCH and RSCH tests. The RSCH attachment is an original attachment of the UTM-25 that is used to perform compression tests. It can be used to perform the RSCH by applying shear loads in one direction (positive). The upper side of this attachment is screwed up into the UTM actuator while the bottom side is attached to the top of DST aluminum plate at center (Khajeh-Hosseini, 2015; Jweihan, 2018).

The second attachment is designed specifically as coupling of two pieces to perform the FSCH test. It provides the capability to apply dynamic shear loads in two directions (up and down). Figure 3-32 shows the coupling details. This coupling connects the UTM-25 actuator ram directly to the DST aluminum plate. It consists of two metal pieces linked firmly by a pin and an adjustable

nut. Piece 1 is screwed-down in the middle at the top of the DST aluminum plate, while Piece 2 is screwed-up into the actuator ram of the UTM-25 (Khajeh-Hosseini, 2015; Jweihan, 2018).

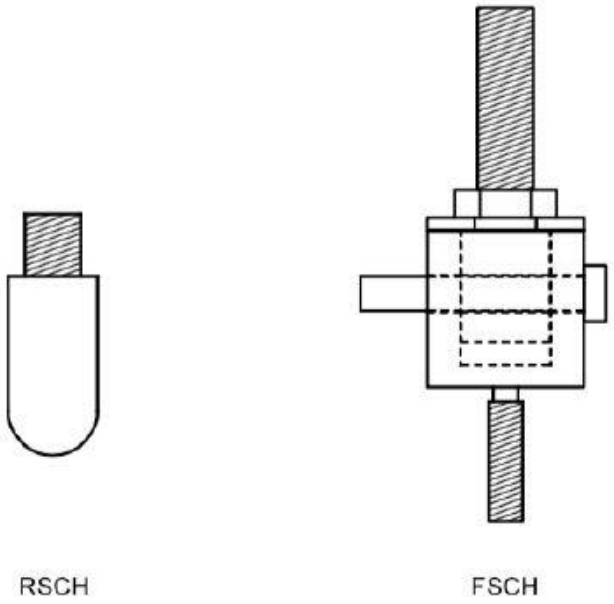

Figure 3-31. Loading Attachments for the DST (Khajeh-Hosseini, 2015)

The Liner Variable Differential Transducers (LVDT) mounts is designed to hold two axial LVDTs. The LVDTs are used in the DST device to measure the relative vertical displacement between the aluminum plate and the steel plates while shearing the specimens. Each mount consists of an aluminum LVDT holder, two pairs of steel clamps, a threaded rod (3/8”-16, 8.5” Long), and four nuts (3/8”-16), as shown in Figure 3-33. The steel clamps along with the LVDT holder and adjustable nuts are fixed on the threaded rod. The LVDT holder attaches to the top of the aluminum plate and able to accommodate two different sizes of LVDTs (Khajeh-Hosseini, 2015; Jweihan, 2018).

.

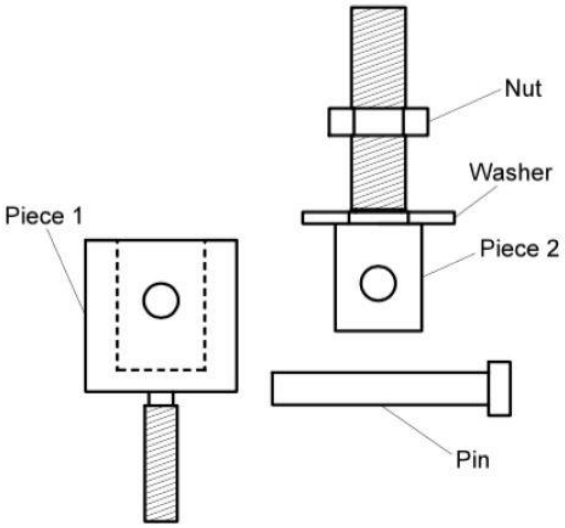

Figure 3-32. DST Coupling Attachment Details (Khajeh-Hosseini, 2015)

The LVDT mounts are installed over the steel plates of the DST sample in a direction perpendicular to the plates plan. The LVDT holder should be placed exactly over the DST middle plate on its centerline. An adjustable bolt on the top of each LVDT holder is used to control its location. The LVDT mounts should be fixed at equal distances in related to the center of the middle aluminum plate, as shown in Figure 3-34 (Khajeh-Hosseini, 2015; Jweihan, 2018).

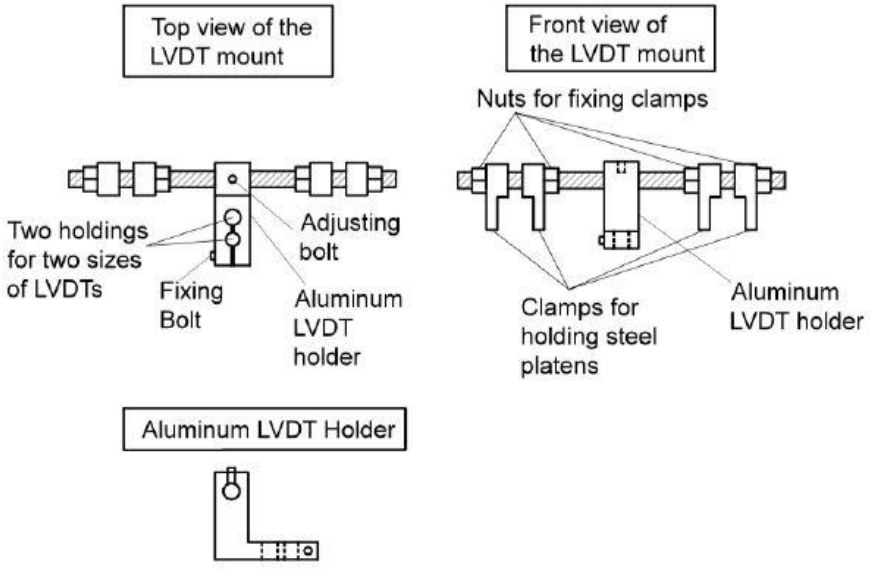

Figure 3-33. LVDT's Mount Components (Khajeh-Hosseini, 2015)

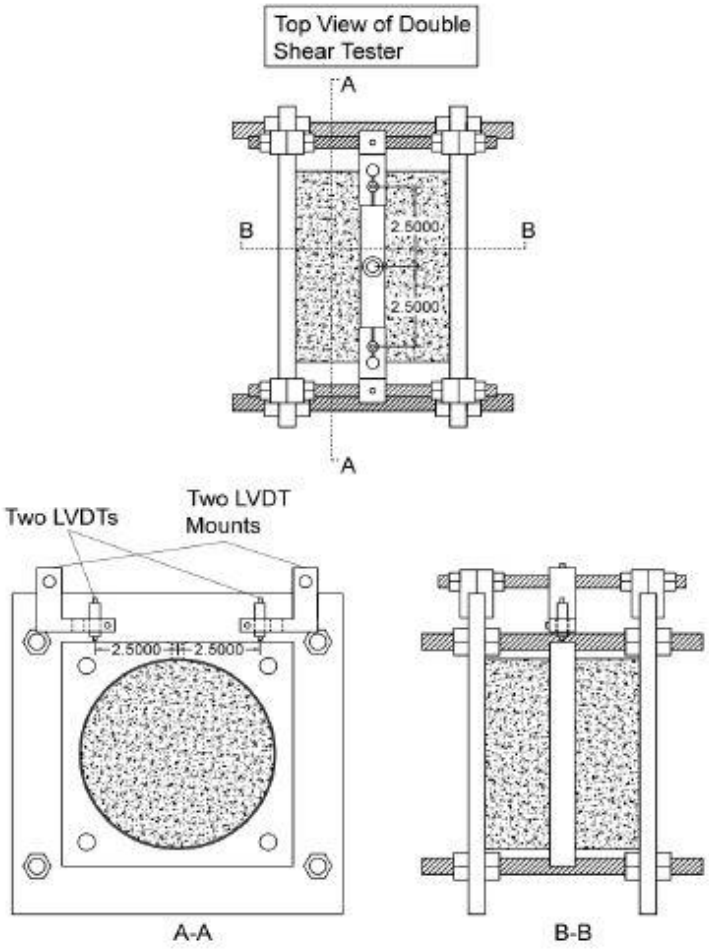

Figure 3-34. Position of the LVDT mount assembly on the DST (Khajeh-Hosseini, 2015).

3.2.4 DST Evaluations

The DST has been developed in the university of Texas at Arlington (UTA) to measure the mechanical shear properties of asphalt concrete in a laboratory. It replicates the loading conditions and constraints of the Superpave Shear Tester (SST). The device is able to measure the inherent shear parameters for rutting resistance prediction of asphalt mixes as an average for two asphalt concrete specimens at the same time. The parameters include the dynamic shear modulus, phase angle and permanent shear deformation (Khajeh-Hosseini, 2015; Jweihan, 2018).

Khajeh-Hosseini, (2015) performed the DST tests utilizing a UTM-25 to measure the shear parameters for four different asphalt mixes. The mixes include three dense graded hot asphalt mixes and a Stone Matrix Asphalt mix (SMA). From each mix, three sets of specimens were selected to perform the FSCH and RSCH procedures using the DST device. The results obtained from the tests were analyzed statistically to study the reliability and repeatability of the test measurements by studying the coefficient of variation (COV) of the results.

The results obtained from the FSCH test proved the ability of the DST device to provide repeatable and reliable measurements to the dynamic shear modulus and phase angle of asphalt mixes at only load frequencies ranged from 10 to 0.5 Hz. The results obtained at low frequencies have limited the DST due to a high variability. Table 3-9 summaries the FSCH test results for shear dynamic modulus and phase angle of the four mixes at 30°C. It can be observed from the table that the average values of the shear dynamic moduli of all mixes decreased as the load frequency decreased while the phase angle followed unclear trend with the load frequency. Moreover, the degrees of variation in the shear dynamic moduli of the dense graded mixtures (Mixes 1, 2 and 4) were generally lower than or close 10 % at load frequencies of 0.5 Hz to 10 Hz. Similarly, for these mixes, the COVs of the phase angle were low at load frequencies of 0.5 Hz to 10 Hz (Khajeh-Hosseini, 2015).

However, the COVs for the SMA mixture (Mixture 3) are relatively high for the shear dynamic modulus and the phase angle at all frequencies. The high variations of this mixture might be happened due to the difficulty in hand working and compacting of the SMA specimens comparing with the others of the dense graded mixes (Khajeh-Hosseini, 2015).

Table 3-9. FSCH Test Results of the original DST, Shear Dynamic Modulus and Phase Angle (Khajeh-Hosseini, 2015)

FSCH- Shear Dynamic Modulus |G*| (MPa) at 30°C											
Mixture #	Frequency	10	5	2	1	0.5	0.2	0.1	0.05	0.02	0.01
Mixture 1	Average	707.3	521.3	384.7	306.0	245.7	179.7	147.7	122.7	94.3	81.7
	COV %	4.3	3.4	4.6	6.5	7.7	11.2	15.0	19.1	24.8	30.8
Mixture 2	Average	1145.0	920.3	701.0	569.0	469.0	342.3	267.7	213.0	160.0	129.7
	COV %	6.4	7.0	7.8	8.4	8.7	10.0	10.7	11.7	13.8	15.5
Mixture 3	Average	802.7	622.7	455.3	375.7	306.3	225.0	180.3	147.3	111.7	92.7
	COV %	18.7	22.7	25.9	27.9	30.1	34.7	39.4	44.1	50.7	56.3
Mixture 4	Average	1099.0	848.3	621.3	481.0	386.3	288.7	232.7	195.3	156.0	138.3
	COV %	8.7	9.1	10.5	11.2	11.8	14.2	13.3	13.6	13.5	14.8
FSCH- Phase Angle (Degree) at 30°C											
Mixture #	Frequency	10	5	2	1	0.5	0.2	0.1	0.05	0.02	0.01
Mixture 1	Average	31.4	33.4	33.8	33.8	31.3	23.9	22.8	26.9	26.3	27.1
	COV %	1.4	1.5	2.9	3.9	7.9	8.9	11.9	9.8	11.6	13.5
Mixture 2	Average	24.4	26.2	27.9	29.1	27.8	21.7	21.9	27.0	27.2	29.1
	COV %	3.6	6.0	5.7	5.6	3.7	8.1	9.4	8.0	9.2	8.8
Mixture 3	Average	27.2	29.8	31.7	32.0	30.1	23.2	22.8	26.9	26.6	27.9
	COV %	12.5	11.9	12.2	13.5	9.3	21.6	23.9	19.5	20.6	20.1
Mixture 4	Average	26.4	29.3	31.3	32.8	31.8	23.8	22.8	26.6	25.4	26.0
	COV %	2.7	3.6	4.1	3.7	4.3	7.1	7.5	8.2	9.6	10.4

The results obtained from the RSCH test proved the ability of DST to measure the permanent shear deformation of asphalt concrete under cyclic loads. Table 3-10 summaries the average values and COVs of the measured permanent shear deformation of each mixes at 2,845 and 5,000 loading cycles at 50°C. It can be observed from the table that the average values of the permanent shear deformation of the dense graded mixes are close together whereas the SMA mix has the lowest average shear permanent deformation. This is because the SMA mixtures usually resist permanent deformation better than the dense graded mixtures. However, it is recommended to perform more than three permanent shear deformation tests for each mixture due to the mild variability that has been observed for each mixture (Khajeh-Hosseini, 2015).

Table 3-10. RSCH Test Results of the original DST, Shear Permanent Deformation (Khajeh-Hosseini, 2015)

RSCH- Shear Permanent Deformation (%) at 50 °C			
Mixture 1	Cycle	2,845	
	Average	0.8701	
	COV %	10.35	
Mixture 2	Cycle	2,845	5,000
	Average	0.8658	0.9777
	COV %	11.94	12.74
Mixture 3	Cycle	2,845	5,000
	Average	0.7512	0.822
	COV %	10.94	9.73
Mixture 4	Cycle	2,845	5,000
	Average	0.9448	1.0717
	COV %	9.02	9.4

Khajeh-Hosseini, (2015) has concluded that the device has proved its ability to provide repeatable measurements to the three shear parameters of asphalt concrete. However, the high variability of the measured shear dynamic modulus and phase angle at low load frequencies have limited the DST reliability. Therefore, it was recommended for further improvements for the DST device to improve the testing procedure and to reduce the tests variability.

Jweihan, (2018) was performed another study to assess the variability of the tests results obtained from the DST device. His study aimed for two objectives. The first objective was aimed to restrict the vertical movement of the DST middle plate during the tests only in the vertical direction. This was achieved by utilizing the mini linear guides system by which the DST supporting plate and middle aluminum plates were modified, as shown previously in Figure 3-27, and Figure 3-30, respectively. The second objective was aimed to assess the variability of the

results obtained with the improved device through conducting the two common Superpave Shear Tester (SST) tests: the FSCH and RSCH (Jweihan, 2018).

Two dense graded asphalt mixes were tested with the modified DST device. The test results proved the ability of the modified DST device to provide reliable measurements with relatively low coefficient of variations for the measured parameters. According to the FSCH tests results, the coefficient of variability of the measured shear dynamic modulus have increased from 10.2 % to 20.2% and from 7.5% to 23.5% for mixes Type-B and Type-D, respectively, with decreasing the shear load frequencies from 10 Hz to 0.01 Hz. Also, the measured phase angles have recorded general variability less than 11% of both mixes across all load frequencies. Table 3-11 summaries the FSCH test results for the shear dynamic modulus and phase angle obtained by the modified DST device at 30°C (Jweihan, 2018).

The results obtained from the RSCH tests have shown ability of the device to measure the shear permanent deformation of both mixes under cyclic shear loads with a coefficient of variation around 20%. Table 3-12 summaries the RSCH test results for the permanent shear deformation at 5,000 shear load cycles obtained by the modified DST device at 50 °C. Some of this variation, however, was justified to material variability because the mixes were sampled from the asphalt plant at different times. For each mix, sufficient amount of asphalt mix to fabricate six gyratory samples was obtained from a fully loaded asphalt truck leaving the plant. The process was repeated at 3-hour intervals (Jweihan, 2018).

Table 3-11. FSCH Test Results of the Modified DST, Shear Dynamic Modulus and Phase Angle (Jweihan, 2018).

FSCH- Shear Dynamic Modulus |G*| (Mpa) at 30°C											
Mixture	Frequency (Hz)	10	5	2	1	0.5	0.2	0.1	0.05	0.02	0.01
Type-B	Average	1168.14	813.71	549.71	386.14	299.57	195	137.86	103.71	65.57	43.86
	STD	119.63	97.46	70.32	53.74	42.02	29.19	22.15	17.17	11.82	8.87
	COV %	10.2	12	12.8	13.9	14	15	16.1	16.6	18	20.2
Type-D	Average	900.75	634.13	444.25	323	260.25	180.5	134.5	106.13	72	50.75
	STD	67.58	59.64	46.42	39.46	33.45	25.82	22.04	19.03	14.76	11.93
	COV %	7.5	9.4	10.4	12.2	12.9	14.3	16.4	17.9	20.5	23.5
FSCH- Phase Angle (Degree) at 30°C											
Mixture	Frequency (Hz)	10	5	2	1	0.5	0.2	0.1	0.05	0.02	0.01
Type-B	Average	26.8	33.24	36.88	40	39.81	35.92	34.46	38.4	39.32	41.66
	STD	2.81	1.54	1.8	1.82	1.45	1.49	1.5	1.34	1.39	1.19
	COV%	10.5	4.62	4.88	4.56	3.64	4.13	4.34	3.49	3.53	2.86
Type-D	Average	25.17	28.83	31.15	33.52	33.54	28.8	27.14	31.8	32.92	35.83
	STD	1.75	1.93	2.18	2.45	2.59	2.79	2.95	2.82	2.87	2.91
	COV%	6.96	6.7	7.01	7.3	7.73	9.67	10.87	8.86	8.73	8.12

Table 3-12. RSCH test results of the Modified DST, Shear Permanent Deformation (Jweihan, 2018).

RSCH- Shear Permanent Deformation (%) at 50°C		
Mix-B	Average	0.72
	Standard Deviation	0.14
	COV%	19.64
Mix-D	Average	0.53
	Standard Deviation	0.11
	COV%	20.86

Jweihan, (2018) has concluded that the modified DST has successfully satisfied the objectives of a new reliable and simple test device. The device can be adopted as a simple performance test equipment for quality control procedure to measure the fundamental shear properties of asphalt mixes at low cost. Also, the test results can be utilized as inputs to develop prediction models to enhance the pavement performance for rutting resistance. Even though the modified DST has successfully satisfied the objectives of a new inexpensive and simple test device, further modifications are recommended to simplify and improve the testing procedure by making the device lighter in weight and able to accommodate other shapes of the test specimens.

Chapter 4: DST Modifications and STNS Development

As discussed in Chapter 1, this study is aimed at assessing the tests variability obtained by the DST device under different conditions for other specimen shapes of asphalt concrete mixes. Also, it is aimed to develop a new device able to measure the shear properties of asphalt concrete while a normal stress is applied at the same time. This chapter discusses in detail the main modifications to the DST device, and the development of the new device called the "Shear Tester with Normal Stress (STNS)".

4.1 Modifications to the DST device

The DST device loads two identical asphalt specimens of 50mm (1.97″) height and 150 mm (5.906″) diameter, that are glued to an aluminum plate in the middle and to steel plates on the sides. The steel plates are fixed and tightened firmly together by threated rods and adjustable nuts to maintain the specimens' height constant during the test. An original DST sample used to weight around 20.0 kg (44 lb) with side plates of (10″ width, 10″ height and 0.5″ thick).

In this study, the dimensions of all side plate were modified to (10″ height, 8″ width, and 0.5″ thick). Also, the plates were made of aluminum instead of steel. These little modifications reduce the average weight of the DST sample of 150 diameter specimens to around 10.0 kg (22 lb). Figure 4-1 shows the modified DST device. Its main parts are:

- Two identical asphalt concrete specimens.
- Two aluminum side-plates (10″ ×8″ × 0.5″).
- One aluminum middle- plate (7″ × 6.5″× 0.75″).
- Supporting Plate (15″×12″×0.5″) with two bolts of (3/4″-16, 1.5″ long).

- Two Mini-linear rail systems (12mm- standard) with one rail segment attached to each side of the middle plate (6.0″ long), and two carriages attached to each side of the vertical stands of the supporting plate.
- Four steel threaded rods (1/2″-13, 8.5″ long) and fourteen nuts (1/2″-13).
- Two steel grippers with four (3/8″-16) bolts.

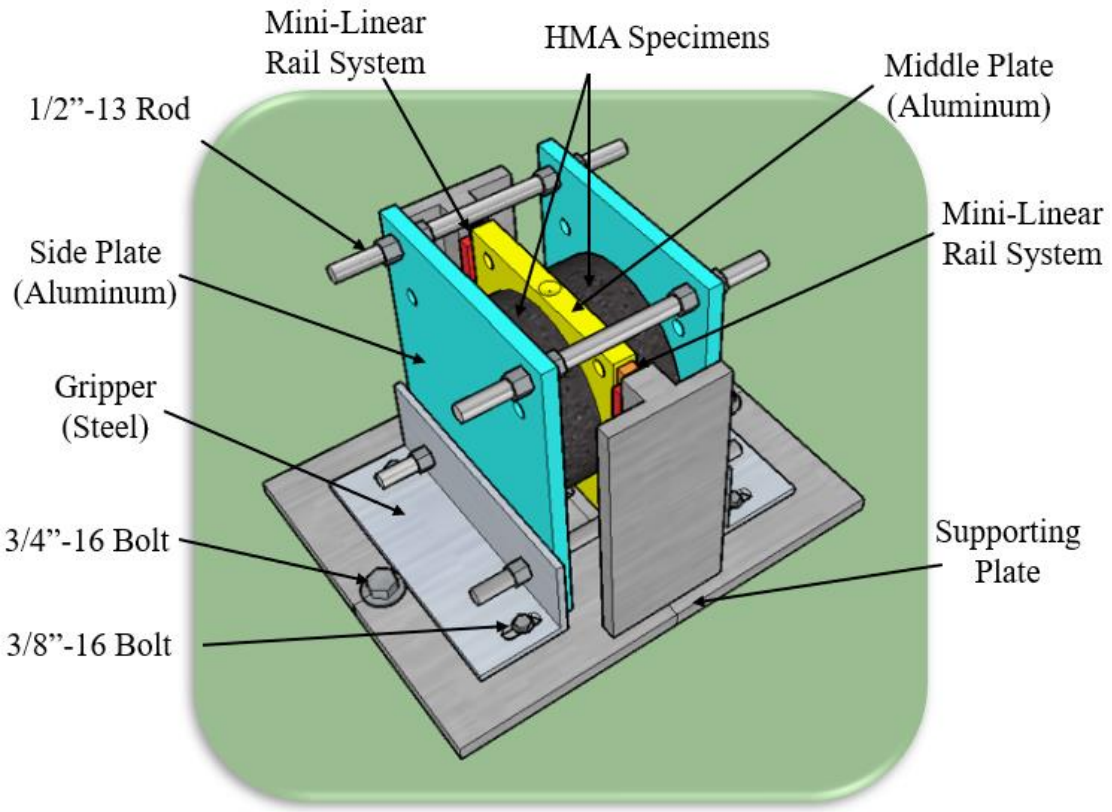

Figure 4-1. Diagram of the DST device.

In addition, DST samples of different shapes can be tested. They include asphalt concrete specimens of 150 mm (5.906″) diameter, 99.06 mm (3.9″) diameter, and rectangular specimens of 125 mm ×75 mm (4.92″ ×2.95″). To simplify the discussion in this research, the diameter size of all specimens was rounded up conventionally, and the specimens' shapes were abbreviated. The notations C6 and C4 indicate for circular specimens with 6.0″ and 4.0″ diameters, respectively.

RH and RV indicate for rectangular specimens cut from horizontal or vertical slices, respectively. The C4 specimens were “drilled core” specimens extracted from the C6 specimens, whereas the rectangular specimens have two different configurations of cutting. The horizontal slices were cut in a way to be sheared perpendicularly to the direction of compaction. The vertical slices were cut to be sheared in the same direction as the compaction. Figure 4-2 illustrates the differences between the shapes of DST samples. The average weights of the DST samples, including the plates and threaded rods with nuts, is about 8.0 kg (17.5 lb) for RH/RV samples and 7.5 kg (16.5 lb) for C4 samples.

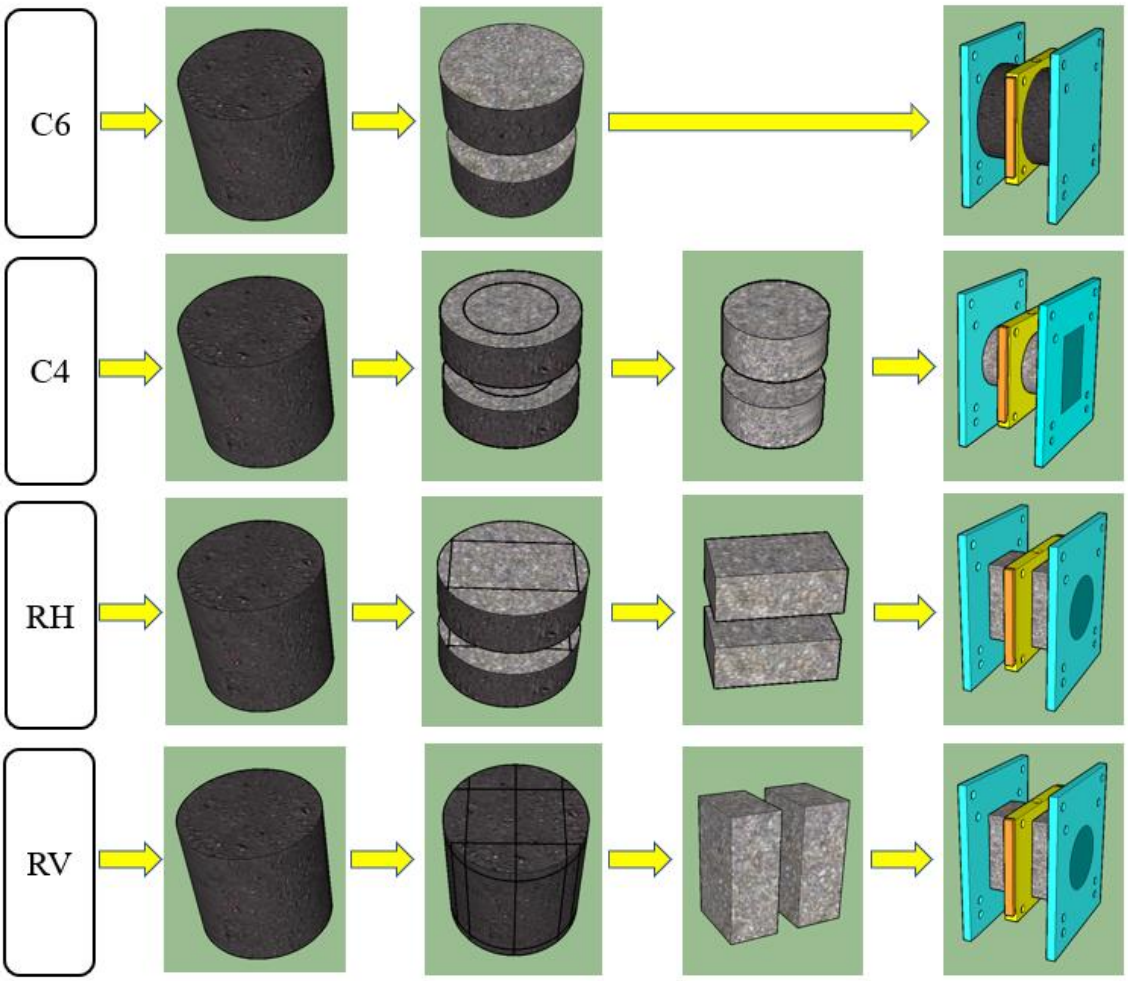

Figure 4-2. The difference between the DST samples.

New sets of aluminum plates for the three DST sample's shapes were fabricated. Each set of the plates can make a group of eight DST samples. Since a DST sample consists of one middle plate and two side plates, sixteen identical side plates and eight middle plates were fabricated for each shape. However, in order to save material and cost, one set of the sixteen side plates was designed to be used for the rectangular and small diameter shapes; one shape at each side of the plates.

The plates have 1/16" depressions match the specimen shape. These depressions were used to contain an epoxy paste of (Devcon™ Plastic Steel Putty (A)) where the specimen should be glued at the center of the plates, as shown in Figure 4-2. The plates of C6 samples have a depression of 5.875″ diameter tapered to 6.0″ at center. Similarly, the plates for both rectangular shapes and C4 samples have a depression of 5.0″× 3.0″ and 4.0″ tapered to 4.1″ diameter, respectively. All DST middle plates have two identical depressions for each DST sample shape at their two sides. The drawings of the DST parts are shown in Appendix A.

In this study, two loading attachments were used to perform the RSCH and FSCH tests. The same attachment used previously by Khajeh-Hosseini, (2015) and Jweihan, (2018) for the RSCH tests was used again in this study. That attachment, shown previously in Figure 3-31, is able to apply repeated shear loads in the downward direction. It is screwed into the UTM actuator from the upper side. It touches the depression of the DST middle plate at center from the lower side.

Regarding the loading attachment of the FSCH tests, Khajeh-Hosseini, (2015) and Jweihan, (2018) used the coupling attachment to perform the FSCH tests. As shown in Figure 3-32, it consists of two pieces and a pin. Its installation was required to line up the two pieces together precisely by adjusting the elevation of the UTM loading table to a point where the

holes of two pieces match. Then the pin was inserted, and the upper nut was tightened the coupling. This complicates the test setup especially that loading table of the UTM machine should be moved up slowly and precisely. Therefore, it was decided to replace the coupling with another attachment that is simpler and easier to install.

The new loading attachment, shown in Figure 4-3(b) consists of two cups are welded together to form a one-unit attachment. Cup 1 includes a 4.0″ long bolt, adjustable nut and washer. The bolt can be moved freely inside the attachment cylinder so that it can be screwed up inside the UTM actuator. It has a small hole of 1/4″ diameter to make the screwing process fast and easy by using a regular screwdriver or pin. Cup 2, on the other hand, consists of a 2.0″ long bolt that is welded to the bottom of Cup 2 at center. This bolt was designed to be screwed down inside a middle plate of DST sample. The drawings of the attachment components are shown in Appendix A.

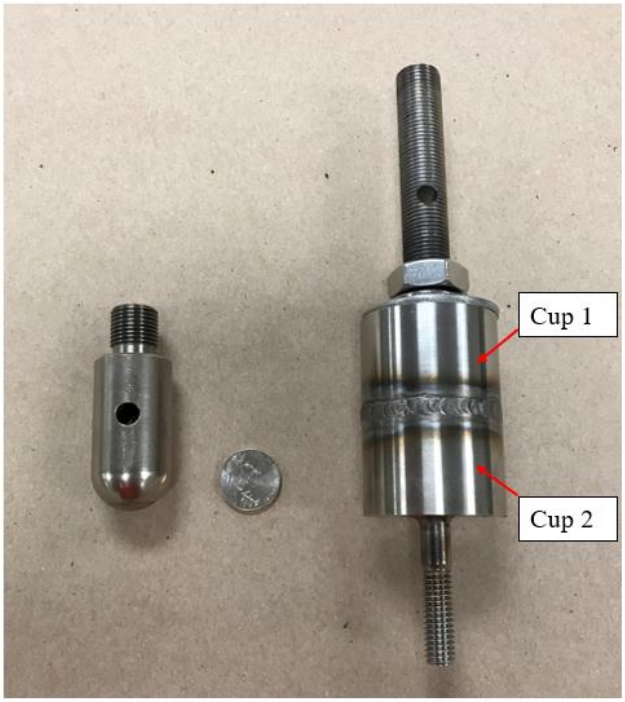

Figure 4-3. The RSCH and FSCH loading attachments.

The new FSCH attachment has a simple installation procedure. After the DST sample is installed and fixed inside the supporting plate on the UTM loading table, the short bolt of the Cup 2 is screwed down inside the middle plate of the DST device by rotating down the whole attachment. Then, the loading table is moved up so that the long bolt of Cup 1 can be screwed up for almost 3/4″ inside the UTM actuator. A regular screwdriver or pin is then inserted temporarily inside the hole of the long bolt to rotate up the bolt inside the actuator ram. Once the head of the bolt, which is hidden inside the Cup 1, is reaches the upper end of the Cup 1, the adjustable nut was tighten down over the attachment. After that, the whole DST device becomes connected to the UTM actuator and the frequent shear loads can be launched. It is preferable to apply a regular "Teflon tape" at the top and bottom threads of the attachment to improve the threads sealability with the UTM actuator and DST middle plate.

Further, a new modification to the original LVDTs holders was done in this study to utilize the current LVDT mounts. As discussed previously, two LVDT mounts were installed on the DST sample to hold the axial LVDTs at equal distances from the center of the DST middle plate. Since the dimensions of the DST plates were minimized in this study, the available room for accommodating the original LVDT holders of (2.5″ long) along with the loading attachments was jammed. Therefore, it was necessary to reduce the length of the LVDT holders to 1.75″.

In this study, an LVDT mount consists of an aluminum LVDT holder, two pairs of steel clamps, a threaded rod (3/8″-16, 8.5″ long), and four nuts (3/8″-16). As shown in Figure 4-4, the steel clamps along with the LVDT holder and adjustable nuts are fixed on the threaded rod. The LVDT holder was designed to accommodate one axial LVDT. It was designed with two different diameters to hold axial LVDTs of 0.315″ diameter of (+/- 0.5 mm span) for the FSCH tests and 0.370″ diameter of (+/- 5.0 mm span) for the RSCH tests. A small adjustable bolt of (#8-32) on

the top of each LVDT holder was used to control its location while the installation. The drawings of the new LVDT holder and clamps are shown in Appendix A.

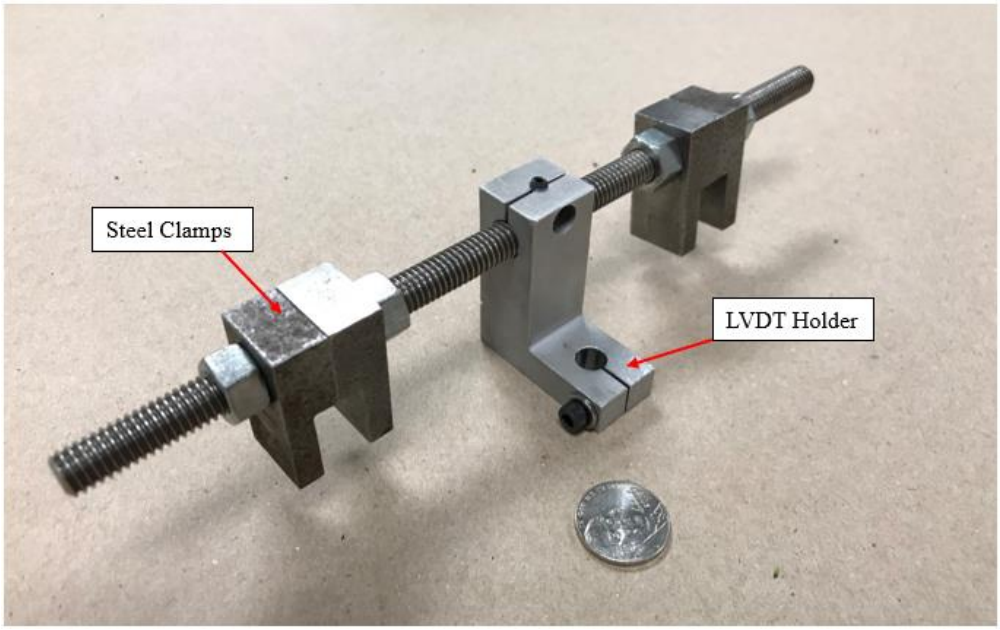

Figure 4-4. The LVDT mount with the new holder- DST device.

4.2 Development of the STNS device

The STNS device is designed to test only one specimen of asphalt concrete. The specimen has the same dimensions as C6. An STNS sample is prepared by sandwiching the specimen between two steel plates using the epoxy paste (Devcon™ Plastic Steel Putty (A)). The first plate is a base plate with a 7″ width, 7″ length, and 0.5″ thick, while the second plate is a middle plate of the STNS device with a 7″ width, 6.5″ length, and 0.75″ thick. Both plates, however, have a 1/16” depression of 5.875″ diameter tapered to 6.0″ at one side only, while the other sides are smooth and without depressions. The average weight of an STNS sample is about 9.0 Kg (20 lb) including the steel plates.

Some new components were utilized for the STNS device. They include Air cylinders, Ball bearing Parallels, and Pillow Block Bearing. As shown in Figure 4-5, the device setup consists of two parallel steel plates at sides, and two steel grippers that are attached to the lower part of the side plates. The side plates along with the grippers are connected together to make the rigid frame setup of the STNS device by using four threaded steel rods (1/2″-13, 9.25″ long) and adjustable nuts (1/2"-13). An STNS asphalt concrete sample is mounted in the device by sliding the linear rail segments of the middle plate inside the mini carriages of the DST supporting plate. The sample base plate is then fixed to the device side plate (A) by using two 1/2″-13, 1.75″ long bolts and adjustable nuts (1/2"-13).

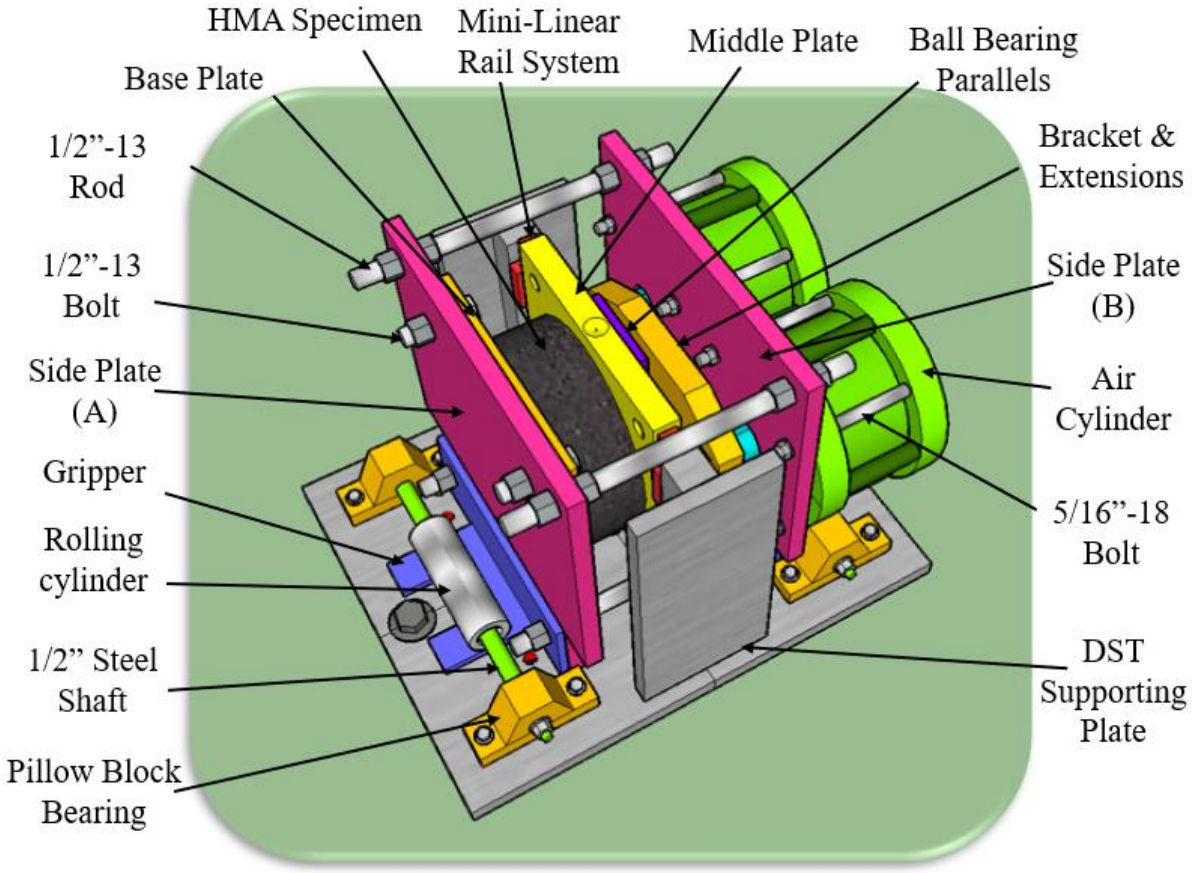

Figure 4-5. Diagram of the STNS device.

Two Air cylinders of (4.0″ bore diameter and 1.5″ stroke) were mounted on the side-plate (B) by using eight bolts of (5/16″-18, 5.0″ long) and their associated nuts. The Air cylinders are manufactured by “Bimba” company (part number FOS-1251.5). A flat steel bracket was designed to connect the piston rods of the air cylinders. Two extension steel cylinders 1.0″ long were also designed to extend the piston rods of the air cylinders. The bracket along with the extension cylinders are screwed to the piston rods of the air cylinders by using two identical bolts of (3/4″-16, 2.5″ long), as shown in Figure 4-6.

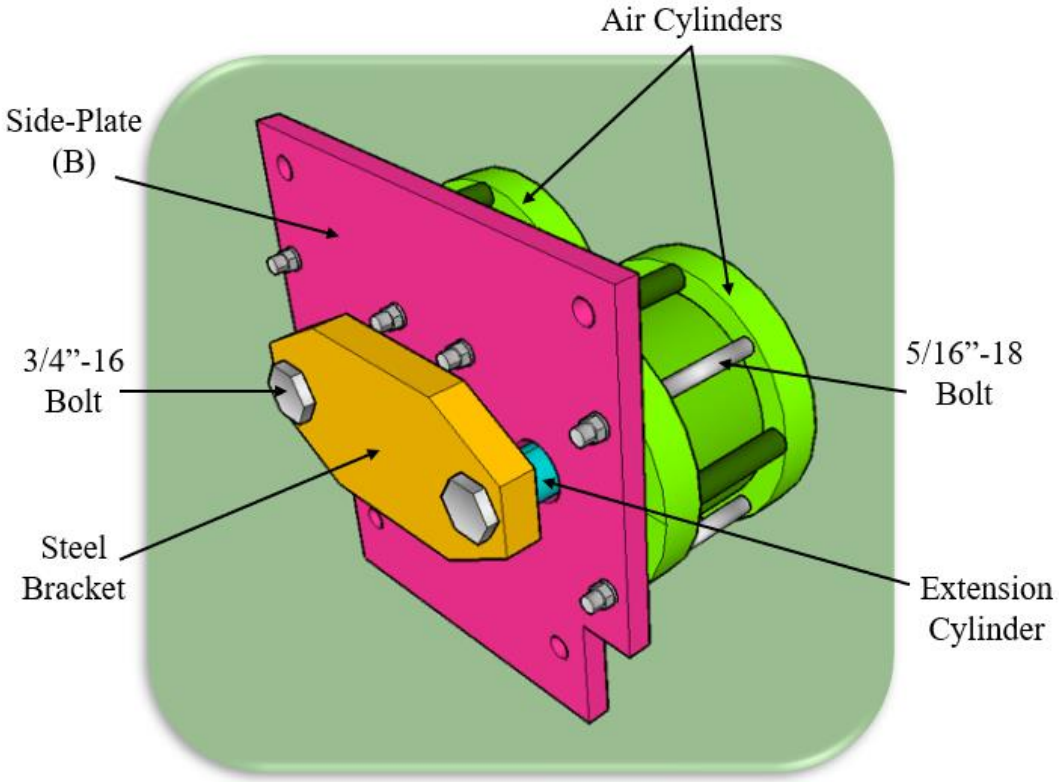

Figure 4-6. Diagram of the side plate (B) with the Air cylinders setup.

Two rolling systems were used to allow the rigid frame setup for free lateral movements while the tests. Each system consists of two standard pillow block bearings of (1/2″ bore diameter), a steel shaft of (1/2″ diameter, 10″ long), and two rolling steel cylinders of (1.25″ diameter, 4.0″

long, 0.25″ thick). The rolling systems were fixed on the DST supporting plate such that the rolling cylinders are located exactly over the center of the grippers legs.

The rolling systems, however, were designed so that the grippers legs can slide laterally with no vertical movements while shearing the asphalt concrete sample. The space between the rolling systems and the underlaying legs of the grippers were tight enough to allow only for the lateral movements. Consequently, it was required to adjust the distance between the “Mounting Surface to the Shaft Center” of the “pillow block bearings” parts to 3/4" instead of the standard distance of 1.0″. This was achieved by shaving a quarter of inch (1/4”) at their bottom. The drawings of the DST parts are shown in Appendix B.

A standard ball bearing parallel of (2.5″ width, 6.0″ long, 0.25″ thick) was used to allow the middle plate for the vertical movements while applying the normal stress. It has very smooth balls of steel of (3/8″ diameter and 3,000 lb load capacity) that slide easily on the smooth face of the device middle plate with no friction. The ball bearing tool was suspended vertically between the middle plate and the steel bracket by using two regular rubber bands attached to the upper threaded rods of the STNS frame.

Similar to the DST tests procedure, loading attachments and LVDT mounts were used to perform the STNS tests. The same loading attachments used for the DST device to perform the RSCH and FSCH tests were used to perform the RSNS and FSNS tests, respectively. The attachments were shown previously in Figure 4-3. New LVDT mounts were designed only for the STNS device. Each mount consists of two parts: an LVDT holder and an ordinary C-clamp of (1.0″ max. opening). The two parts were glued together by using “J-B Weld” epoxy, as shown in Figure 4-7.

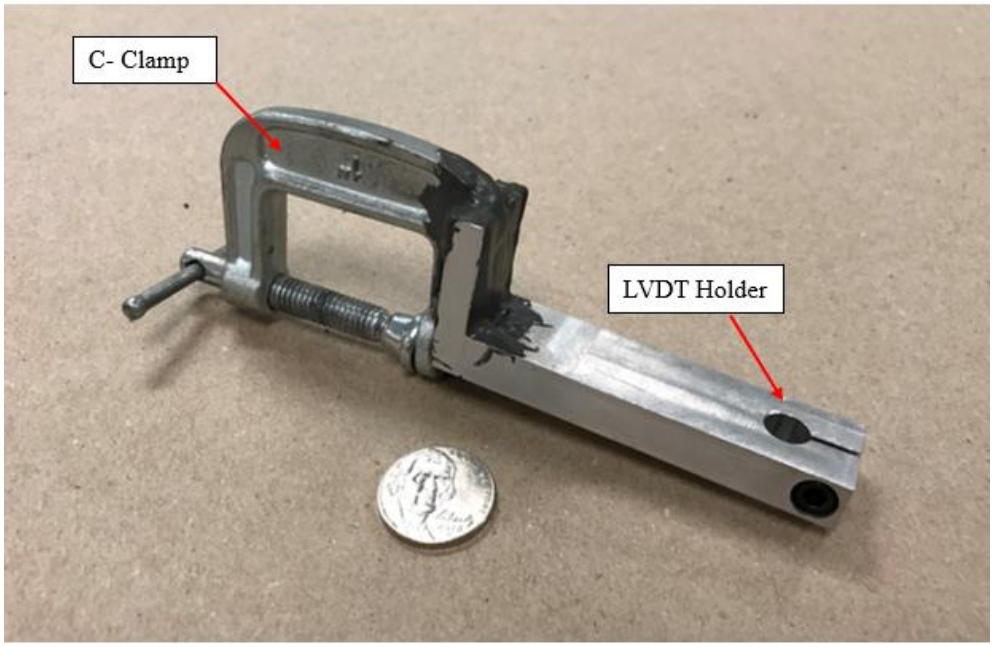

Figure 4-7. The LVDT Mount - SNTS Device.

Two of these mounts were installed on the STNS device to measure the relative vertical displacements between the sample middle and the device side plates while shearing the sample. The mounts were installed firmly on the side plate (A) by gripping the C-clamps at equal distances in related to the center of the STNS middle plate. As for the FSCH and RSCH tests, these LVDT holders were designed with two different diameters to hold axial LVDTs: 0.315″ diameter (+/- 0.5 mm span) for the FSNS tests and 0.370″ diameter (+/- 5.0 mm span) for the RSNS tests. The drawing of the LVDT holder is shown in Appendix B.

4.2.1 The Concept and Loading Condition of the STNS device

The STNS is a compact device able to shear an asphalt concrete specimen while applying an additional normal stress to the specimen at the same time. Even though the STNS is designed to be installed inside the UTM-25 testing system, its' concept and loading condition are different than that of the DST. In this device, an asphalt concrete specimen is sheared in the vertical direction

by the UTM-25 actuator. While an air pressure is applied by the UTM-25 pneumatic system to apply a normal load on the specimen. Figure 4-8 illustrates the air pressure circuit from the UTM-25 pneumatic system to the STNS air cylinders.

The laboratory building is supplied with compressed air pressure of 100 psi maximum. An air valve inside the laboratory is connected with the pneumatic system of the UTM-25 testing machine. The pneumatic system consists of two air filters, an air tank, and a pneumatic valve. The air flows from the laboratory air valve to the air filters fixed to be cleaned from dusts or contaminants materials. Then, the air flows through the air tank to be confined before it passes through the pneumatic valve. The pneumatic valve is used to control the amount of air pressure flows to the UTM-25 chamber. An air pressure sensor inside the UTM-25 chamber connected directly with the CDAS is used to control and record the air pressure during the STNS tests.

The STNS loading conditions are illustrated in Figure 4-9. First, a shear force is applied by the UTM-25 actuator on the middle plate of an STNS asphalt concrete specimen, and an initial pressure is applied into the air cylinders, as illustrated in Step (1). The pressure then extends the pistons of the air cylinders toward the middle plate. As a result, the applied pressure is transmitted from the flat bracket to the middle plate throughout the steel balls of the suspended “ball bearing parallel” tool, as illustrated in Step (2). Since the middle plate can only move vertically inside the guides system of the supporting plate, a reaction force acts directly onto the side-plate (B), as illustrated in Step (3). Since the device has a rigid frame setup and the two side plates are connected together by four threaded rods, the reacted forces transmit through the threaded rods to the side plate (A). In this way, the transmitted forces act directly onto the asphalt specimen inducing a normal stress to the specimen, as illustrated in Step (4).

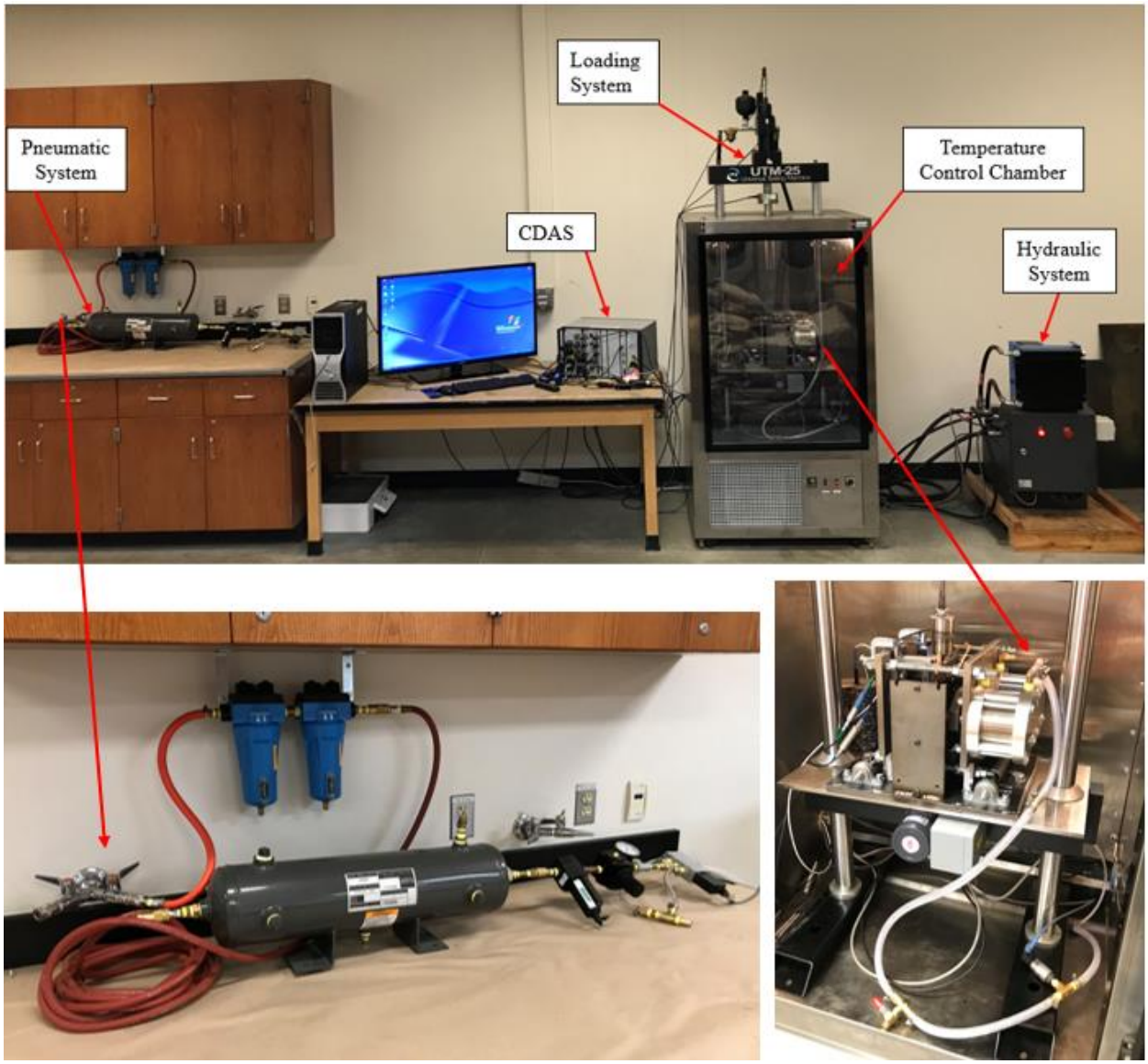

Figure 4-8. The air pressure circuit for the STNS air cylinders.

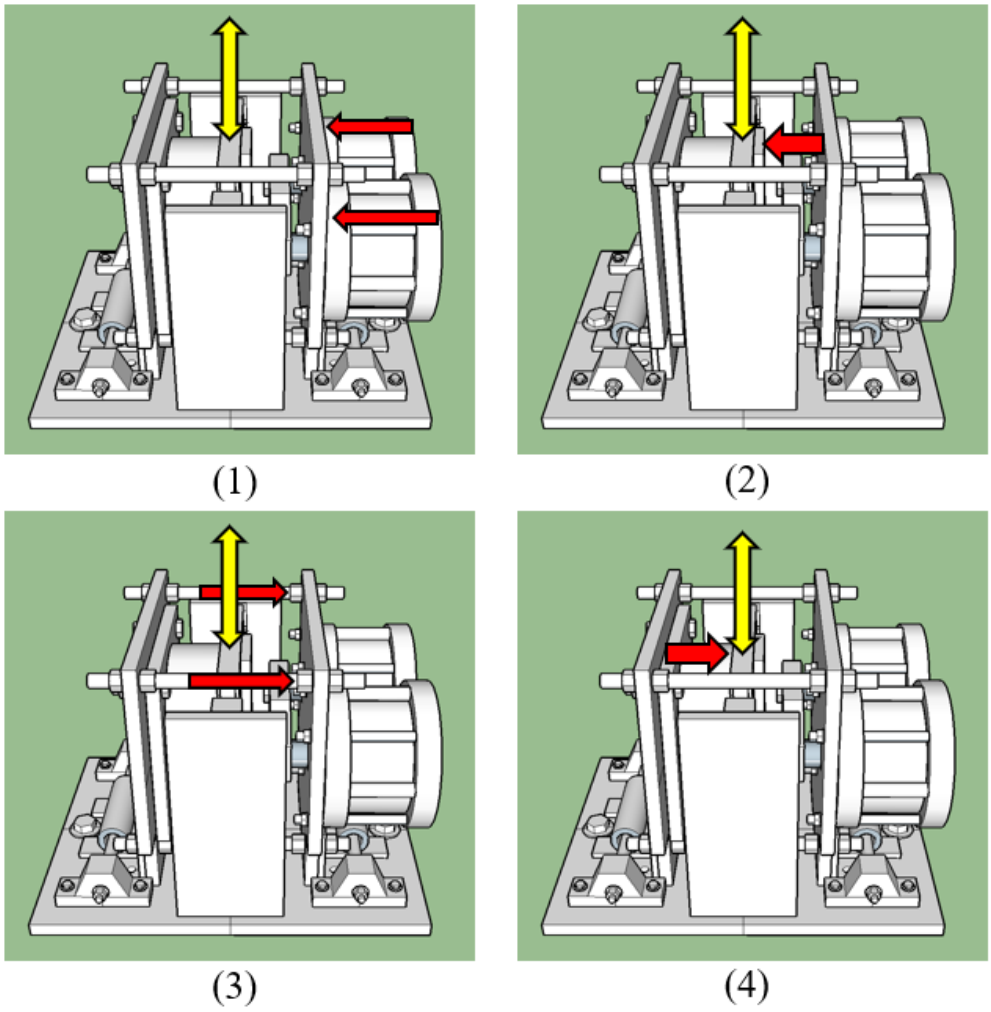

Figure 4-9. Illustration to the loading concept of the STNS device.

A lubricant grease is used to eliminate any potential friction between the STNS parts while the movements. Since the tested specimen of asphalt concrete has a surface area different from the total internal area of the air cylinders, the final pressure (P_f) applied on the specimen will not be the same as the pressure (P_i) in the air circuit. Equation (4-1) calculates the pressure applied on the specimen. In this equation, the friction between the STNS parts is negligible due to the use of lubricant material. The pressure (P_f) transmitted to the specimen is 91.7% of the pressure inside the air cylinders (P_i).

$$P_f = \frac{F}{A'} = \frac{8\,P_i}{8.72} = 91.7\ \%\ Pi \qquad (4\text{-}1)$$

Where,

P_i: Inisial pressure in the air circuit,

P_f: Final pressure applied on the specimen,

A: Total internal area of two air cylinder $= 2 \times \pi r^2 = 8\pi$

F: Acting force $= A \times Pi = 8\pi\ Pi$

A': Area of the specimen $= \pi r^2 = 8.72\pi$

Chapter 5: Materials and Testing Methods

In this chapter, the methodologies of the experimental work are discussed in detail. They include seven steps that were performed in sequences in the laboratory after collecting asphalt mixes from the asphalt plant. Figure 5-1 shows the steps followed in this study.

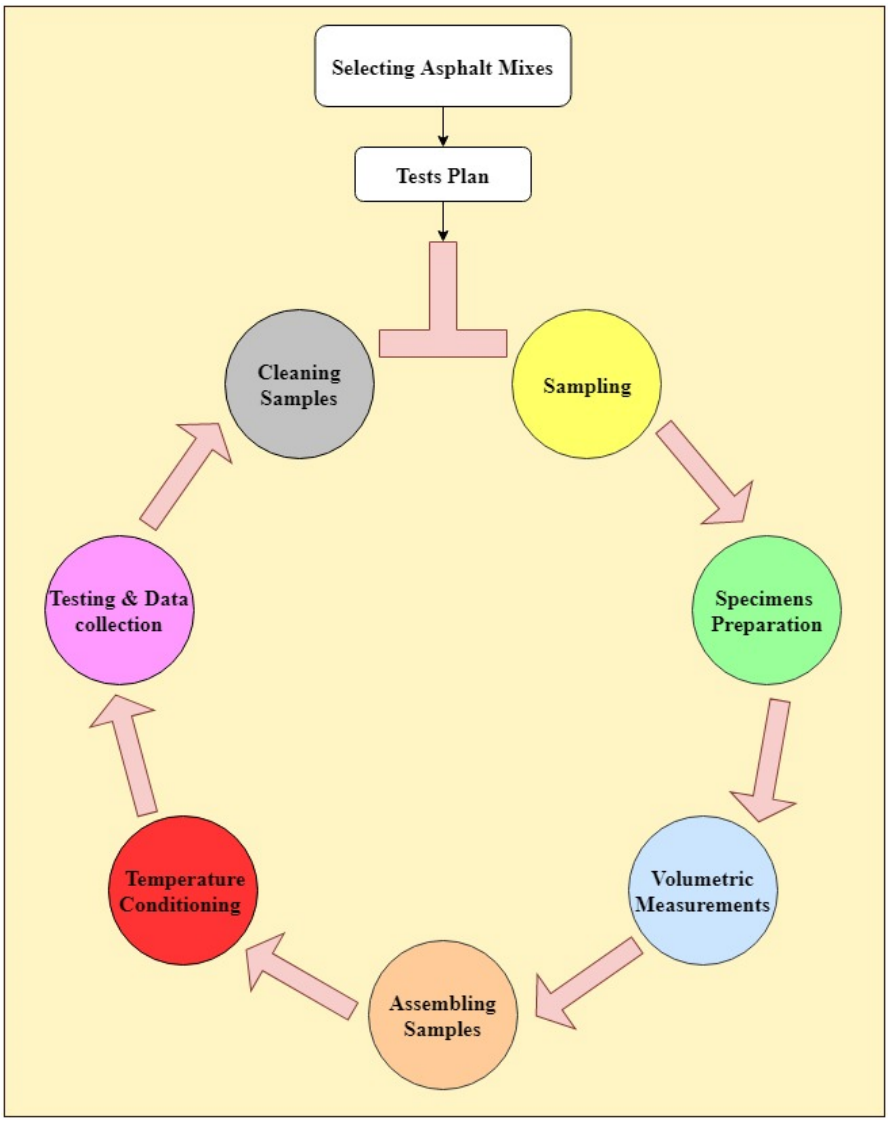

Figure 5-1. Testing Methods of This Study.

5.1 Selecting Asphalt Mixes

Two common types of asphalt mixes are usually used in Texas for paving fixable pavements: the dense graded conventional mixes (DG), and Superpave asphalt mixes (SP). The DG mixes are well-graded HMA mixtures that have a gradual gradation from course to fine aggregates. According to the TxDOT-340 and 341 specifications, the dense graded mixes are classified in five different types (A, B, C, D, and F) based on the maximum sieve size and the intended use of each mixture within the pavement layers, as shown in Table 5-1.

Table 5-1. Master Gradation Limits (% passing by weight or volume) of the Dense Graded (DG) Asphalt Mixes (TxDOT-340 and 341, 2015).

Sieve Size	A	B	C	D	F
	Coarse Base	Fine Base	Coarse Surface	Fine Surface	Fine Mixture
2″	100.0*				
1-1/2″	98.0–100.0	100.0*			
1″	78.0–94.0	98.0–100.0	100.0*		
3/4″	64.0–85.0	84.0–98.0	95.0–100.0	100.0*	
1/2″	50.0–70.0	–	–	98.0–100.0	100.0*
3/8″	–	60.0–80.0	70.0–85.0	85.0–100.0	98.0–100.0
#4	30.0–50.0	40.0–60.0	43.0–63.0	50.0–70.0	70.0–90.0
#8	22.0–36.0	29.0–43.0	32.0–44.0	35.0–46.0	38.0–48.0
#30	8.0–23.0	13.0–28.0	14.0–28.0	15.0–29.0	12.0–27.0
#50	3.0–19.0	6.0–20.0	7.0–21.0	7.0–20.0	6.0–19.0
#200	2.0–7.0	2.0–7.0	2.0–7.0	2.0–7.0	2.0–7.0
* Defined as maximum sieve size. No tolerance allowed.					

The Superpave mixes (SP) are products of the Superpave mix design method. They have different aggregate gradation limits than the dense graded mixes. According to the TxDOT-344 specification, the SP mixes are classified for four different types (SP-A, SP-B, SP-C, and SP-D)

based on the maximum sieve size and the intended use of each mixture within the pavement layers, as shown in Table 5-2.

Table 5-2. Master Gradation Limits (% passing by weight or volume) of the Superpave (SP) Asphalt Mixes (TxDOT-344, 2015).

Sieve Size	SP-A Base	SP-B Intermediate	SP-C Surface	SP-D Fine Mixture
2″	100*			
1-1/2″	98.0–100.0	100*		
1″	90.0–100.0	98.0–100.0	100.0*	
3/4″	Note 2	90.0–100.0	98.0–100.0	100.0*
1/2″	–	Note 2	90.0–100.0	98.0–100.0
3/8″	–	–	Note 2	90.0–100.0
#4	19.0–90.0	23.0–90.0	28.0–90.0	32.0–90.0
#8	19.0–45.0	23.0–49.0	28.0–58.0	32.0–67.0
#16	1.0–45.0	2.0–49.0	2.0–58.0	2.0–67.0
#30	1.0–45.0	2.0–49.0	2.0–58.0	2.0–67.0
#50	1.0–45.0	2.0–49.0	2.0–58.0	2.0–67.0
#200	1.0–7.0	2.0–8.0	2.0–10.0	2.0–10.0
* Defined as maximum sieve size. No tolerance allowed.				
Note 2: Must retain at least 10% cumulative.				

In this study, three asphalt mixes were selected: the SP-Type D, SP-Type C, and DG-Type B. The asphalt mixes D and C were selected because they are used for surface layers where rutting usually occurs. The asphalt mix B was selected to assess both devices for measuring the shear properties of asphalt mixes that contain coarse aggregates with a large aggregate size. All mixes were obtained from the “Austin Bridge and Road” asphalt plants, located in Dallas and Fort Worth, Texas. Figure 5-2 shows aggregates size for the three asphalt mixes.

Figure 5-2. Asphalt concrete specimens of the three selected mixes.

The mix design data of both mixes are shown in Appendix E. Table 5-3, 5-4, and 5-5 present the summary of asphalt mixes components of mixes D, C, and B, respectively. The gradation curves of all mixes in order are given in Figure 5-3, 5-4 and 5-5.

Table 5-3. Mix design summary of asphalt mix D

SP-Type D						
Aggregate	Bin No.	1	2	8	9	Total Bin
	Aggregate Source	Limestone-Dolomite	Limestone-Dolomite	Fractionated RAP	RAS	Total
	Percent of Aggregates (%)	56.0	26.4	15.0	2.6	100.0
	in / #	Cumulative Passing (%)				
	3/4"	100.0	100.0	100.0	100.0	**100.0**
	1/2"	100.0	100.0	100.0	100.0	**100.0**
	3/8"	96.0	100.0	96.5	100.0	**97.2**
	#4	45.0	99.3	66.3	100.0	**64.0**
	#8	6.6	87.7	43.6	98.7	**36.0**
	#16	4.4	59.7	35.0	80.0	**25.6**
	#30	2.3	44.5	27.7	62.0	**18.8**
	#50	1.3	23.6	22.8	53.5	**11.8**
	#200	1.1	4.2	7.0	21.7	**3.3**
Asphalt Binder	Substance	Percent (%)	Source & Grade			
	New	5.3	Hunt PG 64-22			
	Recycled	0.8	RAP			
		0.6	RAS			
Additive	Antistripping Agent	0.5	Evotherm			

Table 5-4. Mix design summary of asphalt mix C

SP-Type C							
Aggregate	Bin No.	1	2	3	8	9	Total Bin
	Aggregate Source	Limestone-Dolomite	Limestone-Dolomite	Limestone-Dolomite	Fractionated RAP	RAS	Total
	Percent of Aggregates (%)	27.0	30.3	26.0	15.0	1.7	100.0
	in / #	Cumulative Passing (%)					
	1"	100	100	100	100	100	100.0
	3/4"	100.0	100.0	100.0	100.0	100.0	100.0
	1/2"	74.7	100.0	100.0	100.0	100.0	93.2
	3/8"	41.6	96.0	100.0	100.0	100.0	83.0
	#4	5.0	45.0	99.3	66.3	100.0	52.4
	#8	1.9	6.6	87.7	43.6	98.7	33.5
	#16	1.1	4.4	59.7	35.0	80.0	23.8
	#30	1.1	2.3	44.5	27.7	62.0	17.8
	#50	1.1	1.3	23.6	22.8	53.5	11.2
	#200	1.1	1.1	4.2	7.0	21.7	3.1
Asphalt Binder	Substance	Percent (%)	Source & Grade				
	New	4.7	Hunt PG 64-22				
	Recycled	0.8	RAP				
		0.4	RAS				
Additive	Antistripping Agent	0.5	Evotherm				

Table 5-5. Mix design summary of asphalt mix B

DG- Type B						
Aggregate	Bin No.	1	2	3	8	Total Bin
	Aggregate Source	Limestone-Dolomite	Limestone-Dolomite	Limestone-Dolomite	Fractionated RAP	Total
	Percent of Aggregates (%)	30.0	16.0	29.2	24.8	100.0
	in / #	Cumulative Passing (%)				
	1-1/2"	100.0	100.0	100.0	100.0	100.0
	1"	97.0	100.0	100.0	100.0	99.3
	3/4"	70.0	100.0	100.0	100.0	92.8
	3/8"	21.0	96.0	100.0	96.5	79.2
	#4	5.0	37.0	99.0	66.3	55.4
	#8	2.0	3.0	85.0	43.6	37.9
	#30	1.4	1.5	40.0	27.7	20.1
	#50	1.3	1.3	27.0	22.8	14.9
	#200	1.0	1.1	5.0	7.0	3.9
Asphalt Binder	Substance	Percent (%)	Source & Grade			
	New	4.6	Hunt PG 64-22			
	Recycled	1.5	RAP			
		0.0	RAS			
Additive	Antistripping Agent	0.5	Evotherm M1/3G			

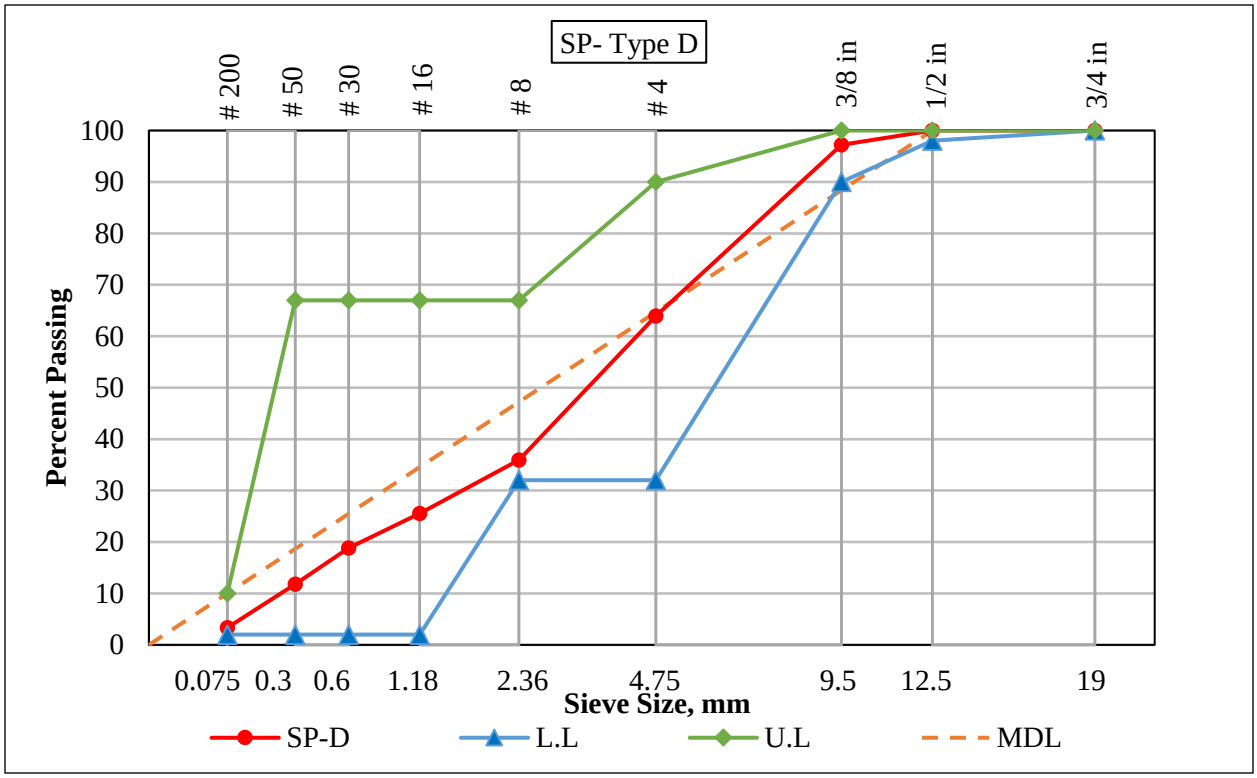

Figure 5-3. Gradation chart of asphalt mix D.

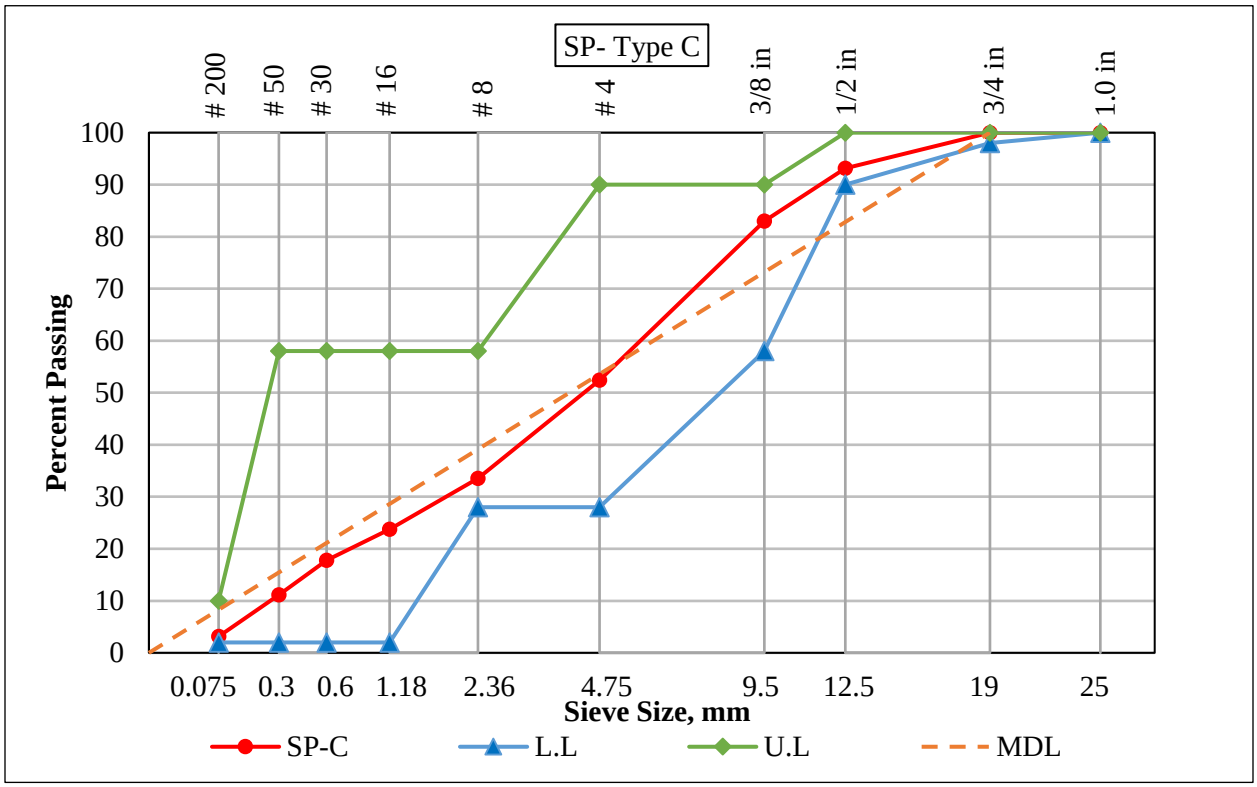

Figure 5-4. Gradation chart of asphalt mix C.

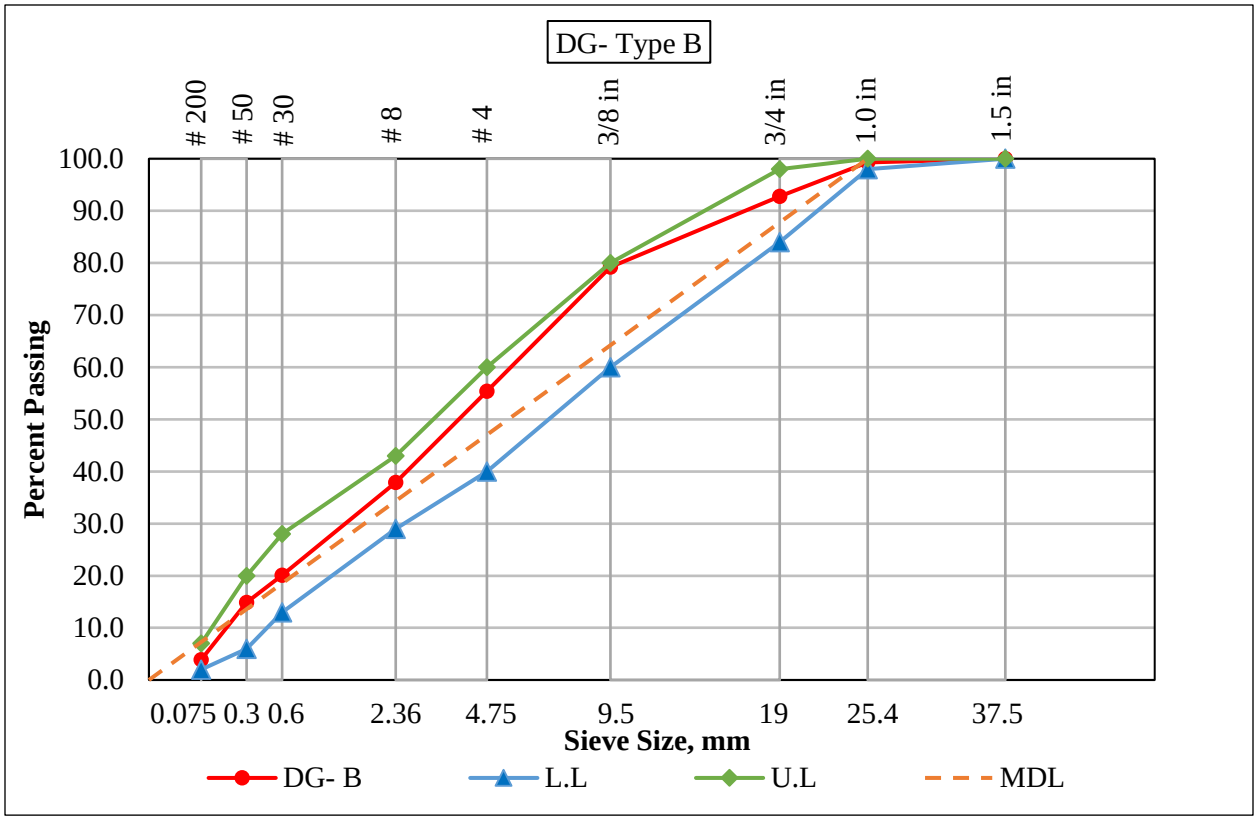

Figure 5-5. Gradation chart of asphalt mix B.

5.2 Tests Plan

This research aims to assess the variability of testing asphalt mixes by varying the daily productions of asphalt mixes and changing the geometry of asphalt concrete specimens that are tested on both devices (DST and STNS). Therefore, the tests plan of this research was divided into two parts of testing groups. The first part includes testing asphalt concrete mixes collected from the asphalt plant at three different intervals of daily productions (at morning, noon, and after noon). The testing specimens of this part had the C6 samples of 150 mm diameter and 50 mm height. Also, they were tested in both devices test temperatures 30ºC and 50ºC for the frequency sweep tests (FSCH &FSNS) and repeated shear tests (RECH & RSNS), respectively. Figure 5-6 illustrates the first part of testing groups.

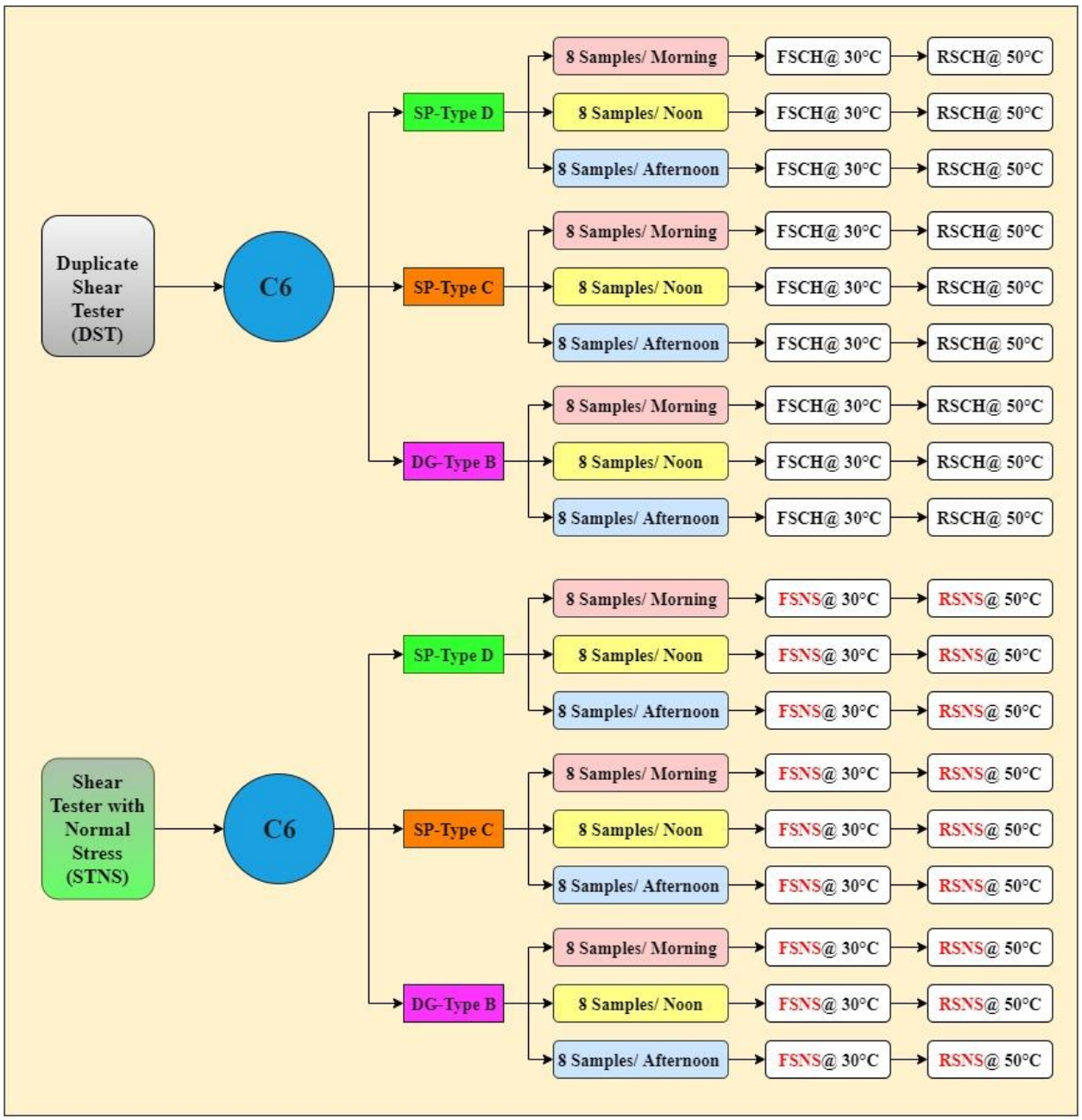

Figure 5-6. The first part of testing groups

The second part of testing groups includes testing of asphalt concrete specimens of different shapes only with the DST device. All specimens in this part were made from mixes collected at noon time. They included the C4, RH, and RV samples. All specimens were also tested at test

temperatures 30ºC and 50ºC for the FSCH and RECH tests, respectively. Figure 5-7 illustrates the second part of testing groups.

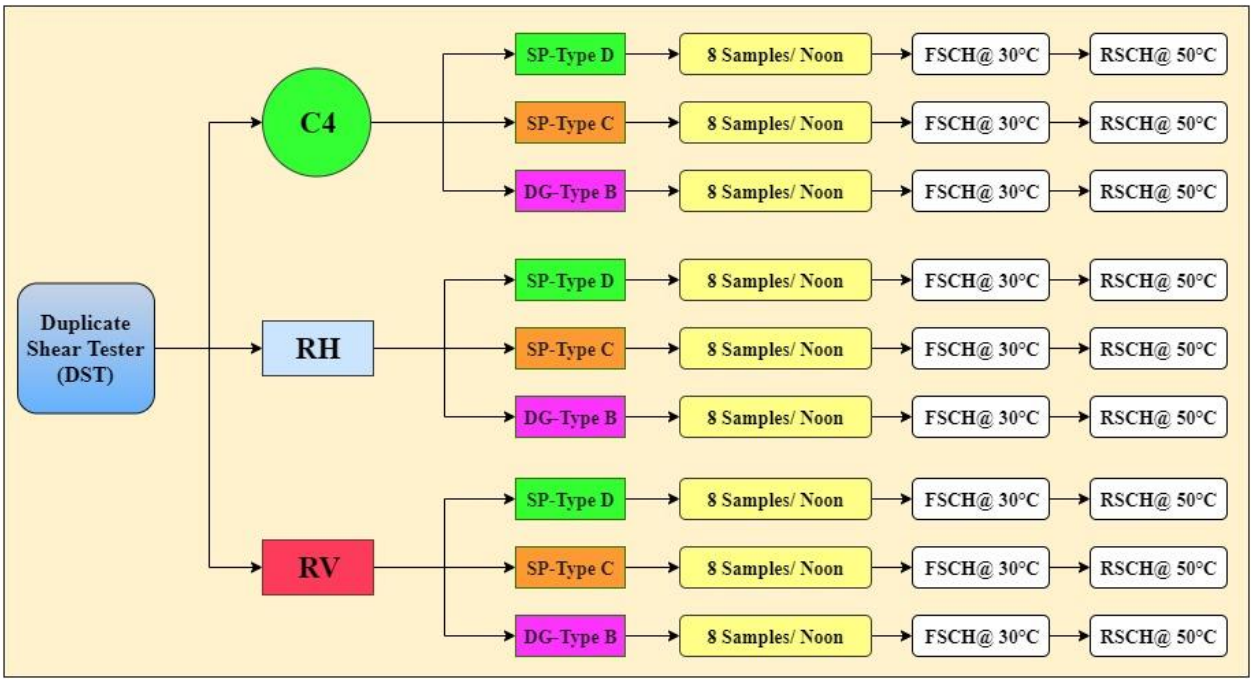

Figure 5-7. The second part of testing groups

5.3 Asphalt Mixes Sampling

All mixes were sampled at three times of daily production: morning, noon, and afternoon. The time of sampling was the same for all mixes to be from (8:00 am to 9:00 am) for the morning; from (12:00 pm to 1:00 pm) for the noon; and from (2:00 pm to 3:00 pm) for the afternoon. The required quantities of asphalt mixes of each mixture were estimated to be 350 lb at morning and afternoon time, and 1200 lb at noon time. These quantities include an extra 60% for each mixture to account for any potential waste in materials while the preparations.

The asphalt mixes were collected in bags from fully loaded trucks leaving the asphalt plant in the morning and afternoon, whereas the mixes of noon time were collected in bags from a bucket of loader loaded directly from the silo of the plant, as shown in Figure 5-8. Each bag of the

collected materials contains about 30lb of material. Table 5-9 summaries the sampling details for each asphalt concrete mix.

a) Morning and Afternoon b) Noon

Figure 5-8. Sampling Methods of Asphalt Mixes

Table 5-6. Sampling details of Asphalt Mixes

SP-Type D				
Day and Date: Tuesday- June 11,2019				
Asphalt Plant: Austin Road and Bridge, 11143 Goodnight Lane, Dallas, TX 75229				
Time			No. of Bags	Sampling Method
From	To	Interval		
8:00 AM	8:12 AM	Morning (M)	6	Truck
8:50 AM	9:04 AM	Morning (M)	6	Truck
12:33 PM	1:04 PM	Noon (N)	40	Loader
2:05 PM	2:15 PM	After Noon (AN)	6	Truck
2:19 PM	2:30 PM	After Noon (AN)	6	Truck

Table 5-6. Sampling details of Asphalt Mixes (Cont.)

SP-Type C				
Day and Date: Tuesday- June 11,2019				
Asphalt Plant: Austin Road and Bridge, 11143 Goodnight Lane, Dallas, TX 75229				
Time			No. of Bags	Sampling Method
From	To	Interval		
8:17 AM	8:30 AM	Morning (M)	6	Truck
8:35 AM	8:41 AM	Morning (M)	6	Truck
12:00 PM	12:22 PM	Noon (N)	40	Loader
2:34 PM	2:45 PM	After Noon (AN)	6	Truck
2:50 PM	3:02 PM	After Noon (AN)	6	Truck
DG-Type B				
Day and Date: Wednesday- July10,2019				
Asphalt Plant: Austin Road and Bridge, 11481 Co Rd 53, Celina, TX 75009				
Time			No. of Bags	Sampling Method
From	To	Interval		
8:00 AM	8:10 AM	Morning (M)	5	Truck
8:30 AM	8:40 AM	Morning (M)	5	Truck
12:05 PM	12:30 PM	Noon (N)	35	Loader
2:00 PM	2:10 PM	After Noon (AN)	5	Truck
2:20 PM	2:30 PM	After Noon (AN)	5	Truck

The theoretical maximum specific gravity (Gmm) of each mix was measured at the asphalt plant according to the standard test method AASHTO T 209 “Theoretical Maximum Specific Gravity (Gmm) and Density of Hot Mix Asphalt (HMA)”. Table 5-7 gives the (Gmm) values of each mix.

Table 5-7. Theoretical Maximum Specific Gravity of Asphalt Mixes

Asphalt Mixes	Gmm
SP-Type D	2.580
SP-Type C	2.601
DG-Type B	2.596

The sampled quantities of asphalt mixes were then transferred to the pavement lab at UTA to be compacted by using a Superpave Gyratory Compactor (SGC) in according to the standard test method TxDOT- 241-F "Compacting Bituminous Specimens Using the Superpave Gyratory Compactor (SGC)". According to the TxDot-241-F specification, a warm mix asphalt (WMA) must be compacted at specific temperatures based on the specified performance grade (PG) of asphalt binder used in the mixture, as shown in Table 5-8. Since all mixes contain an asphalt binder of PG 64-22, all mixes were reheated in an oven and compacted at 250°F temperature.

Table 5-8. Compaction Temperatures of Asphalt Mixes (Tex-241-F, 2015)

PG Grade	Compaction Temperatures
58-28 and 64 - 22	250 °F (121 °C)
64- 28 and 70-22	275 °F (135 °C)
70 -28, 76-22 and 76-28	300 °F (149 °C)

As recommended in AASHTO T-320, the asphalt mix should be compacted to 1.0 air void percentage higher than the target percentage of the test specimens. Table 5-9 shows the recommended air void contents based on the shear test types. A 1.0 percent offset is enough to achieve an appropriate percentage of air voids in the test specimen. This is because the air void content of the test specimen reduces after cutting the top and bottom ends of the compacted specimen. Since the frequency sweep shear tests are performed theoretically in the linear viscoelastic behavior domain, the same test samples that were used for the FSCH & FSNS tests were later used for the RSCH& RSNS tests, respectively. Therefore, it was decided in this research to compact all samples at 153 mm (6.0″) height and to a target air void content of 8.0%. Each compacted sample, however, was cut to obtain to test specimens of asphalt concrete that made

either one DST sample or two SNTS samples. All details of the compacted gyratory samples are given in Appendix F.

Table 5-9. Appropriate Air Void Percentage for Compacted SST Specimens (AASHTO T-320, 2004)

Test	Air Voids, %
Repeated Shear Test	3.0 ± 0.5
Simple Shear Test	7.0 ± 0.5
Shear Frequency Sweep Test	7.0 ± 0.5

5.4 Specimen Preparations

All asphalt concrete specimens of this study were prepared from compacted Superpave gyratory samples. All specimens were cut at constant height of 50 mm (1.97″) as recommended in AASHTO T320, and they were cut in different shapes and dimensions to be tested in both devices. Figure 5-9 shows these shape of cut samples.

Figure 5-9. Asphalt Concrete Specimens After Cutting.

Before cutting, the compacted gyratory samples were left to cool-off at room temperature for around 24 hours. A wet saw equipped with a 20.0″ diamond asphalt cutting blade of 0.15″ thickness was used to cut the gyratory samples. Special holders were designed to make the cutting procedure uniform and provide precise measurements to the specimens.

5.4.1 Cutting Procedure of (C6) Specimens.

The C6 specimens were used for the DST and STNS tests. They were cut by following the same procedure of cutting the SST specimens. Three saw cuts were made to a compacted Superpave gyratory sample of approximately 6.0″ height to obtain two identical specimens of 50 mm (1.97″) height, as illustrated in Figure 5-10.

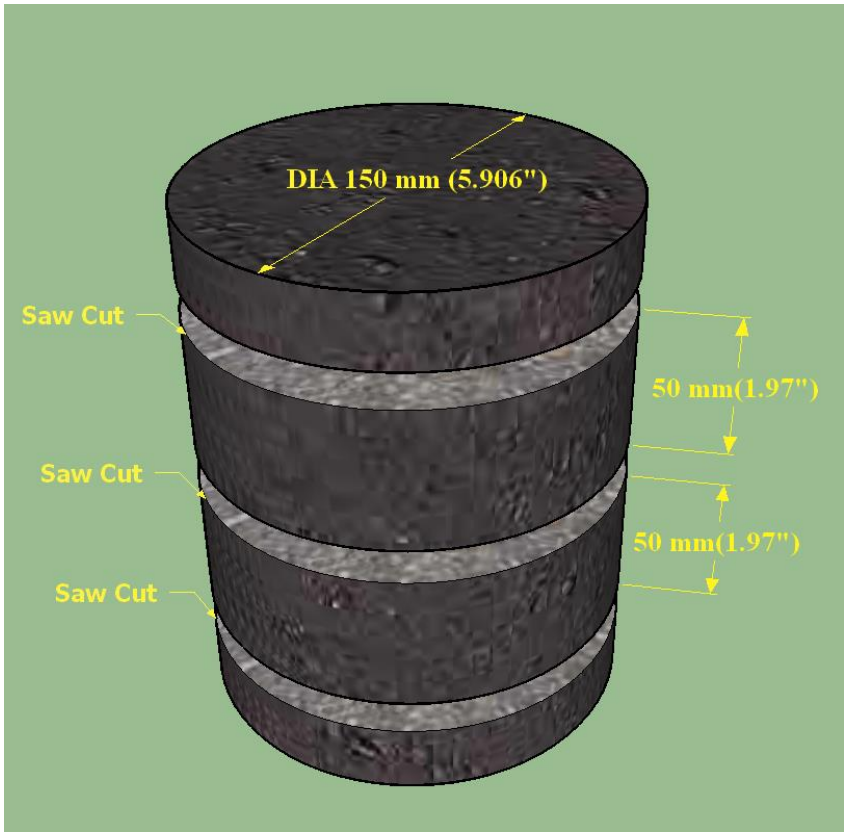

Figure 5-10. Illustration drawing to the Three Saw-cuts preparations of a gyratory sample.

To cut the test specimens safely and precisely, a special sample holder was used to accommodate the gyratory sample while cutting. The holder consists of three circular clamps, a front guide, two back guides, and movable block, as shown in Figure 5-11. The circular clamps were used to hold the sample firmly while cutting. The front guide was used in a specific procedure to control the position of the three saw-cuts before the cutting. The back guides and movable block were used only while preparing the RV specimens. This holder was mounted on a wet saw-cut machine equipped with a 20.0″ diamond blade, as shown in Figure 5-12. The drawings of the holder are shown in Appendix D.

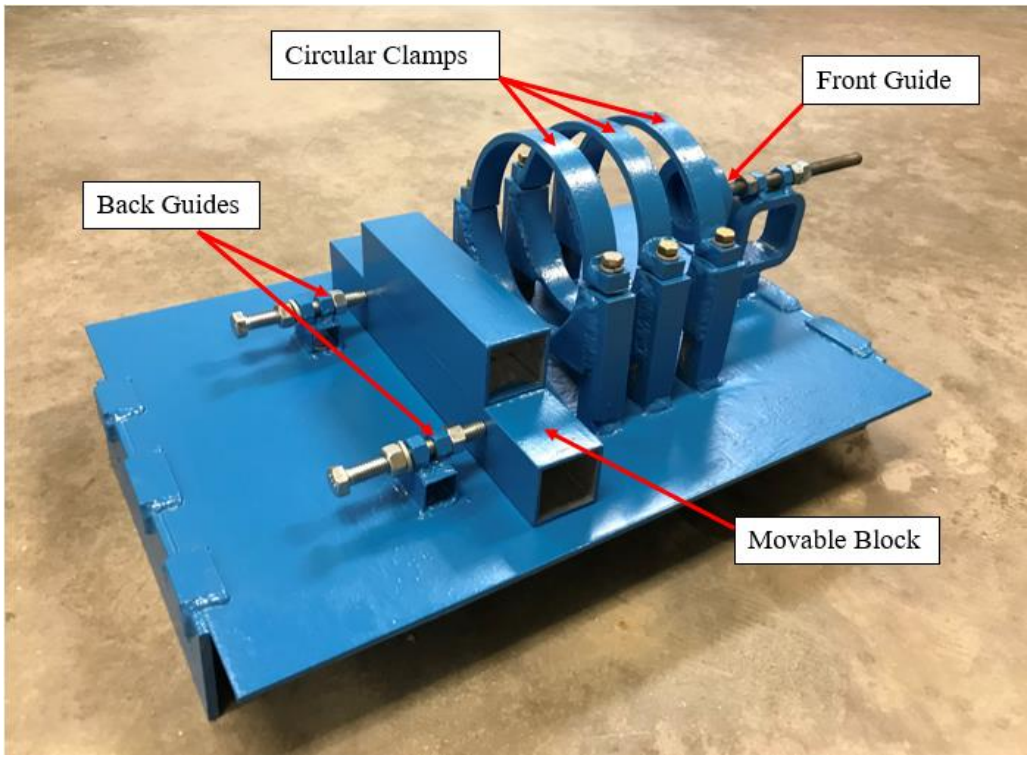

Figure 5-11. Sample Holder of C6 Specimens

Figure 5-12. Saw Cut Machine

The following steps were followed in order to cut two identical C6 specimens of 150 mm (5.906″) diameter and 50 mm (1.97”) height:

- Step 1: Adjusting the front guide so that a 50 mm (1.97″) thick specimen was obtained. This step was done first on a trial sample. Figure 5-13 illustrates the first setup.
- Step 2: Using a new gyratory sample, the first cut was done to cut a waste slice of around 1.0″ thick. This step was aimed to make a first cut face for the first specimen. Figure 5-14 illustrates the first cut preparation.
- Step 3: The sample was pushed to be touched with the front guide. To start that, the saw cut direction was marked vertically by drawing a line from the upper edge of the sample toward

the center. Then, the clamps bolts were loosed slightly so that the sample was pushed toward the front guide. The sample should not be rotated while pushing in order to keep all successive cut faces parallel to each other. Figure 5-15 illustrates this step.

- Step 4: The second cut was done to get the first specimen of 150 mm (5.906″) diameter and 50 mm (1.97″) height. Figure 5-16 illustrates this step.
- Step 5: The sample was pushed again to be touched with the front guide. Same process of marking and pushing the sample in Step 3 were repeated at this step. The third cut was then done to get the second specimen of 150 mm (5.906″) diameter and 50 mm (1.97″) height. The rest of the sample after the third cut was a waste material. Figure 5-17 illustrates this step.

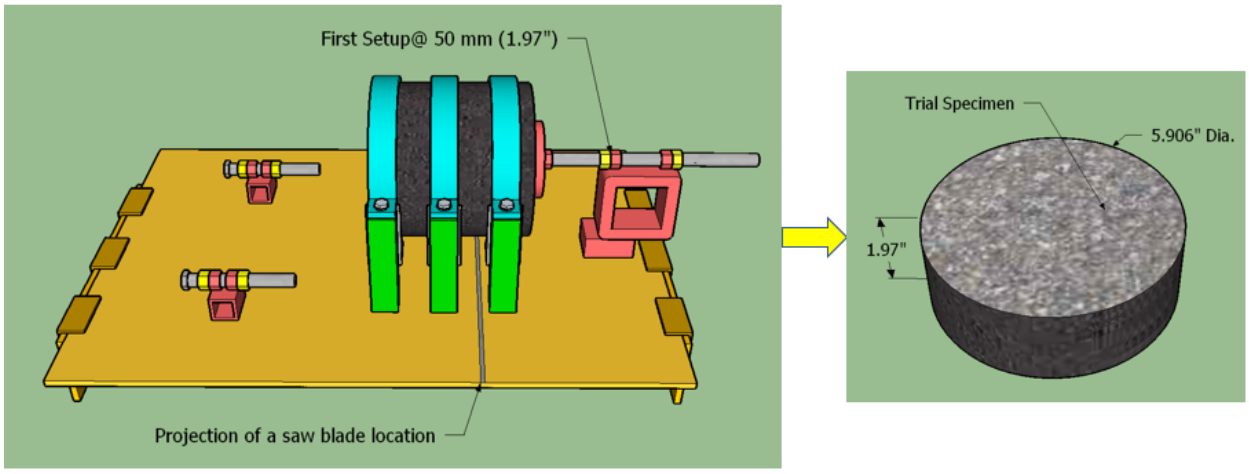

Figure 5-13. Illustration drawings to the first setup of cutting.

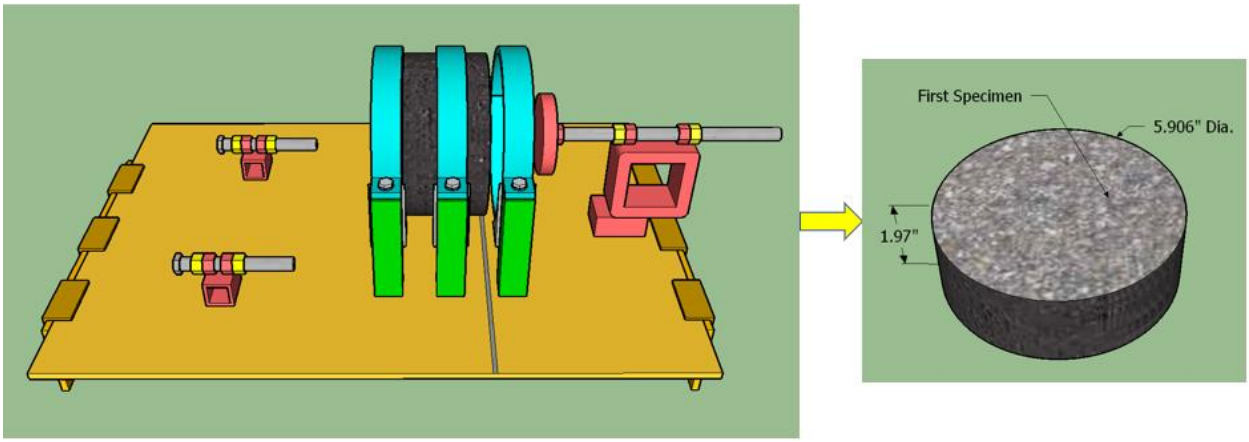

Figure 5-14. Illustration drawings to the Step 2.

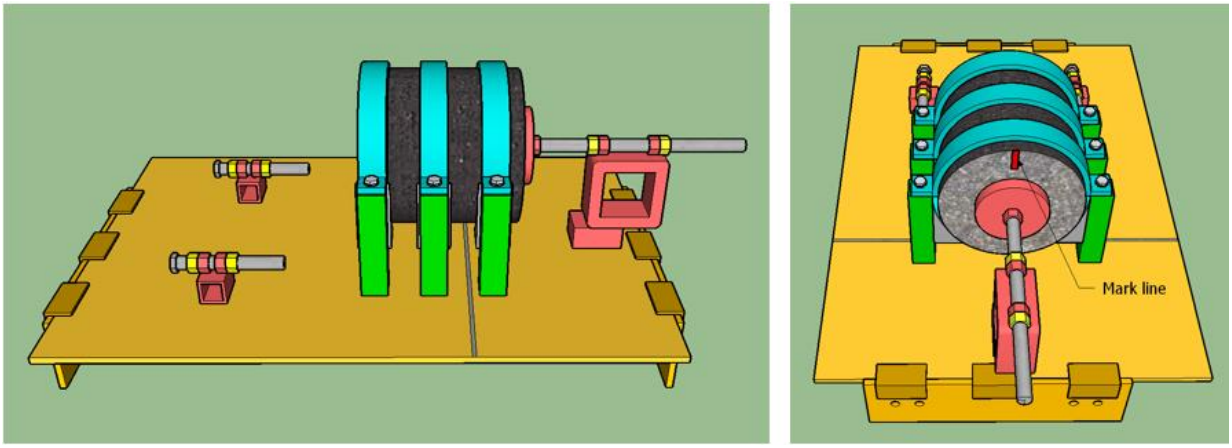

Figure 5-15. Illustration drawings to the Step 3.

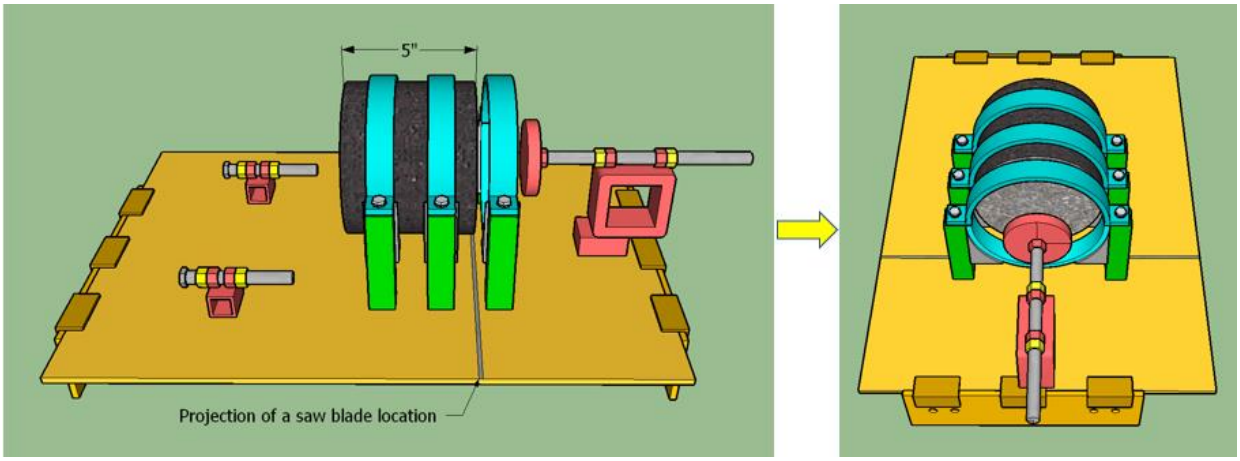

Figure 5-16. Illustration drawings to the Step 4.

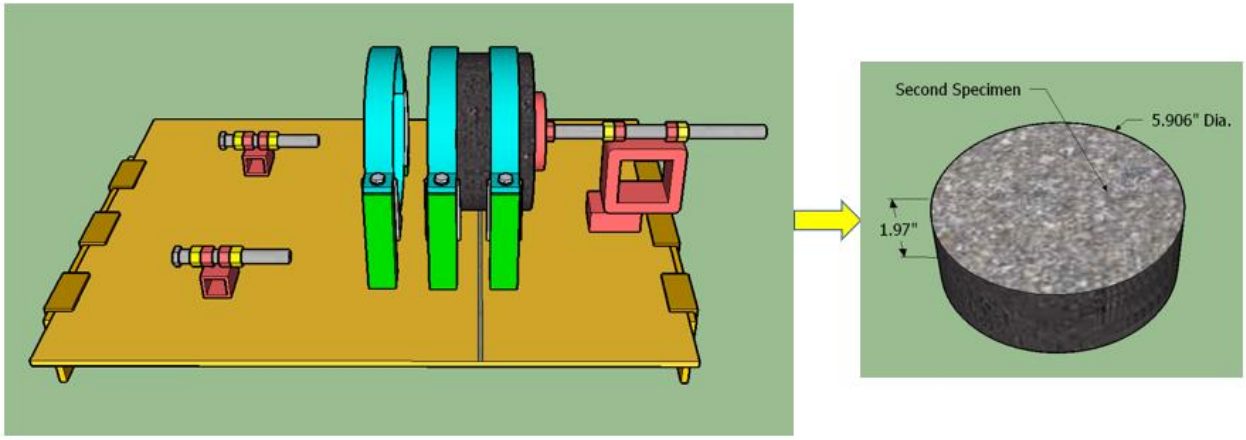

Figure 5-17. Illustration drawings to the Step 5.

5.4.2 Cutting Procedure of (C4) Specimens

The C4 specimens are one of the new DST samples in this study. These specimens were prepared in two phases. The first phase included the same procedure of cutting the C6 specimens, while the second phase included a drilling core technique to extract specimens of 99.06 mm (3.9″) diameter. The drilling core process was done by using an asphalt core bit of 4.0″ diameter attached to a coring machine. An additional sample holder was used to hold the specimen vertically on the ground while the drilling.

The sample holder has two identical semicircular clamps of 6.0″ height and 6.0″ diameter mounted over a base plate of steel, as shown in Figure 5-18. One of these clamps was welded to the base plate while the others was not. The clamps were connected together by six bolts and nuts. The base plate was designed with a 5.0″ diameter hole at center. This hole assures that the drilling bit does not hit the baseplate while the drilling. The drawings of the vertical sample holder are shown in Appendix D.

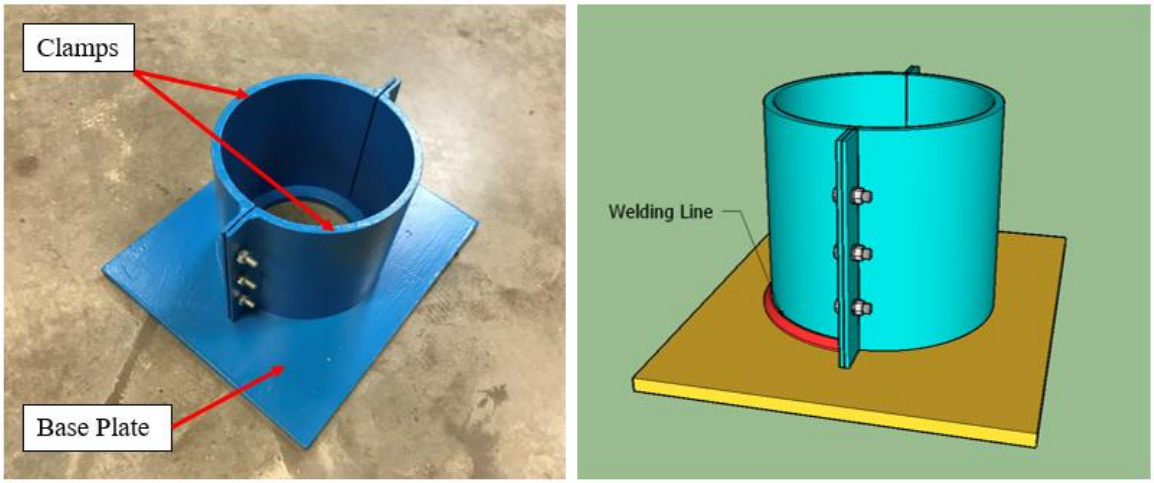

Figure 5-18. Vertical holder of gyratory samples

The following steps were followed to prepare the C4 specimens:

- Step 1: The same procedure of the three saw cuts were performed to a compacted Superpave gyratory sample of 6.0″ height to obtain two identical C6 specimens. This step was done by using the sample holder shown previously in Figure 5-11.
- Step 2: A cut specimen was then placed inside the vertical holder and held firmly by tightening the bolts of the vertical holder.
- Step 3: The vertical holder along with the specimen were centered with the drilling bit that attached to the coring machine, as shown in Figure 5-19.
- Step 4: The first C4 specimen was extracted from inside the drilling bit. Sometimes, a rubber mallet was used gently to extract the cored specimens.
- Step 5: The second C4 specimen was extracted by repeating the same procedure of Step 2 to Step 4.

Figure 5-19. Coring Machine of the C4 Specimens.

5.4.3 Cutting Procedure for the Rectangular Specimens

The rectangular shape specimens of both horizontal and vertical slices were also prepared to be new DST samples in this study. The rectangular specimens were prepared by cutting first a gyratory sample by using the sample holder of C6 specimens, shown in Figure 5-11. Then, a trimming procedure was done to get rectangular shape specimens of 125 mm (4.92″) in length, 75 mm (2.95″) in width, and 50 mm (1.97″) in height.

A steel sample holder was used to hold a test specimen while the trimming. The holder consists of a base plate, four flanges provided with chairs, two “L-shape” grippers, two flat brackets, four bolts of (1/2″-13). The flanges and grippers were fixed on the base plate by using (3/8″-16) bolts. They were used to hold a cut specimen horizontally from four sides around the specimen. The flanges chairs were designed to support the specimen at 1.25″ elevation from the base plate. The brackets were used to grip the specimen vertically from top. The four (1/2″-13)

bolts were used to connect the brackets with the flanges. Similar to the sample holder of 6.0″ gyratory samples, this holder was mounted on a wet saw-cut machine equipped with a 20.0″ diamond blade at center. However, it needs a specific procedure to be used by using additional five blocks of steel. The blocks were used in sequences to unify the cut procedure with high precision. The sample holder and blocks were shown in Figure 5-20 and 5-21, respectively.

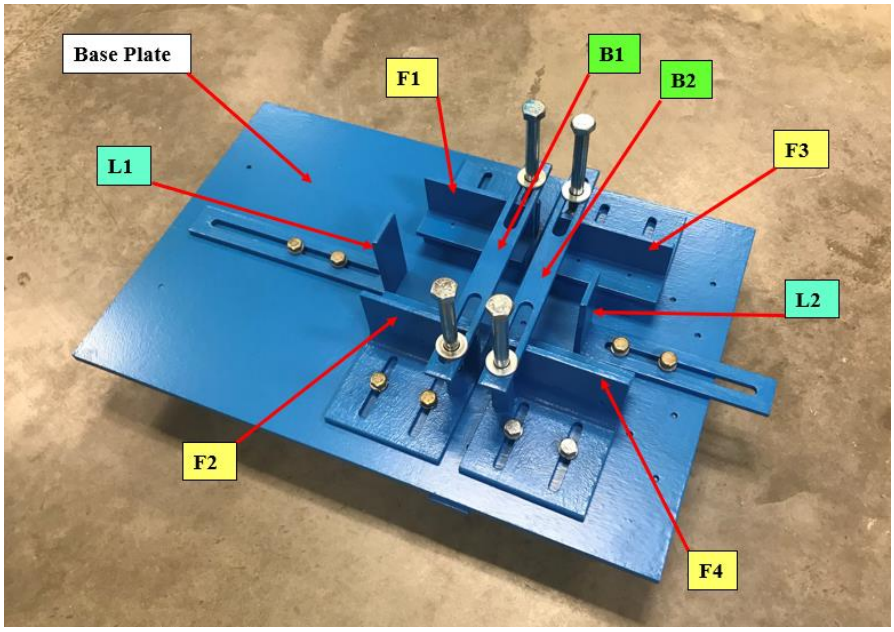

Figure 5-20. Sample Holder of cutting Rectangular Specimens

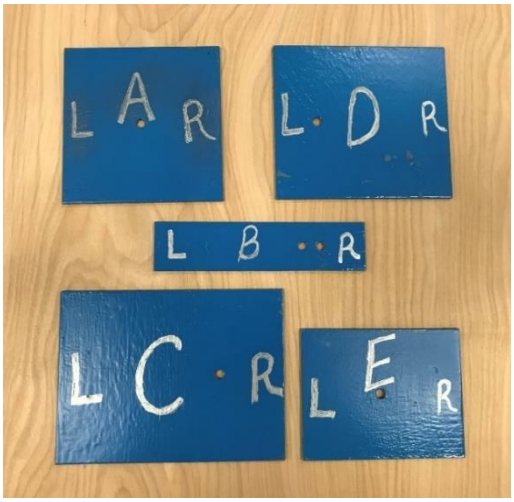

Figure 5-21. Steel Blocks associated to the Rectangular Holder

To demonstrate the trimming procedure simply, the sample holder components and blocks were identified with symbols and alphabet letters, respectively. As shown in Figure 5-22, the four flanges were represented by the symbols (F1, F2, F3, and F4). The symbols (B1 and B2) were used to represent the two brackets, whereas the (L1 and L2) were used for the two “L-shape” grippers. The blocks were identified with the alphabet letters (A, B, C, D, and E). In Figure 5-21, the (R and L) letters on each block represent the right and left sides, respectively. All blocks have one hole of 0.25″ diameter except the block (B) has two holes. The drawings of the sample holder components and blocks are shown in Appendix D.

The trimming procedure started with placing a block between the flanges and “L-shape” grippers on the base plate. A block location was placed correctly on the holder by matching the hole on the block with another identical hole located on the base plate of the holder. A regular pin of 0.25″ diameter was used to allocate the right position of the blocks by matching the blocks hole with the hole on the base plate. Depending on the trimming procedure, the position of determined flanges and grippers were then fixed around the block, followed by removal of the block and placement of the specimen. The remaining flanges, grippers, and brackets were positioned and fixed all around the specimen to be held firmly. Finally, the saw cut trimming was performed. This procedure was performed in sequences to obtain rectangular specimens of horizontal and vertical slices. Blocks (A and B) were used for the horizontal cut slices, whereas the blocks (C, D, and E) were used for the vertical cut slices. Bolts (1/2"-13, 5″ Long) and (1/2"-13, 2″ Long) were used alternatively while the trimming.

The following steps were followed to prepare the RH specimens:

- Step 1: The same procedure of cutting two identical C6 specimens was performed by using the sample holder shown in Figure 5-11.

- Step 2: To start the first cut of trimming, the block (A) was placed on the right position over the base plate by using a regular pin of 0.25″ diameter. The position of flange (F1) was adjusted to be touched with the block side, and the gripper (L2) was pushed to be touched with the right side (R) of the block. Then, the F1 and L2 must be tightened down to the base plate so that their locations were fixed after removing the block. The block was then removed, and a test specimen was placed over the flanges' chairs. The other flanges and gripper were then adjusted and fixed to a position where the specimen was gripped firmly from the four sides. Using two bolts of (1/2"-13, 2.0″ long), the bracket (B1) was then tightened down so that the specimen was held vertically from the top, as shown in Figure 5-22.

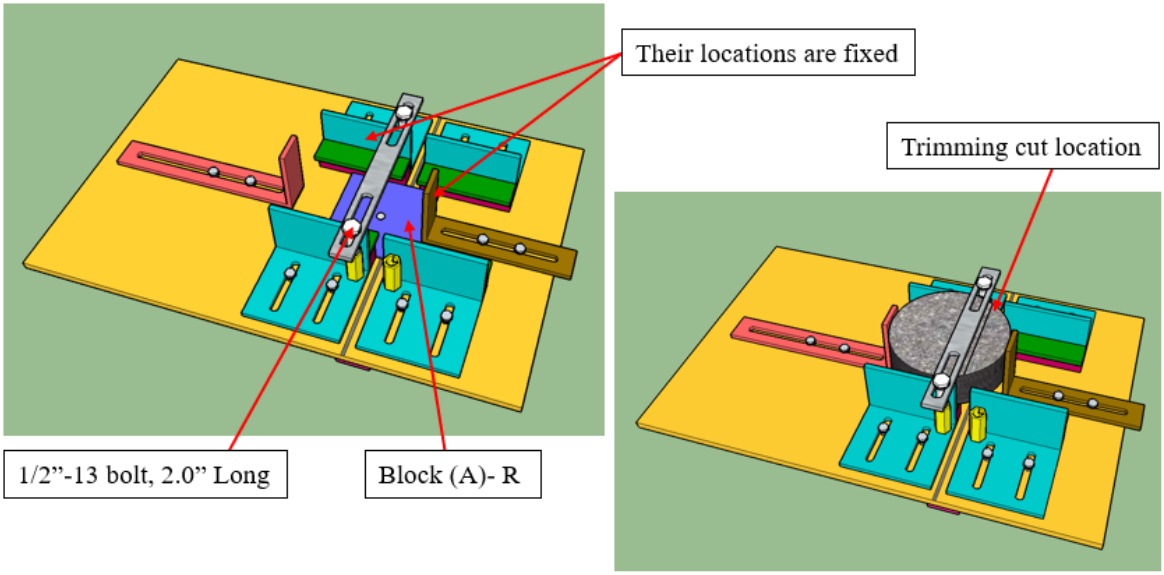

Figure 5-22. Illustration drawings to the first trimming of RH specimens.

- Step 3: To do the second cut of trimming, the block (A) was also placed on the right position over the base plate by using a regular pin of 0.25″ diameter. The position of flange (F1) was adjusted to be touched to the block side, and the gripper (L1) was pushed to be touched with the left side (L) of the block. Then, the F1 and L1 must be tightened down to the base plate so that their locations were fixed after removing the block. The block was then removed, and the

trimmed specimen was flipped horizontally and placed over the flanges' chairs. The other flanges and gripper were then adjusted and fixed to a position where the specimen was gripped firmly from the four sides. Using two bolts of (1/2"-13, 2.0″ long), the bracket (B1) was then tightened down so that the specimen was held vertically from the top, as shown in Figure 5-23.

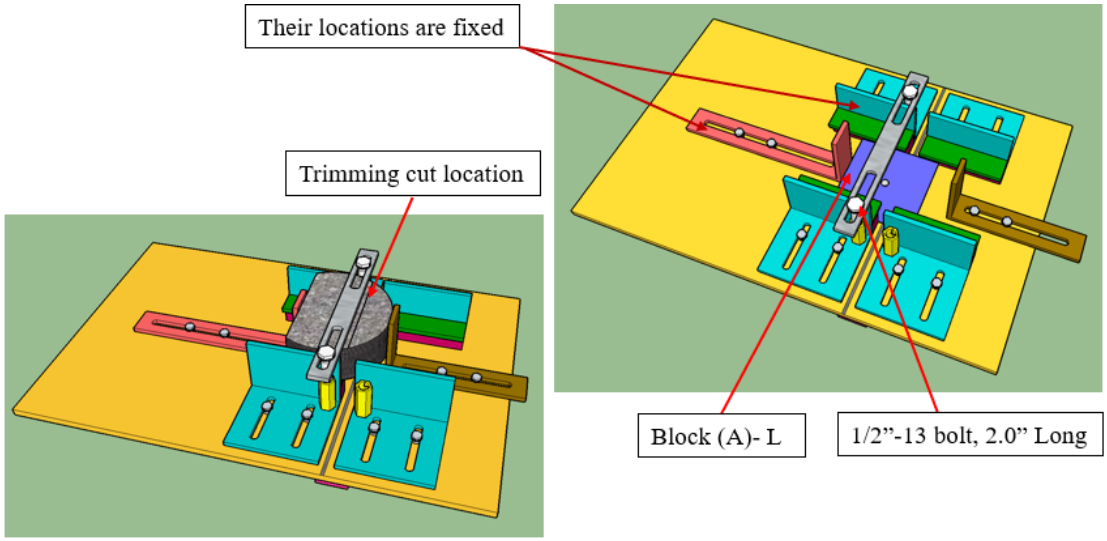

Figure 5-23. Illustration drawings to the second trimming of RH specimens.

- Step 4: To do the third cut of trimming, the block (B) was placed on the right position over the base plate by using a regular pin of 0.25″ diameter inside the right hole (R) of the block. The position of flange (F1) was adjusted to be touched with the block side, and the gripper (L2) was pushed to be touched to the "Right side (R)" of the block. Then, the F1 and L2 must be tightened down to the base plate so that their locations were fixed after removing the block. The block was then removed, and the trimmed specimen was flipped horizontally and placed over the flanges' chairs. The flange (F2) and gripper (L1) were then adjusted and fixed to a position where the specimen was gripped firmly from the four sides. Using two bolts of (1/2"-13, 2.0″ long), the bracket (B1) was then tightened down so that the specimen was held vertically from the top, as shown in Figure 5-24.

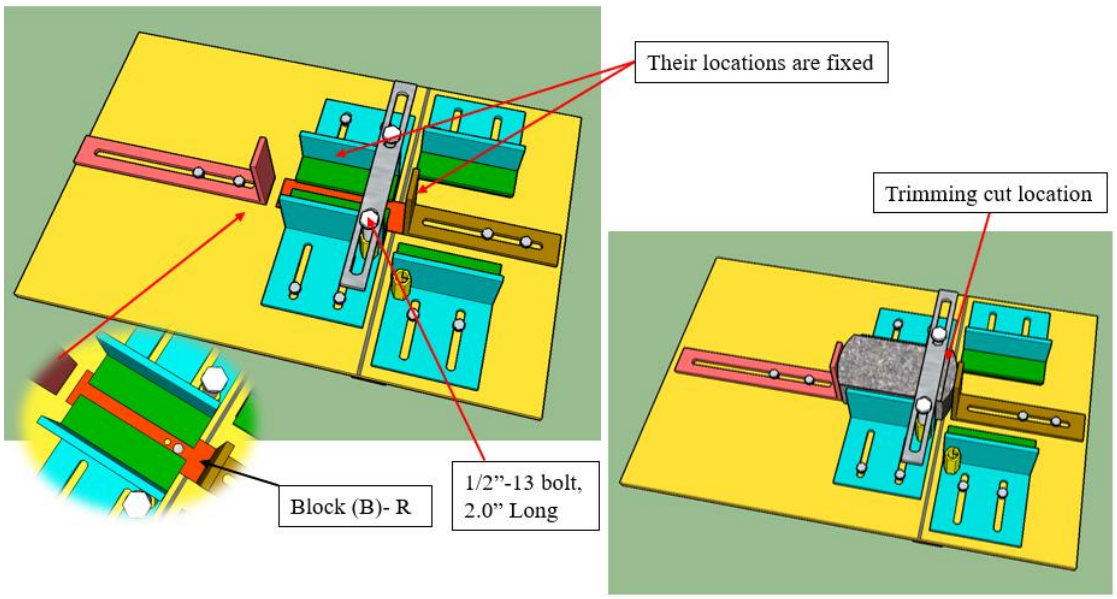

Figure 5-24. Illustration drawings to the third trimming of RH specimens.

- Step 5: To do the fourth cut of trimming, the block (B) was placed on the right position over the base plate by using a regular pin of 0.25″ diameter inside the left hole (L) of the block. The position of flange (F1) was adjusted to be touched with the block side, and the gripper (L1) was pushed to be touched with the "Left side (L)" of the block. Then, the F1 and L1 must be tightened down to the base plate so that their locations were fixed after removing the block. The block was then removed, and the trimmed specimen was flipped horizontally and placed over the flanges' chairs. The flange (F2) and gripper (L2) were then adjusted and fixed to a position where the specimen was gripped firmly from the four sides. Using two bolts of (1/2"-13, 2.0″ long), the bracket (B1) was then tightened down so that the specimen was held vertically from the top, as shown in Figure 5-25.

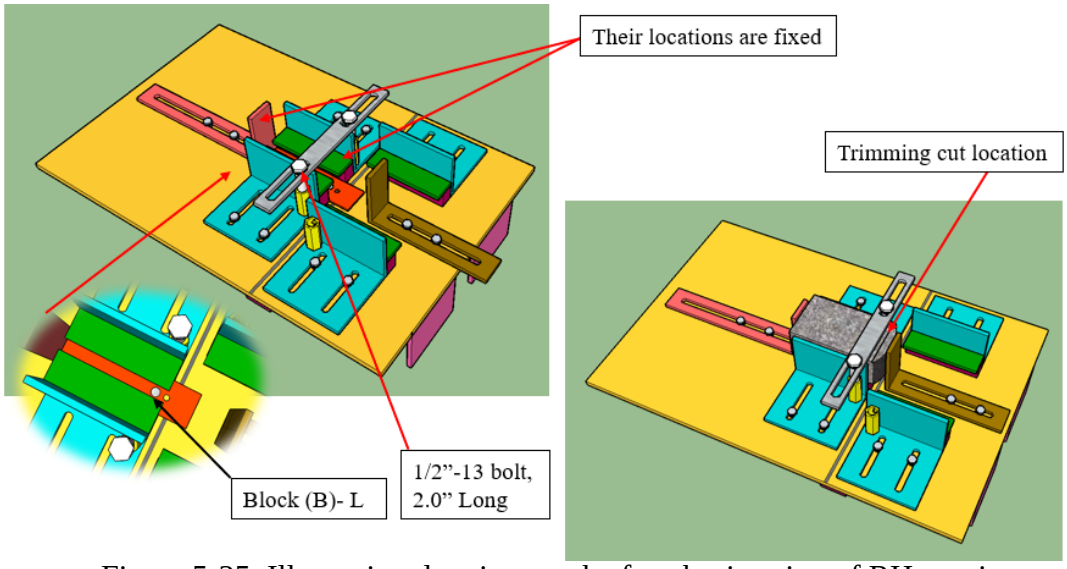

Figure 5-25. Illustration drawings to the fourth trimming of RH specimens.

The following steps were followed to prepare the RV specimens:

- Step 1: Two saw cuts were performed to a compacted Superpave gyratory sample of 6.0″ height to obtain a test specimen of 150 mm (5.906″) diameter and 125 mm (4.92″) height. Figure 5-26 describes the "two saw-cuts" preparations.

This step, however, was done by using the sample holder shown in Figure 5-11. First, a gyratory sample was placed on the sample holder to make the first saw cut by cutting a wasted slice of about 0.5″ thick. Then, the back guides of the holder were adjusted so that the clear distance between the saw blade and the movable block was 125 mm (4.92″). The sample was then flipped horizontally and placed on the holder clamps at a position where the first cut was touched with the movable block's face. After that, the clamps were tightened, and the second saw cut was performed. Figure 5-27 illustrates the sequences of preparing a sample of 125mm (4.92″) height by using the sample holder of 6.0″ gyratory samples.

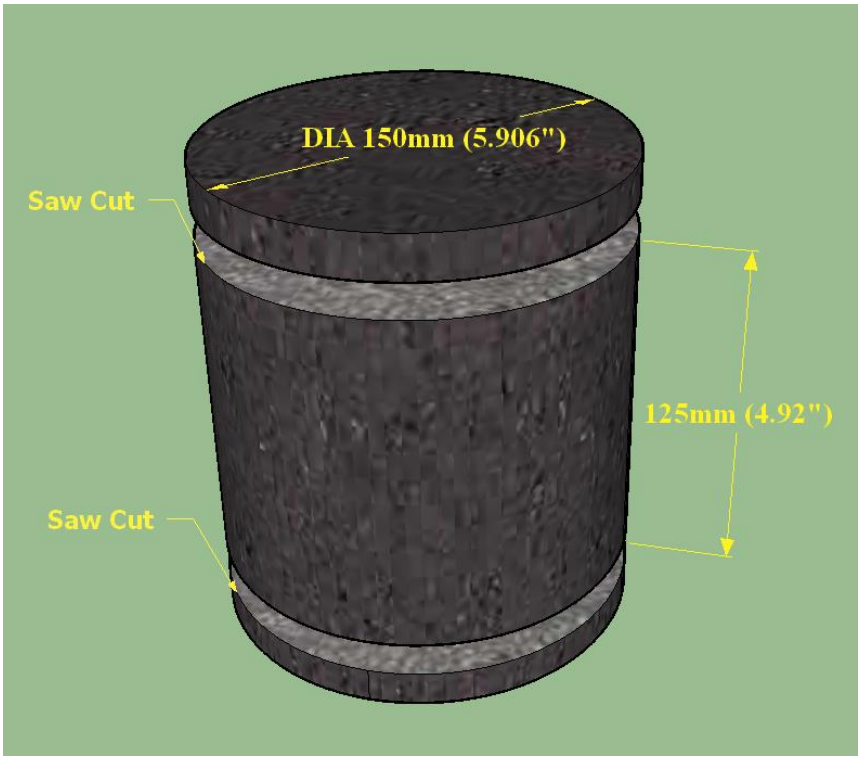

Figure 5-26. Illustration drawing to the “two saw-cuts” preparations.

- Step 2: Using the sample holder shown in Figure 5-20, the first cut of trimming was performed by placing the block (C) on the right position over the base plate by using a regular pin of 0.25″ diameter. The position of flange (F1) was adjusted to be touched with the block side, and the gripper (L2) was pushed to be touched with the right side (R) of the block. Then, the F1 and L2 were tightened down to the base plate so that their locations were fixed after removing the block. The block was then removed, and a test specimen of 125mm (4.92″) height was placed over the flanges’ chairs. The other flanges and gripper were then adjusted and fixed to a position where the specimen was gripped firmly from the four sides. Using two bolts of (1/2"-13, 5.0″ long), the bracket (B1) was then tightened down so that the specimen was held vertically from the top, as shown in Figure 5-28.

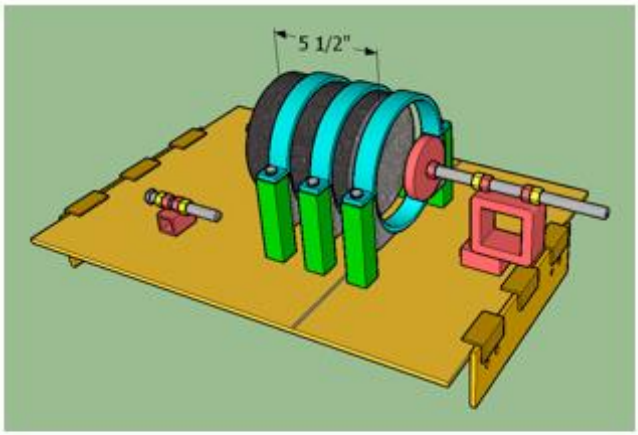

1- The first saw cutting was done to get a slice of 0.5" thick.

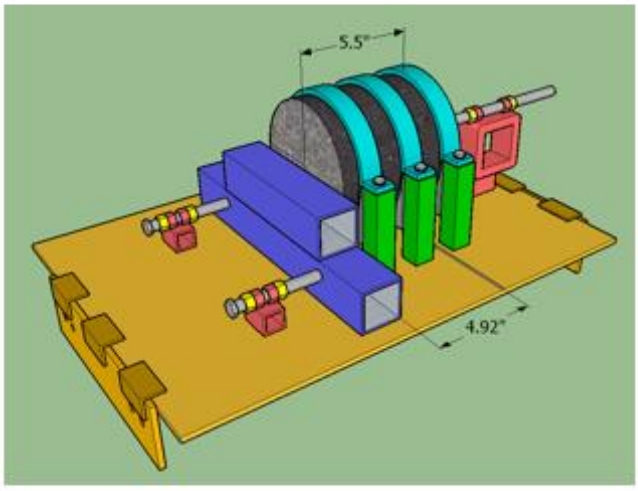

2- The back guides were adjusted.
- The movable block was installed.
- The sample was flipped.

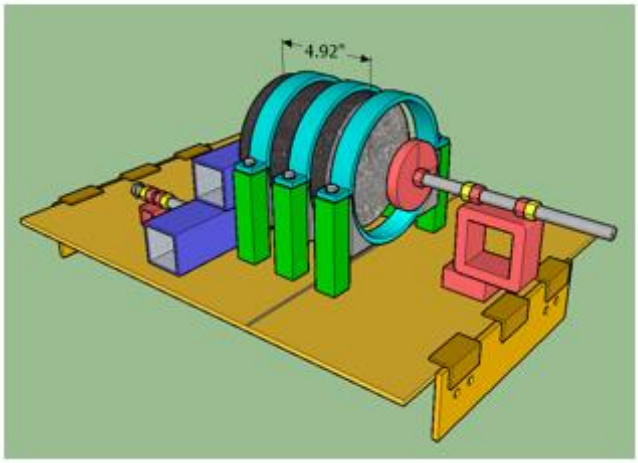

3- The second saw cutting was done.

Figure 5-27. Illustration drawings to the 4.92″ height sample preparations.

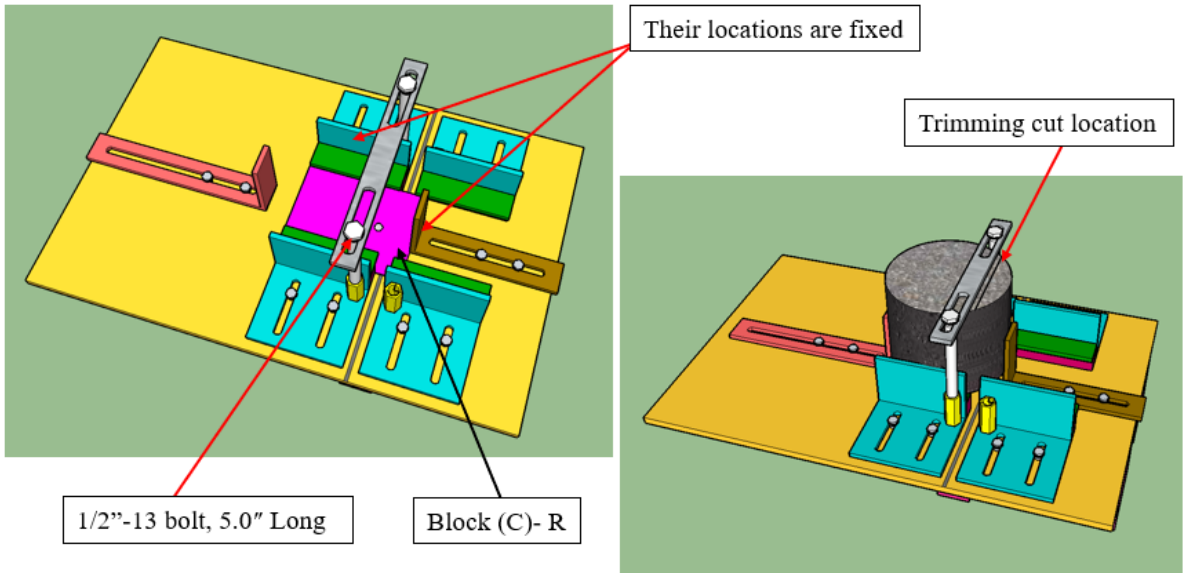

Figure 5-28. Illustration drawings to the first trim of RV specimens.

- Step 3: The second cut of trimming was performed to complete the vertical trimming of the first half of the sample. It was done by placing the block (D) on the right position over the base plate by using a regular pin of 0.25″ diameter. The position of flange (F1 and F3) were adjusted to be touched with the block side, and the gripper (L1) was pushed to be touched with the left side (L) of the block. Then, the F1, F3 and L1 were tightened down to the base plate so that their locations were fixed after removing the block. The block was then removed, and the trimmed specimen of 125mm (4.92″) height was placed over the flanges’ chairs. The other flanges and gripper were then adjusted and fixed to a position where the specimen was gripped firmly from the four sides. Using four bolts of (1/2"-13, 5.0” long), the brackets (B1 and B2) were then tightened down so that the specimen was held vertically from the top, as shown in Figure 5-29.
- Step 4: The third cut of trimming was performed to complete the vertical trimming of the second half of the sample. The locations setup of the F1, F3 and L1 were kept the same from the previous setup of Step 3. The bolts of the bracket (B1), the flanges (F2 and F4), and gripper

(L2) were loosed slightly so that the second half of the sample can be pushed toward the gripper (L1). The flange (F2) and gripper (L2) were then adjusted and fixed to a position where the second half of the sample was gripped firmly from the four sides. Using two bolts of (1/2"-13, 5.0″ long), the bracket (B1) was then tightened down so that the specimen was held vertically from the top, as shown in Figure 5-30.

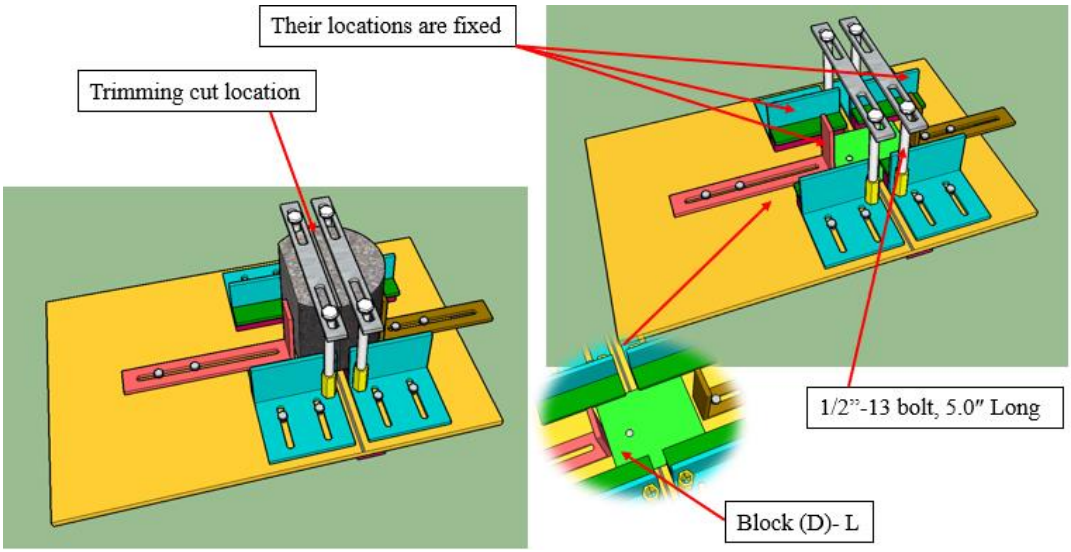

Figure 5-29. Illustration drawings to the second trim of RV specimens.

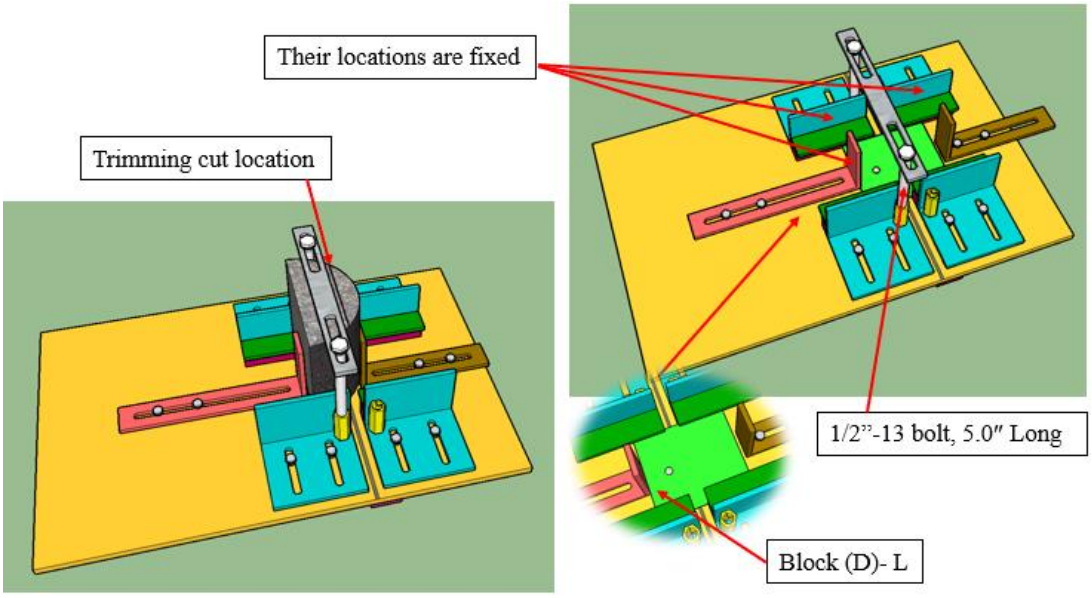

Figure 5-30. Illustration drawings to the third trim of RV specimens.

- Step 5: Starting with the first trimmed specimen obtained from Step 3, the fourth trimming cut was done by using block (E). The position of flange (F1 and F3) were adjusted to be touched with the block side, and the gripper (L2) was pushed to be touched with the right side (R) of the block. Then, the F1, F3 and L2 were tightened down to the base plate so that their locations were fixed after removing the block. The block was then removed, and the trimmed specimen was flipped horizontally and placed over the flanges' chairs. The other flanges and gripper were then adjusted and fixed to a position where the specimen is gripped firmly from the four sides. Using two bolts of (1/2"-13, 2.0" long), the bracket (B1) was then tightened down so that the specimen was held vertically from the top, as shown in Figure 5-31.

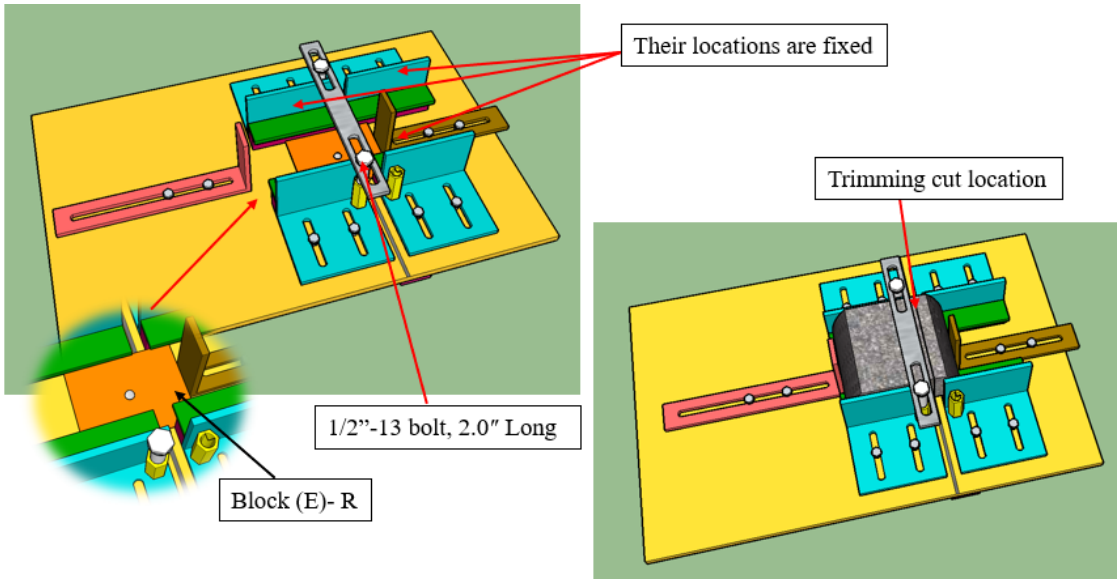

Figure 5-31. Illustration drawings to the fourth trim of RV specimens.

- Step 6: Finally, the fifth trimming cut was done by using also block (E). The position of flange (F1 and F3) were adjusted to be touched with the block side, and the gripper (L1) was pushed to be touched with the left side (L) of the block. Then, the F1, F3 and L1 were tightened down to the base plate so that their locations were fixed after removing the block. The block was then removed, and the trimmed specimen was flipped horizontally and placed over the flanges'

chairs. The other flanges and gripper were then adjusted and fixed to a position where the specimen was gripped firmly from the four sides. Using two bolts of (1/2"-13, 2.0″ long), the bracket (B1) was then tightened down so that the specimen was held vertically from the top, as shown in Figure 5-32.

- Step 7: To get the specimens in pairs, the trimming cuts of Steps 5 and 6 were also done for the second half of sample obtained in Step 4.

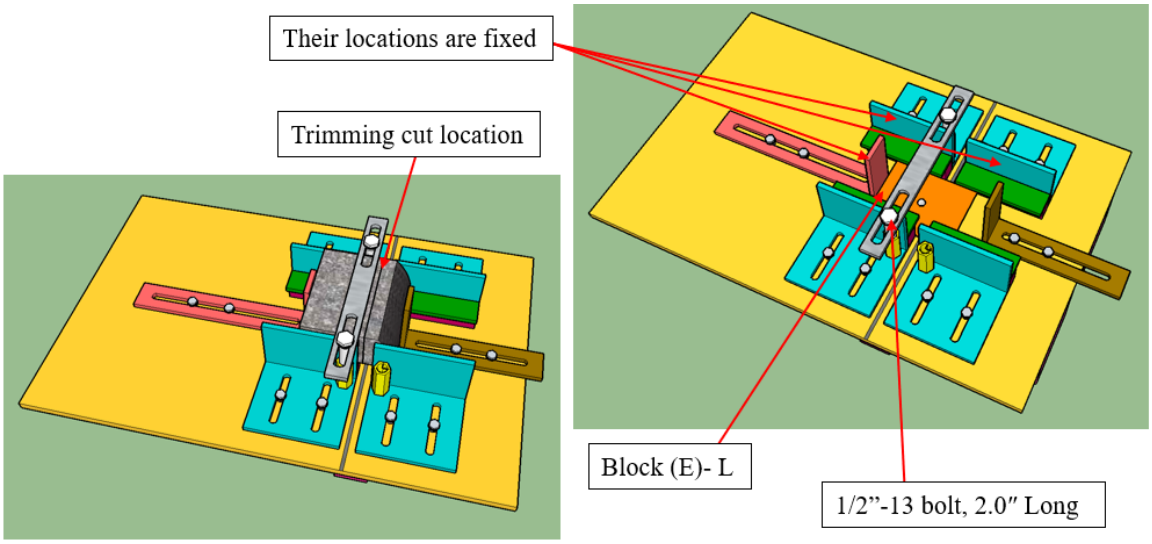

Figure 5-32. Illustration drawings to the fifth trim of RV specimens.

5.5 Volumetric Measurements

After the specimens cut preparations were done for each testing group of the tests plan, all specimens were marked to indicate the mix type and specimen number. The specimens were then left in pairs to dry over a dry towel for at least 24 hours at room temperature, as shown in Figure 5-33.

The volumetric measurements of each specimens' pairs were usually performed after they were dry. The volumetric measurements aim to assure the uniformity of specimens regarding to the air void content and dimensions. The measurements included measuring the average

dimensions and weight of each specimen. The average height of each specimen was calculated by measuring four readings with a caliper according to the standard test method ASTM- D3549.

Figure 5-33. Curing of Asphalt Concrete Specimens

According to the standard test method AASHTO T-320, however, a test specimen should be discarded if the difference between the largest and smallest height of the specimen is more than 2 mm. Same procedure of measuring the average height were also performed to calculate the average length and width for the rectangular specimens. The weight of specimens was measured by using a sensitive scale. The volumetric values of all specimens are listed in Appendix F.

The volumetric measurements were used also to calculate the air void percentage of each specimen. The maximum theoretical specific gravity (G_{mm}) of asphalt mixes were required to calculate the air void percentage of the specimens. The (G_{mm}) values were calculated according to the standard test method AASHTO T-209 "Theoretical maximum specific gravity and density of hot-mix asphalt". Equation 5-1 was used only to calculate the air void percentage of C6 specimens of 150 mm (5.906″) diameter, as required in the standard test method AASHTO T-320. Equations 5-2 and 5-3 were derived to calculate the air void percentage for the C4 specimens of

99.06 mm (3.9″) diameter and rectangular specimens of 125 mm (4.92″) length and 75 mm (2.95″) width, respectively.

$$Mass = 17.671 \times H \times Gmm \times (1 - AV) \quad (5\text{-}1)$$

$$Mass = 7.707 \times H \times Gmm \times (1 - AV) \quad (5\text{-}2)$$

$$Mass = 0.001\ (H \times L \times W) \times Gmm \times (1 - AV) \quad (5\text{-}3)$$

Where:

Mass = Mixture batch weight (grams).

H = Specimen height (millimeters).

L= Specimen length (millimeters).

W= Specimen width (millimeters).

Gmm = Maximum theoretical specific gravity of the mixture (AASHTO T-209).

AV = Percentage of air voids desired in decimal (i.e., 0.04 rather than 4.0 percent).

The volumetric measurements and air voids contents of the specimens were then used to assess the uniformity of the specimen pairs. This assessment was important to select the best pairs for testing especially for the DST samples. For each pair, the difference in average height and air void contents between the specimens were calculated. In this study, the accepted pairs for DST samples should not have a difference in average height more than 2 mm and more than 1.0 percent in air voids content.

5.6 Assembling Samples

Once the volumetric measurements were done of each group of testing specimens, the specimens were glued to the plates by using the epoxy "Devcon™ Plastic Steel Putty (A)". This epoxy was used because it satisfies the AASHTO T 320 requirements for a quick adhesive with a minimum hardened stiffness modulus of 2000 Mpa. Resin and hardener were the two components of this putty that were mixed together in specific proportions. Since this putty get hard quickly within 45 minutes, appropriate quantities of the two components should be determined to be batched at a time. It was determined that mixing 75 cm^3 of the resin with 30 cm^3 of the hardener were enough to glue a one DST sample of C6 specimens, or two DST samples of rectangular or C4 specimens. These quantities satisfy the resin to hardener ratio of (2.5/1), as recommended in the technical specification sheet of the putty.

Immediately after the epoxy putty was mixed properly, the specimens were glued with the plates. Preparing a DST sample is required to glue two asphalt specimens with a middle plate and two side plates, whereas an STNS sample is required to glue one specimen between a middle plate and base plate. The same procedure that used by Jweihan, (2018) for gluing DST samples by using an assembly stand was adopted in this study. The assembly stand was used to assure that all plates are lined up and glued parallel to each other. The assembly stand drawings were shown in Appendix A. Figure 5-34 illustrates the procedure for gluing all DST samples of different shapes. Follows are the steps procedure for gluing a DST sample:

- Step 1: A first side-plate was mounted inside the assembly stand. A thin layer (around 3.0 mm thick) of the epoxy putty was then spread on the specimen groove of the first side-plate. The first specimen was then placed on the epoxy of the first plate.

- Step 2: A second thin layer of the epoxy putty was applied by the scrapper on a first groove of the middle plate. The plate was then mounted over the first specimen inside the assembly stand.
- Step 3: A third thin layer of the epoxy putty was applied by the scrapper on the upper groove of the middle plate. The second specimen of asphalt was then placed on the epoxy over the middle plate.
- Step 4: A fourth thin layer of the epoxy putty was applied by the scrapper on the groove of the second side-plate. The plate was then mounted over the second specimen inside the assembly stand. Then, the glued sample was left in the assembly stand for at least 24 hours at room temperature till the epoxy was completely cured.

Similarly, an STNS sample was glued by following the previous Step 1 and Step 2 of the gluing procedure for a DST sample. Figure 5-35 illustrates the procedure for gluing an STNS sample.

Once the STNS sample was cured, the sample was ready for testing. The assembly procedure for the DST sample was completed it cured by installing four threaded rods of (1/2″-13, 8.5″ long) and two steel grippers on the sample, as shown in Figure 5-36.

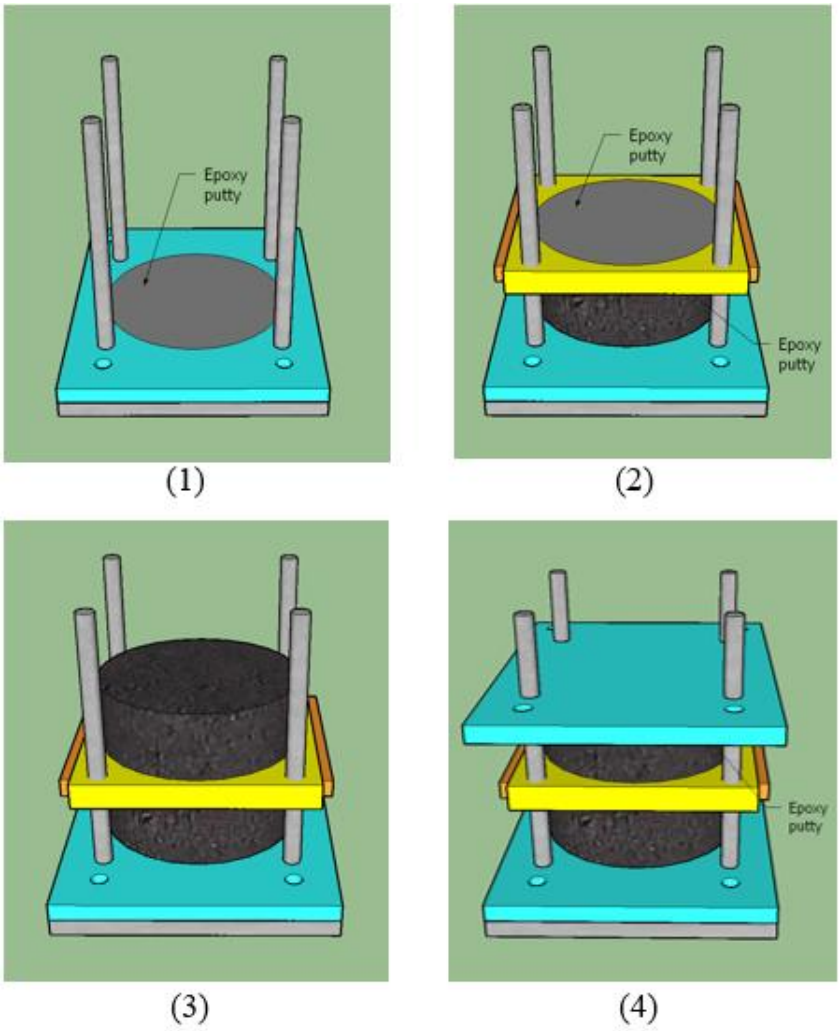

Figure 5-34. Procedure of Gluing a DST Sample.

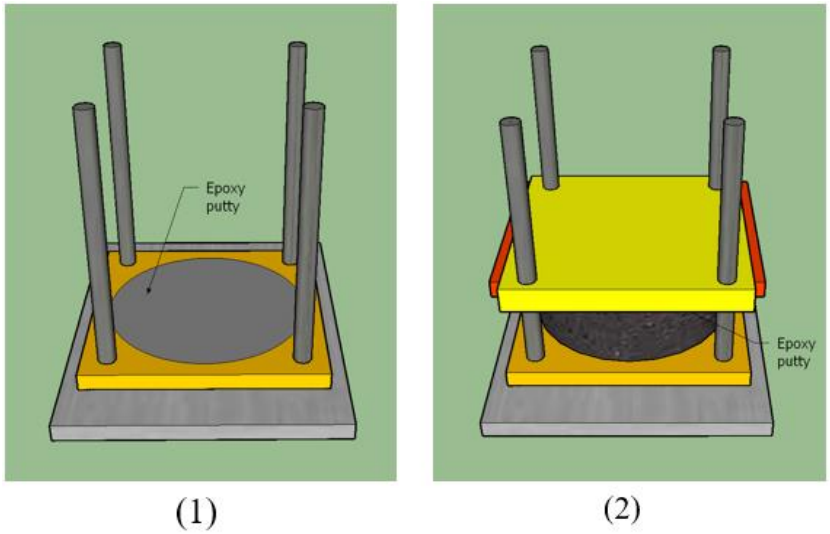

Figure 5-35. Procedure of Gluing an STNS Sample.

Figure 5-36. An assembled DST Sample.

5.7 Testing Temperatures and Conditions

The tests samples were conditioned at appropriate test temperature depending on tests procedure. The samples were conditioned at 30°C for the FSCH and FSNS, and 50°C for the RSCH and RSNS. Since the frequency shear tests are performed theoretically in the linear viscoelastic behavior domain, same test samples that were tested for the FSCH & FSNS tests were tested later for the RSCH& RSNS tests, respectively.

5.8 Executing of the Shear Tests and Collecting the Data

A test sample of DST or STNS device was installed inside the UTM-25 chamber immediately after it was conditioned at tests temperature inside the oven. Since the DST supporting plate is the common part for the two devices, the setup procedure of either DST or STNS device was performed initially by the proper installation of the DST supporting plate inside the UTM-25 chamber.

The following procedure were followed for installing the DST device inside the UTM-25 chamber:

- The supporting plate was fixed inside the UTM-25 chamber on the loading table by using two bolts of (5/8″-18, 2.0″ long). To line up the supporting plate center exactly with the UTM-25 actuator, a guide bolt was screwed on the center of the loading table. This guide matches the central hole of the supporting plate while the installation. Figure 5-37 shows the DST supporting plate installed on the UTM-25 Loading table.

Figure 5-37. Installation of the DST Supporting Plate on the UTM-25 Loading table.

- A DST sample was installed on the supporting plate by inserting the mini linear rails of the sample inside the mini carriages of the supporting plate.
- The sample was fixed to the supporting plate by using four bolts of (3/8″-16, 3/4″ long), which were attached to the sample grippers.
- Depending the shear test procedure, a proper loading attachment was installed. The loading attachments are shown previously in Figure 4-3.

- Two LVDT mounts (Figure 4-4) were installed on the DST sample at equal distances from the center of the sample middle plate. The LVDT holders of 0.315″ hole's diameter were used to hold the small LVDTs of (+/- 0.5 mm span) for the FSCH tests, whereas the LVDT holders of 0.370″ hole's diameter were used to hold the long LVDTs of (+/- 0.5 mm span) for the RSCH tests. Figure 5-38 shows the DST device installed on the loading table inside the UTM-25 chamber.

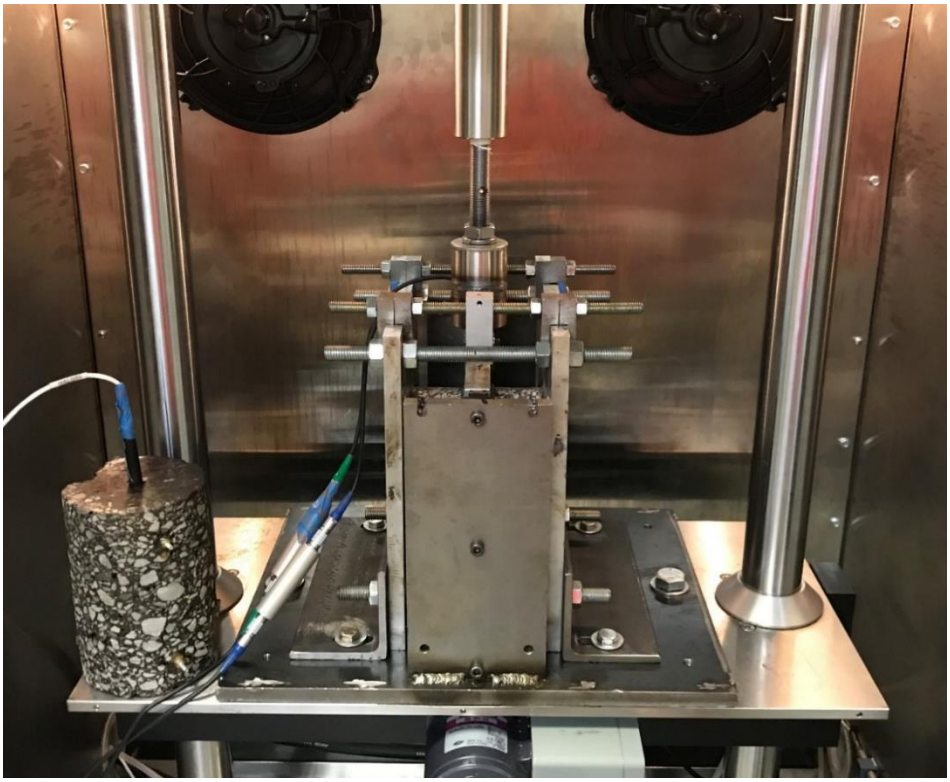

Figure 5-38. DST Device inside the UTM-25 chamber.

The following procedure were followed for installing the STNS device inside the UTM-25 chamber:

- The DST supporting plate was fixed inside the UTM-25 chamber. The same technique of the installation by using the central guide was followed, as shown previously in Figure 5-37.

- An initial setup of the STNS rigid frame was prepared. It includes connecting the two side plates (A& B) together and grippers by four threaded rods of (1/2″-13, 9.25″ long). Also, the setup includes fixing the two-air cylinder to the side plate B, connecting the air cylinders together by using regular fitting tools, installing the bracket plate, and suspending the ball bearing parallel tool by using two rubber bands. Figure 5-39 shows the initial setup of the STNS device frame.

Figure 5-39. Initial Setup of the STNS device frame.

- A lubricant grease material was applied on the base of the supporting plate, the ball bearing parallel, STNS bracket, and between the rolling systems and steel grippers of the STNS device. This technique was important to eliminate any potential friction between the STNS parts while the movements.
- The device frame was then installed on the supporting plate inside the UTM-25 chamber. The rolling systems were then fixed properly so that the frame moved freely only in the horizontal direction. The movements were checked manually by hands.
- A conditioned STNS sample was installed on the device frame. This was done by inserting the mini linear rails of the middle plate inside the mini carriages of the supporting plate. The sample after that was fixed to the side plate (A) by using two bolts of (1/2″-13, 1.75″ long). It

should be mentioned that the lubricant grease was also applied before installing the sample on the sample mini linear rails and the mini carriages of the supporting plate.

- Depending on the shear test procedure, a proper loading attachment was installed. The loading attachments were shown previously in Figure 4-3. Also, an air hose inside the UTM-25 chamber was connected directly to the air cylinders to be supplied with air pressure while testing.
- Two LVDT mounts, shown previously in Figure 4-7, were installed on the STNS sample at equal distances from the middle plate center. The LVDT holders of 0.315″ hole's diameter were used to hold the small LVDTs of (+/- 0.5 mm span) for the FSNS tests, whereas the LVDT holders of 0.370″ hole's diameter were used to hold the long LVDTs of (+/- 0.5 mm span) for the RSNS tests. Figure 5-40 shows the STNS device installed on the loading table inside the UTM-25 chamber.

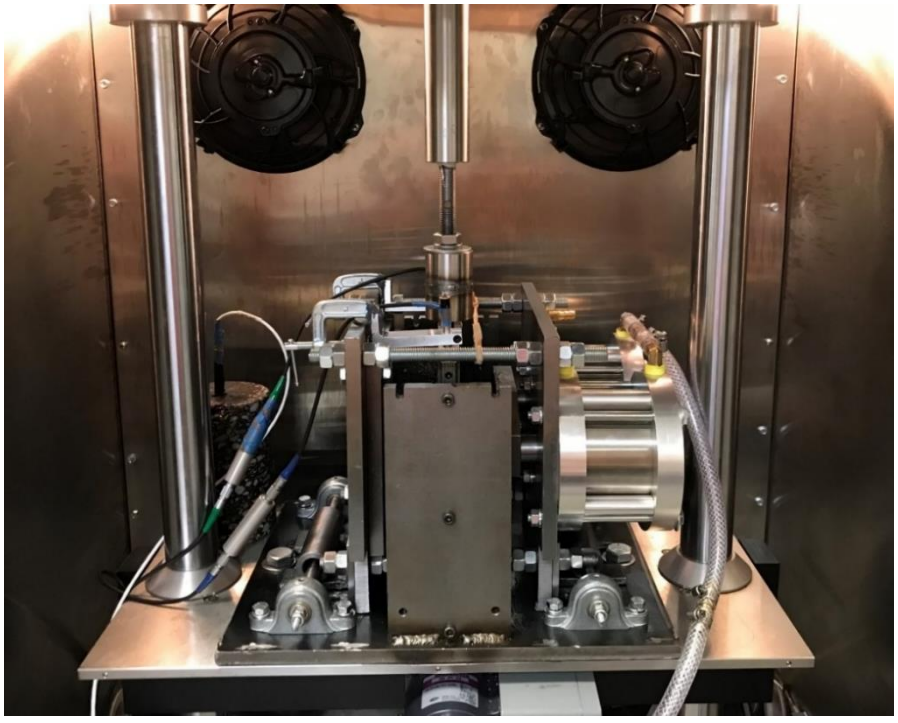

Figure 5-40. STNS Device inside the UTM-25 chamber.

5.8.1 Execution of the FSCH tests

The FSCH tests were executed by using a UTS-023 software. This software is developed by IPC Global™ to measure the dynamic modulus for asphalt mixes under dynamic compressive axial force in according to the standard test method AASHTO TP 62. To utilize this software for the FSCH tests, some inputs in the software had modified: the specimen's diameter, gauge distance and shear stress levels.

The input diameter in the software was modified depending on the number of loaded specimens at a time and the surface area of asphalt concrete specimens. Since a DST sample consists of two identical specimens of asphalt concrete, the input diameter for the FSCH tests compensated the surface area of two surfaces that sheared at the same time. The input diameter varies from FSCH test to another depending on the DST sample geometries. i.e., if the specimens have rectangular of circular shapes of large or small diameters. Table 5-10 summaries the input diameters of different DST samples in the UTS-023 software.

Table 5-10. DST input diameters in the UTS-023 software

Sample Types	Input Diameter (mm)
DST (150 mm) diameter	212.13
DST (99.06 mm) diameter	140.1
DST (125x75 mm)-Horizontal Slices	154.51
DST (125x75 mm)-Vertical Slices	154.51

The input value of the gauge distance was considered as the average plate to plate distance. It was a 50 mm for all FSCH tests since all test specimens have the same average distance of (50 ± 1 mm) between the plates.

The appropriate level of shear stresses at all load frequencies were determined by using the "Tuning condition" in the UTS-023 software. This is one of the software features that is used to determine the dynamic stress levels for each sweep frequency by adjusting the maximum and minimum loading levels to achieve a desirable stain. According to the standard test method AASHTO T-320, the preferable strain of for the frequency sweep tests is 100 micro-strains.

The procedure of determining the appropriate levels of shear stress using the "tuning condition" of the UTS-023 software are followed:

1- The maximum and minimum haversine loads were determined as inputs in the "Tuning Parameters" tab of the UTS-023 software. Since the UTM-25 loading machine can only support dynamic load application in one direction, the minimum load was determined as zero. The maximum load was selected as a first trial value of 2.0 KN starting from "Sweep 1" which is the highest load frequency of 10 Hz.

2- The "haversine pulse" button was selected to apply 10 load cycles in the first sweep. While the loads were applied, the "Average recoverable axial strain (με)" and the "Deviator dynamic stress (kPa)" are recorded at each load cycle. The desired recoverable axial strain at all frequencies of the FSCH test should be 100 micro strain.

3- Considering the linear behavior of the asphalt specimen, the load level was then calculated using equation 5-4, as follow:

$$Load\ Level\ (KN) = \frac{Max.load\ (KN)}{\text{Average recoverable axial strain } (\mu\varepsilon)} \times 100 \qquad (5\text{-}4)$$

4- The outcome of the previous equation was used as new "Maximum load" to be applied again for 10 cycles on the first sweep, as on Step 2. If the result value of the recoverable

axial strain was not close to 100 micro strain, the previous steps of calculating the load level and applying the haversine loads was repeated again for the first sweep.

5- Once the "Average recoverable axial strain (με)" approached a value close to 100 με, the result value of "Deviator dynamic stress (kPa)" was selected as a convenient level for the shear stress for the first sweep.

6- The same procedure was conducted for the other lower frequencies and the appropriate levels of shear stresses were determined. Since the dynamic modulus decreases at lower frequencies, a lower level of maximum load was selected for the next sweep as a first trial. It was observed that about 85 percent of the maximum load of the previous frequency sweep can be selected as the first trial value for the next frequency.

7- After the appropriate levels of shear stresses were determined for of the ten frequencies, they were entered as maximum deviator stresses in the "Test Parameters" tab of the software. The negative values of those levels were also entered as minimum deviator stresses for the all frequencies. Table 5-11 summaries the determined levels of shear stresses at all load frequencies for the FSCH tests.

Table 5-11. Shear stress levels of the FSCH tests.

Sweeps	Sweep 1	Sweep 2	Sweep 3	Sweep 4	Sweep 5	Sweep 6	Sweep 7	Sweep 8	Sweep 9	Sweep 10
Frequency (Hz)	10	5	2	1	0.5	0.2	0.1	0.5	0.02	0.01
Number of load cycles	50	50	20	20	7	7	7	4	4	4
Max Deviator Stress (kPa)	89	77	63	55	47	38	33	29	23	21
Min Deviator Stress (kPa)	-89	-77	-63	-55	-47	-38	-33	-29	-23	-21

Some levels were controlled through the “Transducer Levels” tab of the software while installing a DST sample for testing. The levels include the UTM-25 actuator position and load, the LVDT ranges, and test temperature. The actuator position and load were maintained at zero to prevent any excessive stresses to the specimens while setting up a test sample. The LVDTs levels were maintained closed to zero the middle of their ranges so that they have an enough span to measure the cyclic strains during the tests while shearing the sample. Once the setup of the sample was completed, the frequency sweep test was executed and the shear stress and stain at each frequency were recorded by the software.

The measured average dynamic shear modulus |G*| and phase angle (δ) at each applied load frequency are the main parameters that are obtained from the FSCH tests. Figure 5-41 shows a screenshot of a FSCH test for a tested DST sample at 30°C. The figure shows all resulted measurements including the load frequencies, cycle counts and dynamic modulus. It also shows the applied sinusoidal shear loads and the corresponding strains were measured by the LVDTs at Sweep 2 of 5 Hz frequency.

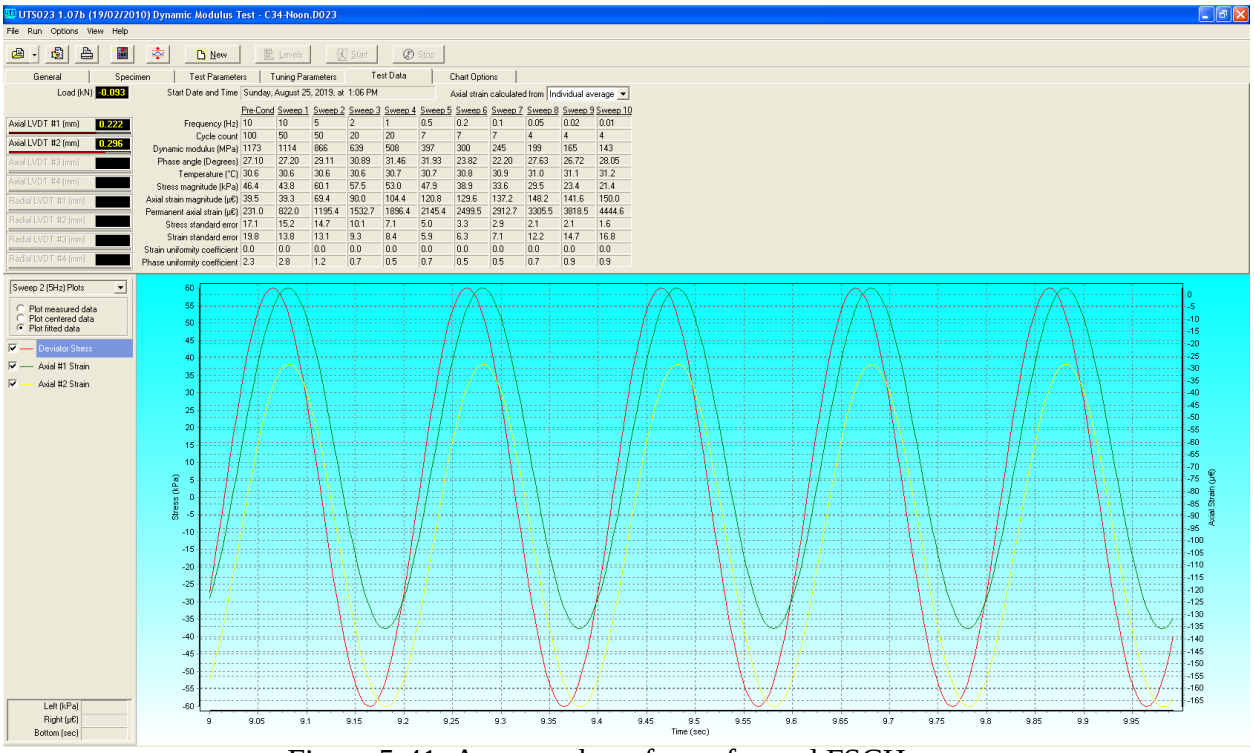

Figure 5-41. A screenshot of a performed FSCH test.

5.8.2 Execution of the FSNS tests

Similar to the FSCH tests, the FSNS tests were executed by using a UTS-023 software. The input diameter for the FSNS tests was 150 mm because the STNS device can accommodate one asphalt concrete specimen of 150 mm diameter at a time. The gauge distance was also considered as 50 mm because all specimens have the same average distance of (50 ± 1 mm) between the plates. The UTM-25 actuator position and load, the LVDT ranges, and test temperature were also controlled through the "Transducer Levels" tab of the software same as for the FSCH tests.

Since the STNS device accommodates one specimens of asphalt concrete, the appropriate level of shear stresses for the FSNS tests were assumed as 50% of the determined levels for the FSNS tests with the DST device. Table 5-12 the used shear stresses at all load frequencies for the FSNS tests.

Table 5-12. Shear stress levels of the FSNS tests.

Sweeps	Sweep 1	Sweep 2	Sweep 3	Sweep 4	Sweep 5	Sweep 6	Sweep 7	Sweep 8	Sweep 9	Sweep 10
Frequency (Hz)	10	5	2	1	0.5	0.2	0.1	0.5	0.02	0.01
Number of load cycles	50	50	20	20	7	7	7	4	4	4
Max Deviator Stress (kPa)	45	39	32	28	24	19	17	15	12	11
Min Deviator Stress (kPa)	-45	-39	-32	-28	-24	-19	-17	-15	-12	-11

The loading shaft diameter was modified in the software to assure that the selected deviator stresses correspond to the applied shear stresses on the test specimen. As mentioned earlier, the UTS-023 software is normally used to measure the dynamic modulus of asphalt concrete mixes according to AASHTO TP 62. The dynamic modulus test is typically performed on a compacted asphalt concrete cylinder by applying a dynamic axial compressive force to the specimen with or without an additional confining pressure depending on the test procedure.

A direct relationship between the developed shear stress (τ) in the FSNS tests and the deviator stress (σ_d) considered in the software for the dynamic modulus test was derived as shown in Equation (5-5). Therefore, the loading shaft diameter (d_s) was assumed to be zero in the software so that the developed shear stress was equal to the applied deviator stresses.

$$F_V = F_A + P_C\left[D^2 - {d_s}^2\right]$$

$$\sigma_d = \sigma_v - P_c$$

$$\sigma_d = \frac{F_A + P_C\left[D^2 - {d_s}^2\right]}{\frac{\pi}{4}.D^2} - P_c = \frac{4\,F_A}{\pi.D^2} - P_c\left(\frac{d_s}{D}\right)^2$$

$$F_A = \frac{\pi}{4}\left[\sigma_d.D^2 + P_c.\ {d_s}^2\right]$$

$$\tau = \frac{F_A}{\frac{\pi}{4}.D^2} = \frac{\frac{\pi}{4}\left[\sigma_d.D^2 + P_c.\ {d_s}^2\right]}{\frac{\pi}{4}.D^2}$$

$$\tau = \sigma_d + P_c\left(\frac{d_s}{D}\right)^2 \qquad (5\text{-}5)$$

Where:

F_V: Total axial loads applied on the specimen (KN),

F_A: Axial load applied by the UTM-25 actuator (KN),

P_C: Confining pressure applied on the specimen (kPa),

σ_d: Deviator stress (kPa),

σ_v: Total vertical stress applied on the specimen (kPa),

d_s: Loading shaft diameter (mm),

D: Diameter of a tested asphalt concrete specimen (mm),

τ: Shear stress developed on the specimen (kPa).

According to the applied normal stress in the FSNS tests, it was decided to apply a confining air pressure of 113 kPa (16.39 Psi) through the air cylinders of the STNS device. This pressure value was selected based on the previous stress levels that were determined for the SST

tests. As discussed in the literature review of the SST test methods, both tests of the Repeated Shear at Constant Stress Ratio Test (RSCSR) and the Repeated Shear Test at Constant Height (RSCH) were conducted to measure the accumulative permeant deformation of an asphalt specimen that is subjected to repeated haversine shear loads of 5,000 cycles or until a 5% of accumulative permanent stain is reached.

For the RSCSR test, the ratio of the applied axial to the shear load is maintained constant within a range of 1.2 to 1.5 (McGennis, et al., 1994). The stresses values of this test were selected to simulate the real in-place stresses of pavements based on the asphalt content in the HMA layer and the base layer conditions for stabilized or un-stabilized base layers, as shown previously in Table 3-6. The RSCH test, however, is conducted by applying repeated shear stress of 69 kPa.

Using the constant ratio of 1.5 for the applied axial to shear load and 69 kPa for the applied shear load, an axial stress of 103.5 kPa (15 Psi) was obtained. The final pressure (P_f) transmitted to the STNS specimen is 91.7 % of the applied air pressure (P_i) inside the air cylinders, as shown previously in Equation (4-1). Therefore, the needed applied pressure into the air cylinders is 113 kPa (16.35 Psi). This pressure was selected as input in the UTS-025 software to be applied at all load frequencies.

The measured average dynamic shear modulus |G*| and phase angle (δ) at each applied load frequency are the main parameters that are obtained from the FSNS tests. Figure 5-43 shows a screenshot of a FSNS test for a tested STNS sample at 30°C. The figure shows all inputs of load frequencies, number of cycles, maximum and minimum deviator stresses, and the applied confining pressure at each load frequency. It also shows the applied sinusoidal shear loads and the corresponding strains were measured by the LVDTs at Sweep 5 of 0.5 Hz frequency.

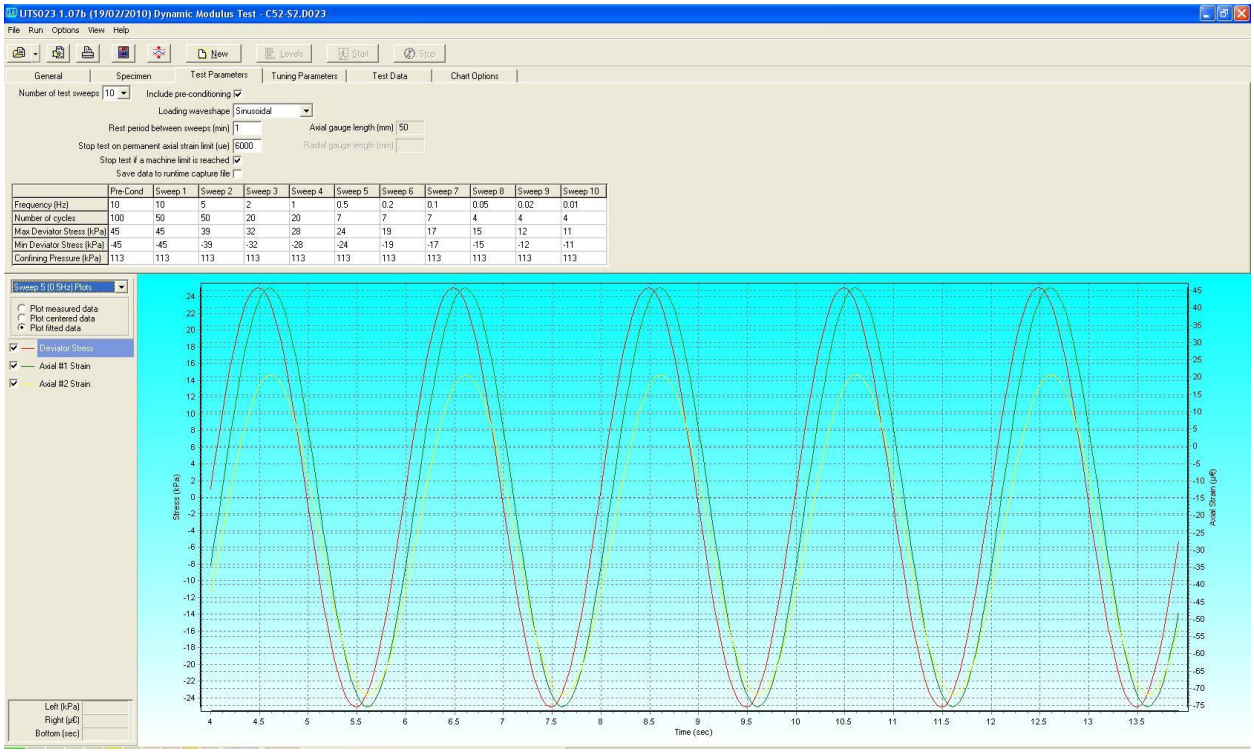

Figure 5-42. A screenshot of a performed FSNS test.

5.8.3 Execution of the RSCH tests

The RSCH tests were executed by using a UTS-014 software. This software is also developed by IPC Global™ to measure the permanent deformation of asphalt specimens under repeated cyclic pluses or static axial load. As modified in the UTS-023 software, the diameter of the specimen, gauge distance, and shear stress levels were modified in the UTS-014 software to be used for the RSCH tests.

The input diameters of tested samples were modified depending on the geometries of DST samples, similar to the FSCH tests, as summarized previously in Table 5-10. Also, the gauge distance value was unified for all samples to be 50 mm as it represents the average plate to plate distance. The UTM-25 actuator position and load, the LVDT ranges, and test temperature were also controlled through the “Transducer Levels” tab of the software before launching the tests.

A seating stress of 3.4 kPa was selected in the software to assure a proper initial seating of the actuator's head on the middle plate of DST samples. Since the RSCH tests are performed according to the standard test method AASHTO T-320, the test applies a cyclic haversine loads of 69 kPa stress level for periods of 0.1 seconds followed by 0.6 seconds of rest. The repeated loads applied for 5,000 cycles or till a 5% permanent deformation was reached, whichever comes first.

The accumulated permanent deformation of asphalt concrete is the only parameter that is measured in the RSCH tests. It is measured by calculating the average readings of the total permanent deformation recorded by two LVDTs mounted on a tested DST sample. Figure 5-43 shows a screenshot of a RSCH test for a tested DST sample at 50°C. The figure shows all input parameters in the software as well as two permanent deformation curves that are measured by the LVDTs for the first 5,000 repeated load cycles.

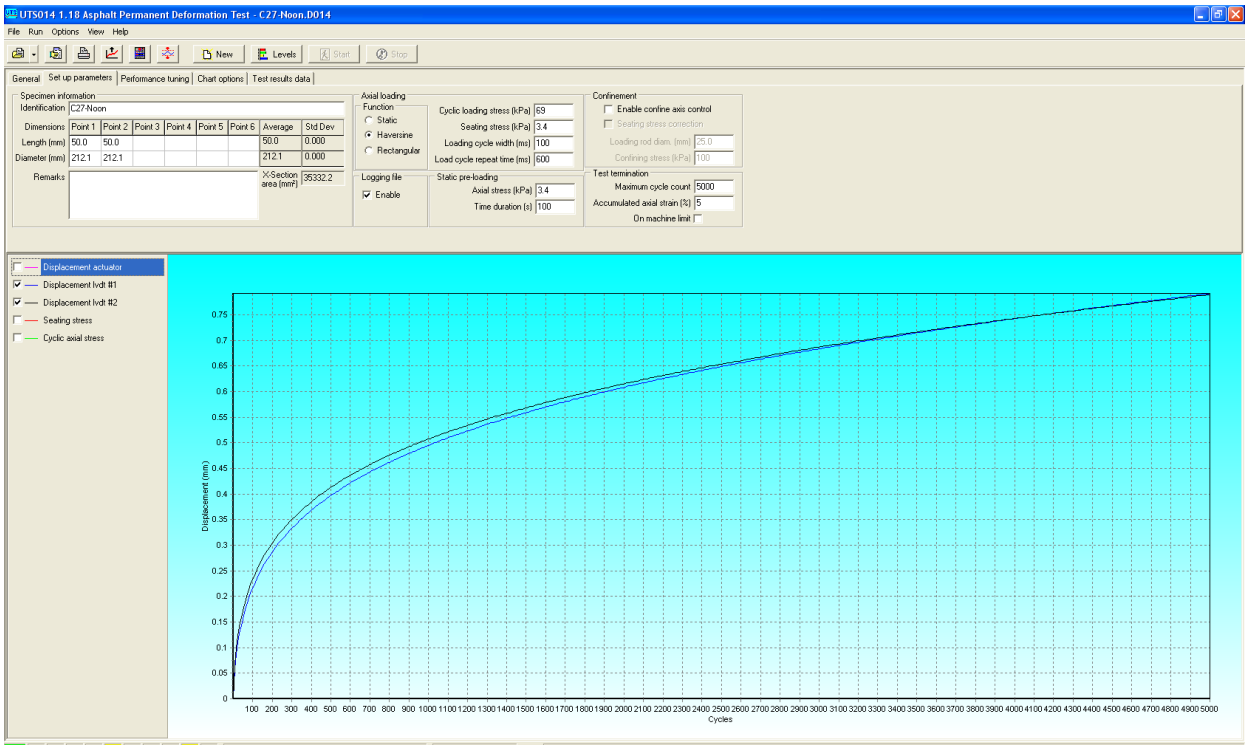

Figure 5-43. A screenshot of a performed RSCH test.

5.8.4 Execution of the RSNS tests

The RSNS tests were executed similarly to the RSCH tests, but with an additional confining pressure of 113 kPa (16.39 Psi) applied through the air cylinders. The input diameter in the software was 150 mm because the STNS device loads only one asphalt concrete specimen of 150 mm diameter. The gauge distance was considered as 50 mm because all specimens have the same average distance of $(50 \pm 1\ \text{mm})$ between the plates. The UTM-25 actuator position and load, the LVDT ranges, and test temperature were also controlled before launching the tests through the "Transducer Levels" tab of the software.

The following test parameters were used for the RSNS test:

- Seating stress of 3.4 kPa.
- Haversine loads of 69 kPa.
- Applied loads for 5,000 cycles or till 5% permanent deformation was reached, whichever comes first.
- Confining air pressure of 113 kPa (16.39 Psi).
- Loading Shaft diameter (d_s) is zero.

The accumulated permanent deformation of asphalt concrete is the only parameter that is measured in the RSNS tests. It is measured by calculating the average readings of the total permanent deformation recorded by two LVDTs mounted on a tested DST sample. Figure 5-44 shows a screenshot of a RSNS test for a tested STNS sample at 50°C. The figure shows all input parameters in the software as well as two permanent deformation curves that are measured by the LVDTs for 5,000 repeated load cycles.

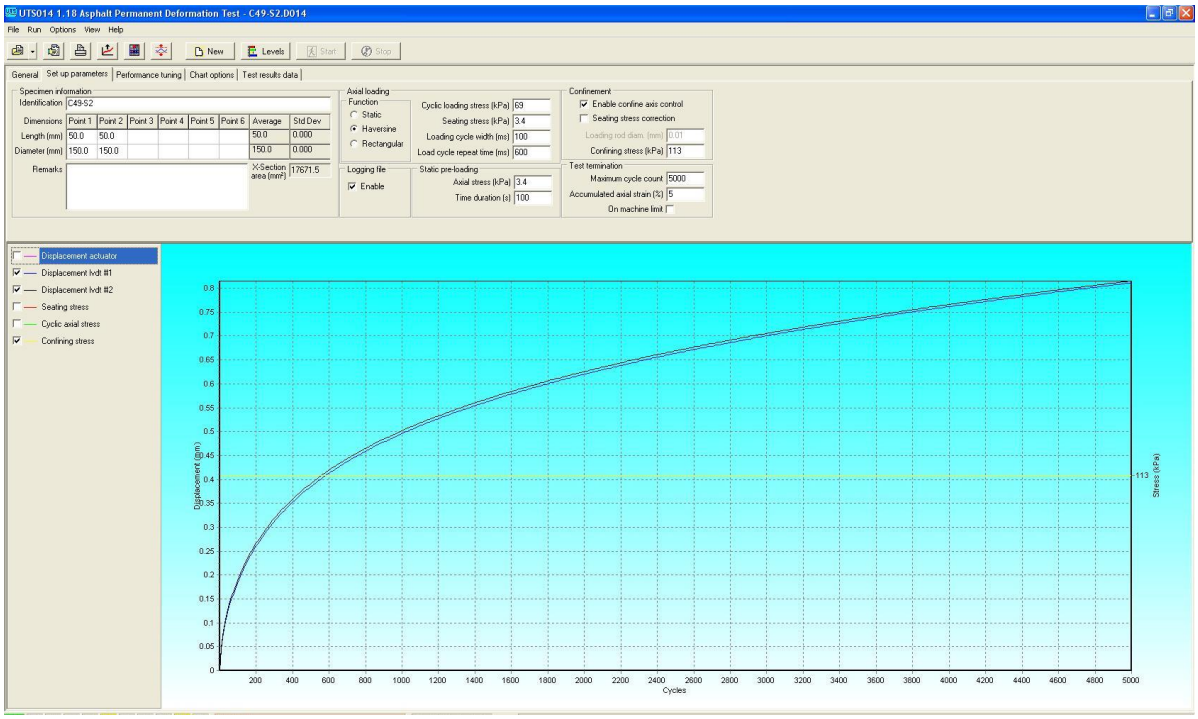

Figure 5-44. A screenshot of a performed RSNS test.

5.9 Cleaning Samples

The cleaning was performed after conducting all tests on each samples group. It includes removing the asphalt concrete and the glue materials on the plates in order to use them for preparing another testing group. The tested samples were placed inside a hot air oven at 204°C (400 °F) for at least 3 hours before they were cleaned by a steel scraper and wire brush. An acetone was used after that to remove any residual on the plates.

Chapter 6: Tests Results and Discussion

After conducting all laboratory tests, the results data were extracted in form of Microsoft Excel tables. Three shear parameters were obtained from the data of each asphalt mix: the shear dynamic modulus |G*| and phase angle (δ) from the FSCH & FSNS tests, and the total permanent deformation (PD) from the RSCH & RSNS tests. The raw data recorded from the DST and STNS devices are given in Appendix G.

The first part of this chapter is an introduction presents the average values of the measured shear parameters of each mix. Also, it discusses the variability of the measured parameters of each mix based on the calculated coefficient of variation (COV). The second part of this chapter compares the test results of both devices by using the Analyses of Variances (ANOVA) technique.

6.1 Introduction

As discussed in Chapter 5, the collected data in the frequency shear and repeated shear tests that performed with the DST and STNS devices were used to calculate the shear dynamic modulus |G*|, shear phase angle (δ), and the total permanent deformation (PD) of asphalt mixes. Eight replicate samples were tested for each loading condition in the frequency sweep and repeated shear tests protocols. The initial observation of these data showed that most testing groups have a high and low values that affect the consistency of the tests results. Therefore, it was decided to exclude the high and low values from each testing group before conducting the statistical analysis.

The extreme samples were selected from each testing group based on the following:

1- In the FSCH & FSNS tests, the two samples of the highest and lowest values of the shear dynamic modulus |G*| at 10Hz frequency were excluded from the shear dynamic modulus |G*| and phase angle (δ) analysis.

2- In the RSCH & RSNS tests, the two samples of the highest and lowest values of the total permanent deformation (PD) were excluded from the tests results.

The excluded samples at the FSCH & FSNS tests were not necessary the same as the excluded samples for the RSCH & RSNS tests.

To simplify the discussion on the obtained results of each mix, the data are presented in groups based on the testing device and asphalt mixes type. Also, the testing groups designation of each type of the asphalt mixes are abbreviated to indicate for the device, shape or size of the specimens, and the daily time interval of collecting asphalt mixes, respectively. For example, the abbreviation (DST-RH-N) represents the testing group of DST samples that have rectangular specimens cut horizontally and made from asphalt mix collected at Noon. Similarly, the (STNS-C6-M) represents the testing group of STNS samples that have circular specimens of 150 mm ($\cong 6.0''$) diameter and made of the asphalt mix collected in the Morning.

6.1.1 Discussion on the DST device Results.

As discussed in Chapter 5, the DST device is used to measure the average shear parameters of two asphalt specimens at the same time. The FSCH and RSCH tests were the two main tests that performed by this device.

Frequency Sweep Test at Constant Height (FSCH)

The average shear dynamic modulus |G*| of all DST groups of asphalt mixes D, C and B are plotted against the logarithm of frequency loads in Figures 6-1, 6-2, and 6-3 respectively. Figure 6-1 shows, as expected, the average shear dynamic modulus |G*| increased with the load frequency. The (DST-C4-N) group showed the highest |G*| at all frequencies range. The

(DST-C6-M &N) groups showed interchangeable values of the minimum |G*| over the load frequencies. The former group showed the lowest values at lower frequency ranges, while the latter group showed that at frequencies above 2 Hz. The difference between the maximum and minimum values of |G*| is about 60% at 10 Hz frequency.

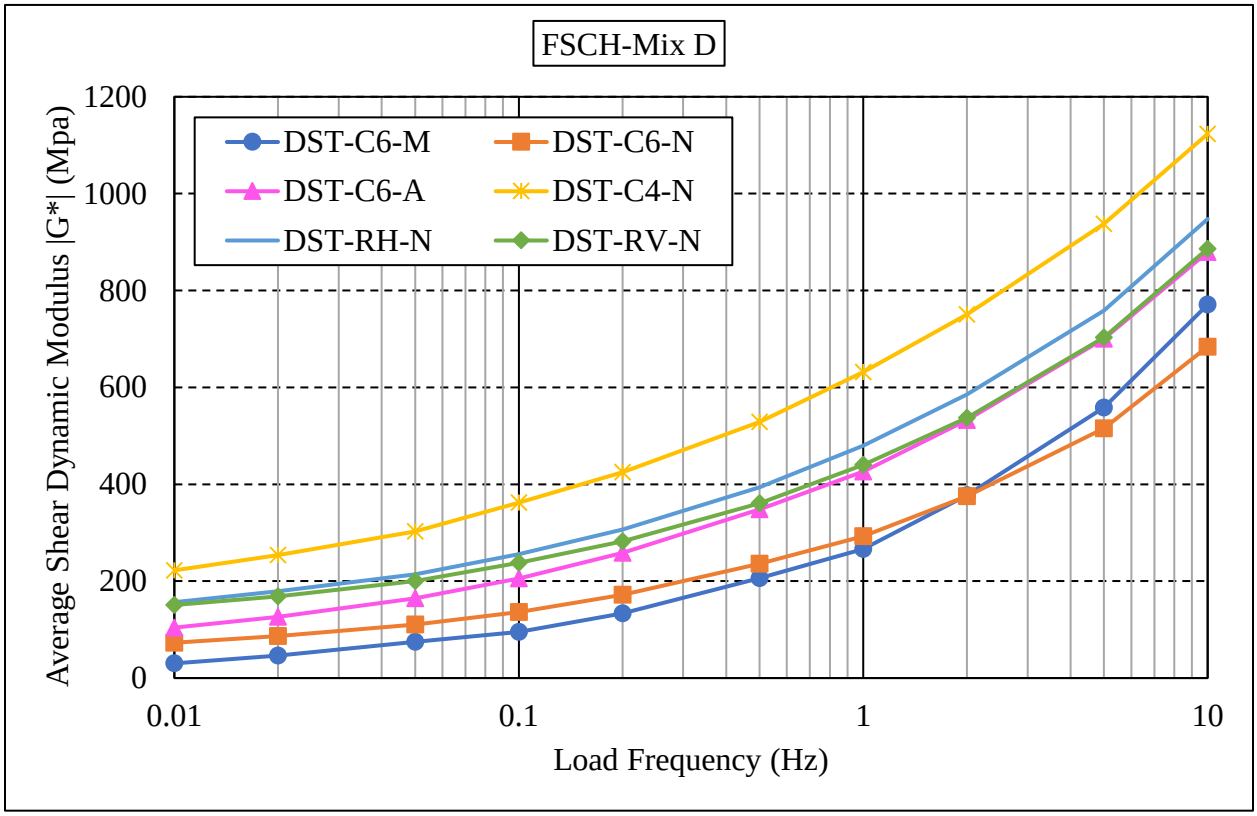

Figure 6-1. Average Shear Dynamic Modulus of DST testing groups- Asphalt Mix D

Figure 6-2 shows, as expected, that the average shear dynamic modulus |G*| of all DST groups of asphalt mix C increased with increasing the load frequency. The (DST-C6-M) group had the lowest |G*| at all frequencies, followed by the (DST-C6-A) group. The (DST-RH-N) group showed the highest |G*| at all load frequencies. The difference between the maximum and minimum |G*| values is about 20% at 10Hz frequency.

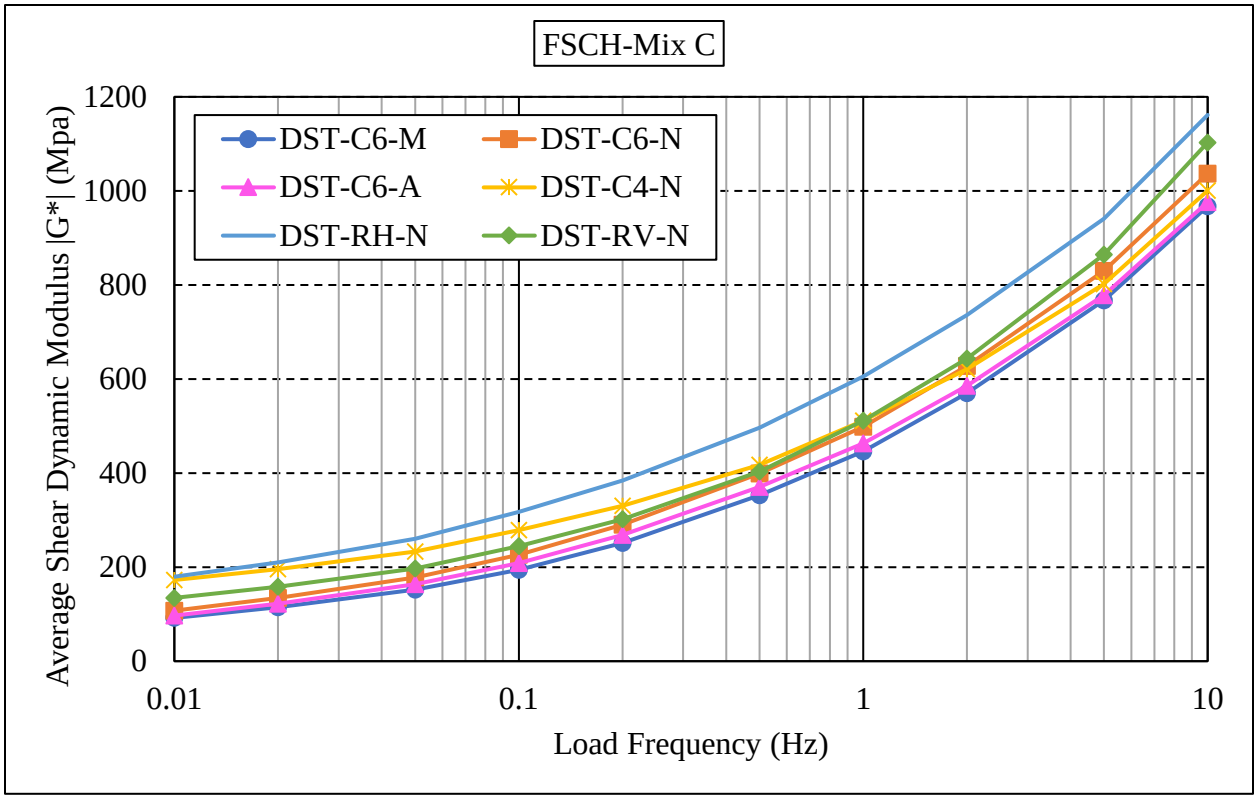

Figure 6-2. Average Shear Dynamic Modulus of DST testing groups- Asphalt Mix C

Figure 6-3 shows, as expected, that the average shear dynamic modulus |G*| of all DST groups of asphalt mix B increased with the shear load frequency. The trends of (DST-C4-N, DST-RV-N & DST-RH-N) groups remained very close together between the frequency 0.01Hz and 0.1Hz, before they diverted gradually to record the highest modulus at 10Hz by the (DST-RH-N) group. The (DST-C6-M, N& A) groups recorded together the minimum moduli at 0.01 Hz and kept marginally close together till the 10Hz frequency. The difference between the maximum and minimum |G*| values is about 30% at 10Hz frequency.

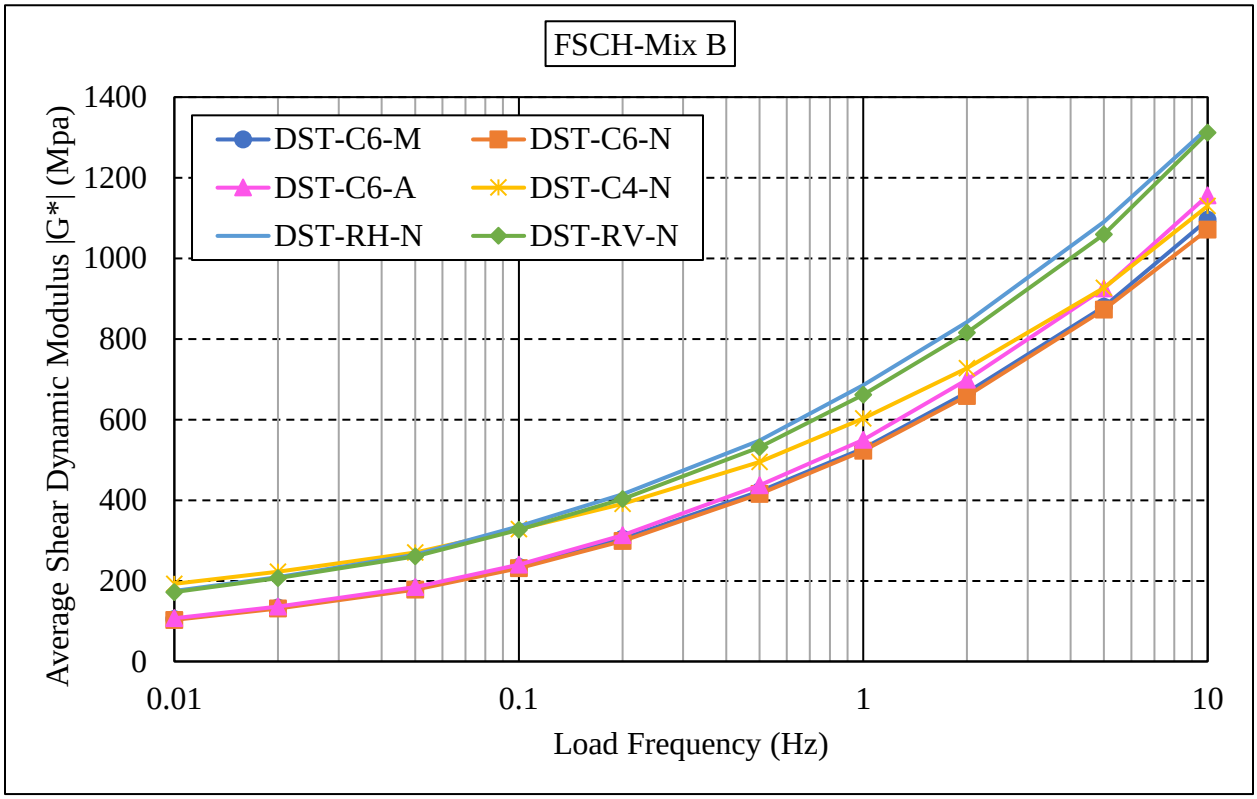

Figure 6-3. Average Shear Dynamic Modulus of DST testing groups- Asphalt Mix B

To assess the variability of the measured parameters of each asphalt mix, the coefficient of variation (COV) was calculated. The COV is defined as the ratio of the standard deviation to the mean value. It gives an indication about the repeatability of the measurements. The calculated COV of the shear dynamic modulus of asphalt mixes C, D, and B are given in Table 6-1 for each DST group.

The shear dynamic modulus of all DST groups of asphalt mix D yielded generally COV values less than 8% at high frequencies of 10Hz and 5.0Hz. However, the (DST-RV-N and DST-C6-N) groups have shown a gradual increasing in the COV above the 0.2 Hz loading frequency. The maximum COV of about 16.5% was recorded at 0.01Hz frequency by the (DST-C6-N) group. The shear dynamic modulus for all DST groups of asphalt mix C had COV values of less than 11% at high frequencies of 10 Hz and 5.0 Hz. However, all groups show inconsistent increasing and

decreasing in the COV values from 2.0 Hz to 0.01 Hz load frequencies. The highest variability of 17% was recorded at 0.01 Hz by the (DST-C6-M) group. For asphalt mix B, the shear dynamic modulus of all DST groups yielded COV values of less than 8.0% at high frequencies from 10 Hz to 1.0 Hz. The highest variability of about 14.5% was recorded at 0.01 Hz by the (DST-RV-N) group.

Table 6-1. COV of Shear Dynamic Modulus (G*) of DST groups- Mixes D, C& B.

Coefficient of Variation (COV%)- Shear Dynamic Modulus of DST groups											
Mixes	Testing Groups	Loads Frequency (Hz)									
		10	5	2	1	0.5	0.2	0.1	0.05	0.02	0.01
Mix D	DST-C6-M	2.2	2.3	2.5	3.1	3.8	5.0	6.3	7.5	8.9	11.0
	DST-C6-N	4.8	4.9	5.5	6.0	7.1	8.6	9.9	11.4	13.8	16.3
	DST-C6-A	7.4	7.8	8.1	8.4	8.2	8.3	8.1	8.1	8.5	8.8
	DST-C4-N	2.8	3.4	4.1	4.3	4.9	5.2	5.2	5.4	5.7	6.1
	DST-RH-N	3.7	4.4	5.5	5.7	5.7	5.8	5.4	4.5	4.2	4.7
	DST-RV-N	7.0	7.9	8.7	8.8	9.5	10.3	11.1	11.6	12.5	12.9
Mix C	DST-C6-M	3.1	3.6	3.7	4.1	4.9	6.5	8.4	10.7	13.9	17.0
	DST-C6-N	8.2	9.7	11.1	12.4	13.8	15.6	16.4	16.5	16.0	15.2
	DST-C6-A	6.4	6.8	7.6	8.6	9.0	9.7	9.7	8.7	7.5	5.9
	DST-C4-N	9.7	10.2	11.5	12.2	12.9	13.8	14.4	14.6	15.5	15.8
	DST-RH-N	3.6	4.5	6.1	6.8	7.7	8.3	8.7	8.6	8.6	8.6
	DST-RV-N	4.0	5.4	6.8	7.7	8.5	8.8	9.8	10.2	11.5	12.2
Mix B	DST-C6-M	3.5	3.6	4.2	4.7	5.1	5.6	6.1	6.6	7.4	8.5
	DST-C6-N	4.1	4.2	5.4	6.3	7.2	8.4	9.0	9.4	9.8	10.1
	DST-C6-A	4.1	4.2	4.3	4.6	5.0	5.8	7.0	8.5	10.9	13.5
	DST-C4-N	6.6	7.0	7.5	7.6	7.7	7.4	7.1	7.2	8.1	9.6
	DST-RH-N	3.5	3.8	5.1	5.9	7.4	8.4	8.4	8.2	7.1	6.3
	DST-RV-N	6.6	6.3	7.3	7.9	8.4	9.3	10.2	10.7	12.9	14.4

According to the average shear phase angle (δ) of all DST groups, Figures 6-4, 6-5, and 6-6 show the plots of average (δ) against the logarithm of frequency loads of all DST groups for asphalt mixes D, C and B, respectively. Figure 6-4 shows the average shear phase angle of all groups followed a similar trend over the frequency ranges. It can be seen clearly that the phase

angle decreased steady for all groups between the frequency intervals from 0.01 Hz to 0.1 Hz and from1 Hz to10 Hz. All trends showed a graduate increasing within the middle frequency interval from 0.1 Hz to 1.0 Hz. The (DST-C6-M) group showed the highest phase angle at all frequencies, followed by the (DST-C6-N) group. The (DST-C4-N) group had the lowest values of phase angle at all frequencies.

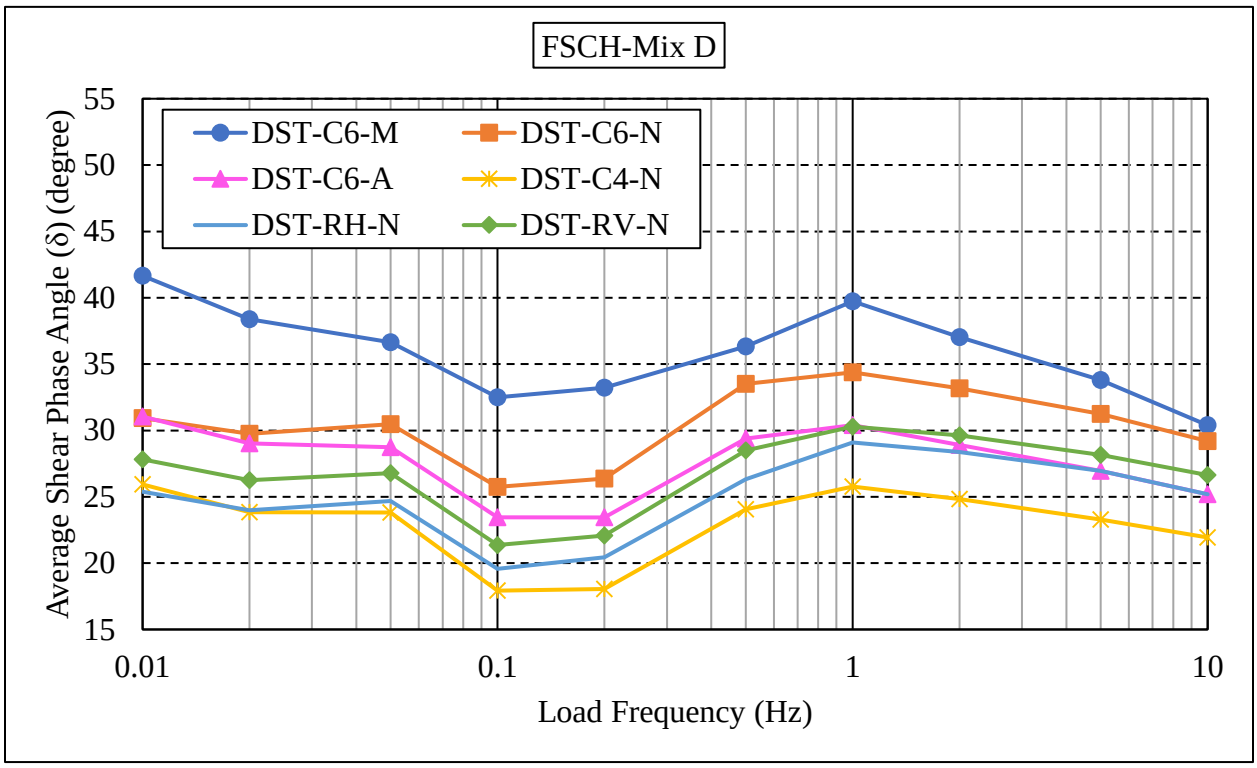

Figure 6-4. Average Shear Phase Angle of DST testing groups- Asphalt Mix D

Figure 6-5 shows that the average shear phase angle of all DST groups of asphalt mix C followed the same trends as for the asphalt mix D at all frequencies. The phase angle of all groups decreased between the frequency intervals of (0.01 Hz to 0.1 Hz) and (1 Hz to10 Hz), while they showed a gradual increasing within the middle interval from 0.1 Hz to 1.0 Hz. The highest phase angles were shown by the (DST-C6-M) group at lower frequency till 2.0 Hz, before it shown by the testing group (DST-RV-N) till the highest frequency. The lowest trend of phase angles was shown by the (DST-C4-N) group at lower frequency till 0.5 Hz, before it shown by the testing

group (DS-RH-N) till the highest frequency. Throughout the frequencies, the phase angle of both (DST-C6 -N& A) groups kept marginally the same values.

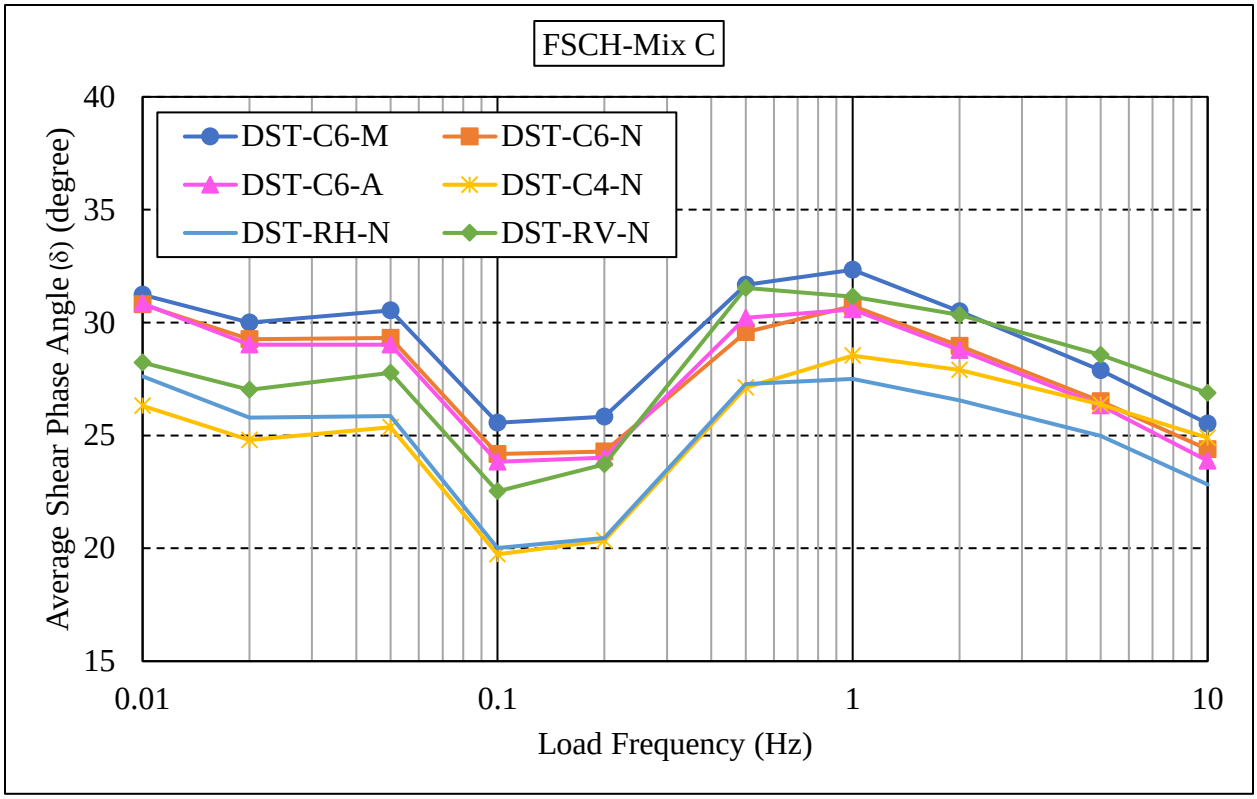

Figure 6-5. Average Shear Phase Angle of DST testing groups- Asphalt Mix C

Figure 6-6 shows that the average shear phase angle of all DST groups of asphalt mix B followed the same trends as for the asphalt mixes D and C at all frequencies. All trends decreased between the frequency intervals of (0.01 Hz to 0.1 Hz) and (1 Hz to10 Hz), while they showed a gradual increasing within the middle interval from 0.1 Hz to 1.0 Hz. All groups of 150 mm diameter specimens (C6) kept very close together and showed the maximum phase angle throughout the frequencies range. The lowest trend of phase angles was for the (DST-C4-N) group at frequencies below 2.0 Hz. Above 2.0 Hz frequency, the lowest phase angle was shown by the (DST-RH-N) group.

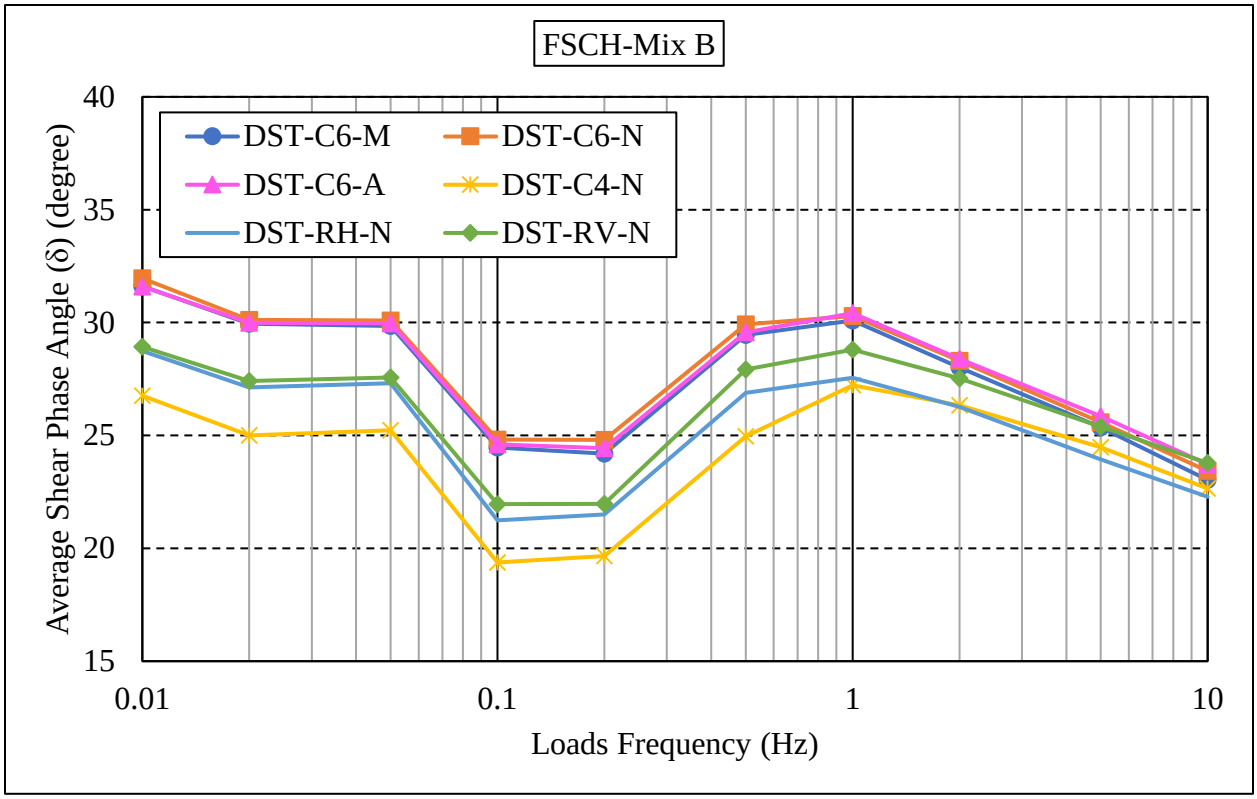

Figure 6-6. Average Shear Phase Angle of DST testing groups- Asphalt Mix B

The calculated COV of the shear phase angle (δ) of asphalt mixes C, D, and B are given in Table 6-2 for all DST groups. As shown in the table, the phase angle of all DST testing groups of asphalt mix D has COV values of less than 8.0% at all frequencies range. The (DST-C6-M) group has the lowest COV values of less than 3.0% at all frequencies.

For the phase angle of asphalt mix C, all DST groups have COV values of less than 10% at all frequencies. The highest variability of about 9.7% was recorded at 10 Hz by the (DST-RH-N) group, followed by the (DST-C6-N) group with about 9.5% COV. The (DST-C6-M) group was recorded low COV values of about 5.5% and 4.5% at 10 Hz and 0.5 Hz frequencies, respectively. The phase angles of all groups of asphalt mix B have COV of less than 8.0 % at all frequencies. The highest variability of about 7.5% were recorded at 0.5 Hz frequency by the (DST-RH-N) group.

Table 6-2. COV of Shear Phase Angle (δ) of DST groups- Mixes D, C& B.

Coefficient of Variation (COV%)- Shear Phase Angle of DST groups											
Mixes	Testing Groups	Loads Frequency (Hz)									
		10	5	2	1	0.5	0.2	0.1	0.05	0.02	0.01
Mix D	DST-C6-M	2.52	2.75	2.14	1.66	2.73	1.80	1.42	1.42	1.63	1.67
	DST-C6-N	3.53	3.18	2.46	2.33	4.02	3.63	3.69	2.57	2.91	2.83
	DST-C6-A	6.24	5.64	5.06	4.33	5.70	5.98	5.50	4.42	4.17	3.47
	DST-C4-N	6.09	4.92	4.55	3.79	7.01	5.47	5.23	3.66	3.63	2.98
	DST-RH-N	5.73	5.34	4.75	3.95	5.41	6.10	7.33	6.93	7.89	7.74
	DST-RV-N	5.26	5.12	4.73	4.34	4.71	5.08	4.09	2.83	2.67	2.76
Mix C	DST-C6-M	5.36	4.46	4.19	4.17	4.37	5.46	6.30	5.31	5.11	4.16
	DST-C6-N	9.36	8.73	8.44	7.79	9.09	9.30	6.93	4.44	2.35	1.30
	DST-C6-A	7.39	7.00	6.33	5.66	5.04	5.86	5.50	4.25	3.92	3.96
	DST-C4-N	5.87	5.56	5.74	5.73	6.83	6.85	6.73	4.16	4.22	4.47
	DST-RH-N	9.69	9.48	7.84	6.43	8.37	6.05	4.03	2.99	3.02	3.33
	DST-RV-N	9.01	7.31	5.86	5.20	5.63	4.68	7.61	6.23	7.24	7.25
Mix B	DST-C6-M	2.73	3.42	2.93	2.75	4.75	3.59	2.95	2.20	2.02	2.01
	DST-C6-N	4.61	5.10	5.10	4.95	6.51	6.63	5.36	3.44	3.24	3.10
	DST-C6-A	3.98	4.28	3.42	3.07	3.02	2.92	3.42	2.95	3.33	2.91
	DST-C4-N	4.14	2.47	2.46	2.32	3.04	3.91	5.03	3.87	4.90	4.83
	DST-RH-N	6.77	6.22	5.42	4.42	7.36	5.80	4.17	2.70	2.56	2.46
	DST-RV-N	4.75	3.54	2.79	3.08	3.22	5.31	6.07	4.05	4.73	5.42

Repeated Shear Test at Constant Height (RSCH)

For the RSCH tests results, Figures 6-7 shows the average permanent deformation of all DST groups for asphalt mixes D, C, and B, respectively. All groups of the three mixes recorded generally permanent deformations of less than 1.1 mm at 5,000 load cycles. The maximum deformation of about 1.1 mm was recorded for mix D by the (DST-C6-N) group, while the minimum deformation of about 0.7 mm was recorded for mix B by the (DST-RV-N) group. Generally, both rectangular groups showed high values for mix D, followed for mixes C and B, respectively. The other groups of large and small diameters showed generally inconsistent increasing and decreasing in the permanent deformation for the three mixes.

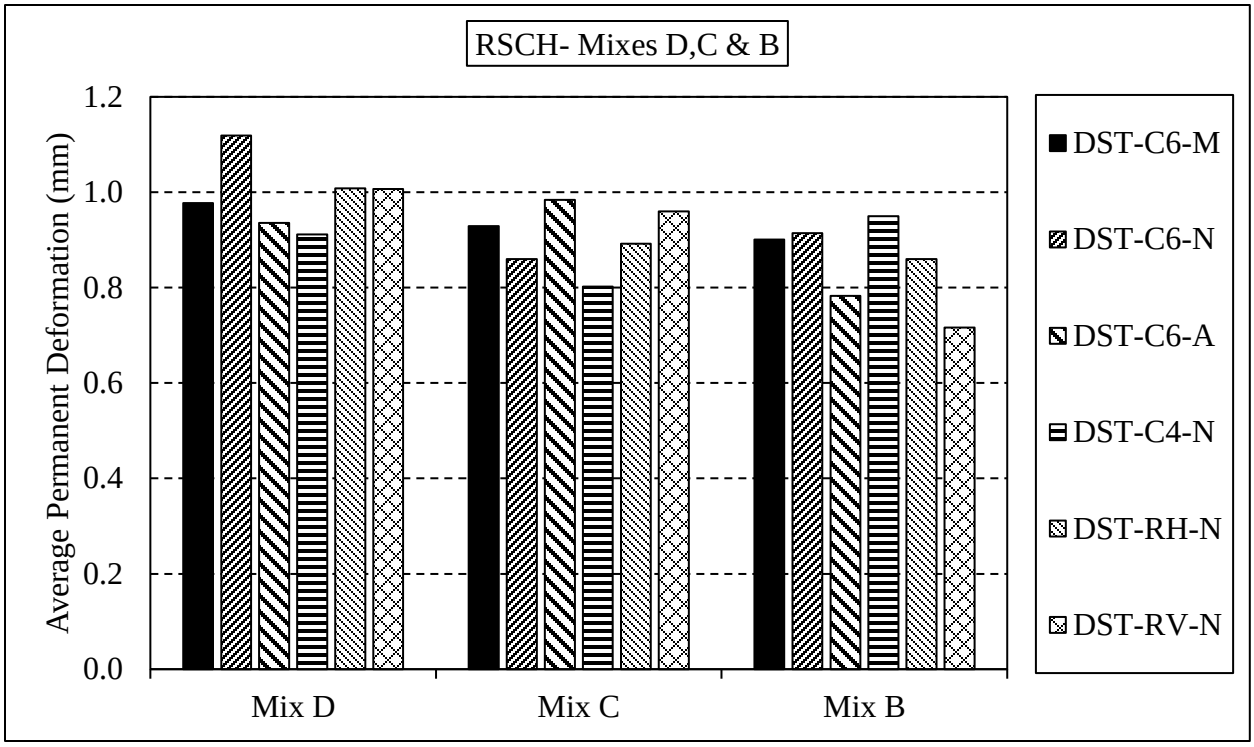

Figure 6-7. Average Permanent Deformation of all DST groups- Mixes D, C& B.

The calculated COV of permanent deformation of all DST groups are given in Table 6-3 for the mixes D, C and B. The permanent deformation of all groups of asphalt mixes D and C yielded generally COV values of less than 13%. For mix B, all groups yielded COV values of less than 8.0% except that for the (DST-C6-M and DST-RV-N) groups as they showed the highest variability of about 17%.

Table 6-3. COV of Permanent Deformation of all DST groups- Mixes D, C& B

Coefficient of Variation (COV%)- Permanent Deformation of DST groups			
Testing Groups	Mix D	Mix C	Mix B
DST-C6-M	11.74	4.91	16.88
DST-C6-N	9.93	7.55	5.91
DST-C6-A	2.77	12.93	7.34
DST-C4-N	12.39	6.22	5.63
DST-RH-N	11.44	7.51	6.08
DST-RV-N	11.10	11.25	16.99

6.1.2 Discussion on the STNS Results

As discussed in Chapter 5, the STNS device was used to measure the shear parameters of only one asphalt specimen by applying the frequency sweep and repeated shear tests protocols under applying an applied normal stress of 113 kPa (16.35 Psi). The STNS tests were performed only on C6 specimens of 150 mm (5.906″) diameter. The FSNS and RSNS tests were the main tests that performed by this device.

Frequency Sweep Test at Normal Stress (FSNS)

The average shear dynamic modulus |G*| of all STNS groups of asphalt mixes D, C and B are plotted against the logarithm of loads frequency in Figures 6-8, 6-9, and 6-10, respectively. The Figures show that the shear dynamic modulus increased, as expected, with the load frequencies. In Figures 6-8, and 6-9 the maximum shear dynamic modulus for asphalt mixes D and C was recorded by the (STNS-C6-N) group, whereas the minimum shear modulus was recorded by the (STNS-C6-M) group. The difference between the maximum and minimum values of |G*| is about 30% and 80% at 10 Hz frequency for asphalt mixes D and C, respectively. In Figure 6-10, the maximum shear dynamic modulus of asphalt mix B was given by the (STNS-C6-A) group, while the minimum values were recorded by the (STNS-C6-N) group. The difference between the maximum and minimum values of |G*| is about 45% at 10 Hz frequency.

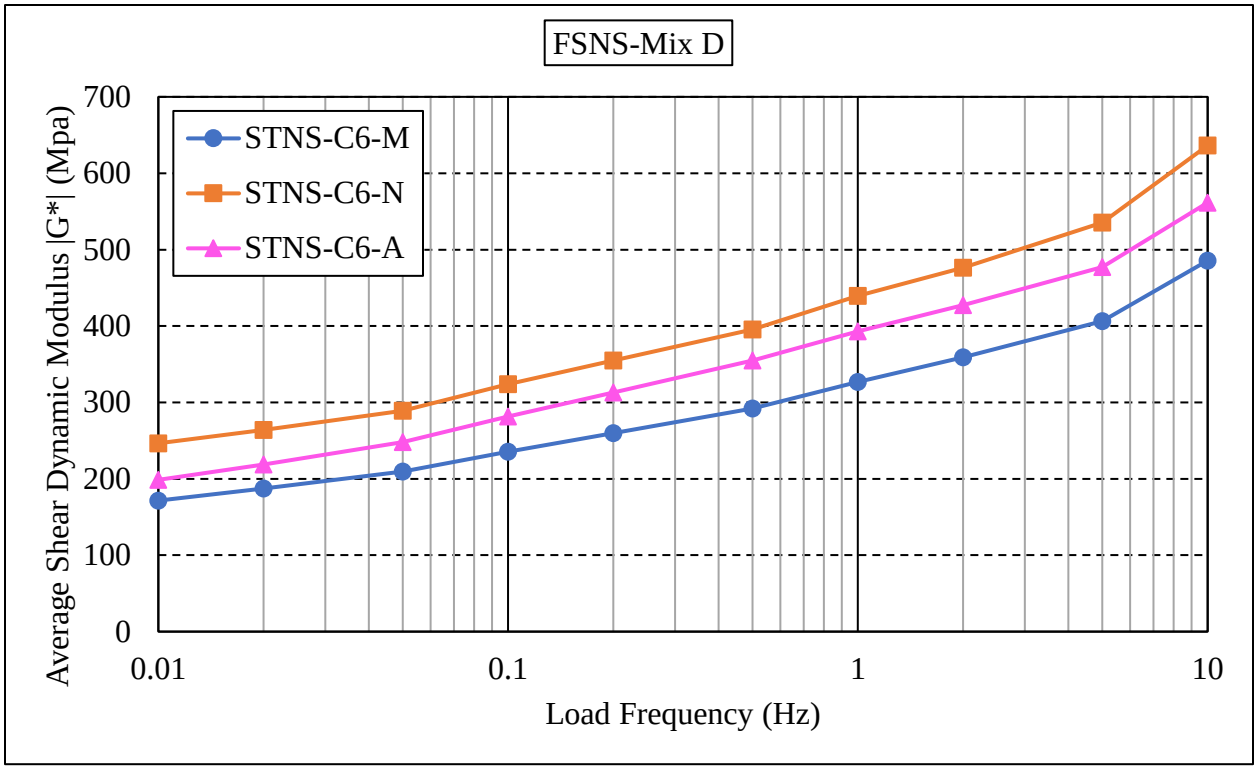

Figure 6-8. Average Shear Dynamic Modulus of asphalt Mix D- STNS device

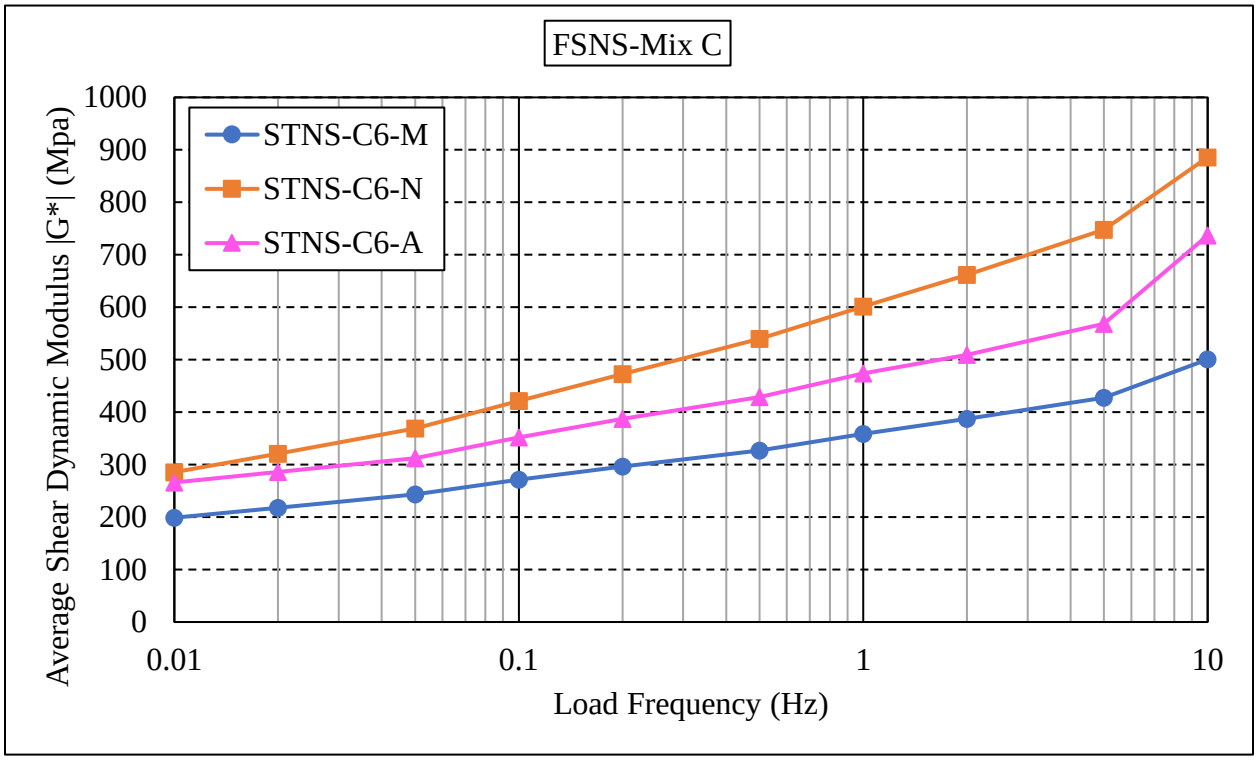

Figure 6-9. Average Shear Dynamic Modulus of asphalt Mix C- STNS device

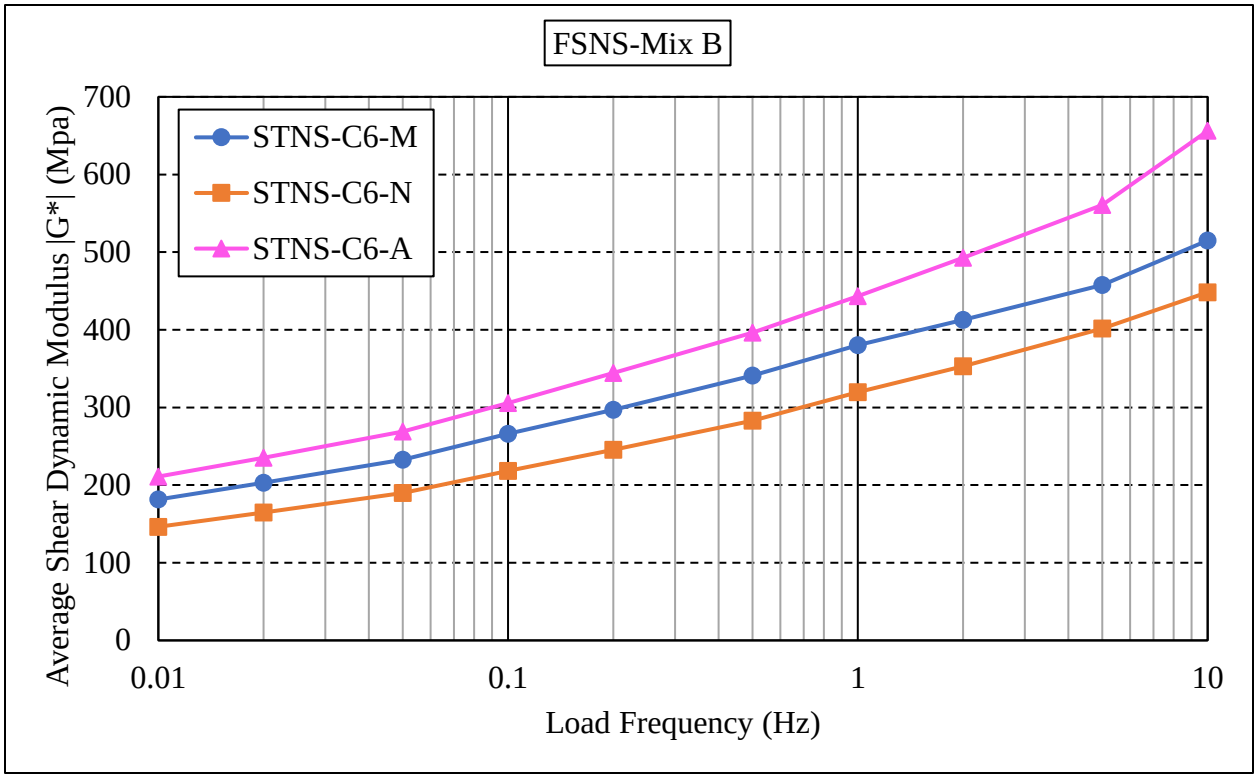

Figure 6-10. Average Shear Dynamic Modulus of asphalt Mix B- STNS device

The calculated COV of the shear dynamic modulus |G*| of all STNS groups are given in Table 6-4 for asphalt mixes D, C, and B, respectively. As shown in the table, the maximum COV values of less than 24% was recorded by the (STNS-C6-A) group at all frequencies for asphalt mix D. The (STNS-C6-N) group recorded the minimum COV values of less than 15% at all frequencies.

For asphalt mix C, both (STNS-C6-N& A) groups have COV values of less than 35% at all frequency loads. The (STNS-C6-M) showed the minimum COV values of around 22% in average at all frequency loads. Similarly, for asphalt mix B, the (STNS-C6-N& A) groups showed COV values of less than 38% at all frequency loads. The test group (STNS-C6-M) showed COV values of less than 11% at all frequency loads.

Table 6-4. COV of Shear Dynamic Modulus (G*) of STNS groups- Mixes D, C& B.

Coefficient of Variation (COV%)- Shear Dynamic Modulus of STNS groups										
Mixes	Testing Groups	Load Frequency (Hz)								
		10	5	2	1	0.5	0.2	0.1	0.05	0.02	0.01
Mix D	STNS-C6-M	16.6	15.3	15.0	14.7	14.4	13.7	13.7	13.4	14.1	14.8
	STNS-C6-N	10.3	14.2	14.6	13.5	12.4	10.7	9.9	9.2	10.2	11.7
	STNS-C6-A	21.4	16.5	16.6	17.5	17.9	19.3	20.3	20.4	22.2	23.5
Mix C	STNS-C6-M	21.9	21.8	22.0	22.0	21.6	20.8	21.0	20.7	21.7	22.8
	STNS-C6-N	34.7	33.8	31.7	29.7	28.6	25.9	25.0	23.5	23.9	24.4
	STNS-C6-A	28.6	22.5	22.7	23.5	23.9	25.7	25.9	26.5	29.2	31.3
Mix B	STNS-C6-M	9.1	6.5	7.0	7.3	7.7	8.1	8.6	9.2	9.8	10.3
	STNS-C6-N	33.8	29.6	28.6	27.3	26.0	24.2	22.3	20.8	19.1	18.4
	STNS-C6-A	36.4	37.4	36.4	35.2	34.3	32.2	30.7	29.6	28.6	28.1

According to the average shear phase angle (δ) of all STNS groups, Figures 6-11, 6-12, and 6-13 show the plots of shear phase angle against the logarithm of frequency loads of all STNS groups for asphalt mixes D, C and B, respectively. In these Figures, the phase angle decreased gradually from 0.01Hz to 0.1Hz loads frequency and showed inconsistent increasing and decreasing above 0.1 Hz load frequency. The (STNS-C6-A) group showed generally the lowest phase angles at all frequencies for asphalt mix D, and showed the opposite for asphalt mixes C and B. Also, the (STNS-C6-M) group showed generally a moderate phase angle for asphalt mix D, and low phase angle for asphalt mix C. For asphalt mix B, both (STNS-C6-N& M) groups have marginally low phase angles at load frequencies from 0.01 Hz to 0.2 Hz and from1.0Hz to 10Hz.

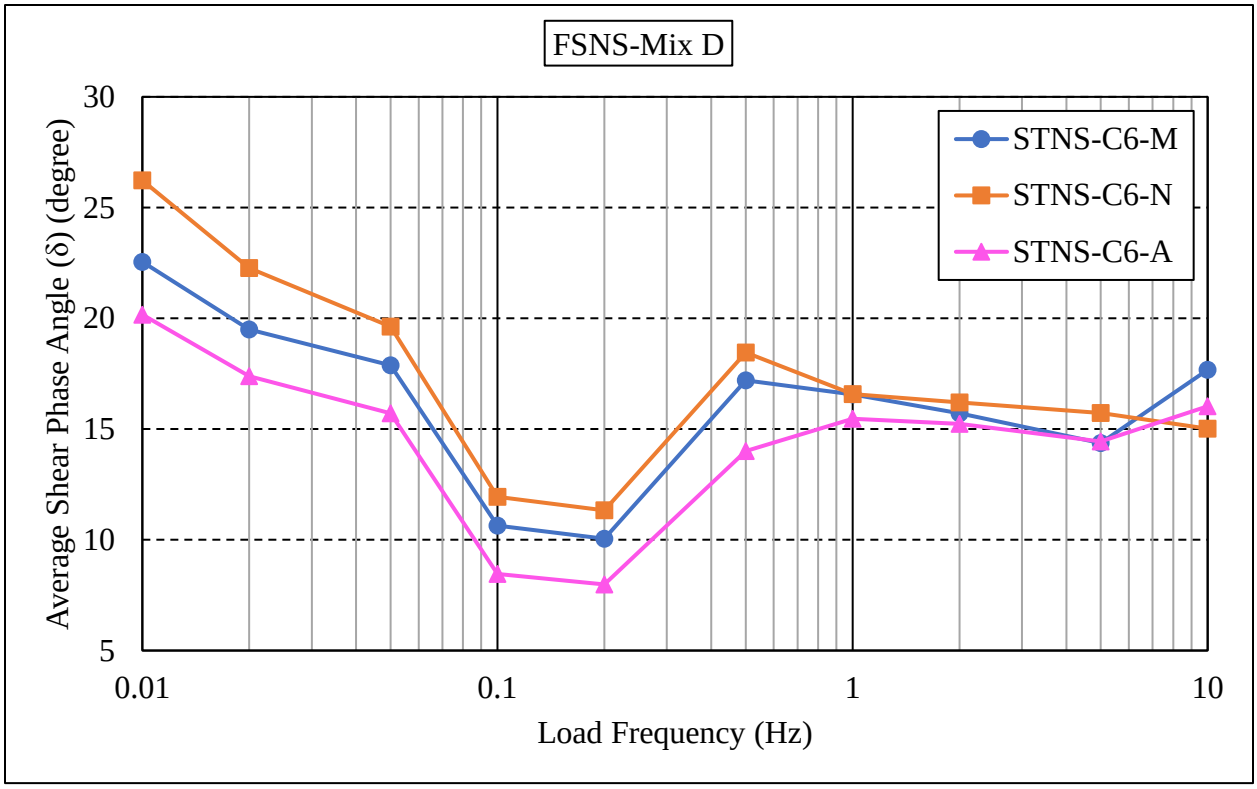

Figure 6-11. Average Shear Phase Angle of asphalt Mix D- STNS device

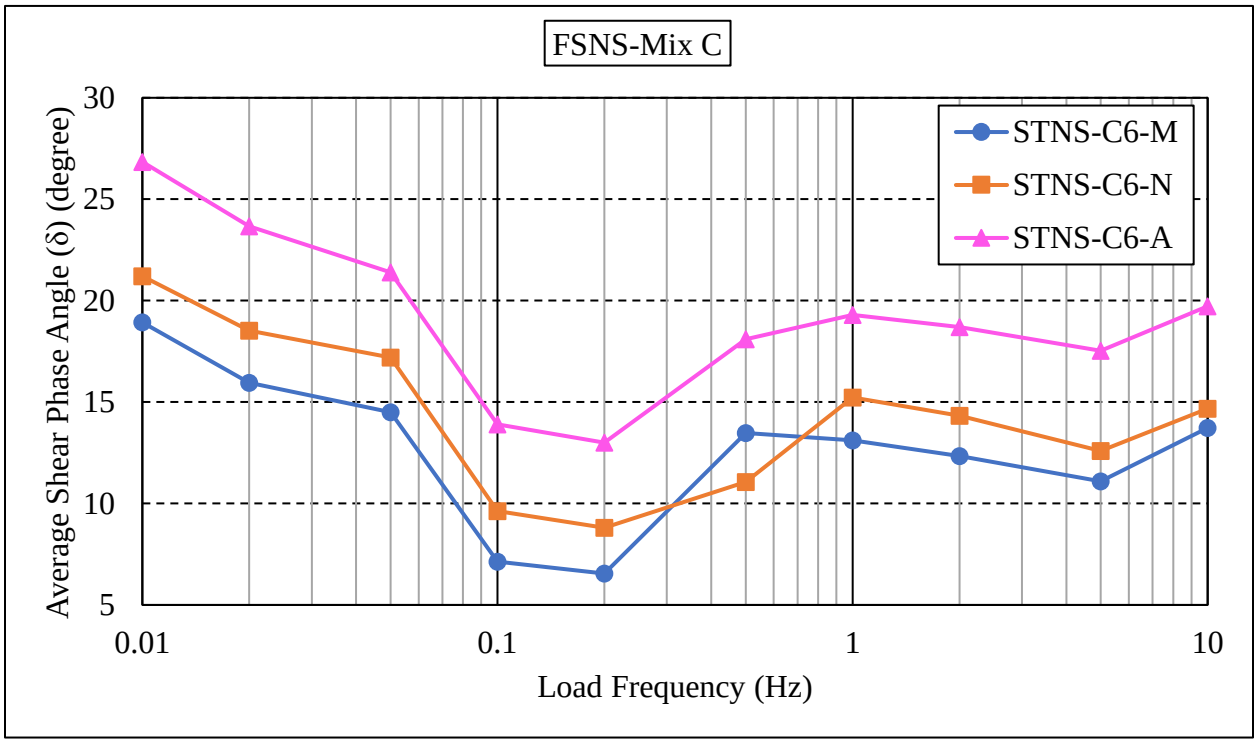

Figure 6-12. Average Shear Phase Angle of asphalt Mix C- STNS device

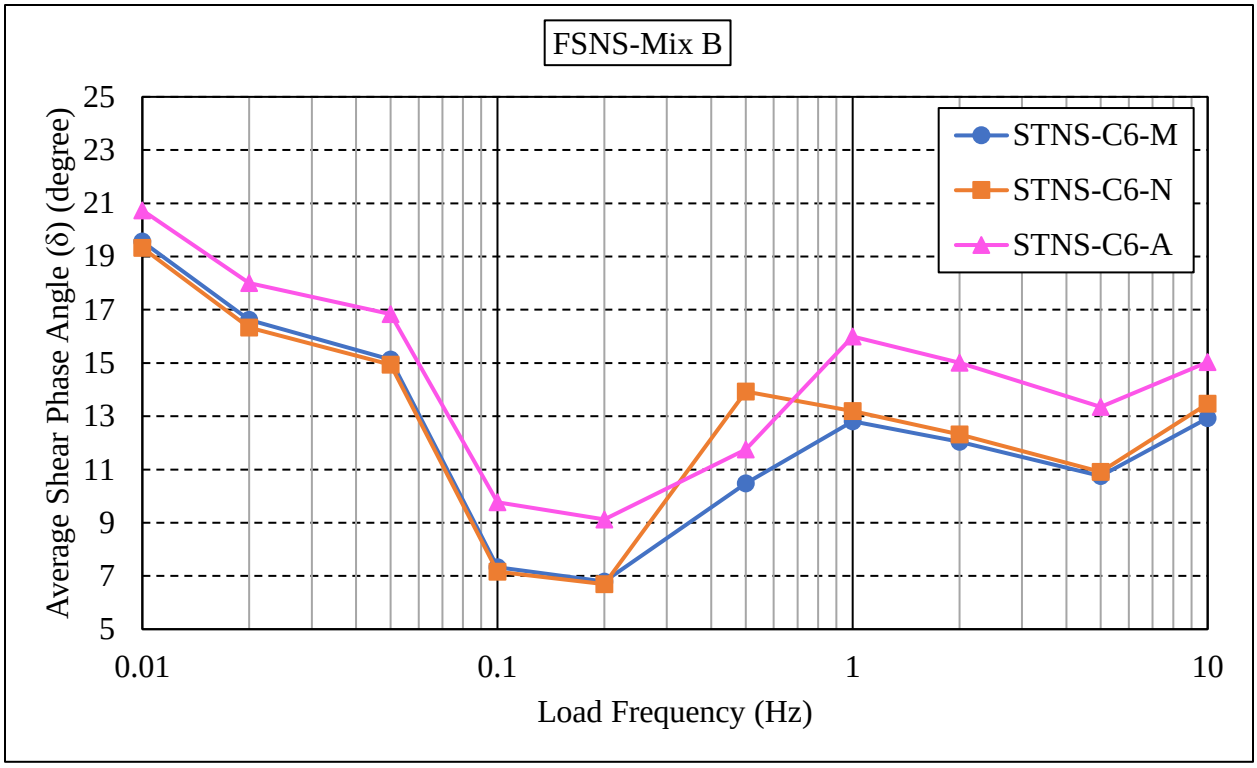

Figure 6-13. Average Shear Phase Angle of asphalt Mix B- STNS device

The calculated COV of the shear phase angle (δ) of all STNS groups are given in Table 6-5 for asphalt mixes D, C, and B, respectively. For the three mixes, some groups showed significant COV values ranged from about 35% to 65% at low load frequencies of (0.2Hz and 0.1Hz). At high load frequencies, however, the COV values were less than 30% for asphalt mix D. The (STNS-C6-A) group yielded the highest COV values for mix D at all frequencies comparing to the (STNS-C6-M & N) groups. For asphalt mix C, all groups yielded generally COV values of less than 35% at high load frequencies. The (STNS-C6-M & A) groups had higher COV values for mix C than that for the (STNS-C6-N) group. For asphalt mix B, the COV values of all groups were less than 26% at high load frequency. The (STNS-C6-N) had the highest COV values for mix B at high load frequencies comparing to the other groups.

Table 6-5. COV of Shear Phase Angle (δ) of STNS groups- Mixes D, C& B.

Coefficient of Variation (COV%)- Shear Phase Angle of STNS groups											
Mixes	Testing Groups	Load Frequency (Hz)									
		10	5	2	1	0.5	0.2	0.1	0.05	0.02	0.01
Mix D	STNS-C6-M	22.29	14.45	11.71	11.44	5.10	22.79	22.46	12.93	12.93	11.90
	STNS-C6-N	19.15	22.08	19.72	18.52	16.51	33.15	32.33	21.06	21.70	21.76
	STNS-C6-A	29.34	24.73	22.96	24.52	33.37	54.15	54.54	28.48	27.81	25.20
Mix C	STNS-C6-M	31.44	28.64	26.09	26.64	19.78	64.21	63.60	31.18	29.50	24.64
	STNS-C6-N	22.29	21.90	20.71	19.43	26.14	40.13	37.17	20.59	19.92	17.84
	STNS-C6-A	25.93	33.14	27.67	26.62	26.91	41.44	40.92	25.48	25.79	22.28
Mix B	STNS-C6-M	21.81	16.89	13.28	11.69	15.88	31.14	29.76	14.68	14.29	13.52
	STNS-C6-N	25.20	19.31	16.77	17.59	19.53	37.87	36.13	15.48	13.44	10.77
	STNS-C6-A	13.16	15.02	14.14	14.77	20.10	29.44	29.84	15.04	13.06	11.43

Based on the results of COV values for shear dynamic modulus and phase angle, it can be seen that the obtained variabilities with the STNS device were relatively higher than that with the DST device. The high variabilities might be occurred due to a technical fault for compaction process since high differences in results were observed for the specimens cut from the same compacted gyratory cylinder. This observation was common for all STNS pairs of the three mixes.

As discussed in the previous chapters, each Superpave gyratory sample was prepared to make two STNS samples, or one DST sample. Since the gyratory samples were compacted at a height of around 6.0″ (152 mm), different distribution of the aggregates might be happened while placing the mix inside the mold of the SGC. This fault, however, would affect the mechanical properties of the compacted asphalt mix sample.

Further, it was decided to investigate if the observed variations between the STNS specimens have a relation with their location in the compacted gyratory samples. Therefore, the top “T” and bottom “B” specimens were identified while cutting the specimens pairs for the last

mix, asphalt mix B. The results proved that there is no clear trend for the observed values for the top or the bottom specimens.

Consequently, the author recommends performing an STNS sample from asphalt mixes of homogenous aggregates distribution. This can be obtained by coring asphalt samples from pavements surface in the fields, or by compacting gyratory sample at short height of maximum 4.0″ (100 mm) in the lab. However, preparing the STNS specimens of 1.97″ (50 mm) height should be cut from the middle of the gyratory sample. In these cases, the effect of aggregates distribution would be less.

Repeated Shear Test at Normal Stress (RSNS)

For the RSNS tests results, Figures 6-14 shows the average permanent deformation of all STNS groups of asphalt mixes D, C, and B, respectively. As for the DST groups, all STNS groups recorded generally permanent deformations of less than 1.1 mm at 5,000 load cycles for the three mixes. The minimum permanent deformations of less than 0.7 mm were observed for asphalt mix C by all groups. The maximum deformation of about 1.1 was recorded by the (STNS-C6-N) group for asphalt mix B. Both (STNS-C6-N& A) groups showed equal permanent deformation for mix D. The testing group (STNS-C6-A), also, showed equal deformations for asphalt mixes C and B.

The calculated COV of permanent deformation of all STNS groups are given in Table 6-6 for asphalt mixes D, C and B. The maximum COV values of about 17% and 14% were recorded by the testing group (STNS-C6-N) for asphalt mix B and D, respectively. For mix C, the (STNS-C6-A) group has a COV value of about 12%, followed by COV value of about 10.5% recorded by the (STNS-C6-M) group. In contrast, the (STNS-C6-A) group recorded the lowest COV value of about 4% for asphalt mix D. For each asphalt mix, however, it can be seen that at

least one STNS group yielded COV value of less than 8.0%. Generally, the COV values of permanent deformation measurements obtained with the STNS device could be comparable with those obtained by the DST device.

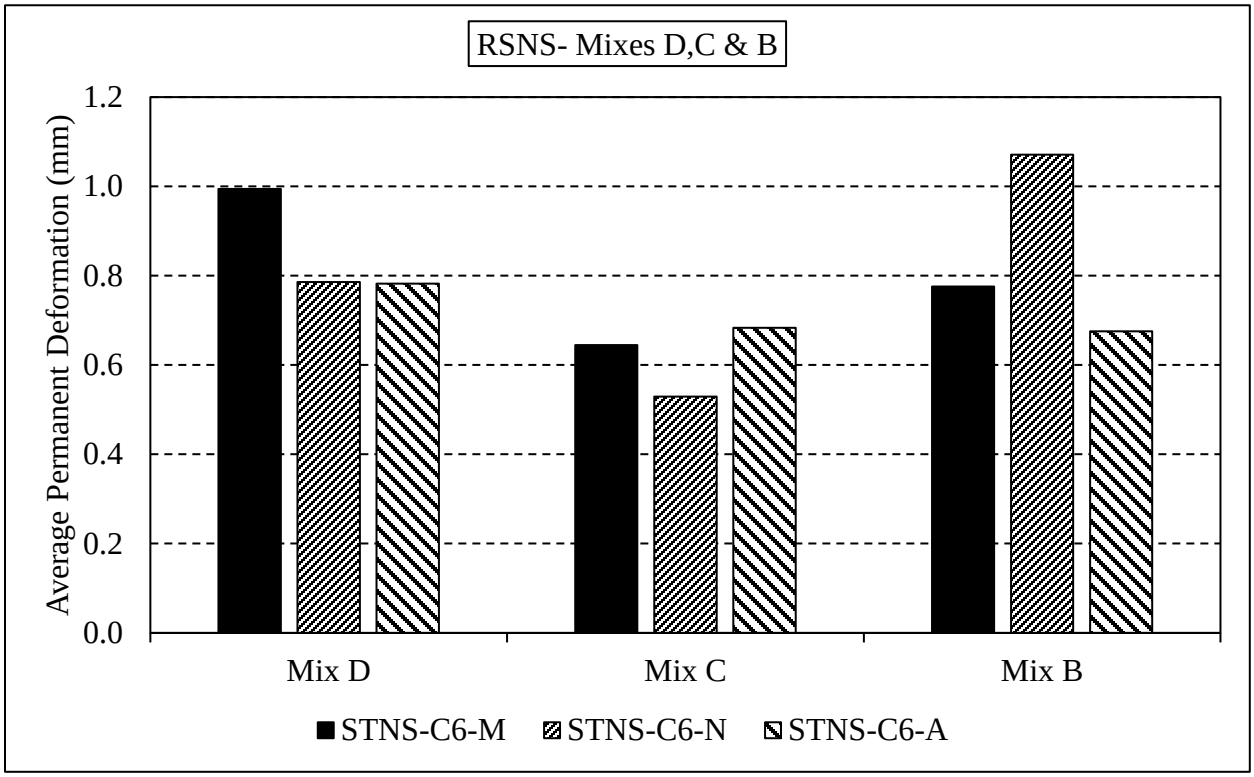

Figure 6-27. Average Permanent Deformation of all asphalt mixes-STNS device.

Table 6-6. COV of Permanent Deformation of all STNS groups- Mixes D, C& B.

Coefficient of Variation (COV%)- Permanent Deformation of STNS groups			
Testing Groups	Mix D	Mix C	Mix B
STNS-C6-M	6.30	10.43	7.72
STNS-C6-N	14.34	6.67	17.05
STNS-C6-A	3.83	11.96	13.59

6.2 Statistical Comparison of Test Results Using ANOVA

An analysis of variance (ANOVA) technique was conducted to compare the test results by using the "Statistical Analysis System (SAS)" software. The comparison includes testing the equality of population means of test results for asphalt concrete samples that were:

1- collected at different times during the daily production (morning (M), noon (N), and afternoon (A));
2- prepared with different sample sizes and shapes (circular with 150mm (C6) and 99.06 mm (C4) diameters, and rectangular cut from horizontal (RH) and Vertical (RV) slices);
3- tested under different conditions with the DST device and the STNS device.

The probability value or "*P-value*" was used to interpret the differences between the mean values of the test results. The "*P-value*" is defined as "the lowest level (of significance) at which the observed value of the test statistic is significant" (Walpole., et al. 2011, Page 333). It was decided in this research to interpret the results of "*P-value*" at 95% level of confidence to study the effect of different four factors on the shear dynamic modulus |G*| at 10Hz loading frequency and the accumulated permanent deformation (PD) at 5,000 load cycles. The reason for selecting these two parameters is that the G*@10Hz frequency is closer than the other frequencies to the loading frequency that the mixes would be experienced in the field under real truck traffics, whereas the accumulated (PD) at 5,000 load cycles is the only shear parameter obtained from the repeated shear tests.

The comparison study between the tested samples on both devices was limited only to get answers for the following questions:

Question* 1:*

a) Would different daily production times of asphalt mixes affect the values of the G*@10Hz and the accumulated PD measured by the DST device?
b) Would different daily production times of asphalt mixes affect the values of the G*@10Hz and the accumulated PD measured by the STNS device?

***Question* 2**: Would the diameter of the circular specimens affect the values of the G*@10Hz and the accumulated PD for asphalt mixes produced at the same time of day?

***Question* 3**: Would the cut directions for rectangular specimens affect the values of the G*@10Hz and the accumulated PD for asphalt mixes produced at the same time of day?

***Question* 4**: Would the DST and STNS devices give different results for the values of the G*@10Hz and the accumulated PD for asphalt mixes produced:

a) in the morning?
b) at noon?
c) in the afternoon?

Table 6-7 shows a summary of the previous questions' categories, and the "*P-value*" results of both G*@10Hz and accumulated PD for each asphalt mix.

To interpret the "*P-value* "results, one-way ANOVA F-test hypotheses were created as follow:

$$H0:\ \mu 1 = \mu 2 = \cdots = \mu k$$

$$H1: \text{at least one mean is different.}$$

The null hypotheses (H0) indicates that all group means are statically equal, whereas the alternative hypotheses (H1) indicates that at least one group's mean is different from the other mean groups. The "*P-values*" were compared independently with the designated level of significance of α =0.05 for the 95% level of confidence. The null hypothesis was rejected when the $p \leq \alpha$; in that are the means are statically significant. To simplify the comparison, the word "***Significant***" was used to indicate that the group's means are different, whereas the word "***Insignificant***" was used to indicate that the group's means are equal. Tables 6-8 summarizes the hypotheses results at 95% level of confidence.

Table 6-7. "*P-value*" results from the ANOVA analysis

QUS	Studying Factors	Comparison Items			Shear Parameters	P-value		
		Devices	Specimens	Times		Mix D	Mix C	Mix B
1-a	Daily time production	DST	C6	M, N, A	G* @10Hz	<0.0001	0.1524	0.0115
					PD	0.0103	0.0748	0.1019
1-b	Daily time production	STNS	C6	M, N, A	G* @10Hz	0.0393	0.0307	0.1190
					PD	0.0002	0.0037	0.0001
2	Diameter	DST	C6, C4	N	G* @10Hz	<0.0001	0.5088	0.1282
					PD	0.0094	0.1164	0.2997
3	Rectangular cut directions	DST	RH, RV	N	G* @10Hz	0.0616	0.0390	0.7892
					PD	0.9802	0.2214	0.0236
4-a	Testing condition	DST, STNS	C6	M	G* @10Hz	<0.0001	<0.0001	<0.0001
					PD	0.7542	<0.0001	0.1149
4-b	Testing condition	DST, STNS	C6	N	G* @10Hz	0.1420	0.2730	<0.0001
					PD	0.0004	<0.0001	0.0730
4-c	Testing condition	DST, STNS	C6	A	G* @10Hz	0.0002	0.0235	0.0005
					PD	<0.0001	0.0008	0.0396

Table 6-8. Hypotheses results at 95% level of confidence

QUS	Studying Factors	Comparison Items			Shear Parameters	95% level of confidence		
		Devices	Specimens	Times		Mix D	Mix C	Mix B
1-a	Daily time production	DST	C6	M, N, A	G* @10Hz	Significant	Insignificant	Significant
					PD	Significant	Insignificant	Insignificant
1-b	Daily time production	STNS	C6	M, N, A	G* @10Hz	Significant	Significant	Insignificant
					PD	Significant	Significant	Significant
2	Diameter	DST	C6, C4	N	G* @10Hz	Significant	Insignificant	Insignificant
					PD	Significant	Insignificant	Insignificant
3	Rectangular cut directions	DST	RH, RV	N	G* @10Hz	Insignificant	Significant	Insignificant
					PD	Insignificant	Insignificant	Significant
4-a	Testing condition	DST, STNS	C6	M	G* @10Hz	Significant	Significant	Significant
					PD	Insignificant	Significant	Insignificant
4-b	Testing condition	DST, STNS	C6	N	G* @10Hz	Insignificant	Insignificant	Significant
					PD	Significant	Significant	Insignificant
4-c	Testing condition	DST, STNS	C6	A	G* @10Hz	Significant	Significant	Significant
					PD	Significant	Significant	Significant

It can be observed from the Table 6-8 that each factor has different effects on the G*@10Hz and accumulated PD values. However, the answers for the previous questions are follows:

Answers-Q1:

a) Using the DST device, the daily times production affects the values of both parameters for mix D, while it affects only the G*@10Hz value for mix B.

b) Using the STNS device, the daily times production affects the values of both parameters for mixes D and C, while it affects only the accumulated PD value for mix B.

Answer-Q2: The diameter size affects only the value of both G*@10Hz and accumulated PD for mix D samples tested with the DST device.

Answer-Q3: The rectangular cut directions affect the value of G*@10Hz for mix C, and the value of accumulated PD for mix B samples tested with the DST device.

Answers-Q4:

a) Using asphalt mixes produced in the Morning, both devices would **not** give different values of the accumulated PD for mixes D and B.

b) Using asphalt mixes produced at Noon, both devices would **not** give different values of the G*@10Hz for mixes D and C. It also would **not** give different value of the accumulated PD for mix B.

c) Using asphalt mixes produced in the afternoon, both devices would give different values of both parameters for mixes D, C, and B.

The ANOVA analysis proved that testing asphalt mixes with the DST and STNS devices affects sometimes the values of G*@10Hz and accumulated PD, but it does not show which of both devices gives usually higher values for the measurements than the other. Figure 6-28, 6-29 and 6-30 show Box and Whisker plots of the G*@10Hz values for all mixes tested with the two devices at Morning, Noon and Afternoon, respectively. The figures show that the DST device provides usually higher values for the G*@10Hz than the STNS devices at all times for the three mixes.

The accumulated PD plots for the three mixes samples collected at Morning, Noon and Afternoon and tested with the two devices, are shown in Figures 6-31, 6-32 and 6-33, respectively. It is clearly seen that no clear trend for the accumulated PD measured by the two devices. In Figures 6-31 and 6-32, the DST device provide higher PD values than the STNS device except that for mix D samples collected in the morning and mix B samples collected at noon as the DST provides relatively lower value for the PD than the STNS. Figure 6-33 show that the DST provide higher PD values than the STNS device for all samples collected in the afternoon.

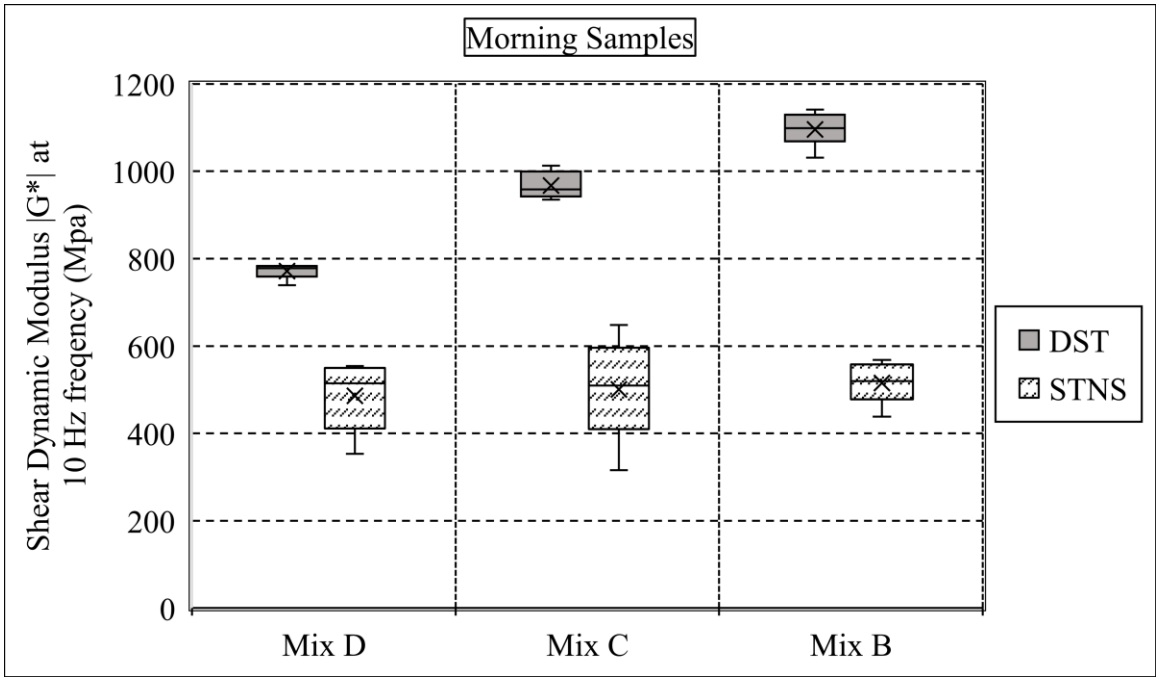

Figure 6-28. G*@10Hz for samples collected at Morning.

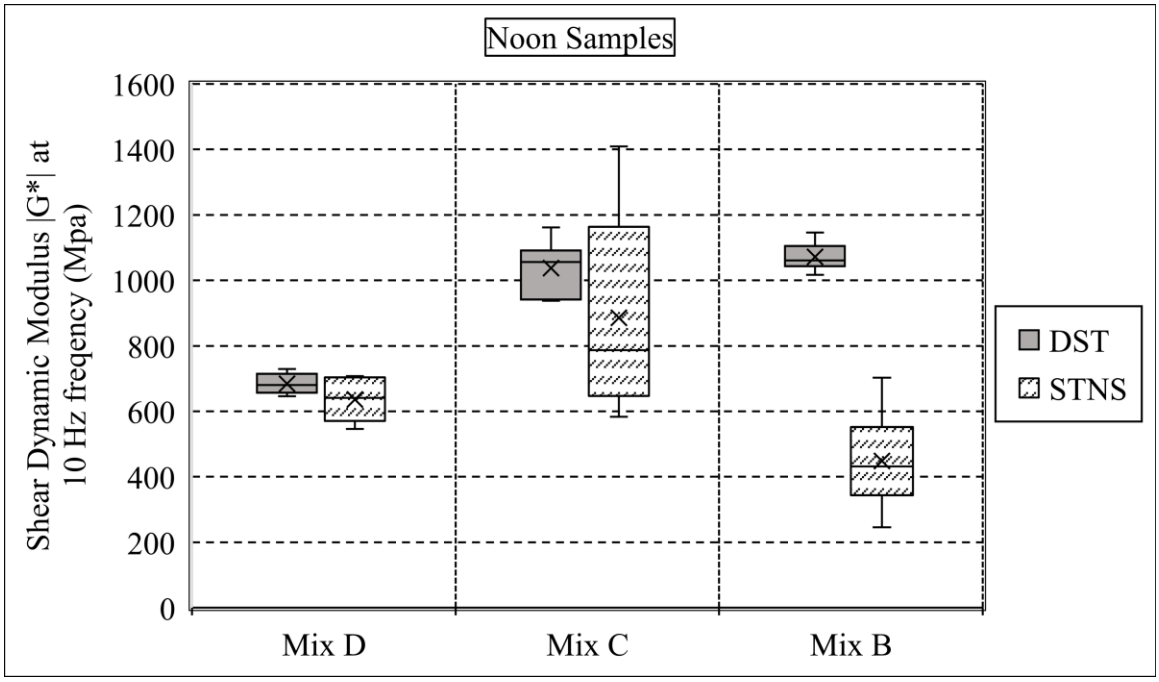

Figure 6-29. G*@10Hz for samples collected at Noon.

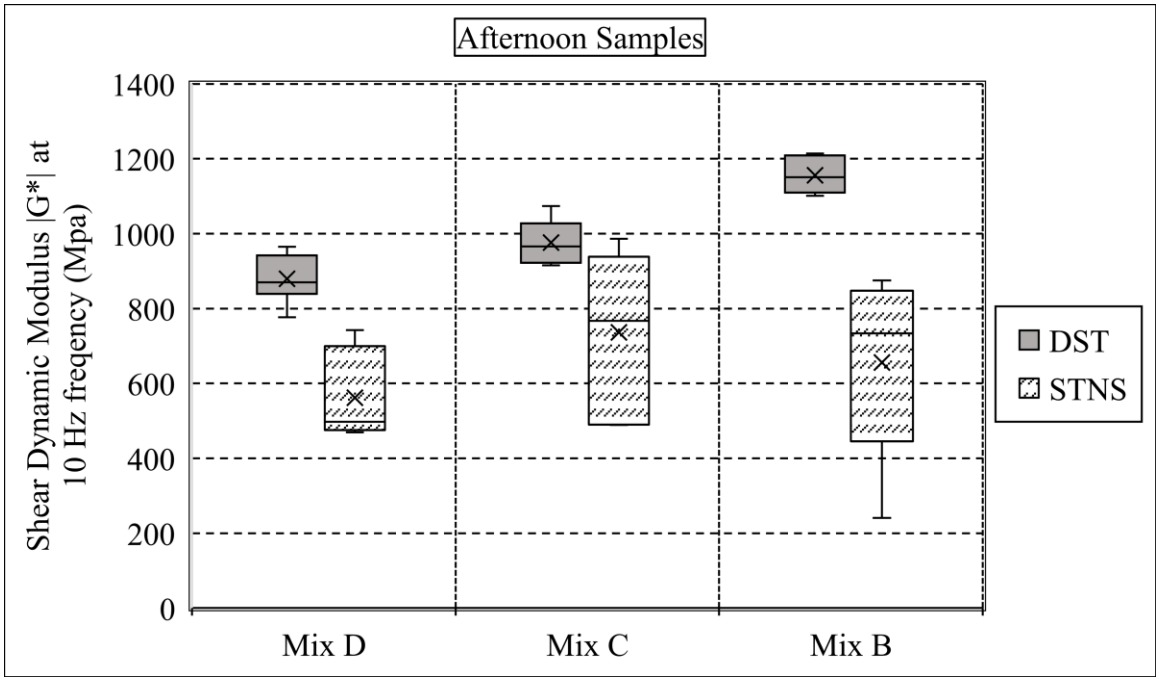

Figure 6-30. G*@10Hz for samples collected at Afternoon.

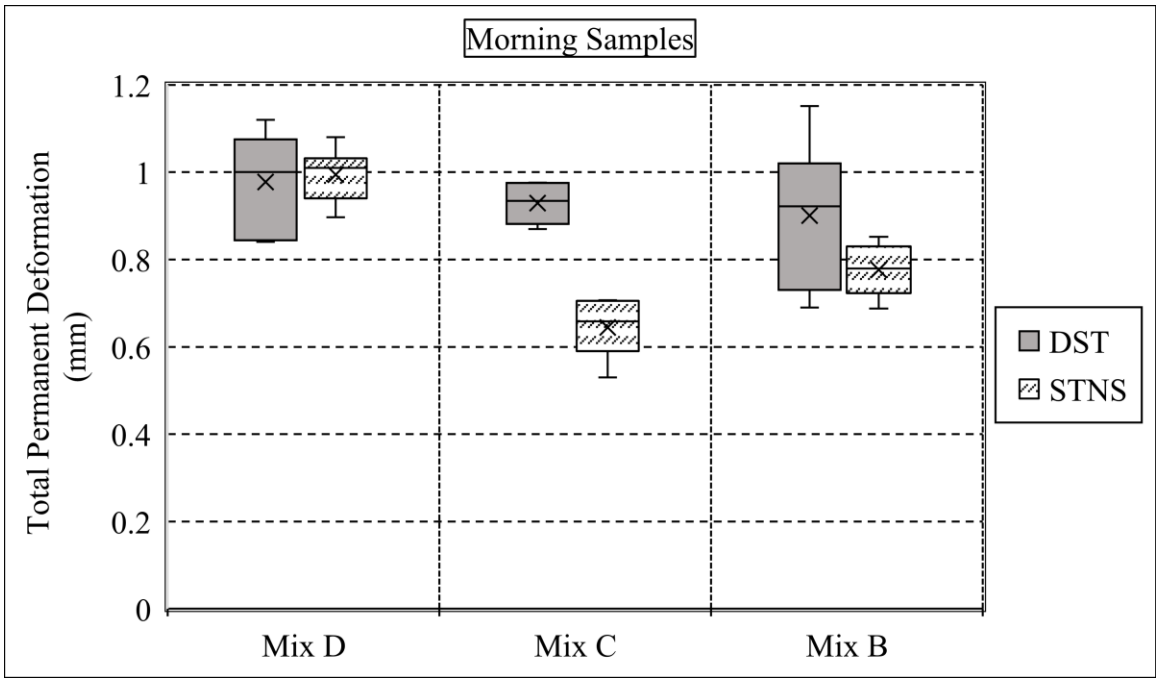

Figure 6-31. PD for samples collected at Morning.

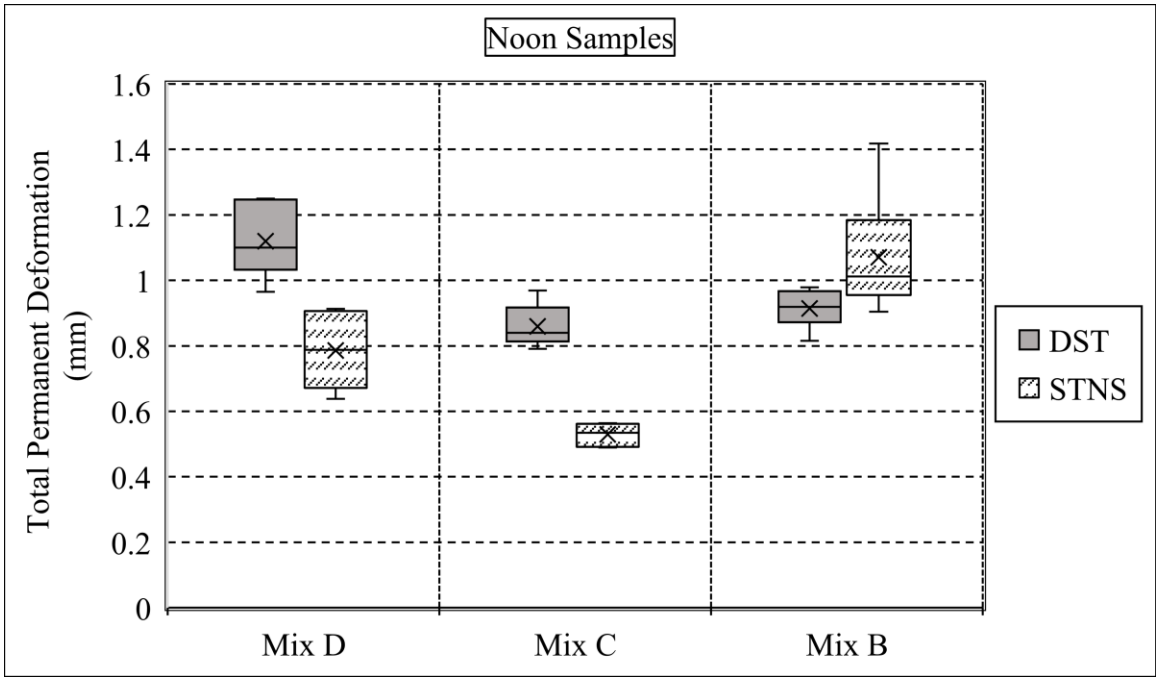

Figure 6-32. PD for samples collected at Noon.

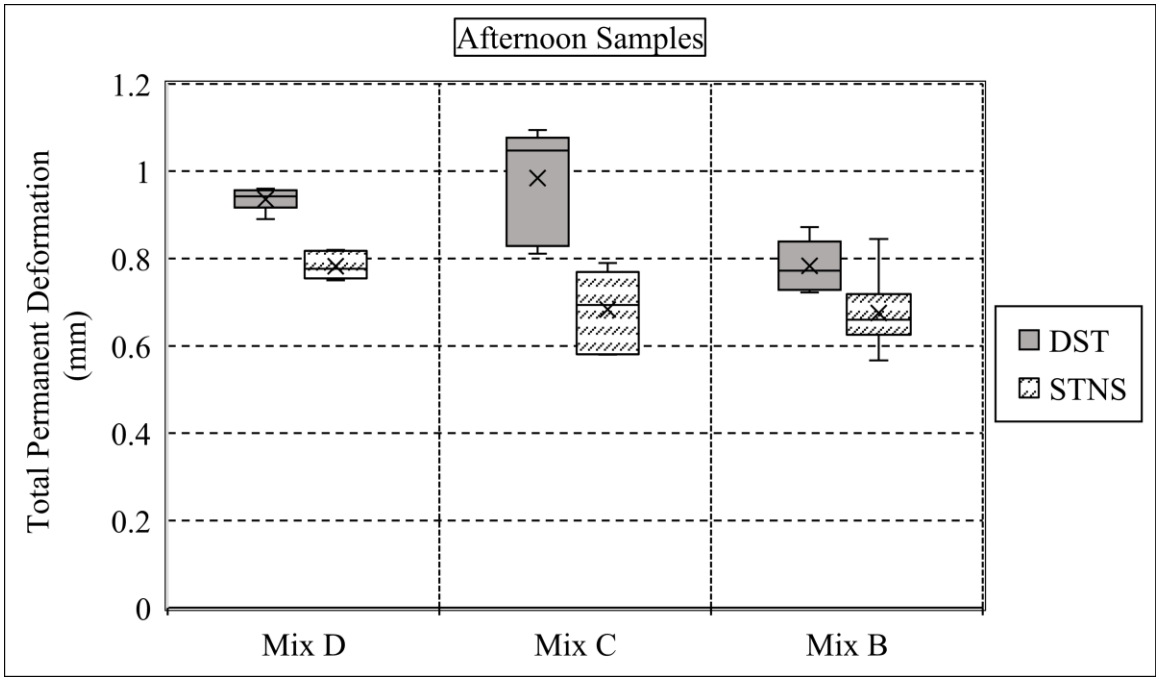

Figure 6-33. PD for samples collected at Afternoon.

Chapter 7: Conclusions and Recommendations

7.1 Conclusions

The need for a proper laboratory test method for evaluating the resistance of asphalt mixes to rutting is quite important. Since 90% of rutting in asphalt pavement occurs due to the shear deformation of asphalt mixes, this research is aimed to develop reliable, simple and inexpensive laboratory test devices for measuring the fundamental shear properties of asphalt mixes and to assess the effect of different testing factors on the test results.

The DST was developed in the University of Texas at Arlington as a replacement test device to the Superpave Shear Tester (SST). It is able to perform the two common SST tests: the FSCH and RSCH in according to the standard test method AASHTO T-320 (Khajeh-Hosseini, 2015). In this study, the author enhanced the shear tests procedure for asphalt pavements through modifying the DST device and developing a new shear tester device that is able to measure the shear properties of asphalt mixes under normal stress.

The DST device was modified to be lighter in weight and able to accommodate other shapes of test specimens including large and small circular diameter specimens, and rectangular specimens cut horizontally and vertically from gyratory compacted samples. The new device is called the “Shear Tester with Normal Stress (STNS)”. The STNS device was developed successfully with only simple and inexpensive testing attachments. It was developed to simulate the state of stresses within the rutting zone of asphalt pavements where the asphalt mix is subjected to states of shear and normal stresses simultaneously under the loading provided by truck wheels.

Similar to the DST device, the STNS proved its ability to shear an asphalt concrete specimen under the same loads condition and constrains of the frequent and repeated shear tests

protocols in accordance to the standard test method AASHTO T-320, but with an additional normal stress applied on the specimen. Two tests were performed by this device through utilizing a universal testing machine (UTM-25): the Frequency Shear Test at Normal Stress (FSNS), and the Repeated Shear Test at Normal Stress (RSNS).

Three asphalt mixes were tested on both devices. According to the TxDOT specifications 340, 341 and 344, (2015), they are Superpave asphalt mixes (types D and C), and dense graded asphalt mix type B. All mixes were tested with the DST device for the (FSCH and RSCH tests) and with the STNS device for the (FSNS and RSNS tests) at an applied normal stress of 113 kPa (16.35 Psi). Both frequency sweep tests were conducted at 30°C, whereas the repeated shear tests were conducted at 50°C. Three shear parameters were obtained from each device for different mixes: the shear dynamic modulus |G*| and shear phase angle (δ) from the FSCH & FSNS tests, and the total permanent deformation (PD) from the RSCH & RSNS tests.

The test results proved the ability of the modified DST device to provide repeatable measurements with relatively low coefficient of variations (COV) for the measured shear parameters. The shear dynamic modulus of all DST groups yielded generally COV values of less than 8%, 11% and 8% for asphalt mixes D, C, and B, respectively, at high load frequencies of 10 Hz and 5.0 Hz. The phase angle of all DST groups had generally low COV values of less than 8.0% for asphalt mixes D and B, and less than 10% for asphalt mix C at all loading frequencies. The permanent deformation (PD) measurements of all DST groups yielded generally low COV values of less than 13% for asphalt mixes D and C, and less than 8% for mix B except that for some testing groups of asphalt mix B as they had a COV values of about 17%.

The test results of all STNS testing groups showed generally high variabilities for the measured shear dynamic modulus and phase angle. At high load frequencies of 10Hz and 5.0Hz,

the COV values of the shear dynamic modulus were less than 24%, 35%, and 38% for asphalt mixes D, C, and B, respectively. Some testing groups, however, yielded reasonable COV values for the shear dynamic modulus of less than 10% for asphalt mixes D and B, and less than 22% for asphalt mix C, at high load frequencies. The phase angle measurements showed comparable variabilities to that of shear dynamic modulus at high load frequencies. The COV values of shear phase angle were less than 30%, 35%, and 26% for asphalt mixes D, C, and B, respectively.

The reasons behind the observed high variabilities of the shear dynamic modulus and phase angle measurements with the STNS device were justified due to a technical fault for the compaction process at a height of 6.0″ (152 mm). The fault, most likely, were led to non-uniform distribution of aggregates which affected the mechanical properties of the cut samples. A further investigation was also proved that the high variabilities have no relation of whether the test specimens were cut from the top or bottom of the gyratory samples.

According to the COV values of the permanent deformation (PD) measurements with the STNS device, they were comparable to those obtained by the DST device. The maximum COV value of the permeant deformation at 5,000 load cycles were less than 14%, 12%, and 17% for asphalt mixes D, C and B, respectively. For each asphalt mix, however, there is at least one testing group had low COV value of less than 8.0%.

An analysis of variance (ANOVA) technique was conducted to compare the tests results by using the "Statistical Analysis System (SAS)" software. The comparison includes testing the influence of four different factors on the mean values of the G*@10Hz frequency and the accumulated permanent deformation (PD) at 5,000 load cycles by using the calculated "*P-value*" at 95% level of confidence. The analysis studied the significance of the mean values under different:

1- time of daily production for asphalt mixes (Morning, Noon, and Afternoon).
2- diameter for test specimens (150 mm (C6) versus 99.06 mm (C4)).
3- cut directions for rectangular specimens (Horizontal (RH) versus Vertical (RV)).
4- tests conditions by using the DST and STNS devices (Constant Height (CH) versus Normal Stress (NS)).

The ANOVA results proved that each testing factor has different effects on the value of both G*@10Hz and accumulated PD. Follows are summary of findings obtained from the analysis:

a) Using the DST device, the daily times production affects the values of both parameters for mix D, while it affects the G*@10Hz value for mix B.
b) Using the STNS device, the daily times production affects the values of both parameters for mixes D and C, while it affects only the accumulated PD value for mix B.
c) The diameter size affects only the value of both G*@10Hz and accumulated PD for mix D samples tested with the DST device.
d) The rectangular cut slices affect the value of G*@10Hz for mix C, and the value of accumulated PD for mix B samples tested with the DST device.
e) Testing asphalt mixes with both devices sometimes affects the values of the G*@10Hz and accumulated PD and sometimes does not make a difference.
f) The DST device provides usually higher value for the G*@10Hz measurements than the STNS device for all mixes at all times of asphalt mix daily production. For the PD values, no clear trends were shown for mixes D and B tested with the two devices.

In general, the DST and STNS devices have successfully satisfied the objectives of reliable and simple test procedures for measuring the fundamental shear properties of asphalt mixes at low

cost comparing to the SST. Their results had some variations that can be attributed to material variability since the mixes were collected at the asphalt plant from different loaded trucks. However, the outputs from these devices can be used to develop prediction models to enhance the asphalt pavement performance against rutting.

7.2 Recommendations

This study leads to the following recommendations for future work:

- Investigate if the STNS device can be improved further so that the results will have smaller variability by:
  - Making samples from field cut cores.
  - Making each sample from a single gyratory cylinder of about 4.0″ tall.
  - Accommodating other specimen shapes.
- Perform the FSCH and FSNS tests at temperatures higher than 30°C (86°F) to investigate the effect of temperature on the shear dynamic modulus (G*) and shear phase angle (δ).
- Study the effect of the magnitude of the normal stress on the FSNS and RSNS test results.

References

AASHTO R 68-15. (2015). Preparation of Asphalt Mixtures by Means of the Marshall Apparatus. American Association of State Highway and Transportation Officials AASHTO.

AASHTO T 246-10. (2015). Resistance to Deformation and Cohesion of Hot Mix Asphalt (HMA) by Means of Hveem Apparatus. American Association of State Highway and Transportation Officials AASHTO.

AASHTO T 245-15. (2015). Resistance to Plastic Flow of Asphalt Mixtures Using Marshall Apparatus. American Association of State Highway and Transportation Officials AASHTO.

ASTM-E1703/E1703M. (2015). Standard Test Method for Measuring Rut-Depth of Pavement Surfaces Using a Straightedge.

AASHTO R48-10. (2013). Standard Practice for Determining Rut Depth in Pavements. American Association of State Highway and Transportation Officials AASHTO.

AASHTO T-320. (2004). Standard Method of Test for Determining the Permanent Shear Strain and Stiffness of Asphalt Mixtures Using the Superpave Shear Tester (SST). In Standard Specification for Transportation Materials and Methods of Sampling and Testing (Vol. Part 2B). American Association of State Highway and Transportation Officials AASHTO.

ASTM-D6433. (2016). Standard practice for roads and parking lots pavement condition index surveys. doi:10.1520/D6433-16.

AASHTO T 209-12. (2015). Theoretical Maximum Specific Gravity (Gmm) and Density of Hot Mix Asphalt (HMA).

Brown E. R., and S. A. Cross. (1992). A National Study of Rutting in Hot Mix Asphalt (HMA) Pavements, NCAT Report No. 92-05, Auburn University, Auburn, AL.

Brown, E. R., Kandhal, P. S., & Zhang, J. (2001). Performance Testing for Hot Mix Asphalt. National Center for Asphalt Technology (No. NCAT 01-05).

Bahuguna, S. (2003). Permanent deformation and rate effects in asphalt concrete: Constitutive modeling and numerical implementation. Ph.D. Thesis. Case Western Reserve University.

Christensen, D. W., Bonaquist, R. F., & Handojo, T. (2002). Field Shear Test for Hot Mix Asphalt. Transportaion Research Board (TRB), National Cooperative Highway Research Program (NCHRP). Transportation Research Board National Research Council.

Christensen, D. W. (2003). Sensitivity Evaluation of Field Shear Test using Improved Protocol and Indirect Tension Strength Test. National Cooperative Highway Research Program.

Chowdhury, A., & Button, J. (2002). Evaluation of superpave shear test protocols (No. FHWA/TX-02/1819-1,). Texas Transportation Institute, Texas A & M University System.

Chowdhury, A., & Button, J. W. (2003). Precision Statistics for Frequency Sweep at Constant Height Test (No. FHWA/TX-04/0-1819-2,). Texas Transportation Institute, Texas A & M University System.

Collop, A. C., Cebon, D., & Hardy, M. S. A. (1995). Viscoelastic approach to rutting in flexible pavements. Journal of Transportation Engineering, 121(1), 82-93. doi:10.1061/(ASCE)0733-947X (1995)121:1(82)

F. Zhou, E.G. Fernando, and T. Scullion. (2010). Development, Calibration, and Validation of Performance Prediction Models for the Texas M-E Flexible Pavement Design System, Research Report FHWA/TX-10/0-5798-2, Texas Transportation Institute, College Station, TX.

Goodman, S. (2000). Design, Development and Validation of the In-Situ Shear Stiffness Test (InSiSST™) for Asphalt Concrete Pavements. Ottawa, Canada: Carleton University.

Guide, S. M. D. (2001). Westrack Forensic Team Consensus Report. FHWA, US Department of Transportation, Washington, DC.

Harrigan, E. T., Leahy, R. B., & Youtcheff, J. S. (1994). Superpave manual of specifications, test methods and practices. SHRP-A-379, Strategic Highway Research Program, National Research Council, Washington, DC.

Hoffman, B. R., & Sargand, S. M. (2011). Verification of Rut Depth Collected with the INO Laser Rut Measurement System (LRMS) (No. FHWA/OH-2011/18). Ohio Research Institute for Transportation and the Environment, Russ College of Engineering and Technology, Ohio University.

Jweihan, Y. S. (2018). Improvements to the duplicate shear tester.

Khajeh Hosseini, M. (2015). Development of the duplicate shear test for asphalt mixtures.

Khosla, N. P. and Omer, M. S. (1985). Characterization of Asphaltic Mixtures for Prediction of Permanent Deformation, Transportation Research Board, Transportation Research Record 1034, pp.47-55.

Long, F. M. (2001). Permanent deformation of asphalt concrete pavements: A nonlinear viscoelastic approach to mix analyses and design.

Mallela, R., & Wang, H. (2006). Harmonising Automated Rut Depth Measurements: Stage 2 (No. 277). Land Transport New Zealand.

Martin, A. E., & Park, D. W. (2003). Use of the asphalt pavement analyzer and repeated simple shear test at constant height to augment superpave volumetric mix design. Journal of transportation Engineering, 129(5), 522-530.

McGennis, R. B., Anderson, R. M., Kennedy, T. W., & Solaimanian, M. (1994). Background of superpave asphalt mixture design and analysis. Final Report (No. FHWA-SA-95-003).

Moghadas Nejad, F. M., Azarhoosh, A. R., Hamedi, G. H., Azarhoosh, M. J. (2015). Characterization of permanent deformation resistance of precipitated calcium carbonate modified asphalt mixture. Journal of Civil Engineering and Management, 21(5), pp. 615–622.

NHI. (2000). Superpave Fundamentals Reference Manual (NHI Course #131053). Federal Highway Administration - FHWA, National Highway Intitute. U.S. Department of Transportation.

Pavement Interactive. (2018, August 4). Superpave Shear Tester. Retrieved from: https://www.pavementinteractive.org/reference-desk/testing/asphalt-tests/superpave-shear-tester/

Pradhan, M. M. (1995). Permanent deformation characteristics of asphalt-aggregate mixtures using varied materials and molding procedures with marshall method. Ph.D. Thesis. Montana University.

Romero, P., & Anderson, R. (2001). Variability of asphalt mixture tests using Superpave shear tester repeated shear at constant height test. Transportation Research Record: Journal of the Transportation Research Board, (1767), 95-101.

Romero, P., & Mogawer, W. (1998b). Evaluation of ability of superpave shear tester to differentiate between mixtures with different aggregate sizes. Transportation Research Record: Journal of the Transportation Research Board, (1630), 69-76.

Romero, P., & Mogawer, W. (1998a). Evaluation of the superpave shear testing using 19-mm mixtures from the Federal Highway Administration's accelerated loading facility. Journal of the Association of Asphalt Paving Technologists, 67.

Romero, P., & Masad, E. (2001). Relationship between the representative volume element and mechanical properties of asphalt concrete. Journal of materials in civil engineering, 13(1), 77-84.

Roberts, F. L., Kandhal, P. S., Brown, E. R., Lee, D. Y., & Kennedy, T. W. (2009). Hot Mix Asphalt Materials, Mixture Design, and Construction. National Asphalt Pavement Association Education Foundation. Lanham, MD.

Scullion, T., Sun, L., & Zhou, F. (2004). Verification and modeling of three-stage permanent deformation behavior of asphalt mixes. Journal of Transportation Engineering, 130(4), 486-494. doi:10.1061/(ASCE)0733-947X(2004)130:4(486)

Sousa, J.B., Craus, J., C.L. Monismith. (1991). Summary Report on Permanent Deformation in Asphalt Concrete, Strategic Highway Research Program, National Research Council, Washington, D.C., Report No. SHRP-A / IR-91-104.

Sousa, J.B., J.A. Deacon, S.L. Weissman, R.B. Leahy, J.T. Harvey, G. Paulsen, J.S. Coplantz, and C.L. Monismith. (1994a). Permanent Deformation Response of Asphalt Aggregate Mixes, Strategic Highway Research Program, National Research Council, Washington, D.C., Report No. SHRP-A-415.

Sousa, J.B.; Solaimanian, M. and Weissman, S.L. (1994b). Development and Use of the Repeated Shear Test (Constant Height): An Optional Superpave Mix Design Tool. Strategic Highway Research Program, National Research Council. Washington.

Sousa, J. B. (1994). Asphalt-aggregate mix design using the repetitive simple shear test (constant height). National Association of Asphalt Technologists, 63, 299-345.

Sousa, J. B., & Solaimanian, M. (1994). Abridged procedure to determine permanent deformation of asphalt concrete pavements. Transportation Research Record, (1448), 25-33.

Solaimanian, M., & Kennedy, T. W. (1993). Predicting maximum pavement surface temperature using maximum air temperature and hourly solar radiation. Transportation Research Record, 1-1.

Tayebali, A., Khosla, N., Malpass, G., & Waller, H. (1999). Evaluation of superpave repeated shear at constant height test to predict rutting potential of mixes: Performance of three pavement sections in North Carolina. Transportation Research Record: Journal of the Transportation Research Board, (1681), 97-105.

Tex-340. (2014). Dense-Graded Hot-Mix Asphalt (Small Quantity). Texas Department of Transportation.

Tex-341. (2014). Dense-Graded Hot-Mix Asphalt. Texas Department of Transportation.

Tex-344. (2014). Superpave Mixtures. Texas Department of Transportation.

Tex-241-F. (2015). Compacting Bituminous Specimens Using the Superpave Gyratory Compactor (SGC). Texas Department of Transportation.

Walpole, R. E., Myers, R. H., Myers, S. L., & Ye, K. E. (2011). Probability and statistics for engineers and scientists (9th ed.), International Edition. Page 333.

Weissman, S. L., J. Sackman, J. T. Harvey and F. Long. (1999). Selection of Laboratory Test Specimen Dimension for Permanent Deformation of Asphalt Concrete Pavements, Transportation Research Record 1681, pp. 113-120.

Witczak, M. W., Kaloush, K., Pellinen, T., El-Basyouny, M., & Von Quintus, H. (2002). Simple performance test for superpave mix design. NCHRP Report 465. Washington, DC: National Research Council, Transportation Research Board.

White, T. D., Haddock, J. E., Hand, A. J., & Fang, H. (2002). Contributions of Pavement Structural Layers to Rutting of Hot Mix Asphalt Pavements. NCHRP Report, 468. National Research Conuncil. Washington: Transportation Research Board.

Witczak, M. W. (2007). Specification criteria for simple performance tests for rutting (Vol. 1). Transportation Research Board.

Zhang, J., Ray Brown, E., Kandhal, P., & West, R. (2005). An overview of fundamental and simulative performance tests for hot mix asphalt. Journal of ASTM International, 2(5), 1-15. doi:10.1520/JAI12254

Zhang, J., Xie, H., Kandhal, P. S., & Powell, R. D. (2006). Field Validation of Superpave Shear Test on NCAT Test Track. In Performance Tests for Hot Mix Asphalt (HMA) Including Fundamental and Empirical Procedures. ASTM International.

Biographical Information

Yazeed Suleiman Jweihan was born in Jordan at 1989. He received a bachelor's degree in civil engineering with an excellent assessment (honor degree) from Mutah University, Jordan in August 2011. During his study, he achieved a distinguished academic record by listing his name on the Dean's list for four times and once on the University list. He was also awarded the University shield for excellence in 2009. He worked in Jordan as a QC engineer in the pipeline and road construction fields for three years. He received a full scholarship from Mutah University in 2015 to pursue his graduate studies in civil engineering. He started his Master of Science program at the University of Texas at Arlington (UTA) in January 2016. His Master thesis was entitled *"IMPROVEMENTS TO THE DUPLICATE SHEAR TESTER*". He received his M.Sc. in December 2017 and since January 2018 he enrolled for the Ph.D. studies at the UTA. His doctoral research focused on an expanded topic in which several new tests on asphalt concrete are developed and evaluated. The preliminary title of the dissertation is "*ENHANCEMENTS OF SHEAR TESTS FOR ASPHALT CONCRETE*". He has completed this research under the supervision of Prof. Stefan A. Romanoschi and received his Ph. D degree in December 2019.

Appendix A: Duplicate Shear Tester (DST), Parts Drawings

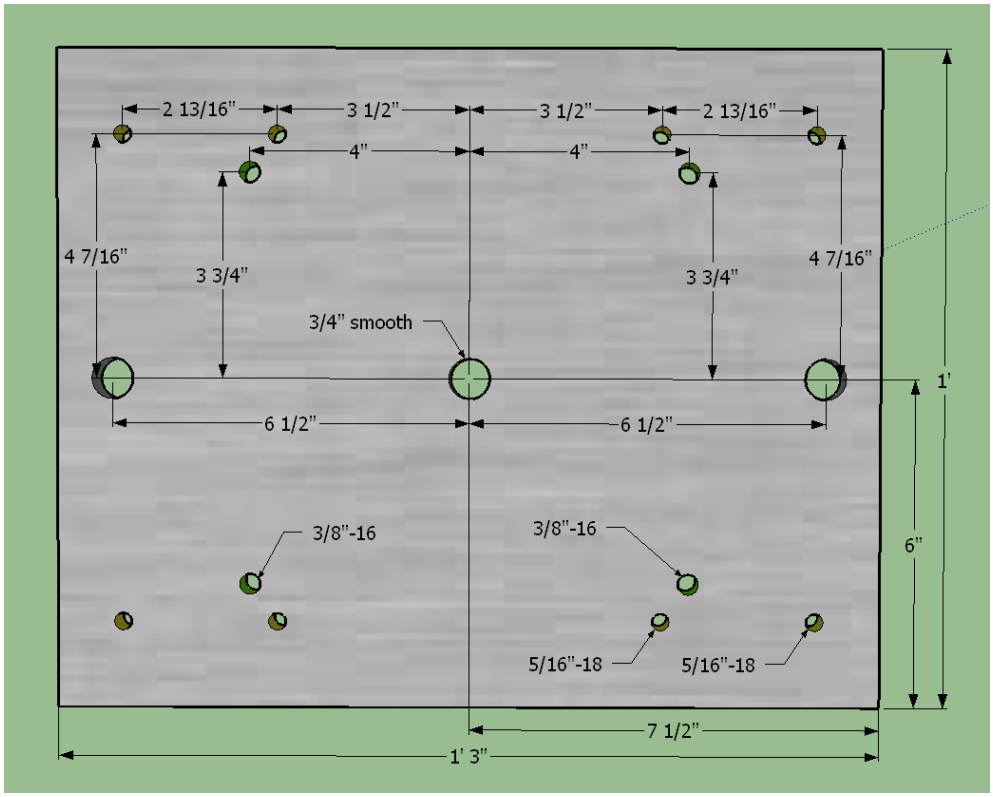

Figure A1. DST Supporting Plate- Holes Location

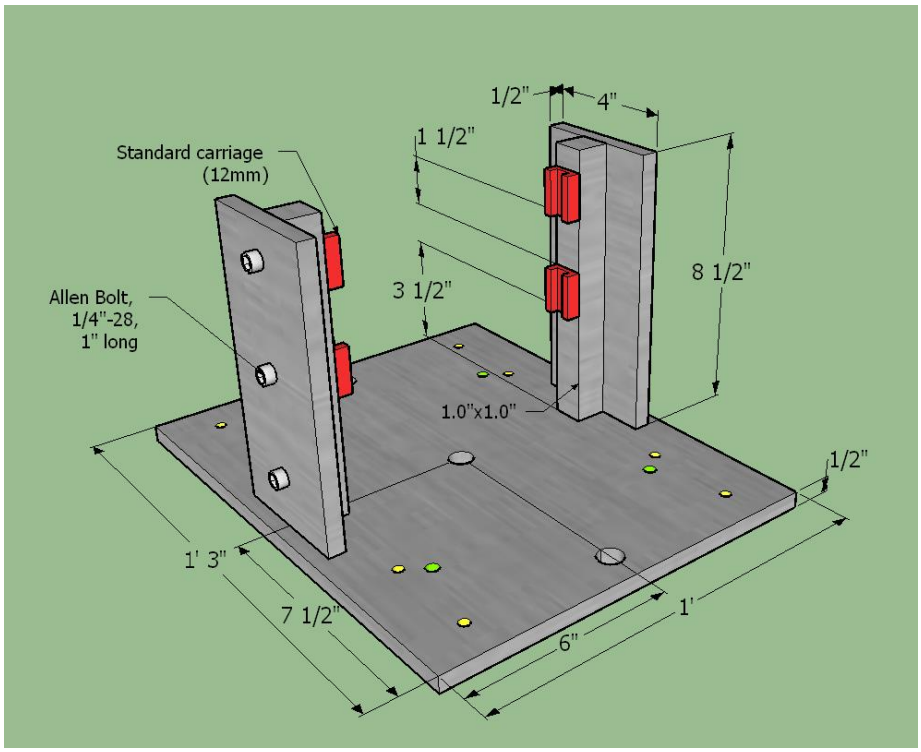

Figure A2. DST Supporting Plate.

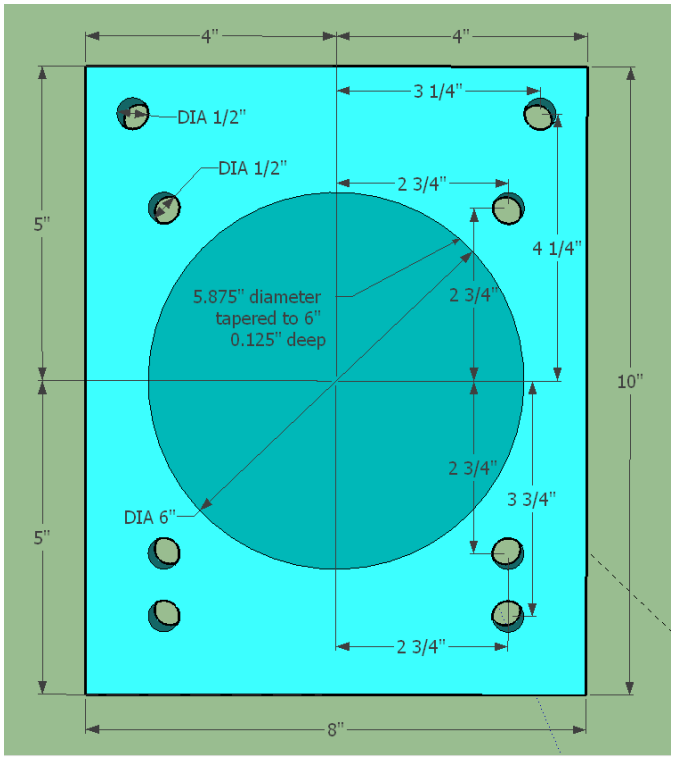

Figure A3. DST Sides-Plate of C6 specimens – Aluminum 1/2" thick.

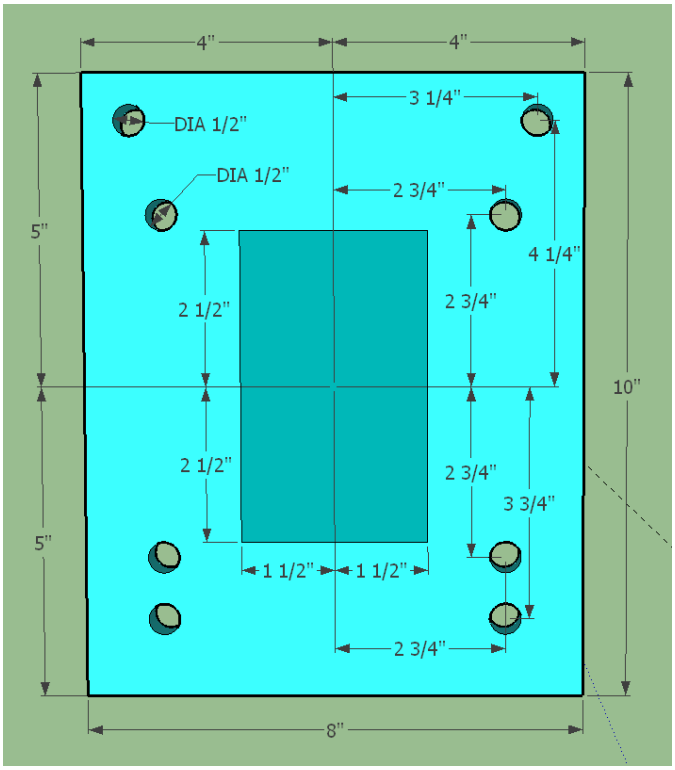

Figure A4. DST Sides-Plate of the Rectangular Specimens- Aluminum 1/2" thick.

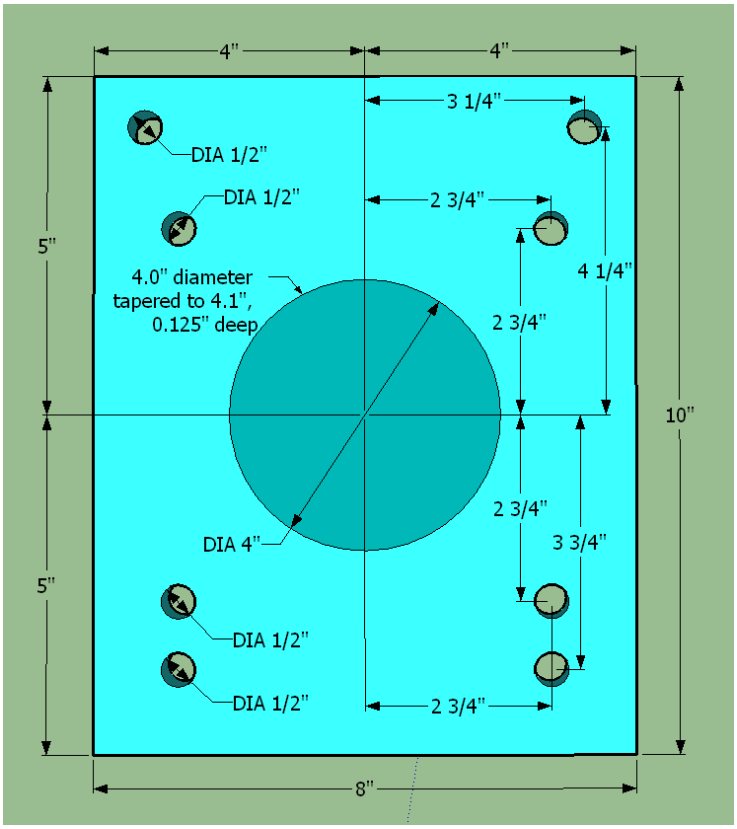

Figure A5. DST Sides-Plate of C4 specimens - Aluminum 1/2" thick.

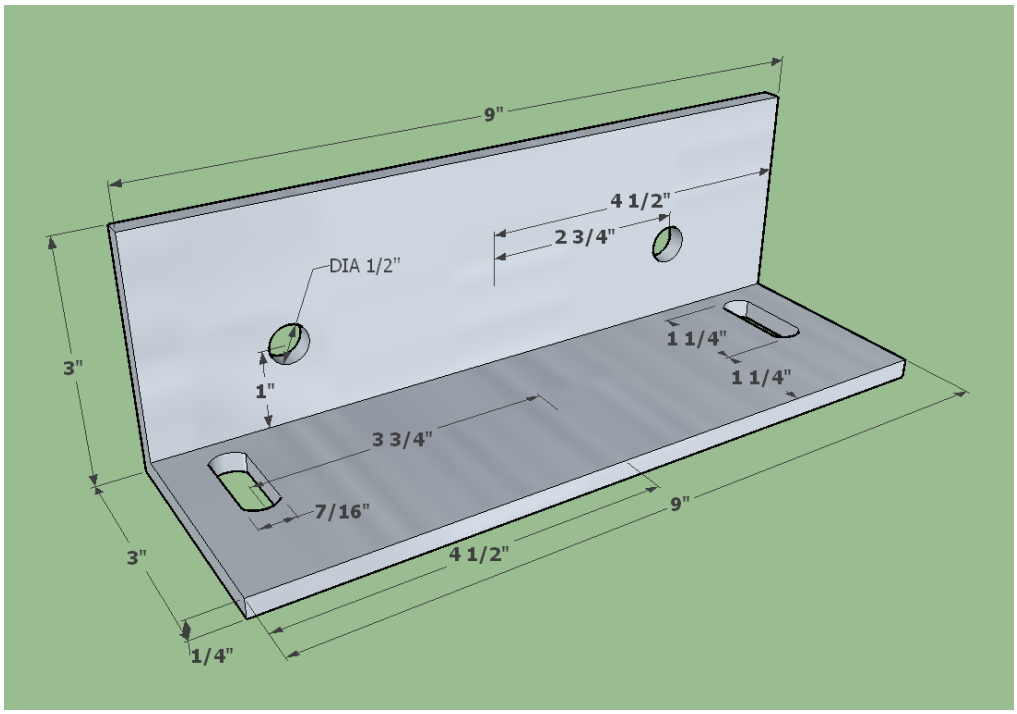

Figure A6. DST Gripper- Steel 1/4” thick.

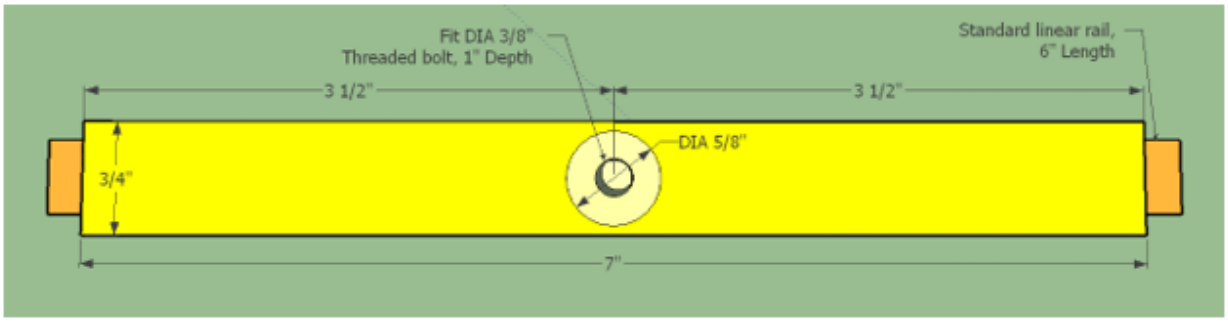

a) Middle-Plate of Aluminum "Top View" Section.

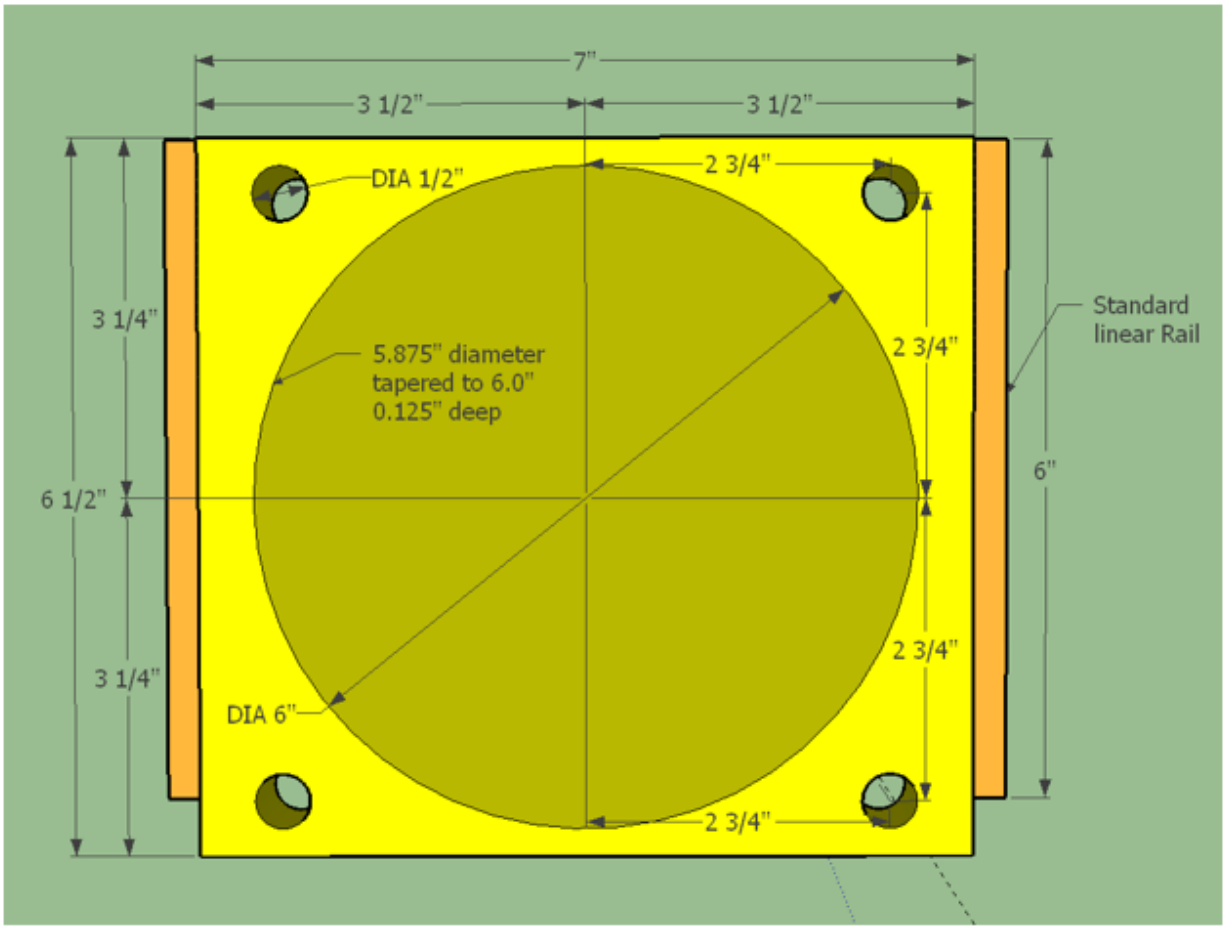

b) Middle- Plate of Aluminum "Front & Back Views" Section (Depression at both faces).

Figure A7. DST Middle-Plate of the C6 specimens - Aluminum 3/4" thick.

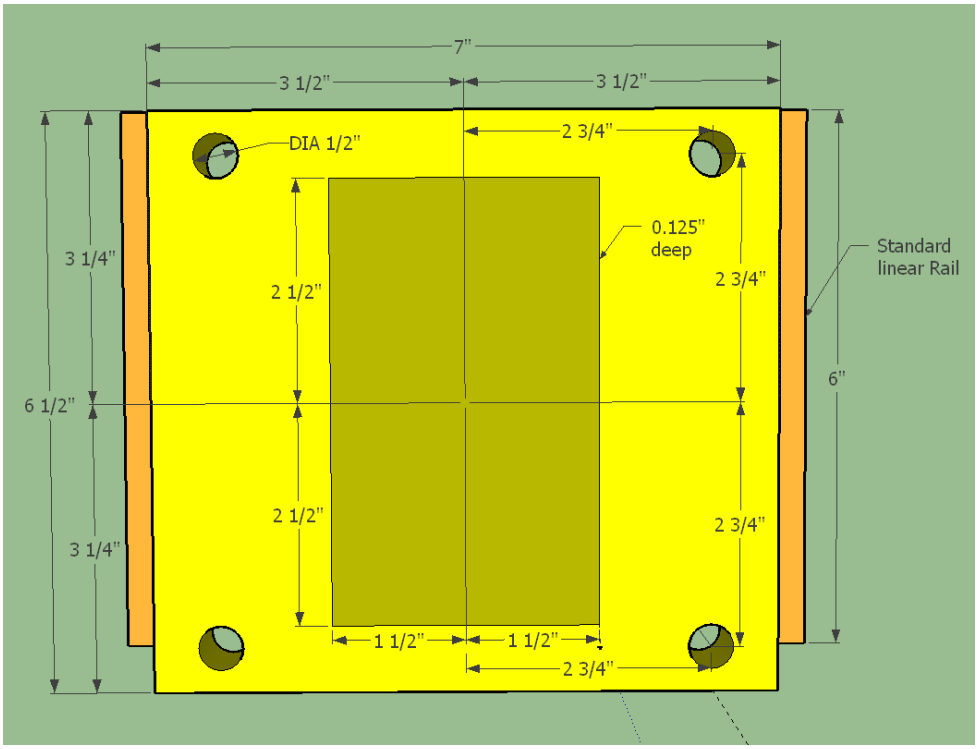

Figure A8. DST Middle-Plate of the Rectangular Specimens- Aluminum 3/4" thick.

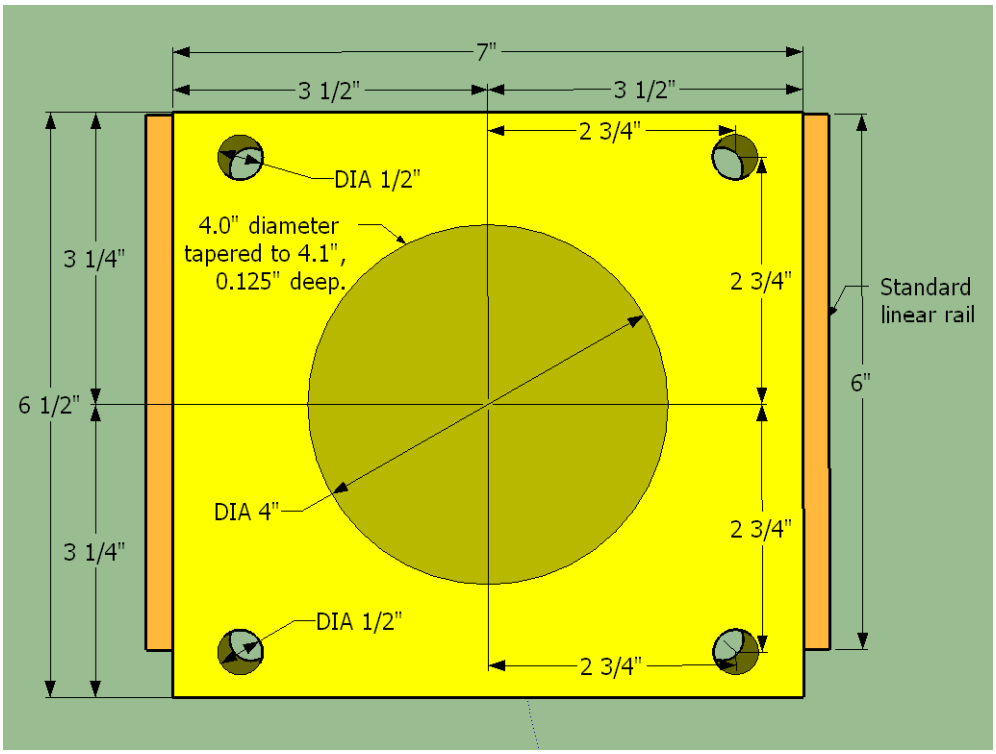

Figure A9. DST Middle-Plate of C4 specimens - Aluminum 3/4" thick.

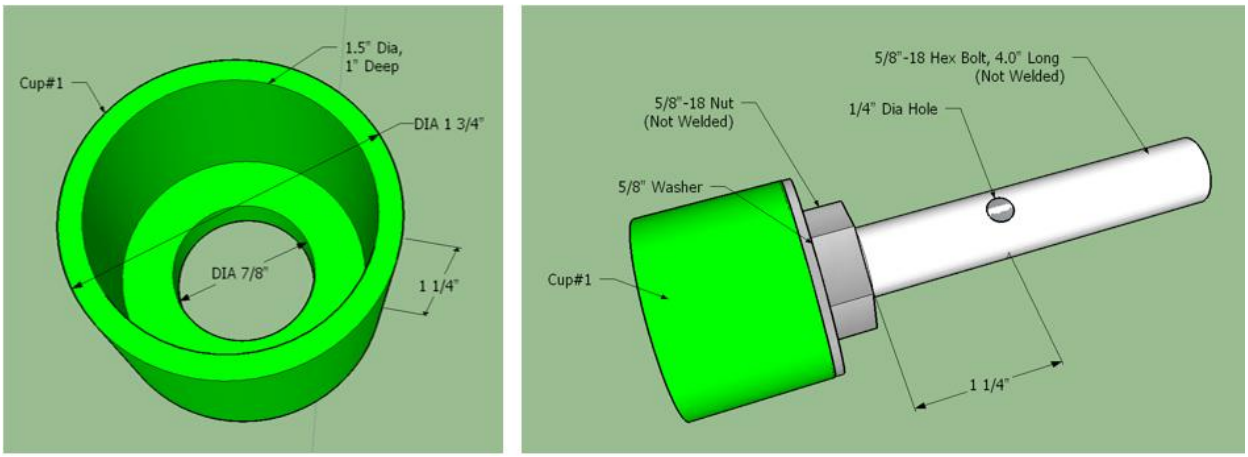

Figure A10. FSCH loading attachment- Cup 1- Steel.

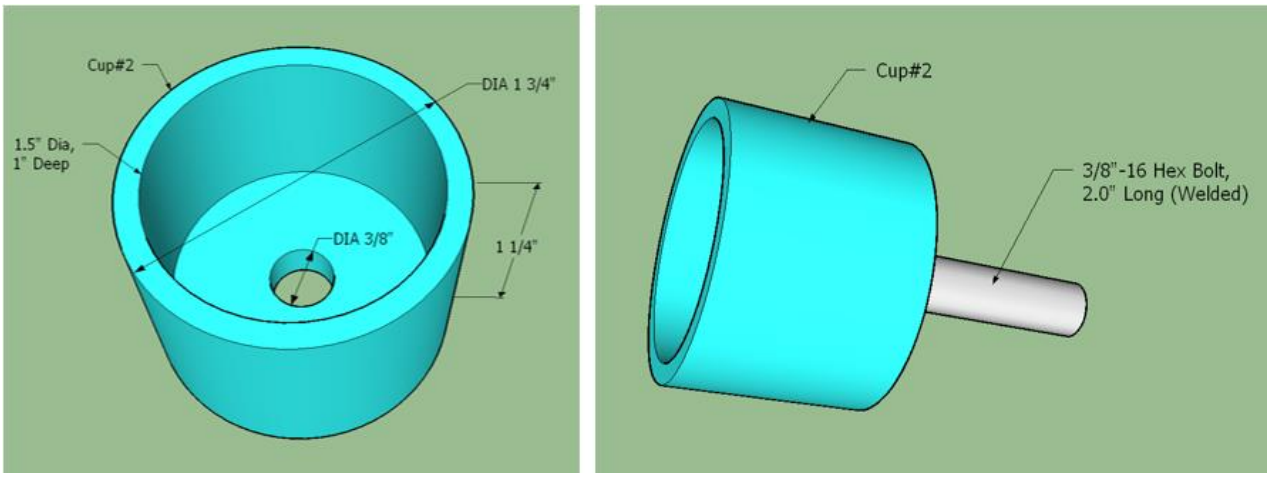

Figure A11. FSCH loading attachment- Cup 2- Steel.

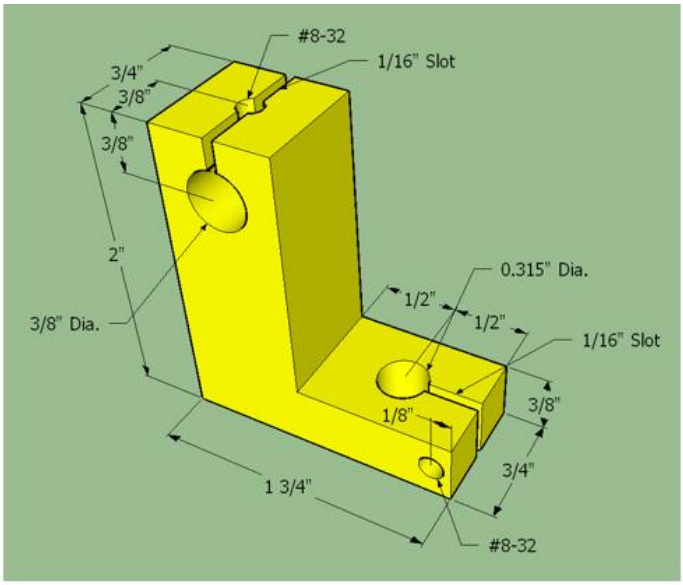

a) LVDT Holder

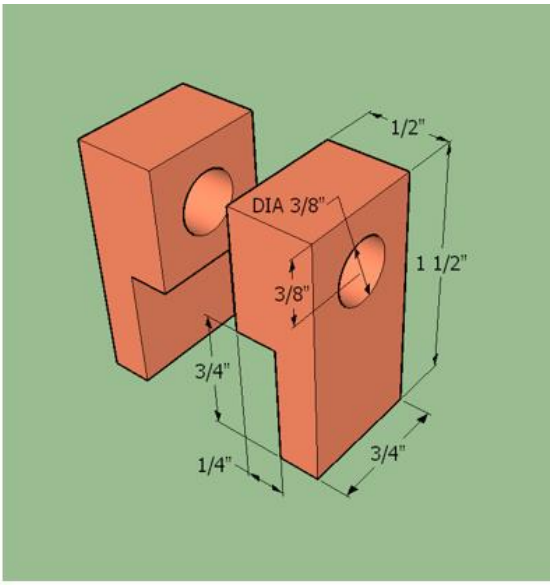

b) LVDT Clamps

Figure A12. LVDT Aluminum Holder and LVDT Steel Clamps- LVDT Mounts of DST device.

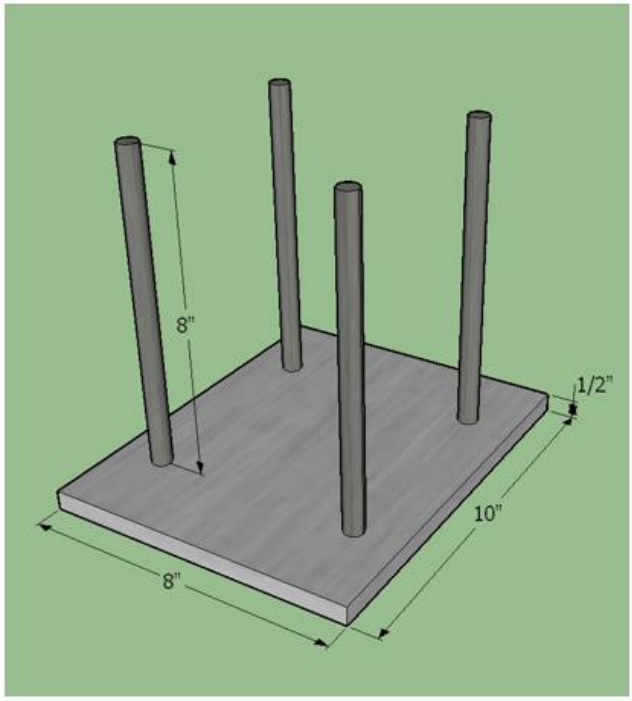

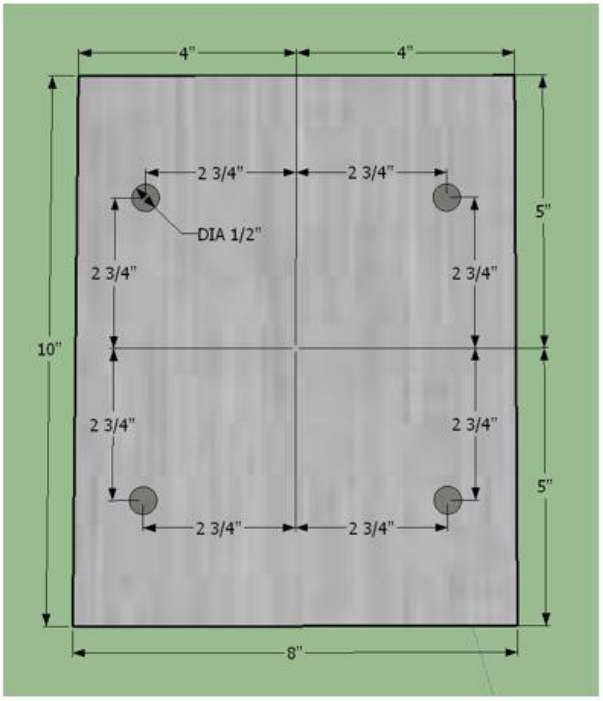

Figure A13. DST Assembly Stand

Appendix B: Shear Tester with Normal Stress (STNS), Parts Drawings

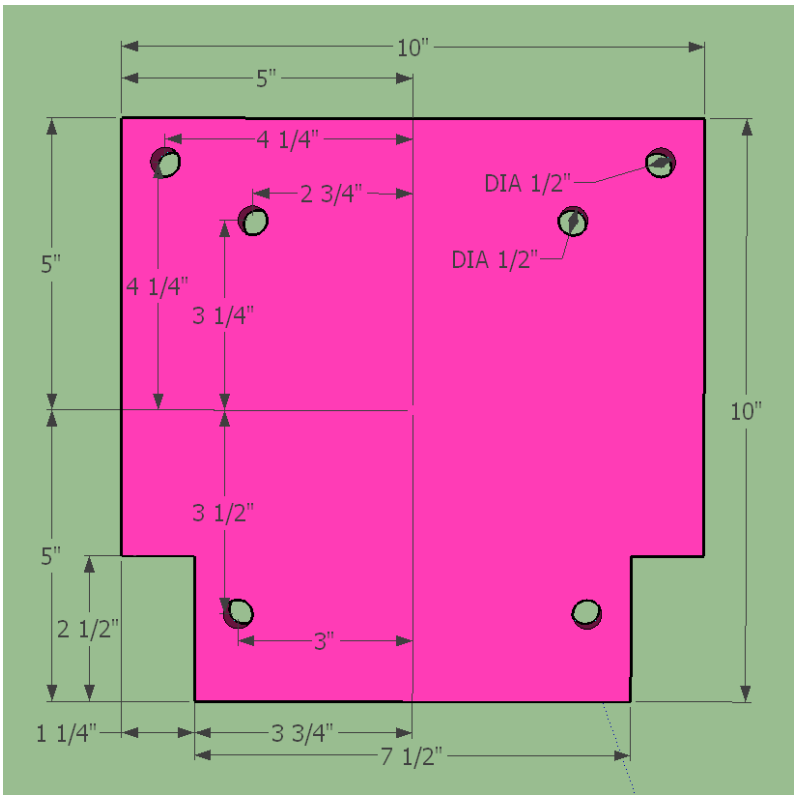

Figure B1. STNS Side-Plate (A)- Steel 1/2” thick.

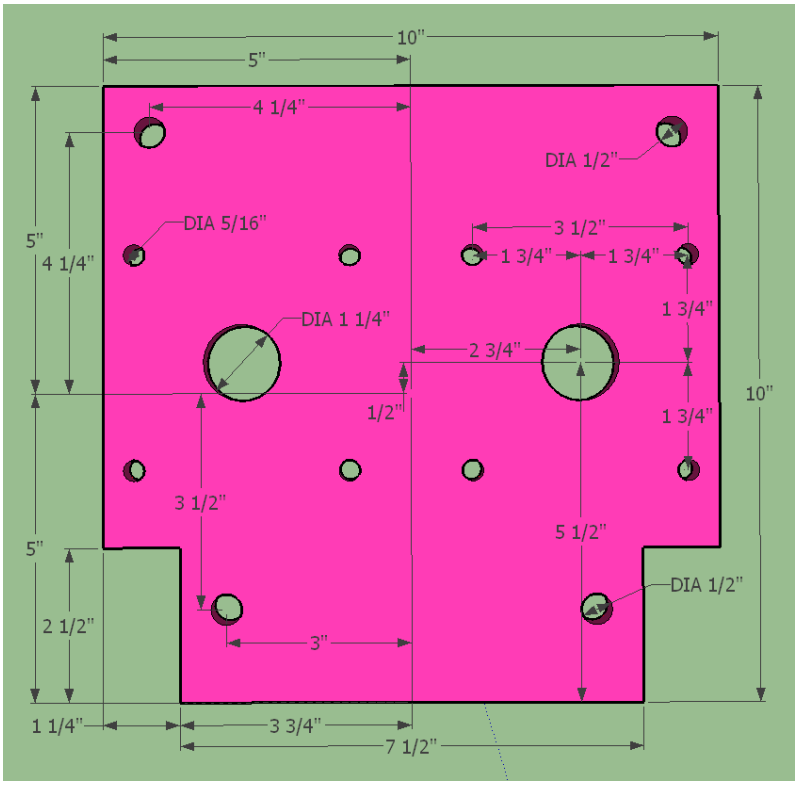

Figure B2. STNS Side-Plate (B)- Steel 1/2” thick.

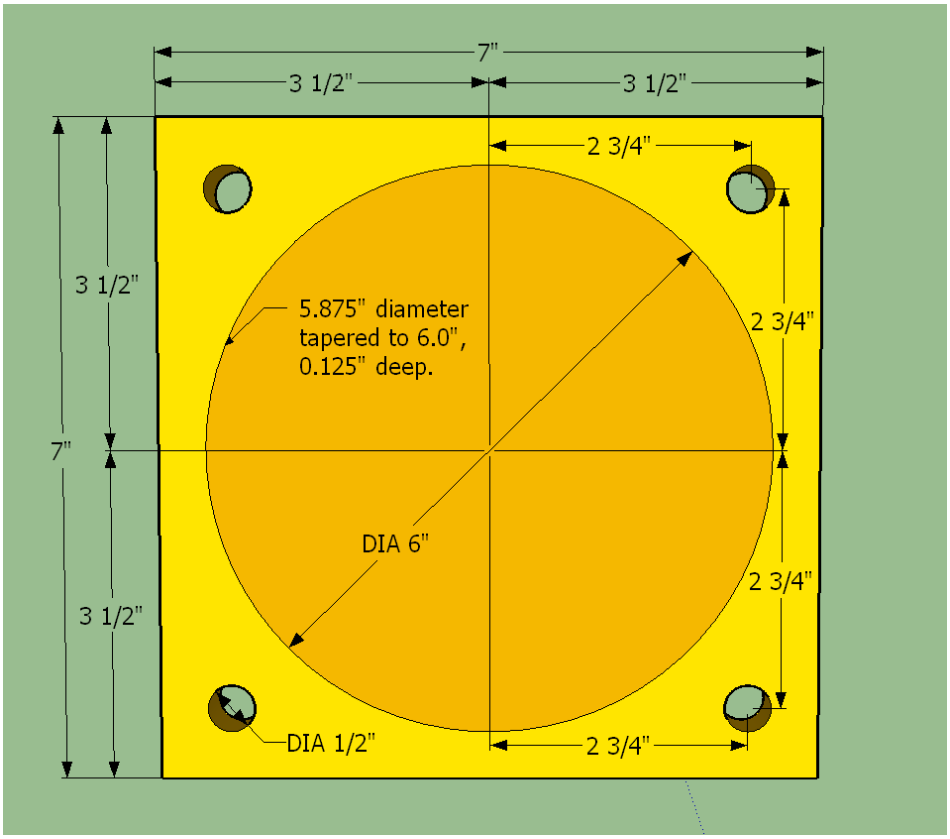

Figure B3. STNS Base Plate- Steel 1/2” thick.

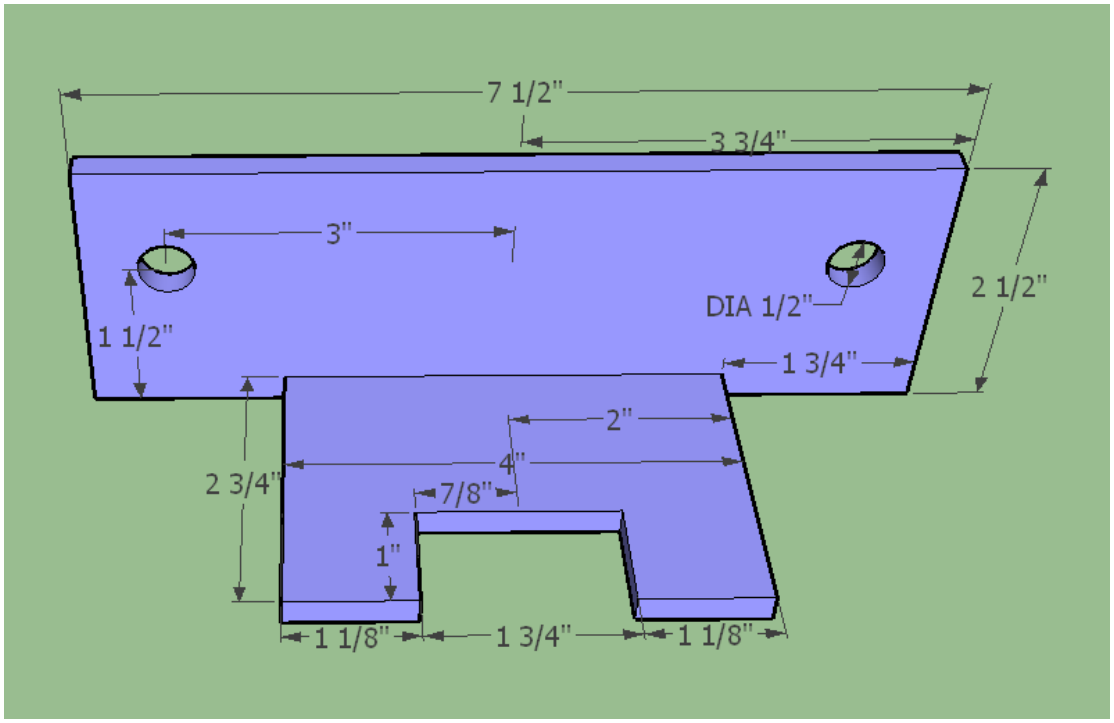

Figure B4. STNS Gripper- Steel 1/4” thick.

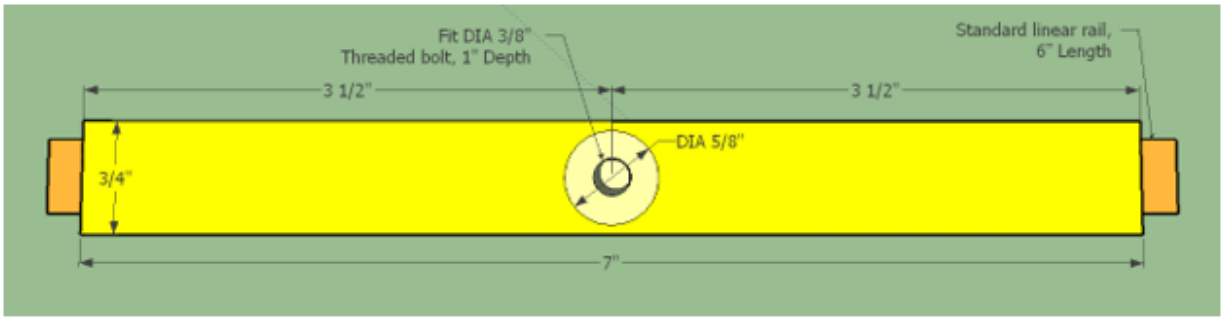

a) Middle-Plate of Steel "Top View" Section.

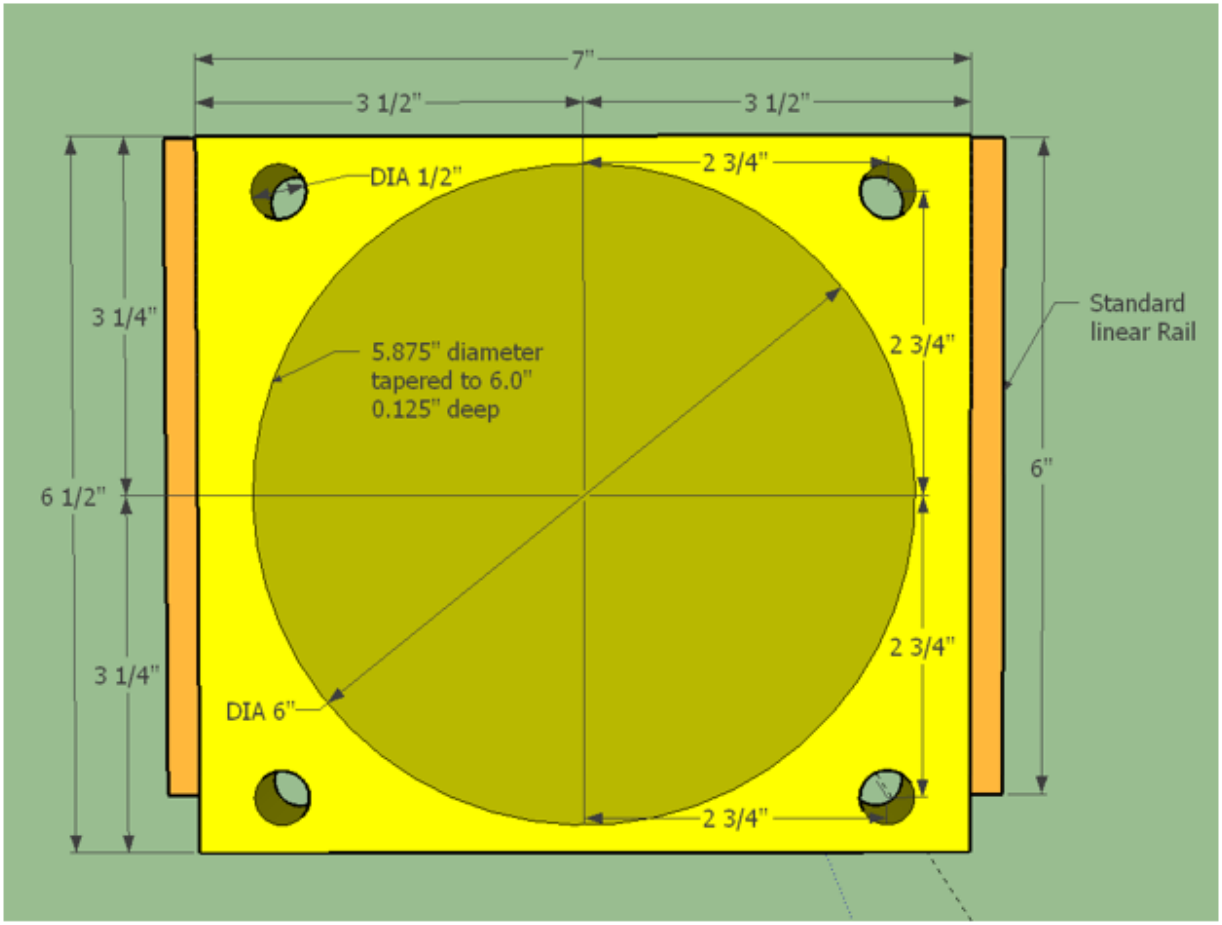

b) Middle- Plate of Steel "Front View" Section (Depression at one face only).

Figure B5. STNS Middle-Plate- Steel 3/4" thick.

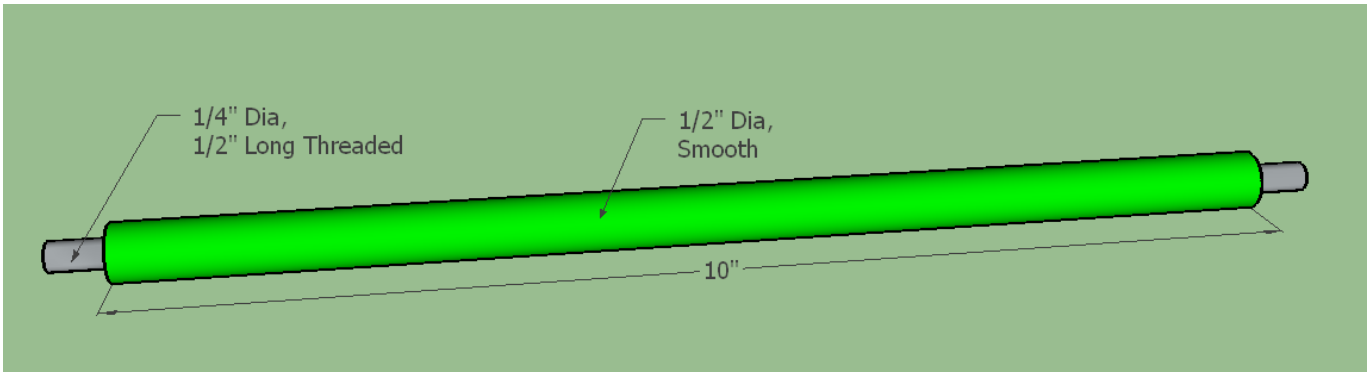

Figure B6. Rolling Systems' Steel Shaft – Steel 10" long.

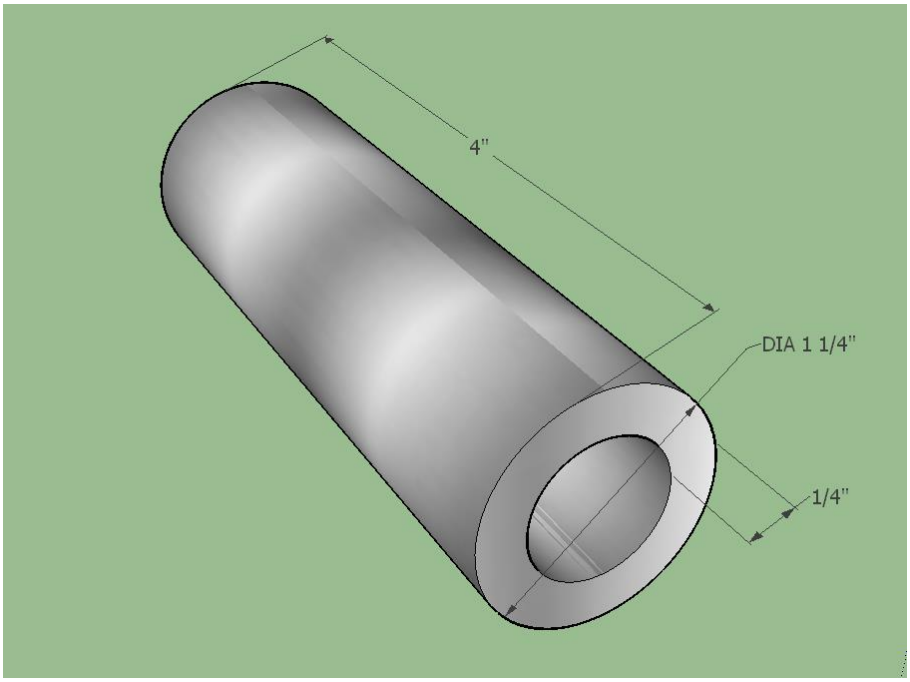

Figure B7. Rolling Cylinder – Steel 4.0" long.

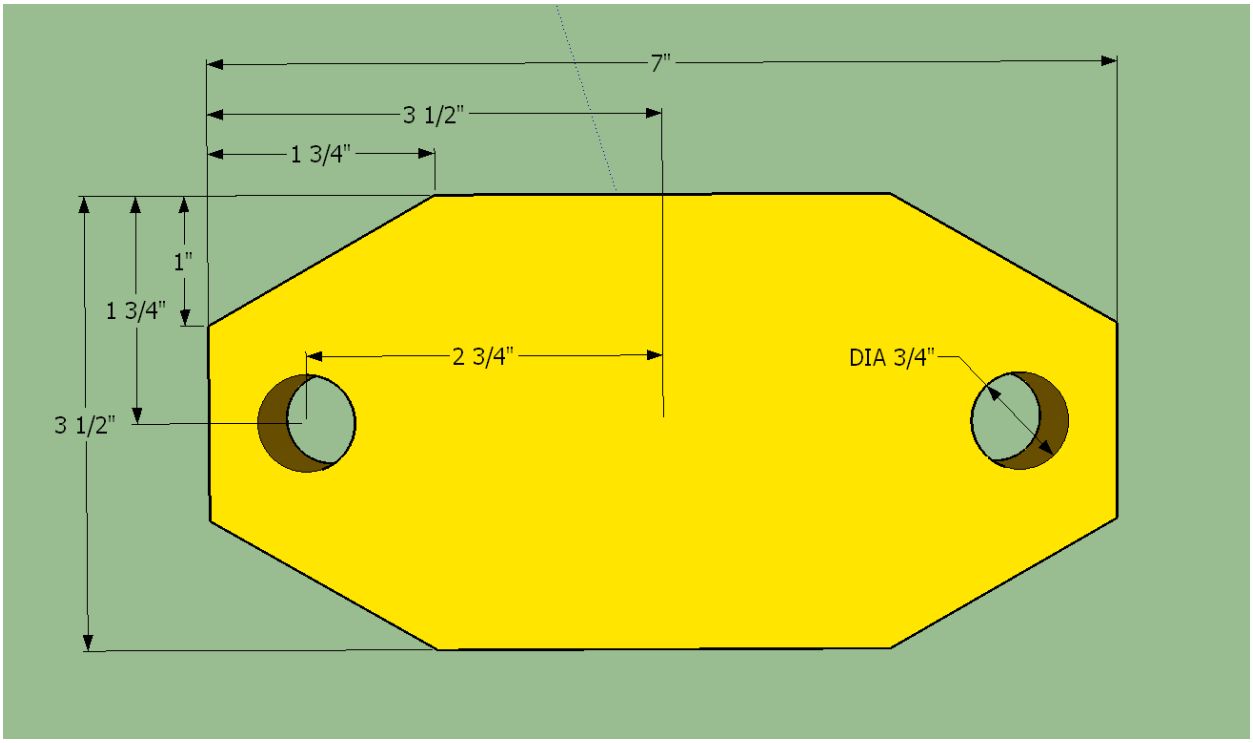

Figure B8. Bracket Plate - Steel 3/4” thick.

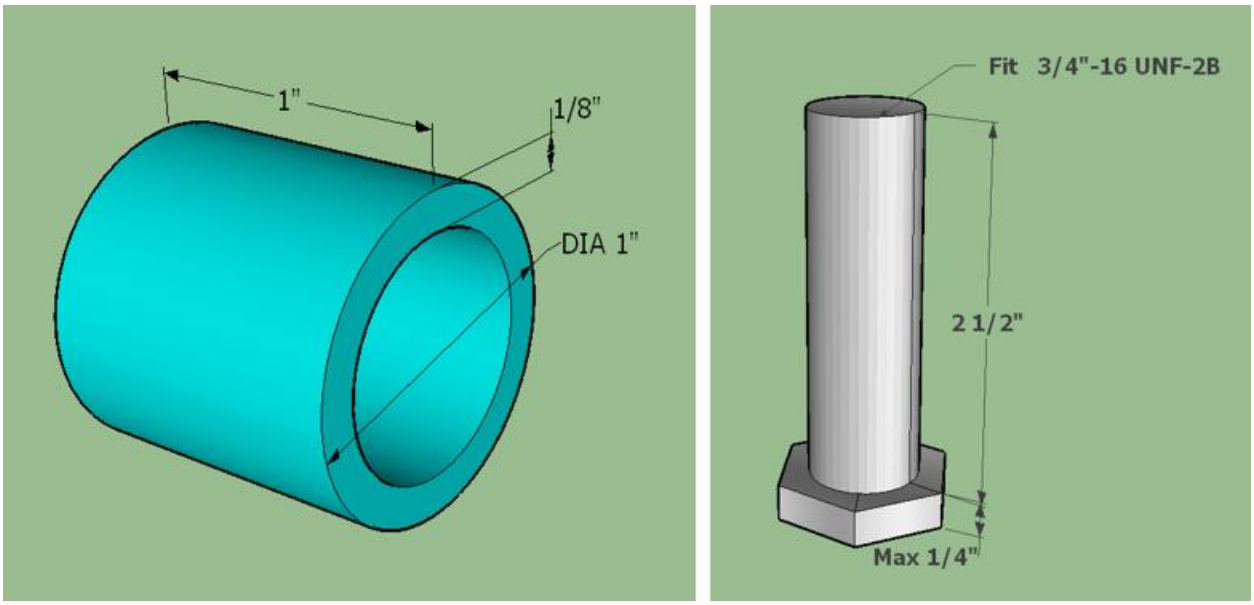

Figure B9. Extension cylinders and Bolts of the Bracket Plate - Steel.

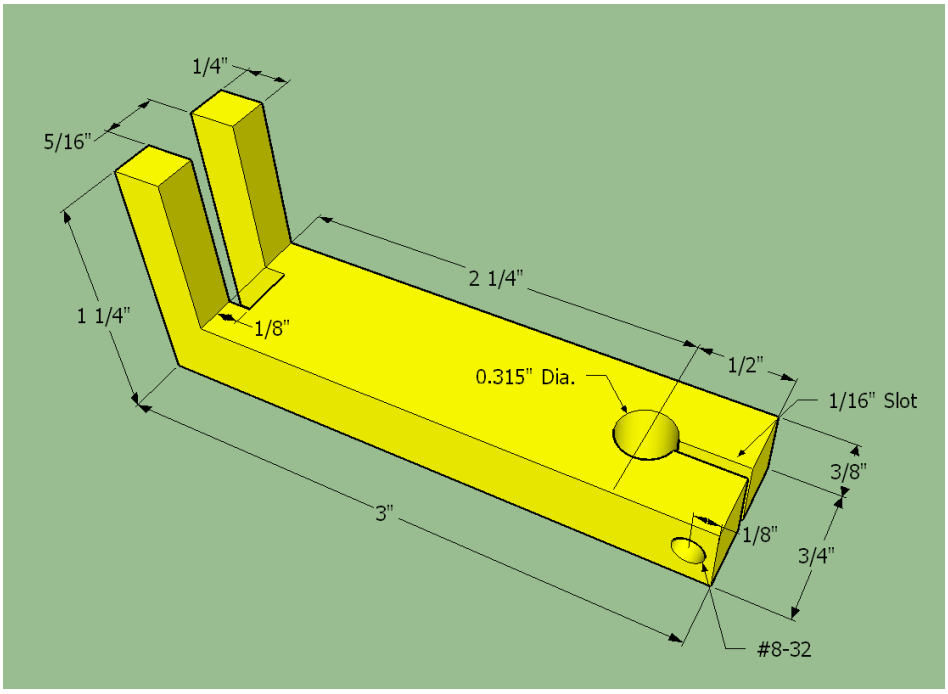

Figure B10. LVDT Holder of the SNTS device- Aluminum

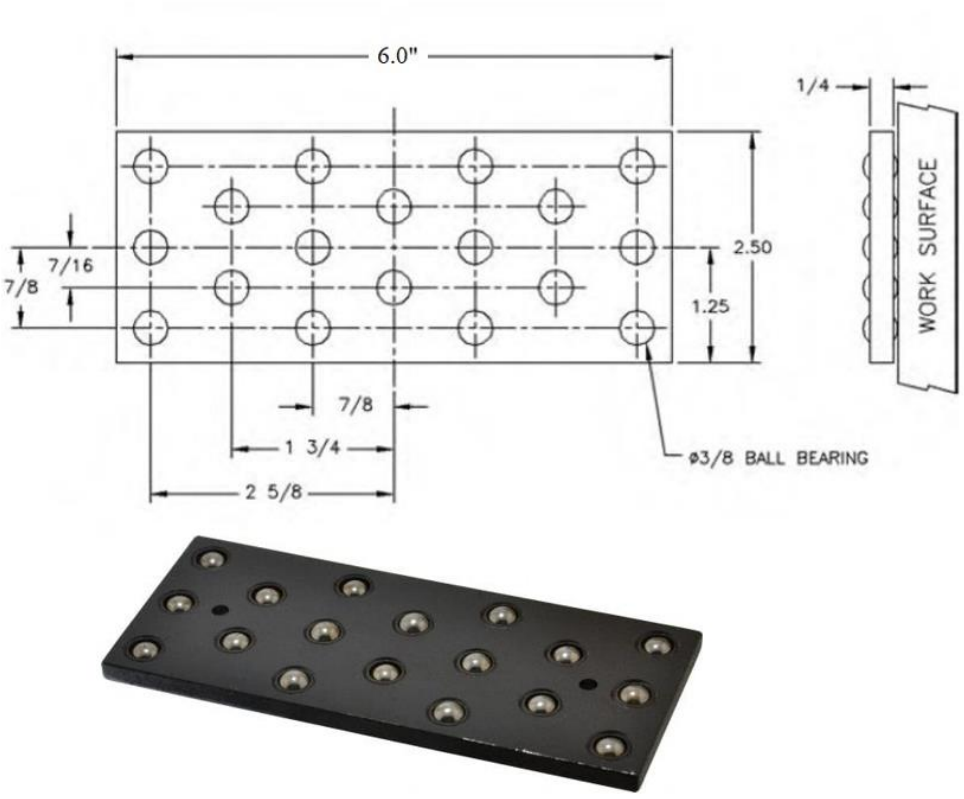

Figure B11. Pall Bearing Parallel (MSCDirect, 2018)

Item	Pillow Block Bearing	Bolt Size	5/16”
Bearing Insert Type	Sleeve	Overall Height	1-7/8"
Bore Dia.	1/2"	Overall Width	1-1/8"
Bolt Hole Center-to-Center	2-13/16"	Overall Length	3-9/16"
Mounting Surface to Shaft Center	1”	Max. Speed	6000 rpm
Bearing Housing Material Type	Zinc Die Cast	Bearing Lubrication	20 Weight Non-Detergent Oil
Bearing Insert Material	Bronze	Dynamic Load Capacity	Max. PV 50,000 lb.
Series	PBDC-BR	Temp. Range	-5 Degrees to 220 Degrees F
Number of Bolts	2	Includes	Oiler Hole

Figure B12. Pillow Block Bearing- 1/2” Bore Diameter (Grainger, 2018)

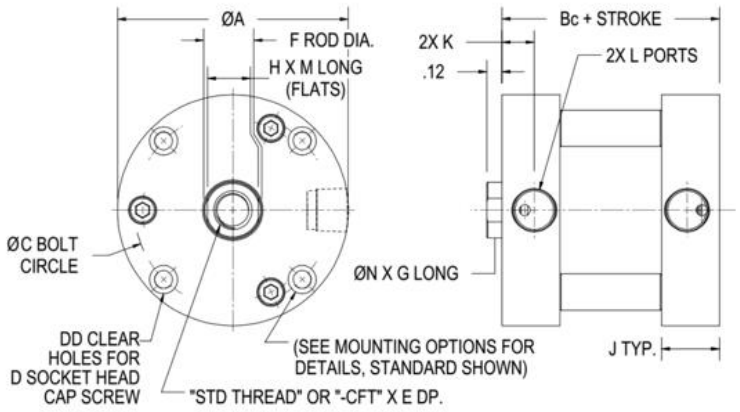

Part No.	FOS-1251.5
Stroke (in)	1.5
A (in)	5.50
B (in)	0.13
Bc (in)	2.44
C (in)	4.94
DD (in)	4
D	5/16
E Standard	3/4-16 UNF-2B
E Coarse	3/4-10 UNC-2B
E Depth (in)	0.8
F (in)	1.0
G (in)	0.21
H (in)	0.87
HH (in)	0.5
J (in)	0.84
K (in)	0.42
L	3/8 NPT
MM (in)	0.2
NN (in)	0.96

Figure B13. Air Cylinders- Single Acting, 4.0” Bore Diameter (Bimba, 2018)

Appendix C: Specimens Cut Preparations, Detailed Drawings

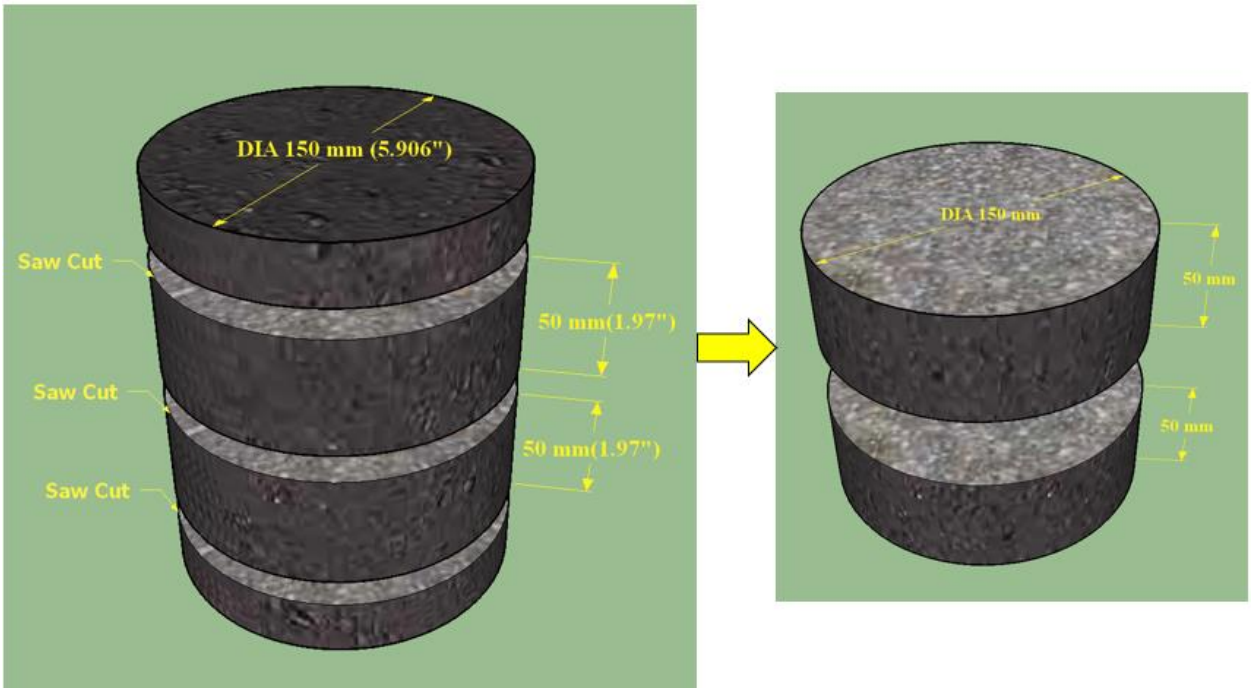

Figure C1. Three Saw-Cuts preparation to the C6 Specimens.

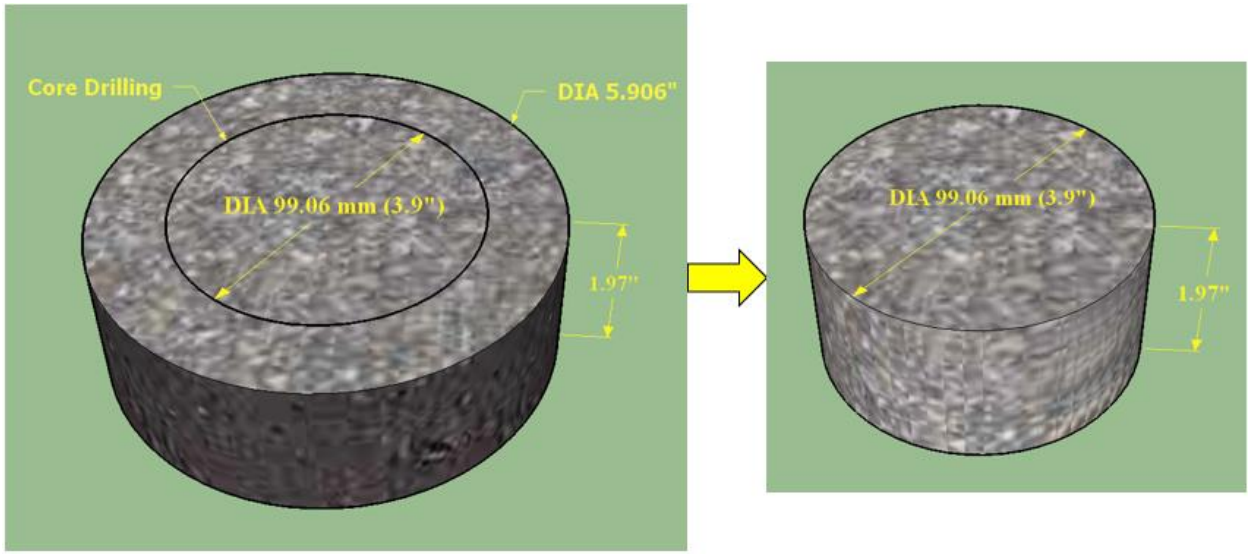

Figure C2. Drilling core preparation to the C4 Specimens.

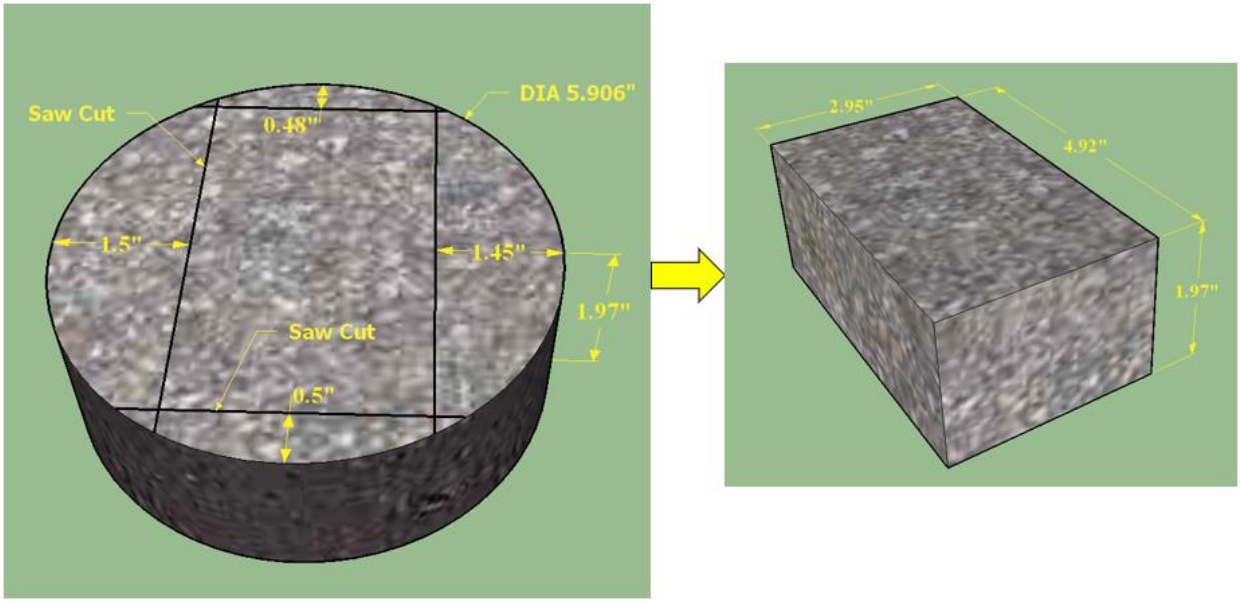

Figure C3. Trimming cut preparation to the RH Specimens.

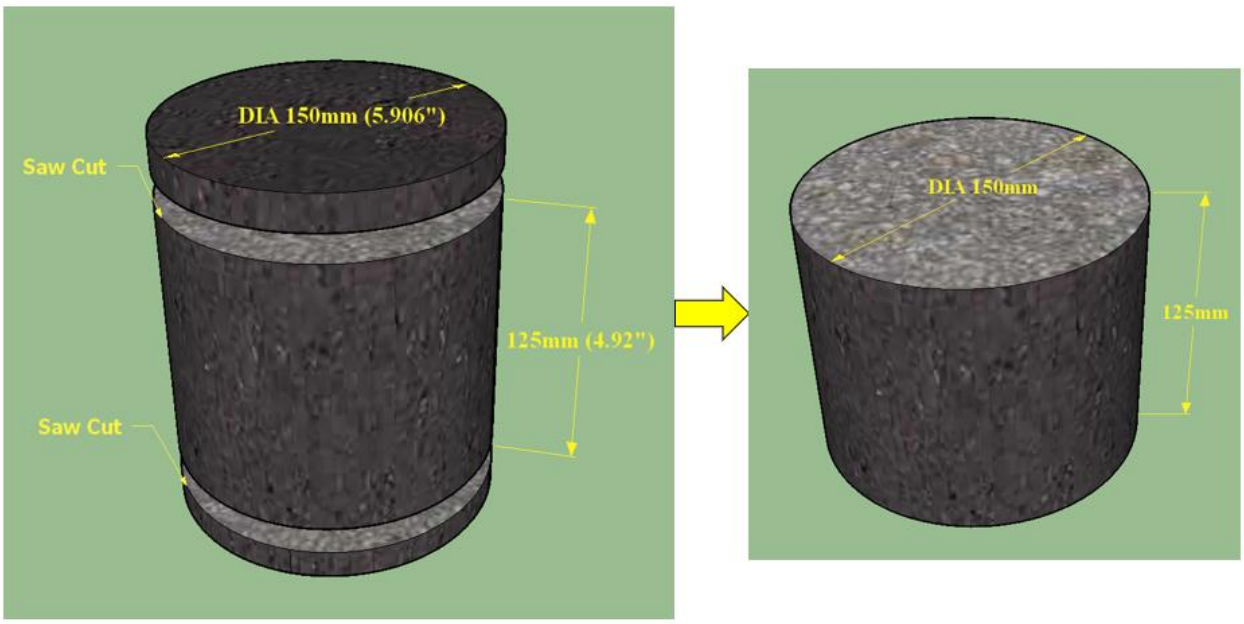

Figure C4. Two Saw-Cuts preparation to a Superpave gyratory sample

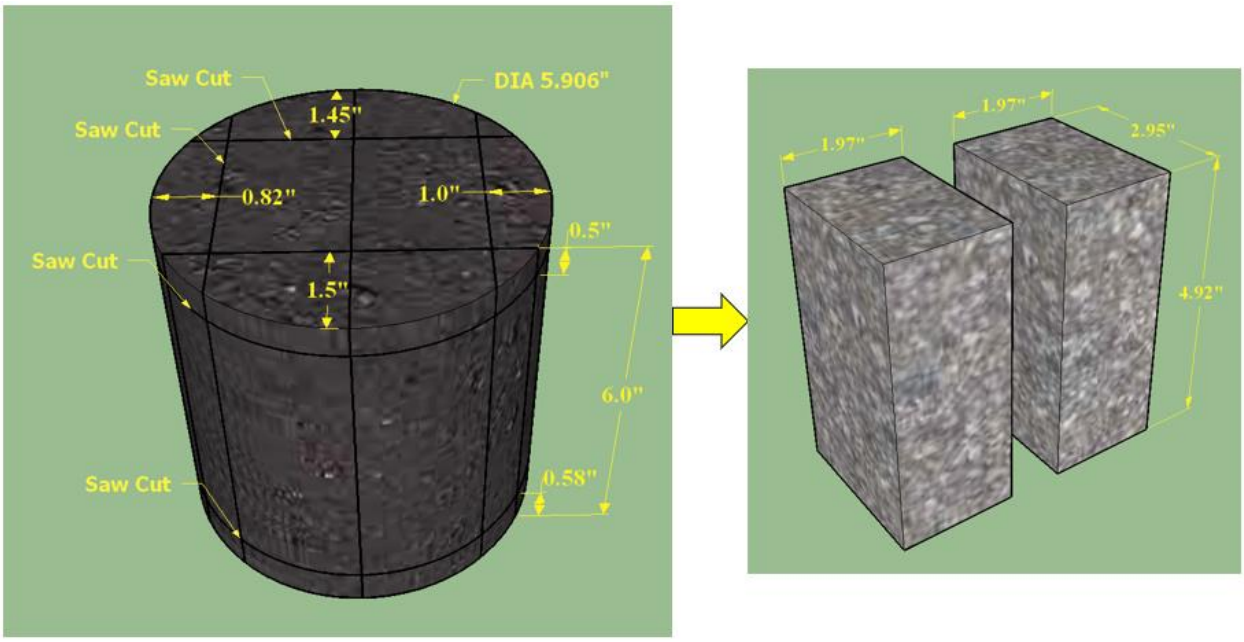

Figure C5. Trimming cut preparation to the RV Specimens.

Appendix D: Sample Holders, Detailed Drawings

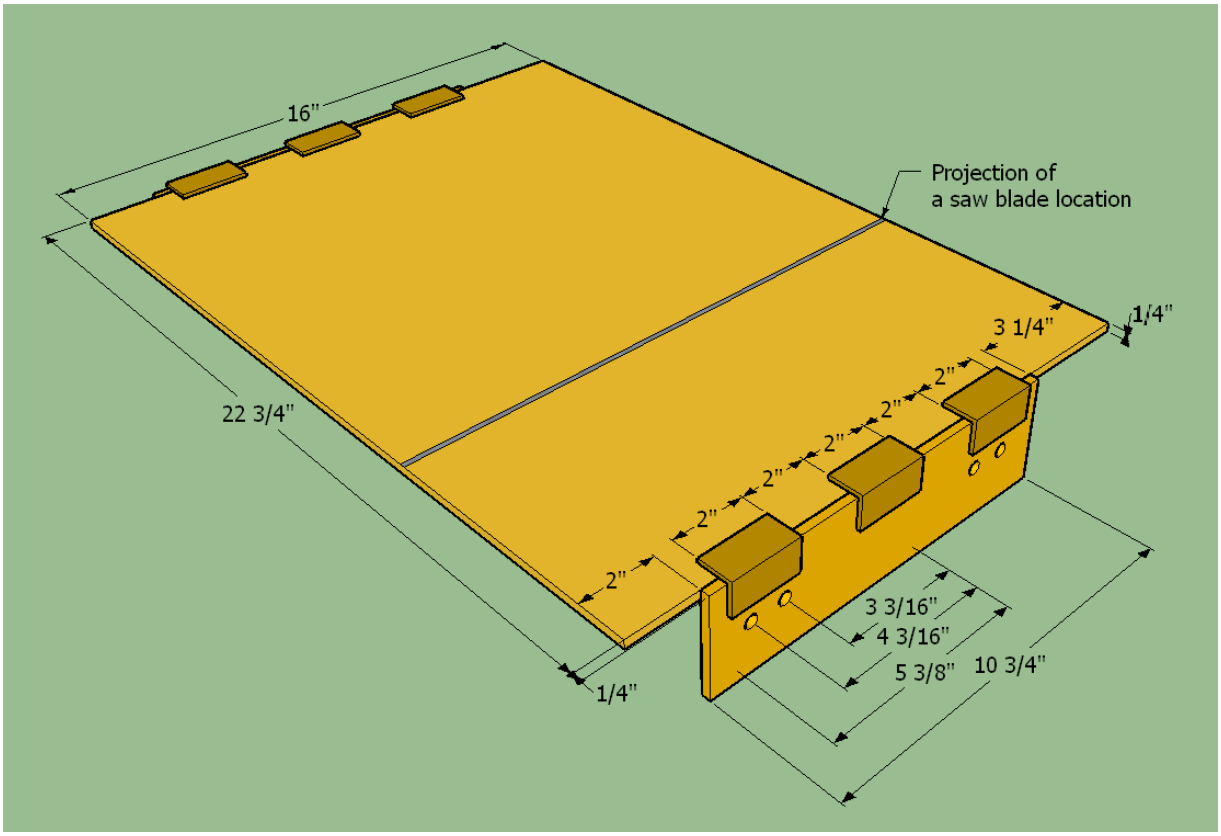

Figure D1. Base Plate- Sample holder of C6 samples.

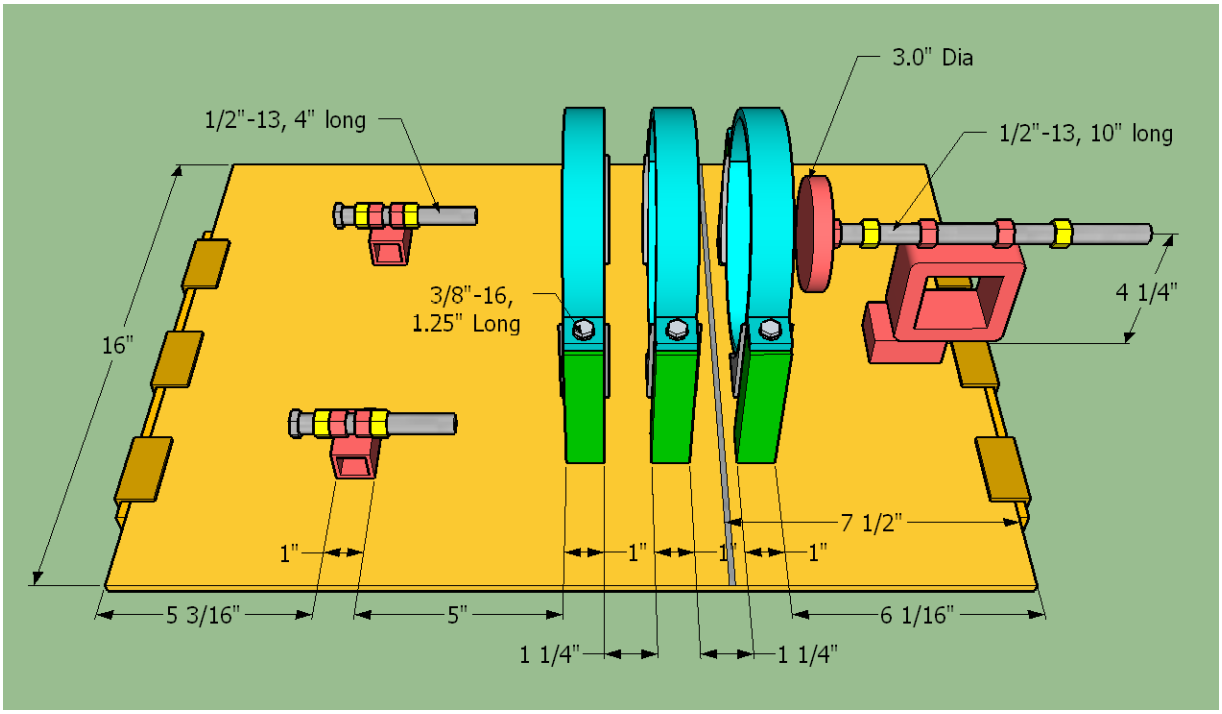

Figure D2. Full View 1- Sample holder of C6 samples.

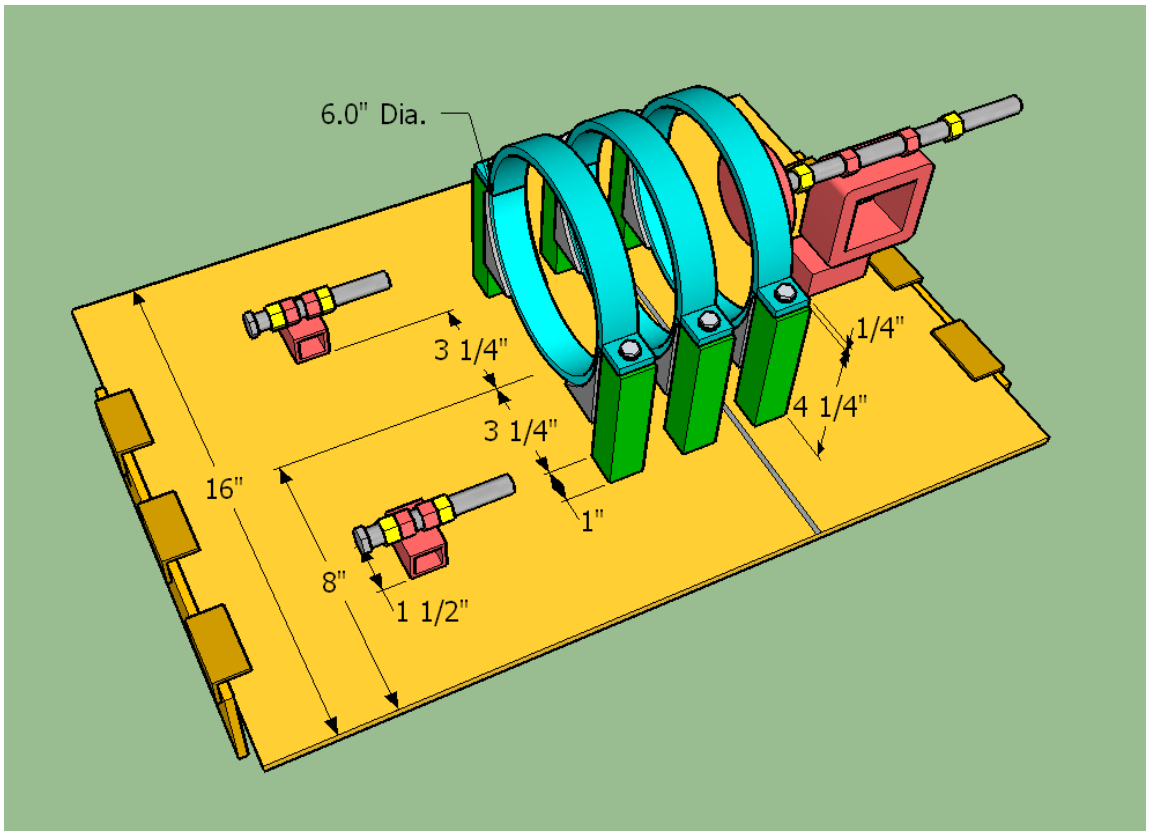

Figure D3. Full View 2- Sample holder of C6 samples.

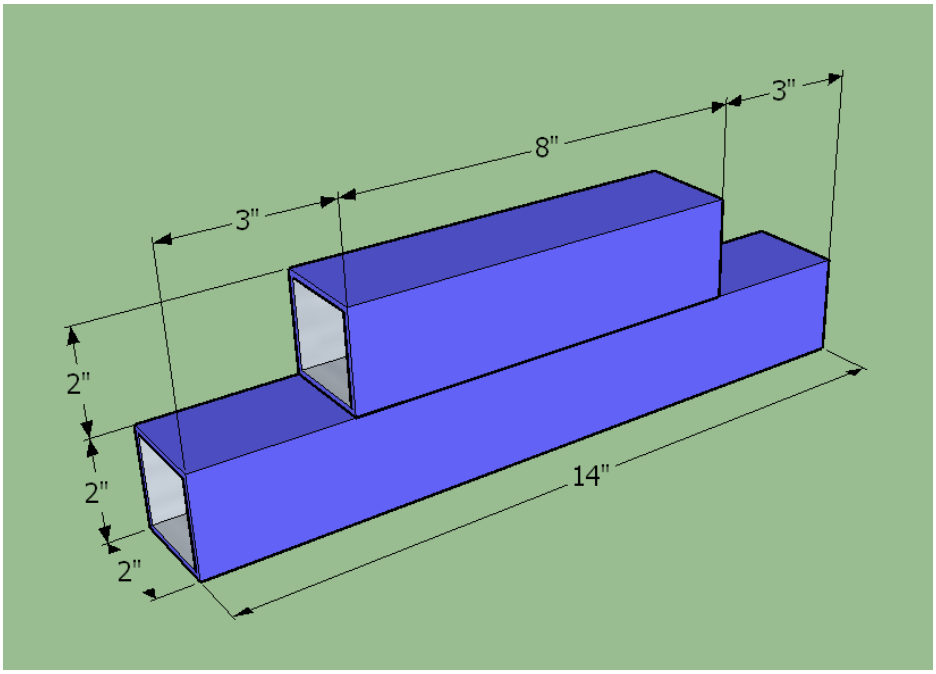

Figure D4. Movable Block- Sample Holder of C6 samples.

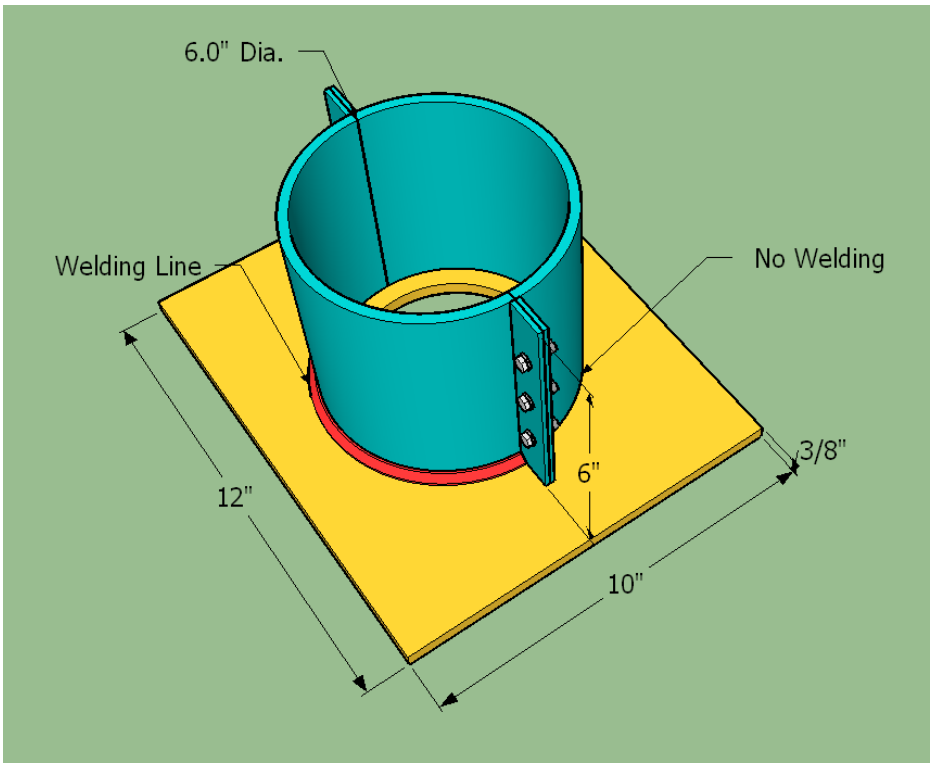

Figure D5. Full View- Vertical holder of gyratory samples.

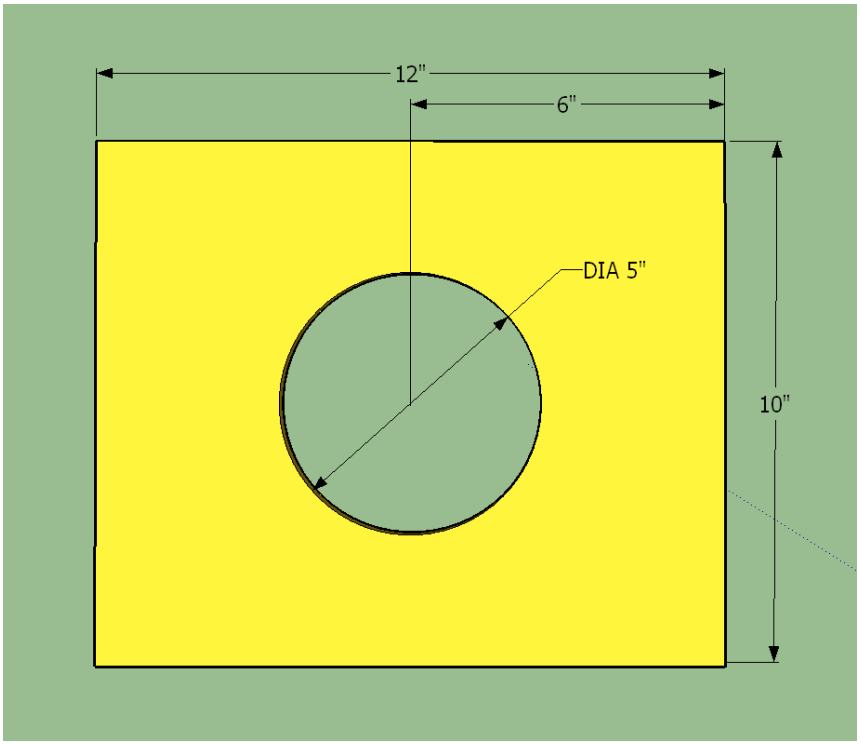

Figure D6. Base Plate- Vertical holder of gyratory samples.

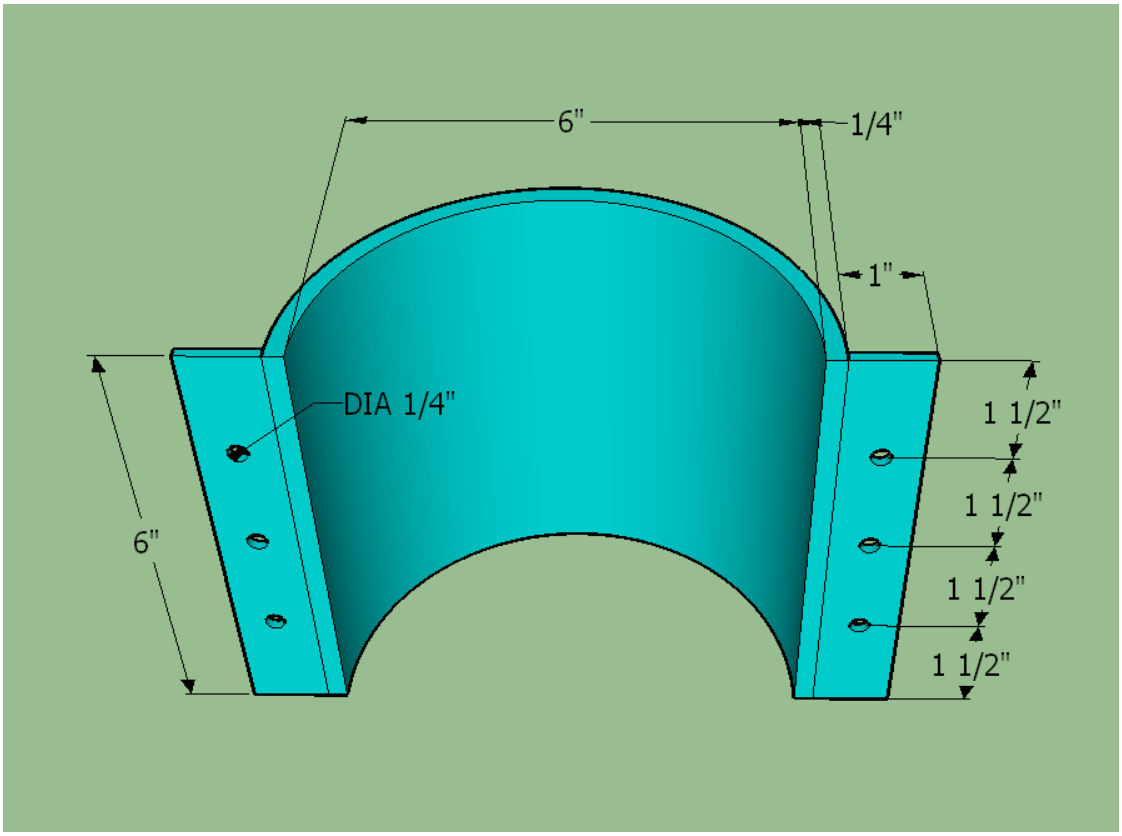

Figure D6. Semicircular Clamps- Vertical holder of gyratory samples.

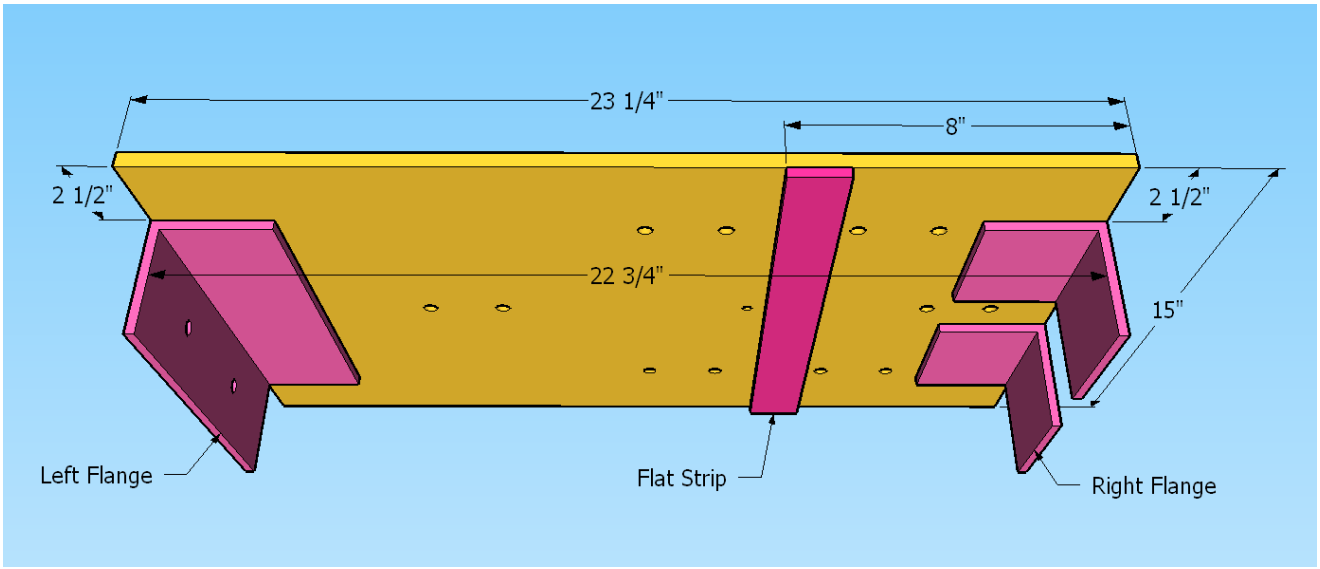

Figure D7. Base Plate Full View- Sample Holder of Rectangular Specimens.

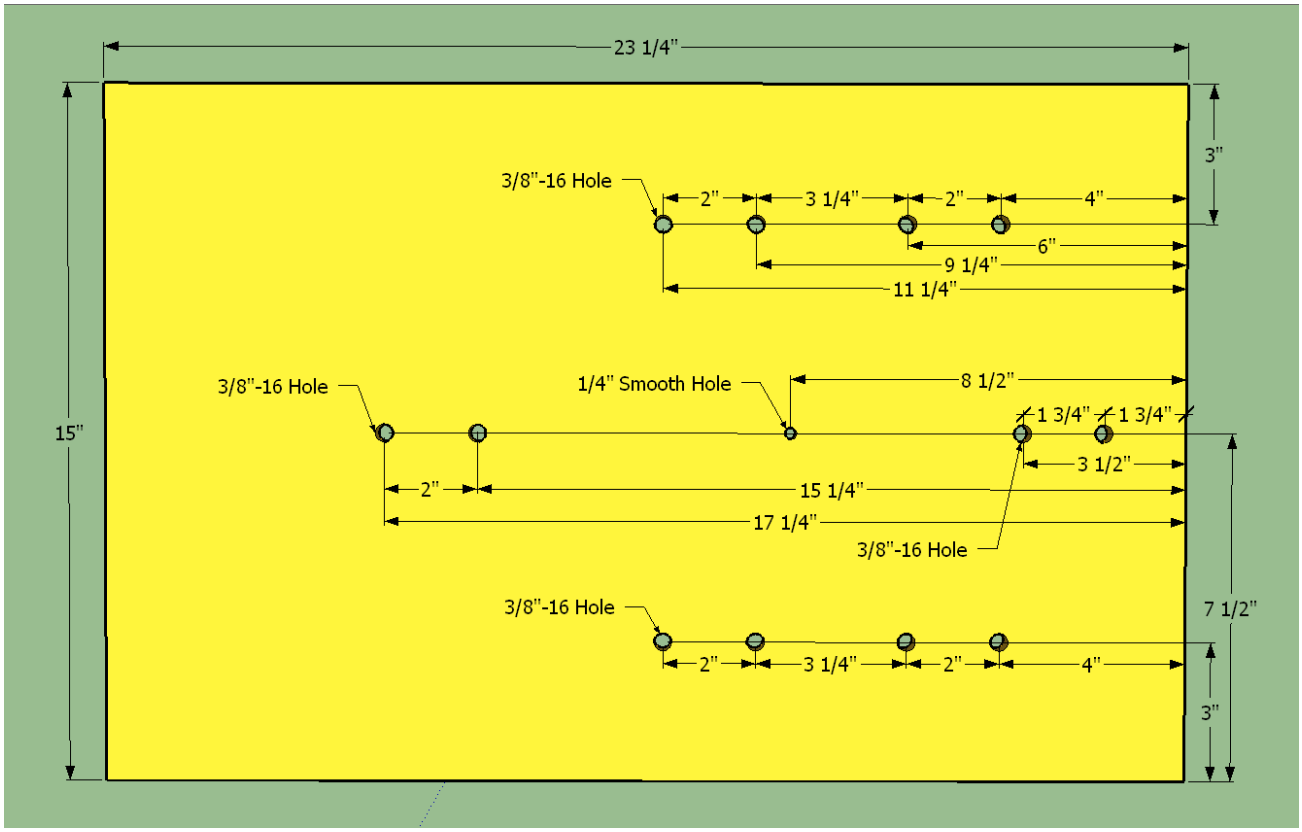

Figure D8. Base Plate Holes Locations- Sample Holder of Rectangular Specimens.

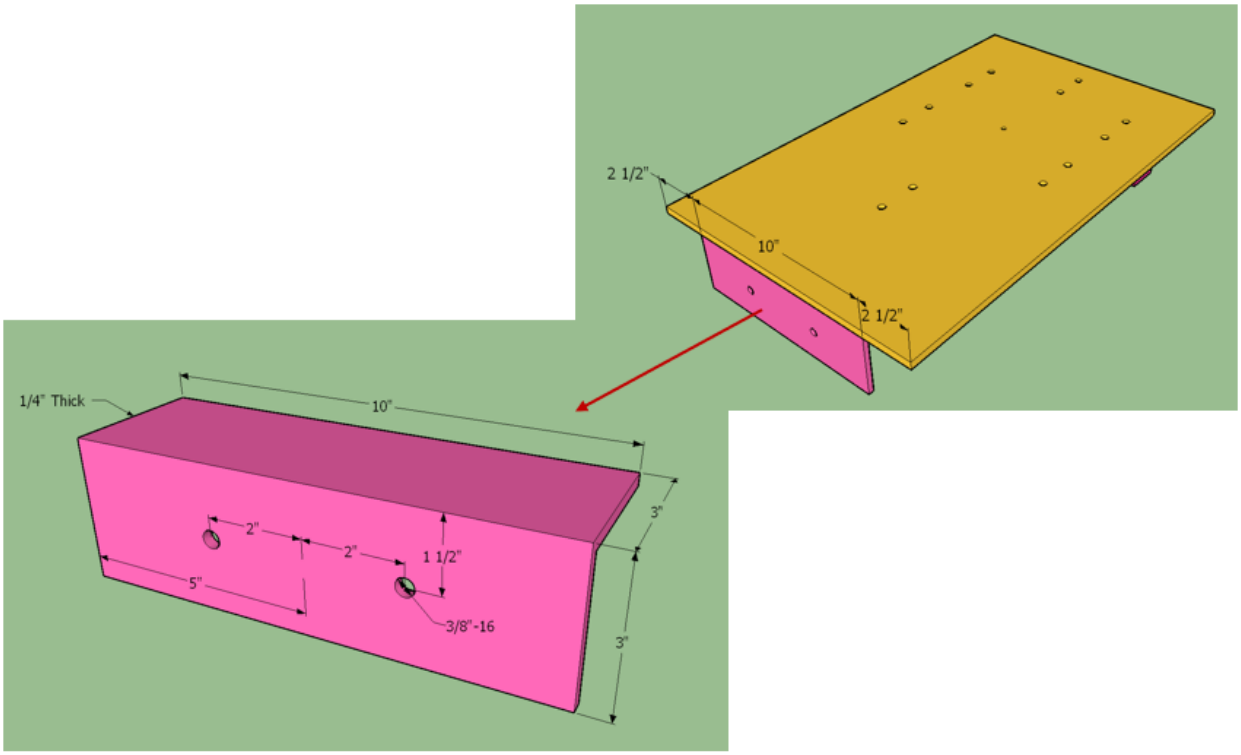

Figure D9. Left Flange of the Base Plate- Sample Holder of Rectangular Specimens.

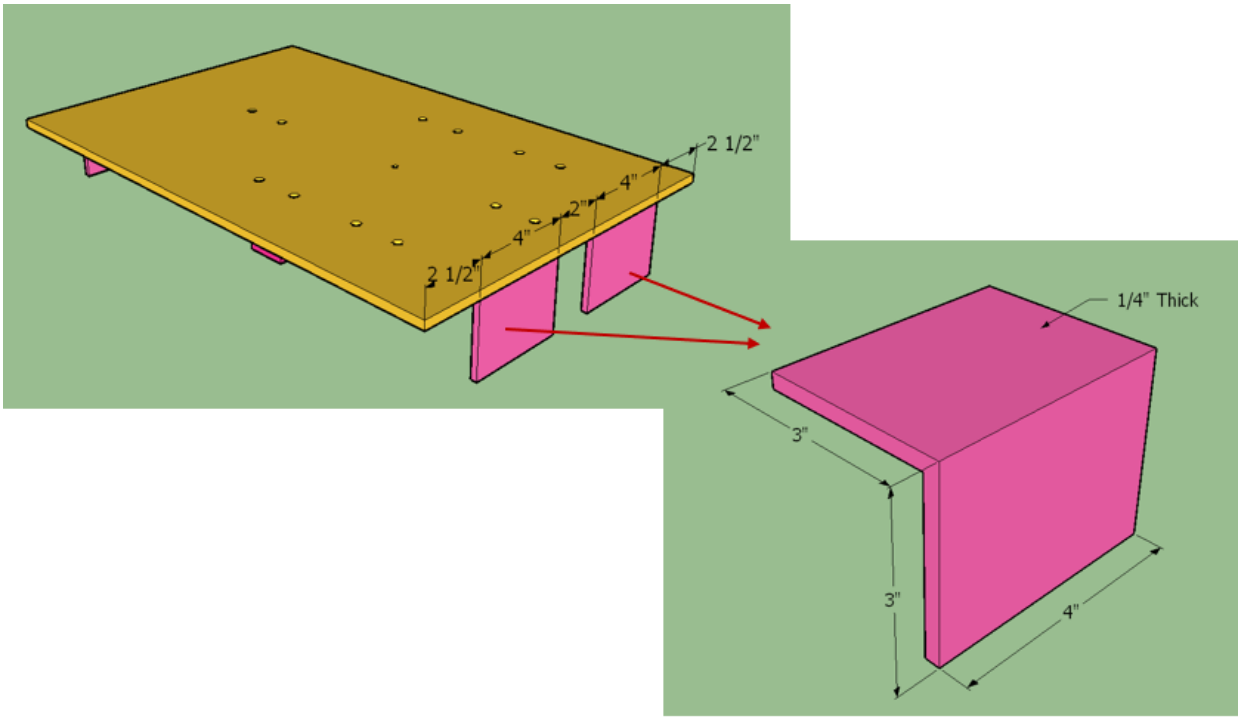

Figure D10. Right Flange of the Base Plate- Sample Holder of Rectangular Specimens.

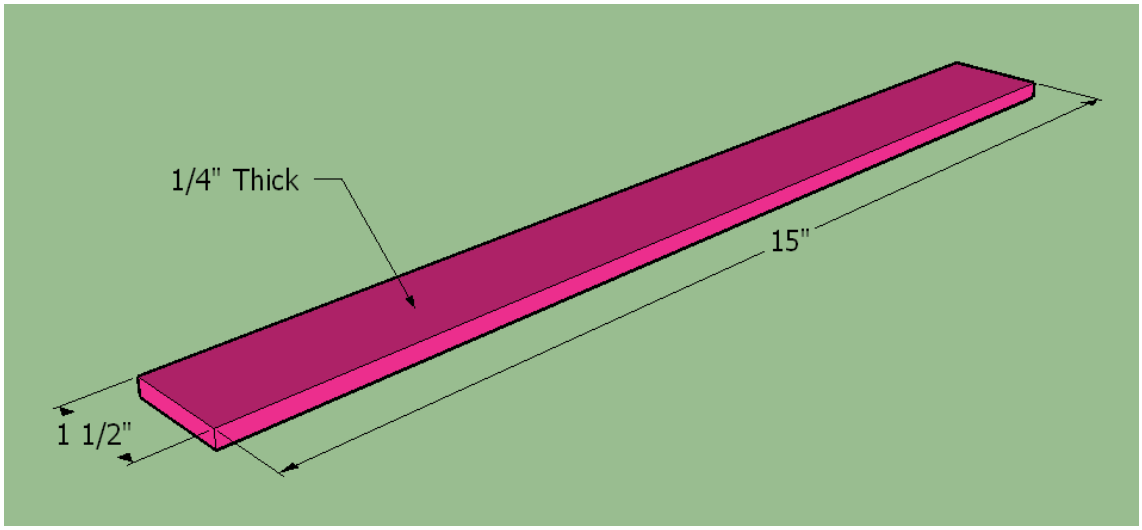

Figure D11. Flat Strip of the Base Plate- Sample Holder of Rectangular Specimens.

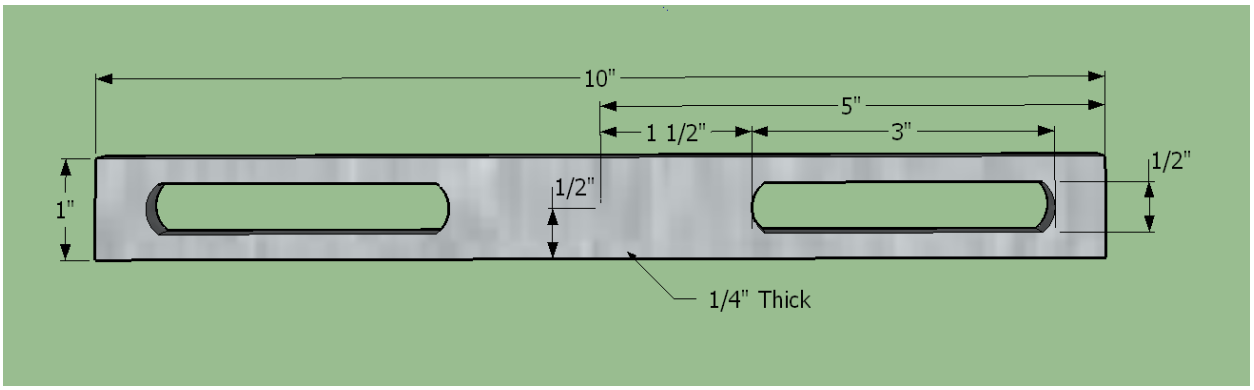

Figure D12. Brackets (B1 & B2)- Sample Holder of Rectangular Specimens.

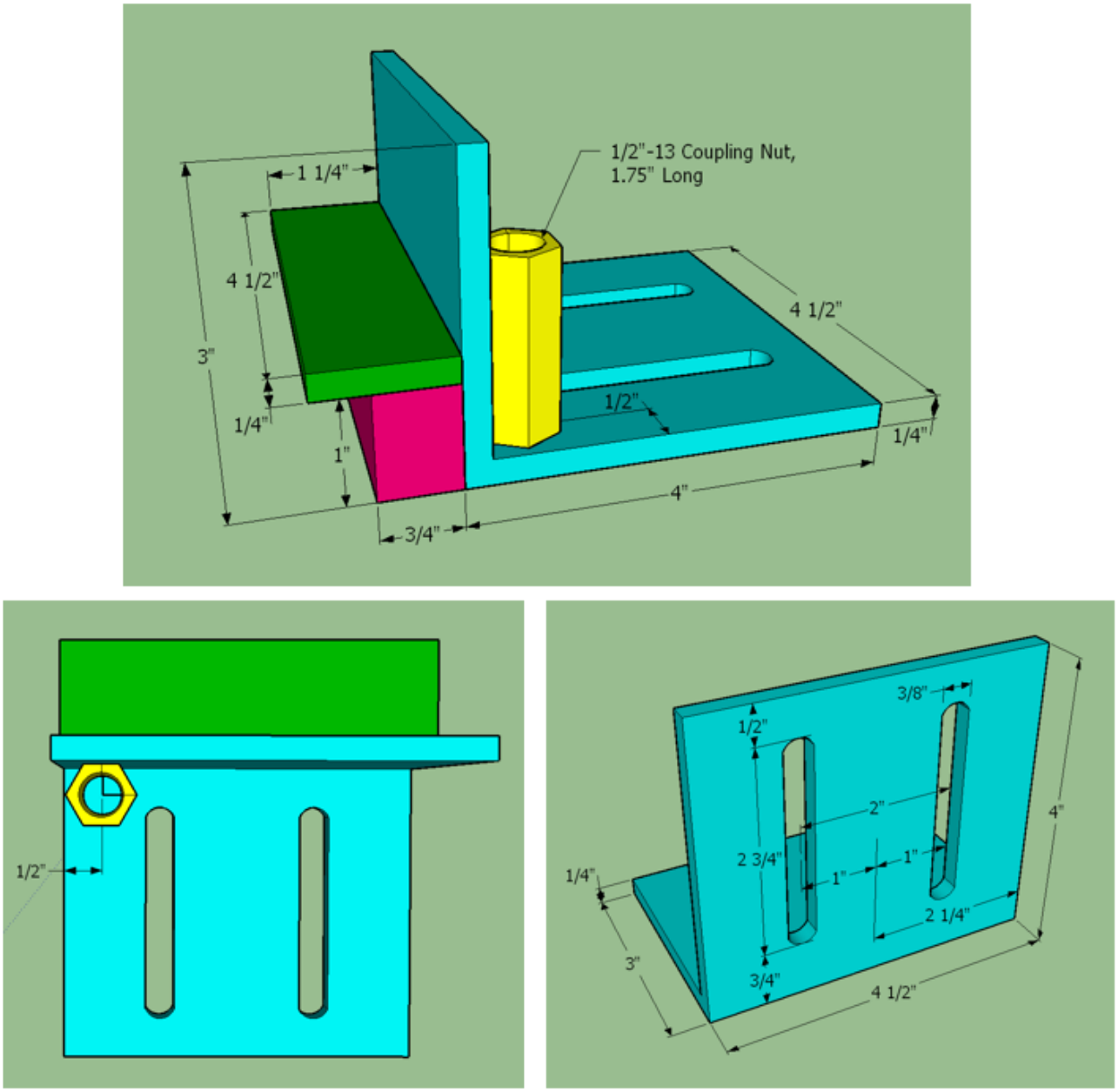

Figure D13. Flanges (F1& F4)- Sample Holder of Rectangular Specimens.

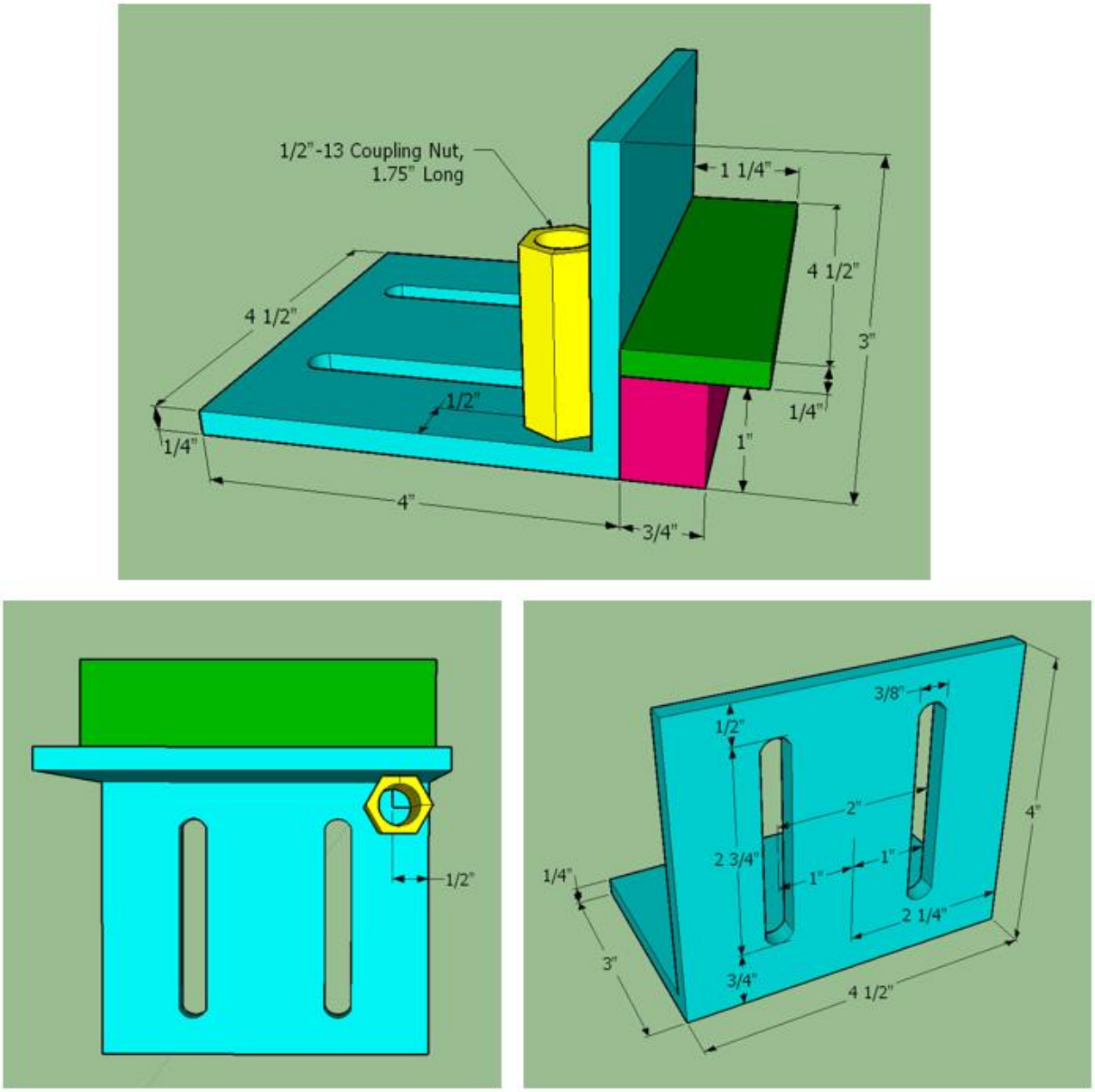

Figure D14. Flanges (F2& F3)- Sample Holder of Rectangular Specimens.

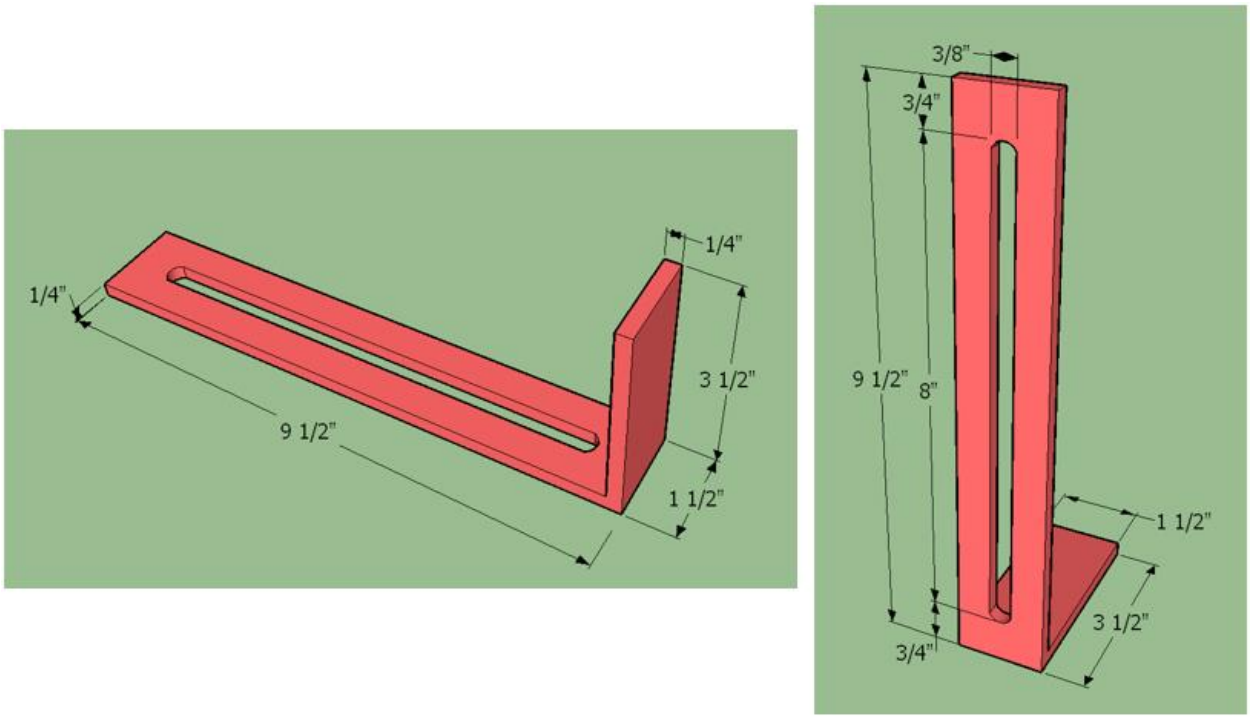

Figure D15. Gripper (L1)- Sample Holder of Rectangular Specimens.

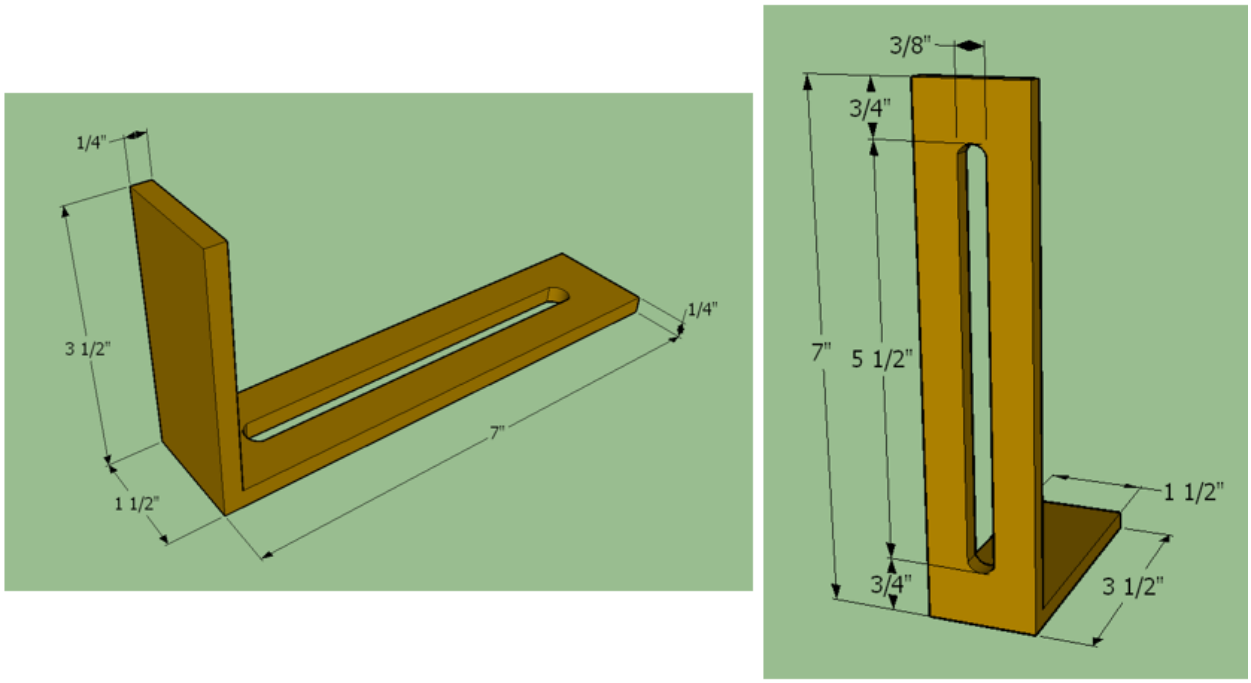

Figure D16. Gripper (L2)- Sample Holder of Rectangular Specimens.

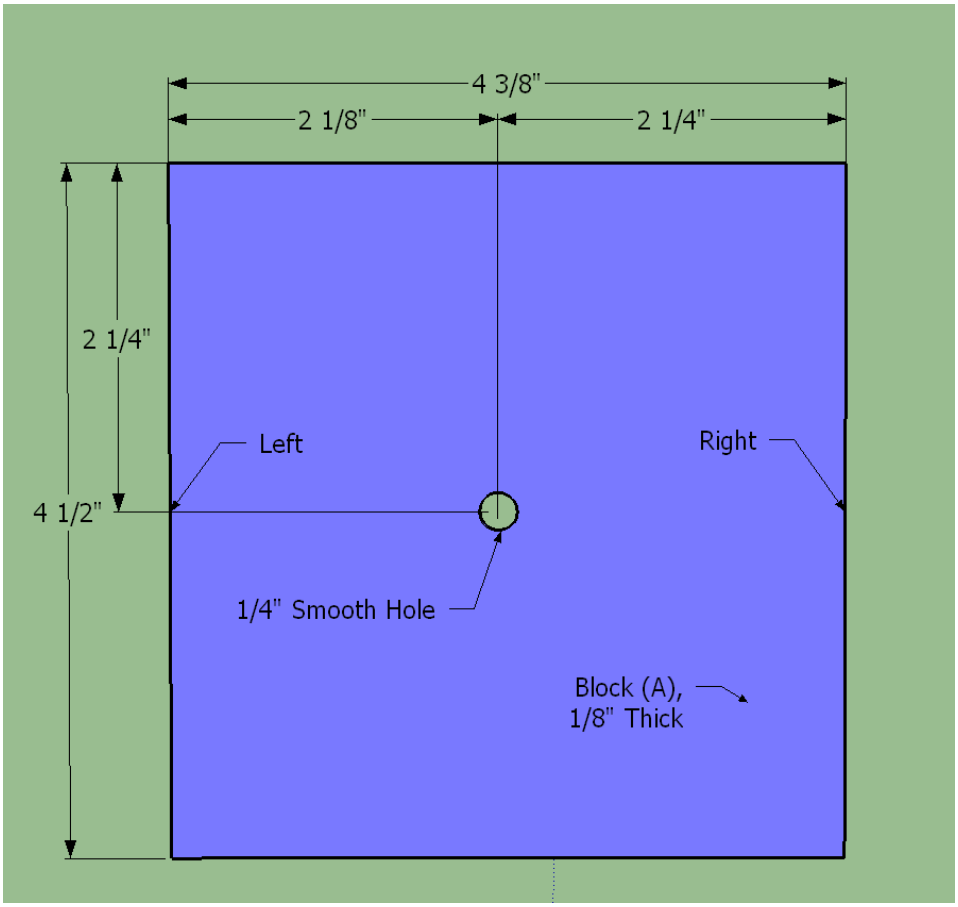

Figure D17. Block (A)- Sample Holder of Rectangular Specimens.

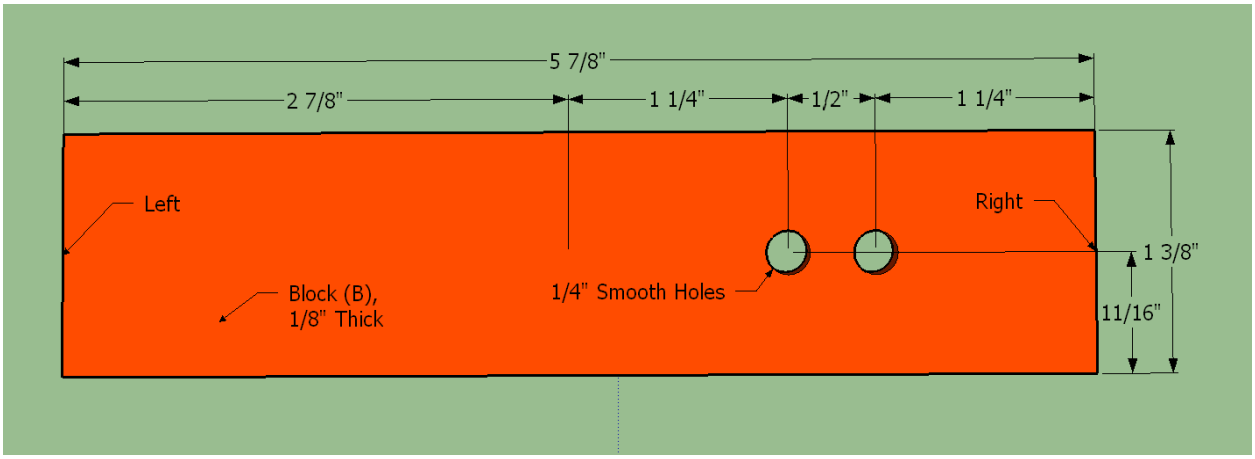

Figure D18. Block (B)- Sample Holder of Rectangular Specimens.

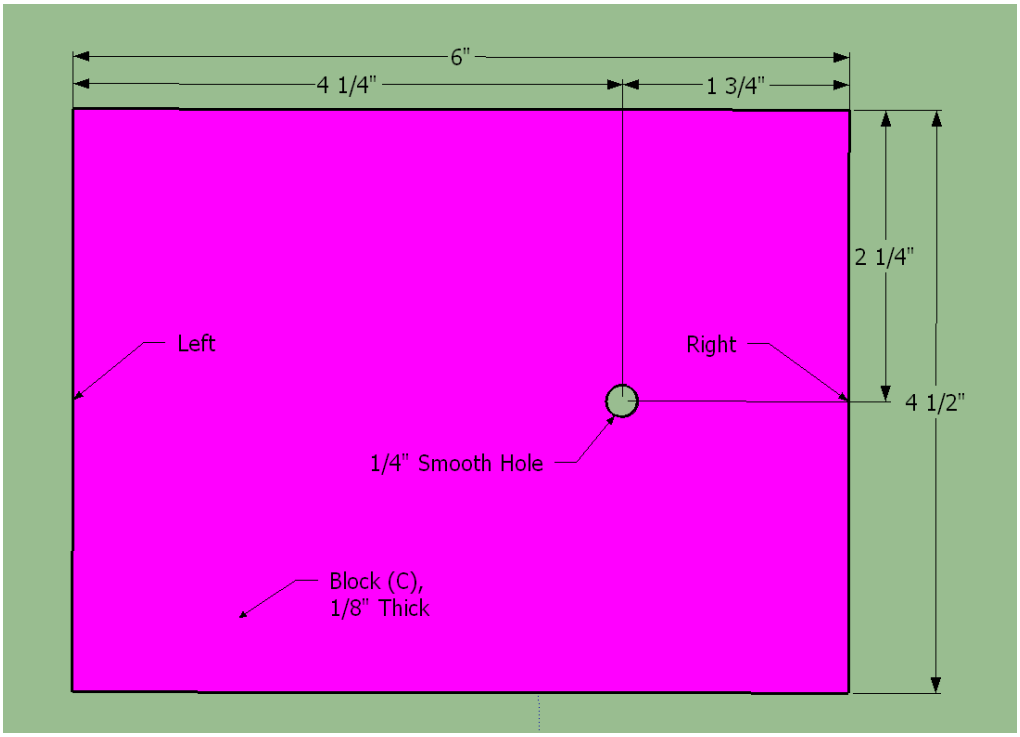

Figure D19. Block (C)- Sample Holder of Rectangular Specimens.

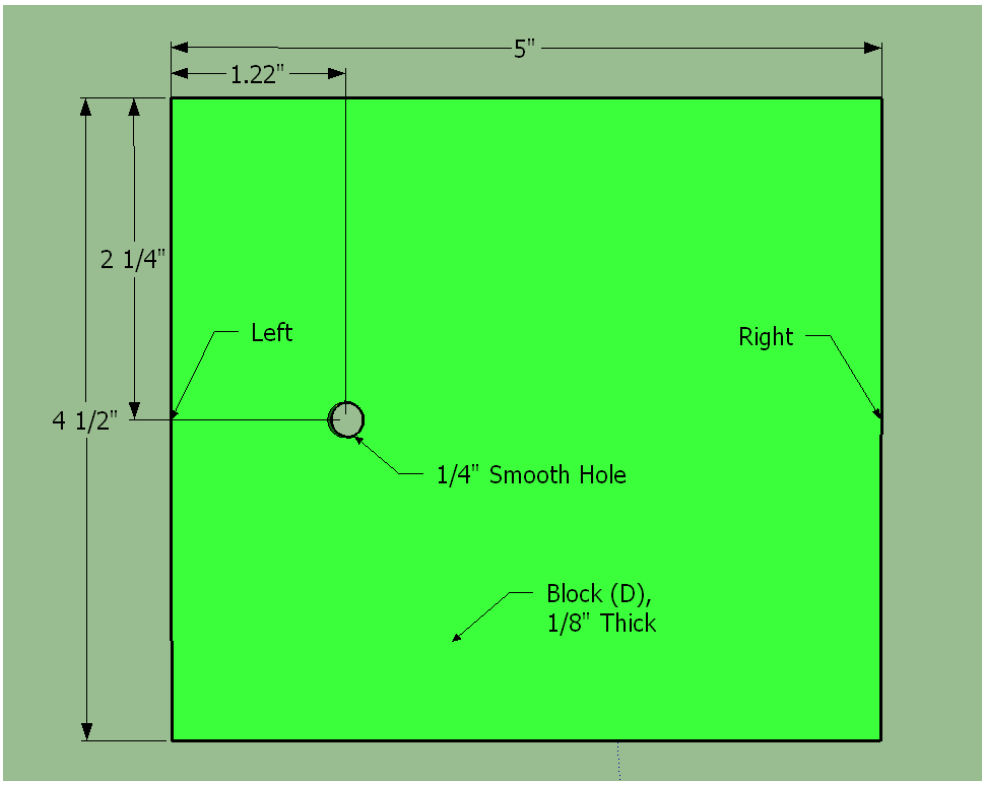

Figure D20. Block (D)- Sample Holder of Rectangular Specimens.

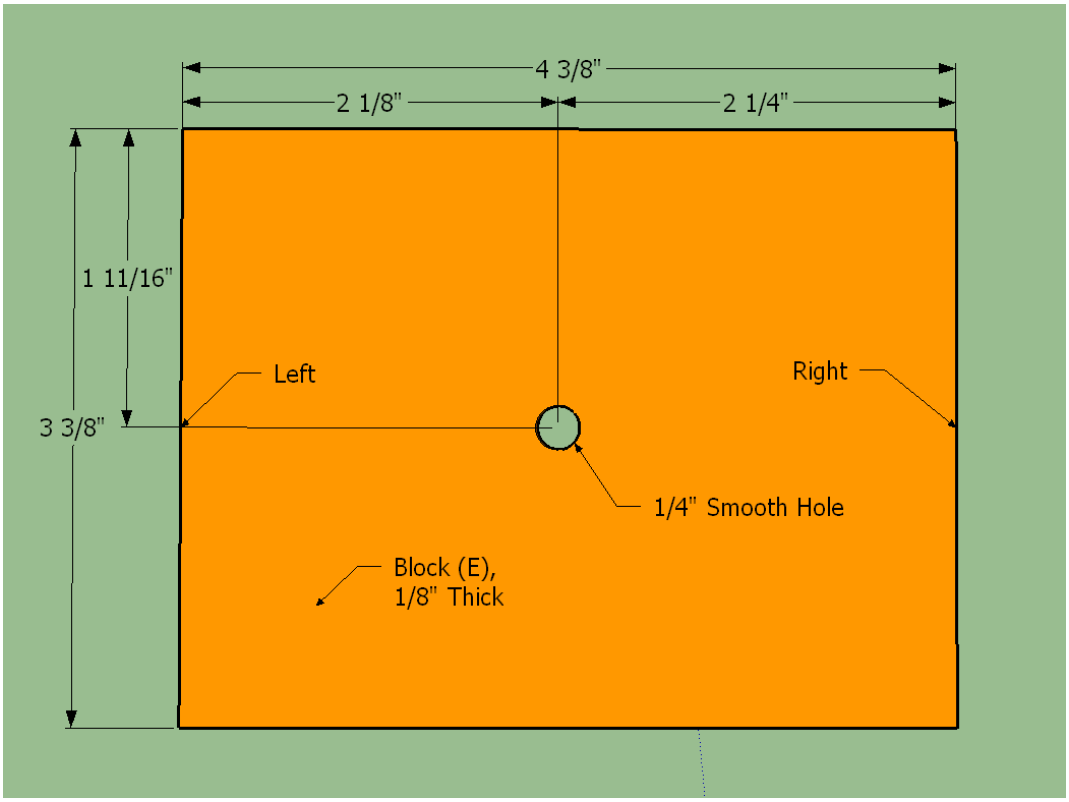

Figure D21. Block (E)- Sample Holder of Rectangular Specimens.

Appendix E: Mix Design Data

Table E1. Mix Design Data of (SP-Type D) Asphalt Concrete Mix

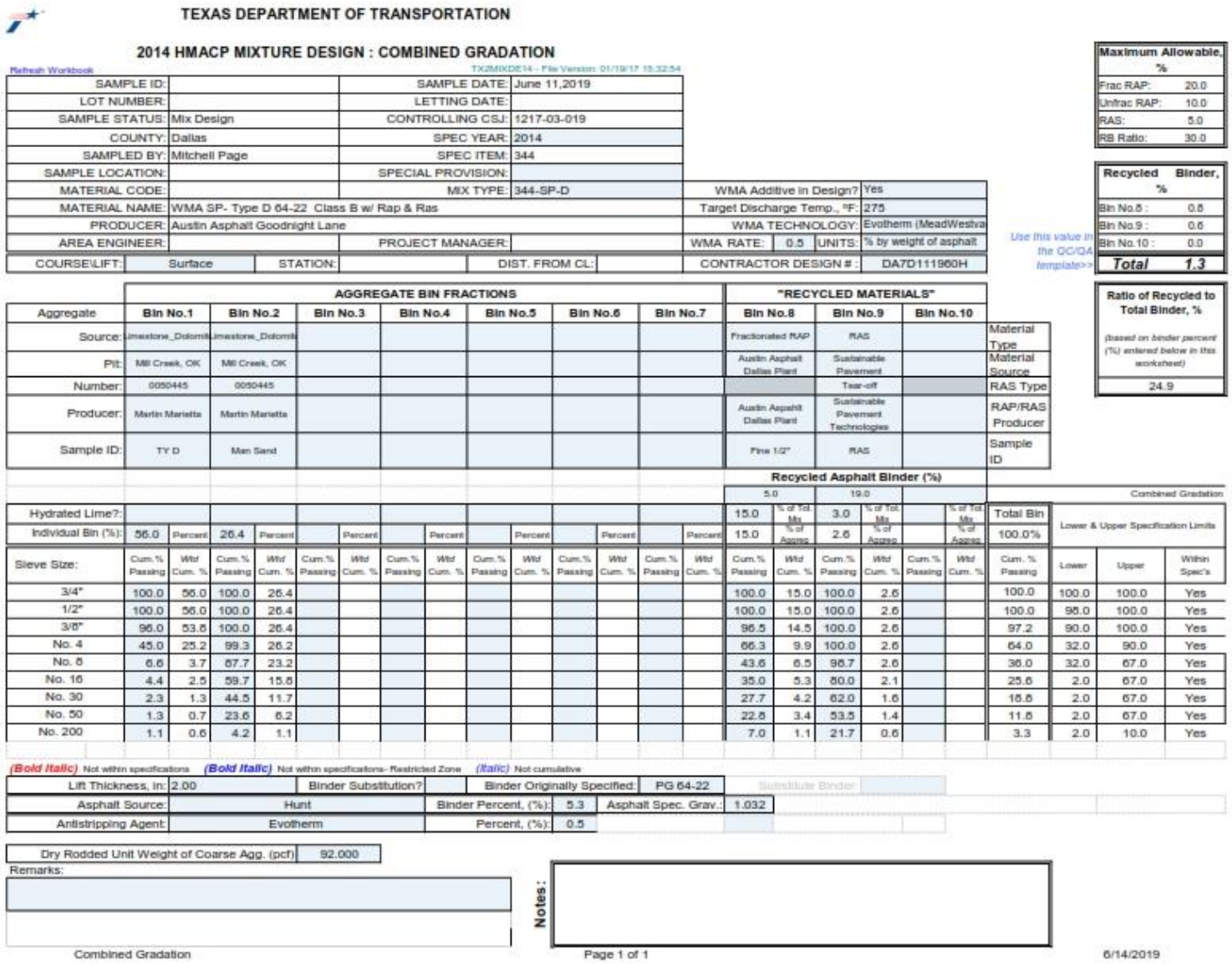

TEXAS DEPARTMENT OF TRANSPORTATION

2014 HMACP MIXTURE DESIGN : COMBINED GRADATION

Refresh Workbook — TXDMIXDES14 - File Version: 01/19/17 15:32:54

SAMPLE ID:		SAMPLE DATE:	June 11,2019
LOT NUMBER:		LETTING DATE:	
SAMPLE STATUS:	Mix Design	CONTROLLING CSJ:	1217-03-019
COUNTY:	Dallas	SPEC YEAR:	2014
SAMPLED BY:	Mitchell Page	SPEC ITEM:	344
SAMPLE LOCATION:		SPECIAL PROVISION:	
MATERIAL CODE:		MIX TYPE:	344-SP-D
MATERIAL NAME:	WMA SP- Type D 64-22 Class B w/ Rap & Ras		
PRODUCER:	Austin Asphalt Goodnight Lane		
AREA ENGINEER:		PROJECT MANAGER:	
COURSE\LIFT:	Surface	STATION:	DIST. FROM CL:

WMA Additive in Design?	Yes		
Target Discharge Temp., °F:	275		
WMA TECHNOLOGY:	Evotherm (MeadWestva		
WMA RATE:	0.5	UNITS:	% by weight of asphalt
CONTRACTOR DESIGN # :	DA7D111960H		

Use this value in the QC/QA template>>

Maximum Allowable, %	
Frac RAP:	20.0
Unfrac RAP:	10.0
RAS:	5.0
RB Ratio:	30.0

Recycled Binder, %	
Bin No.8 :	0.8
Bin No.9 :	0.6
Bin No.10 :	0.0
Total	*1.3*

Ratio of Recycled to Total Binder, %
(based on binder percent (%) entered below in this worksheet)
24.9

	AGGREGATE BIN FRACTIONS							"RECYCLED MATERIALS"			
Aggregate	Bin No.1	Bin No.2	Bin No.3	Bin No.4	Bin No.5	Bin No.6	Bin No.7	Bin No.8	Bin No.9	Bin No.10	
Source:	Limestone_Dolomit	Limestone_Dolomit						Fractionated RAP	RAS		Material Type
Pit:	Mill Creek, OK	Mill Creek, OK						Austin Asphalt Dallas Plant	Sustainable Pavement		Material Source
Number:	0050445	0050445							Tear-off		RAS Type
Producer:	Martin Marietta	Martin Marietta						Austin Asphalt Dallas Plant	Sustainable Pavement Technologies		RAP/RAS Producer
Sample ID:	TY D	Man Sand						Fine 1/2"	RAS		Sample ID

															Recycled Asphalt Binder (%)							Combined Gradation		
															5.0		19.0							
Hydrated Lime?:															15.0	% of Tot Mix	3.0	% of Tot Mix		% of Tot Mix	Total Bin	Lower & Upper Specification Limits		
Individual Bin (%):	56.0	Percent	26.4	Percent		Percent		Percent		Percent		Percent		Percent	15.0	% of Aggres	2.6	% of Aggres		% of Aggres	100.0%			
Sieve Size:	Cum.% Passing	Wtd Cum. %	Cum.% Passing	Wtd Cum. %	Cum.% Passing	Wtd Cum. %	Cum.% Passing	Wtd Cum. %	Cum.% Passing	Wtd Cum. %	Cum.% Passing	Wtd Cum. %	Cum.% Passing	Wtd Cum. %	Cum.% Passing	Wtd Cum. %	Cum.% Passing	Wtd Cum. %	Cum.% Passing	Wtd Cum. %	Cum. % Passing	Lower	Upper	Within Spec's
3/4"	100.0	56.0	100.0	26.4											100.0	15.0	100.0	2.6			100.0	100.0	100.0	Yes
1/2"	100.0	56.0	100.0	26.4											100.0	15.0	100.0	2.6			100.0	95.0	100.0	Yes
3/8"	96.0	53.8	100.0	26.4											96.5	14.5	100.0	2.6			97.2	90.0	100.0	Yes
No. 4	45.0	25.2	99.3	26.2											66.3	9.9	100.0	2.6			64.0	32.0	90.0	Yes
No. 8	6.6	3.7	87.7	23.2											43.6	6.5	98.7	2.6			36.0	32.0	67.0	Yes
No. 16	4.4	2.5	59.7	15.8											35.0	5.3	80.0	2.1			25.6	2.0	67.0	Yes
No. 30	2.3	1.3	44.5	11.7											27.7	4.2	62.0	1.6			18.8	2.0	67.0	Yes
No. 50	1.3	0.7	23.6	6.2											22.8	3.4	53.5	1.4			11.8	2.0	67.0	Yes
No. 200	1.1	0.6	4.2	1.1											7.0	1.1	21.7	0.6			3.3	2.0	10.0	Yes

(Bold Italic) Not within specifications *(Bold Italic)* Not within specifications- Restricted Zone *(Italic)* Not cumulative

Lift Thickness, in:	2.00	Binder Substitution?		Binder Originally Specified:	PG 64-22
Asphalt Source:	Hunt	Binder Percent, (%):	5.3	Asphalt Spec. Grav.:	1.032
Antistripping Agent:	Evotherm	Percent, (%):	0.5		

Dry Rodded Unit Weight of Coarse Agg. (pcf)	92.000

Remarks:

Notes:

Combined Gradation

Page 1 of 1

6/14/2019

Table E2. Mix Design Data of (SP-Type C) Asphalt Concrete Mix

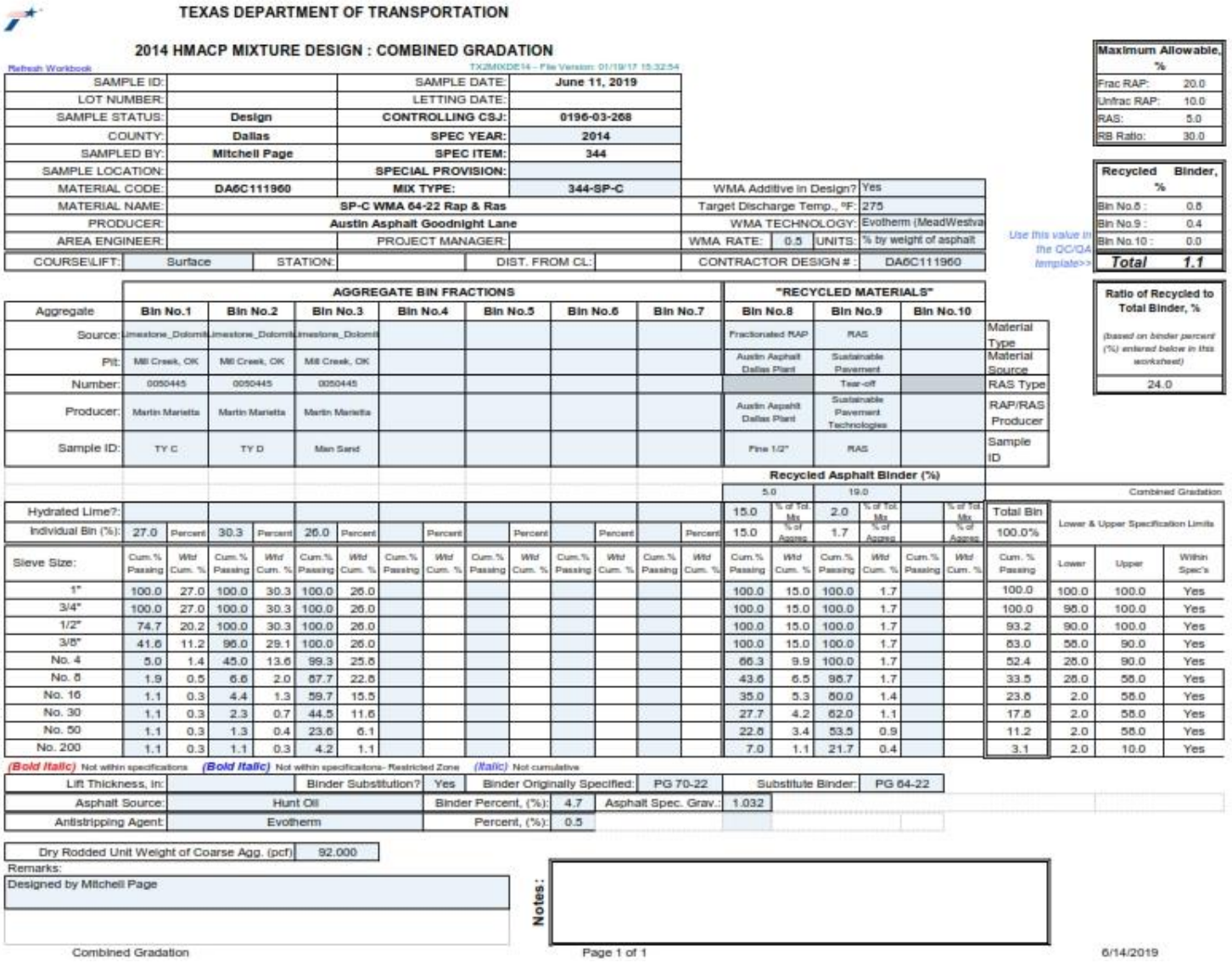

TEXAS DEPARTMENT OF TRANSPORTATION

2014 HMACP MIXTURE DESIGN : COMBINED GRADATION

Refresh Workbook — TX2MIXDE14 – File Version: 01/19/17 15:32:54

SAMPLE ID:		SAMPLE DATE:	June 11, 2019
LOT NUMBER:		LETTING DATE:	
SAMPLE STATUS:	Design	CONTROLLING CSJ:	0196-03-268
COUNTY:	Dallas	SPEC YEAR:	2014
SAMPLED BY:	Mitchell Page	SPEC ITEM:	344
SAMPLE LOCATION:		SPECIAL PROVISION:	
MATERIAL CODE:	DA6C111960	MIX TYPE:	344-SP-C
MATERIAL NAME:	SP-C WMA 64-22 Rap & Ras		
PRODUCER:	Austin Asphalt Goodnight Lane		
AREA ENGINEER:		PROJECT MANAGER:	
COURSE\LIFT:	Surface	STATION:	
DIST. FROM CL:			

WMA Additive in Design?	Yes
Target Discharge Temp., °F:	275
WMA TECHNOLOGY:	Evotherm (MeadWestva
WMA RATE: 0.5	UNITS: % by weight of asphalt
CONTRACTOR DESIGN # :	DA6C111960

Use this value in the QC/QA template>>

Maximum Allowable, %	
Frac RAP:	20.0
Unfrac RAP:	10.0
RAS:	5.0
RB Ratio:	30.0

Recycled Binder, %	
Bin No.8 :	0.8
Bin No.9 :	0.4
Bin No.10 :	0.0
Total	*1.1*

Ratio of Recycled to Total Binder, %
(based on binder percent (%) entered below in this worksheet)
24.0

	AGGREGATE BIN FRACTIONS							"RECYCLED MATERIALS"			
Aggregate	Bin No.1	Bin No.2	Bin No.3	Bin No.4	Bin No.5	Bin No.6	Bin No.7	Bin No.8	Bin No.9	Bin No.10	
Source:	Limestone_Dolomit	Limestone_Dolomit	Limestone_Dolomit					Fractionated RAP	RAS		Material Type
Pit:	Mill Creek, OK	Mill Creek, OK	Mill Creek, OK					Austin Asphalt Dallas Plant	Sustainable Pavement		Material Source
Number:	0050445	0050445	0050445						Tear-off		RAS Type
Producer:	Martin Marietta	Martin Marietta	Martin Marietta					Austin Asphalt Dallas Plant	Sustainable Pavement Technologies		RAP/RAS Producer
Sample ID:	TY C	TY D	Man Sand					Fine 1/2"	RAS		Sample ID

															Recycled Asphalt Binder (%)						Combined Gradation			
															5.0		19.0					Lower & Upper Specification Limits		
Hydrated Lime?:															15.0	% of Tot. Mix	2.0	% of Tot. Mix		% of Tot. Mix	Total Blin			
Individual Bin (%):	27.0	Percent	30.3	Percent	26.0	Percent		Percent		Percent		Percent		Percent	15.0	% of Aggrea	1.7	% of Aggrea		% of Aggrea	100.0%			
Sieve Size:	Cum.% Passing	Wtd Cum. %	Cum.% Passing	Wtd Cum. %	Cum.% Passing	Wtd Cum. %	Cum.% Passing	Wtd Cum. %	Cum.% Passing	Wtd Cum. %	Cum.% Passing	Wtd Cum. %	Cum.% Passing	Wtd Cum. %	Cum.% Passing	Wtd Cum. %	Cum.% Passing	Wtd Cum. %	Cum.% Passing	Wtd Cum. %	Cum. % Passing	Lower	Upper	Within Spec's
1"	100.0	27.0	100.0	30.3	100.0	26.0									100.0	15.0	100.0	1.7			100.0	100.0	100.0	Yes
3/4"	100.0	27.0	100.0	30.3	100.0	26.0									100.0	15.0	100.0	1.7			100.0	95.0	100.0	Yes
1/2"	74.7	20.2	100.0	30.3	100.0	26.0									100.0	15.0	100.0	1.7			93.2	90.0	100.0	Yes
3/8"	41.6	11.2	96.0	29.1	100.0	26.0									100.0	15.0	100.0	1.7			83.0	55.0	90.0	Yes
No. 4	5.0	1.4	45.0	13.6	99.3	25.8									66.3	9.9	100.0	1.7			52.4	25.0	90.0	Yes
No. 8	1.9	0.5	6.6	2.0	87.7	22.8									43.6	6.5	95.7	1.7			33.5	25.0	55.0	Yes
No. 16	1.1	0.3	4.4	1.3	59.7	15.5									35.0	5.3	80.0	1.4			23.6	2.0	55.0	Yes
No. 30	1.1	0.3	2.3	0.7	44.5	11.6									27.7	4.2	62.0	1.1			17.6	2.0	55.0	Yes
No. 50	1.1	0.3	1.3	0.4	23.6	6.1									22.6	3.4	53.5	0.9			11.2	2.0	55.0	Yes
No. 200	1.1	0.3	1.1	0.3	4.2	1.1									7.0	1.1	21.7	0.4			3.1	2.0	10.0	Yes

(Bold Italic) Not within specifications *(Bold Italic)* Not within specifications- Restricted Zone *(Italic)* Not cumulative

Lift Thickness, in:		Binder Substitution?	Yes	Binder Originally Specified:	PG 70-22	Substitute Binder: PG 64-22
Asphalt Source:	Hunt Oil	Binder Percent, (%):	4.7	Asphalt Spec. Grav.:	1.032	
Antistripping Agent:	Evotherm	Percent, (%):	0.5			

Dry Rodded Unit Weight of Coarse Agg. (pcf)	92.000

Remarks:

Designed by Mitchell Page

Notes:

Combined Gradation

Page 1 of 1

6/14/2019

Table E3. Mix Design Data of (DG-Type B) Asphalt Concrete Mix

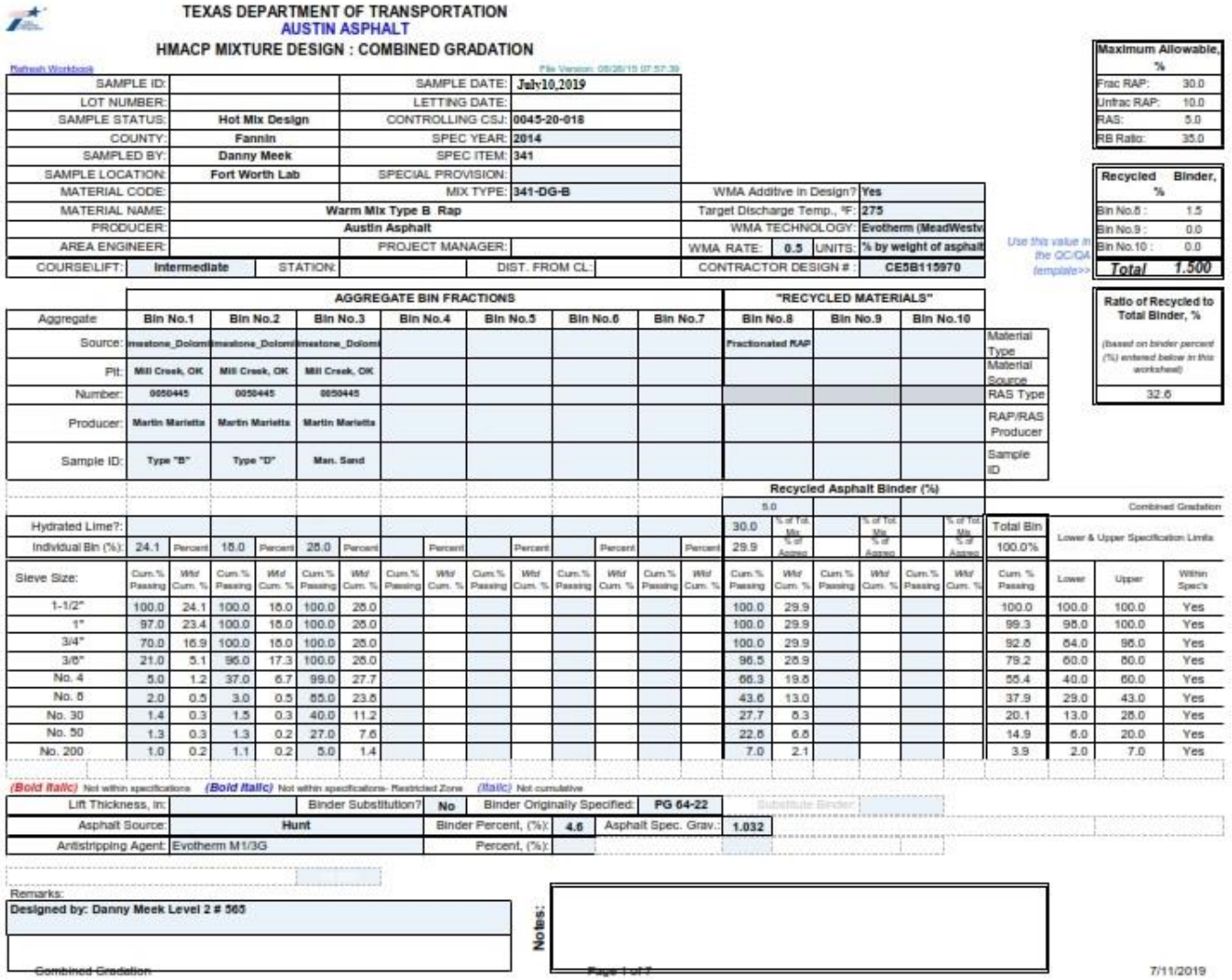

TEXAS DEPARTMENT OF TRANSPORTATION
AUSTIN ASPHALT
HMACP MIXTURE DESIGN : COMBINED GRADATION

Refresh Workbook — File Version: 08/26/15 07:57:39

SAMPLE ID:		SAMPLE DATE:	July10,2019
LOT NUMBER:		LETTING DATE:	
SAMPLE STATUS:	Hot Mix Design	CONTROLLING CSJ:	0045-20-018
COUNTY:	Fannin	SPEC YEAR:	2014
SAMPLED BY:	Danny Meek	SPEC ITEM:	341
SAMPLE LOCATION:	Fort Worth Lab	SPECIAL PROVISION:	
MATERIAL CODE:		MIX TYPE:	341-DG-B
MATERIAL NAME:	Warm Mix Type B Rap		
PRODUCER:	Austin Asphalt		
AREA ENGINEER:		PROJECT MANAGER:	
COURSE\LIFT:	Intermediate	STATION:	DIST. FROM CL:

WMA Additive in Design?	Yes		
Target Discharge Temp., °F:	275		
WMA TECHNOLOGY:	Evotherm (MeadWestv		
WMA RATE:	0.5	UNITS:	% by weight of asphalt
CONTRACTOR DESIGN # :	CE5B115970		

Use this value in the QC/QA template>>

Maximum Allowable, %	
Frac RAP:	30.0
Unfrac RAP:	10.0
RAS:	5.0
RB Ratio:	35.0

Recycled Binder, %	
Bin No.8 :	1.5
Bin No.9 :	0.0
Bin No.10 :	0.0
Total	*1.500*

Ratio of Recycled to Total Binder, %
(based on binder percent (%) entered below in this worksheet)
32.6

	AGGREGATE BIN FRACTIONS							"RECYCLED MATERIALS"			
Aggregate	Bin No.1	Bin No.2	Bin No.3	Bin No.4	Bin No.5	Bin No.6	Bin No.7	Bin No.8	Bin No.9	Bin No.10	
Source:	Limestone_Dolomi	Limestone_Dolomi	Limestone_Dolomi					Fractionated RAP			Material Type
Plt:	Mill Creek, OK	Mill Creek, OK	Mill Creek, OK								Material Source
Number:	0050445	0050445	0050445								RAS Type
Producer:	Martin Marietta	Martin Marietta	Martin Marietta								RAP/RAS Producer
Sample ID:	Type "B"	Type "D"	Man. Sand								Sample ID
								Recycled Asphalt Binder (%)			
								5.0			
Hydrated Lime?:								30.0	% of Tot. Mix		% of Tot. Mix		% of Tot. Mix	Total Bin	Combined Gradation
Individual Bin (%):	24.1	Percent	16.0	Percent	26.0	Percent		Percent		Percent		Percent		Percent	29.9	% of Aggreg		% of Aggreg		% of Aggreg	100.0%	Lower & Upper Specification Limits		

Sieve Size:	Cum.% Passing	Wtd Cum. %	Cum.% Passing	Wtd Cum. %	Cum.% Passing	Wtd Cum. %	Cum.% Passing	Wtd Cum. %	Cum.% Passing	Wtd Cum. %	Cum.% Passing	Wtd Cum. %	Cum.% Passing	Wtd Cum. %	Cum.% Passing	Wtd Cum. %	Cum.% Passing	Wtd Cum. %	Cum.% Passing	Wtd Cum. %	Cum.% Passing	Wtd Cum. %	Cum. % Passing	Lower	Upper	Within Spec's
1-1/2"	100.0	24.1	100.0	16.0	100.0	26.0									100.0	29.9							100.0	100.0	100.0	Yes
1"	97.0	23.4	100.0	16.0	100.0	26.0									100.0	29.9							99.3	95.0	100.0	Yes
3/4"	70.0	16.9	100.0	16.0	100.0	26.0									100.0	29.9							92.8	64.0	96.0	Yes
3/8"	21.0	5.1	96.0	17.3	100.0	26.0									96.5	28.9							79.2	60.0	80.0	Yes
No. 4	5.0	1.2	37.0	6.7	99.0	27.7									66.3	19.8							55.4	40.0	60.0	Yes
No. 8	2.0	0.5	3.0	0.5	85.0	23.8									43.6	13.0							37.9	29.0	43.0	Yes
No. 30	1.4	0.3	1.5	0.3	40.0	11.2									27.7	8.3							20.1	13.0	28.0	Yes
No. 50	1.3	0.3	1.3	0.2	27.0	7.6									22.6	6.8							14.9	8.0	20.0	Yes
No. 200	1.0	0.2	1.1	0.2	5.0	1.4									7.0	2.1							3.9	2.0	7.0	Yes

(Bold Italic) Not within specifications *(Bold Italic)* Not within specifications- Restricted Zone *(Italic)* Not cumulative

Lift Thickness, in:		Binder Substitution?	No	Binder Originally Specified:	PG 64-22
Asphalt Source:	Hunt	Binder Percent, (%):	4.6	Asphalt Spec. Grav.:	1.032
Antistripping Agent:	Evotherm M1/3G	Percent, (%):			

Remarks:
Designed by: Danny Meek Level 2 # 565

Combined Gradation

Notes:

Page 1 of 2

7/11/2019

Appendix F: Asphalt Concrete Gyratory Samples & Volumetric Measurements

Table F1. Superpave Gyratory Samples of Asphalt Mix D

Sample	Interval	Weight (g)	Target height (mm)	Device- Shapes
D01	Morning	6552	156.21	DST- C6
D02	Morning	6515	155.33	
D03	Morning	6531	155.71	
D04	Morning	6560	156.40	
D05	Morning	6533	155.76	
D06	Morning	6531	155.71	
D07	Morning	6532	155.73	
D08	Morning	6531	155.71	
D09	Noon	6516	155.35	DST-RH
D10	Noon	6528	155.64	
D11	Noon	6522	155.49	
D12	Noon	6533	155.76	
D13	Noon	6535	155.80	
D14	Noon	6530	155.68	
D15	Noon	6525	155.56	
D16	Noon	6540	155.92	
D17	Noon	6590	157.11	DST-C6
D18	Noon	6602	157.40	
D19	Noon	6610	157.59	
D20	Noon	6620	157.83	
D21	Noon	6603	157.42	
D22	Noon	6610	157.59	
D23	Noon	6625	157.95	
D24	Noon	6655	158.66	
D25	Noon	6632	158.12	DST-RV
D26	Noon	6611	157.62	
D27	Noon	6630	158.07	
D28	Noon	6630	158.07	
D29	Noon	6615	157.71	
D30	Noon	6610	157.59	
D31	Noon	6625	157.95	
D32	Noon	6623	157.90	

Table F1. Superpave Gyratory Samples of Asphalt Mix D (Cont.)

Sample	Interval	Weight (g)	Target height (mm)	Device- Shapes
D33	Noon	6620	157.83	DST-C4
D34	Noon	6640	158.31	
D35	Noon	6630	158.07	
D36	Noon	6655	158.66	
D37	Noon	6625	157.95	
D38	Noon	6626	157.97	
D39	Noon	6635	158.19	
D40	Noon	6620	157.83	
D49	Afternoon	6631	158.09	DST-C4
D50	Afternoon	6633	158.14	
D51	Afternoon	6630	158.07	
D52	Afternoon	6626	157.97	
D53	Afternoon	6640	158.31	
D54	Afternoon	6635	158.19	
D55	Afternoon	6630	158.07	
D56	Afternoon	6637	158.24	
D57	Noon	6630	158.07	STNS-C6
D58	Noon	6622	157.88	
D59	Noon	6623	157.90	
D60	Noon	6622	157.88	
D61	Morning	6500	154.97	STNS-C6
D62	Morning	6520	155.45	
D63	Morning	6525	155.56	
D64	Morning	6517	155.37	
D65	Afternoon	6513	155.28	STNS-C6
D66	Afternoon	6530	155.68	
D67	Afternoon	6511	155.23	
D68	Afternoon	6521	155.47	

Table F2. Superpave Gyratory Samples Asphalt Mix C

Sample	Interval	Weight (g)	Target height (mm)	Device- Shapes
C01	Noon	6560	155.14	DST-C6
C02	Noon	6560	155.14	
C03	Noon	6565	155.25	
C04	Noon	6575	155.49	
C05	Noon	6570	155.37	
C06	Noon	6560	155.14	
C07	Noon	6574	155.47	
C08	Noon	6555	155.02	
C09	Morning	6560	155.14	DST-C6
C10	Morning	6570	155.37	
C11	Morning	6565	155.25	
C12	Morning	6573	155.44	
C13	Morning	6567	155.30	
C14	Morning	6581	155.63	
C15	Morning	6578	155.56	
C16	Morning	6564	155.23	
C17	Noon	6555	155.02	DST-RH
C18	Noon	6565	155.25	
C19	Noon	6567	155.30	
C20	Noon	6559	155.11	
C21	Noon	6572	155.42	
C22	Noon	6576	155.52	
C23	Noon	6561	155.16	
C24	Noon	6558	155.09	
C25	Noon	6560	155.14	DST-C6
C26	Noon	6557	155.07	
C27	Noon	6573	155.44	
C28	Noon	6578	155.56	
C29	Noon	6572	155.42	
C30	Noon	6566	155.28	
C31	Noon	6568	155.33	
C32	Noon	6560	155.14	

Table F2. Superpave Gyratory Samples of Asphalt Mix C (Cont.)

Sample	Interval	Weight (g)	Target height (mm)	Device- Shapes
C33	Noon	6561	155.16	DST-RV
C34	Noon	6564	155.23	
C35	Noon	6573	155.44	
C36	Noon	6555	155.02	
C37	Noon	6559	155.11	
C38	Noon	6562	155.18	
C39	Noon	6561	155.16	
C40	Noon	6572	155.42	
C41	Afternoon	6555	155.02	DST-C6
C42	Afternoon	6556	155.04	
C43	Afternoon	6558	155.09	
C44	Afternoon	6555	155.02	
C45	Afternoon	6556	155.04	
C46	Afternoon	6560	155.14	
C47	Afternoon	6555	155.02	
C48	Afternoon	6558	155.09	
C49	Afternoon	6555	155.02	STNS-C6
C50	Afternoon	6557	155.07	
C51	Afternoon	6556	155.04	
C52	Afternoon	6557	155.07	
C53	Morning	6555	155.02	STNS-C6
C54	Morning	6557	155.07	
C55	Morning	6559	155.11	
C56	Morning	6557	155.07	
C57	Noon	6558	155.09	STNS-C6
C58	Noon	6555	155.02	
C59	Noon	6562	155.18	
C60	Noon	6558	155.09	

Table F3. Superpave Gyratory Samples Asphalt Mix B

Sample	Interval	Weight (g)	Target height (mm)	Device- Shapes
B01	Noon	6450	152.83	DST-C6
B02	Noon	6400	151.64	
B03	Noon	6460	153.07	
B04	Noon	6430	152.36	
B05	Noon	6440	152.59	
B06	Noon	6443	152.66	
B07	Noon	6476	153.45	
B08	Noon	6476	153.45	
B09	Morning	6540	154.96	DST-C6
B10	Morning	6550	155.20	
B11	Morning	6548	155.15	
B12	Morning	6553	155.27	
B13	Morning	6549	155.17	
B14	Morning	6560	155.44	
B15	Morning	6545	155.08	
B16	Morning	6547	155.13	
B17	Noon	6540	154.96	DST-RH
B18	Noon	6544	155.06	
B19	Noon	6550	155.20	
B20	Noon	6543	155.03	
B21	Noon	6548	155.15	
B22	Noon	6550	155.20	
B23	Noon	6551	155.22	
B24	Noon	6540	154.96	
B25	Noon	6542	155.01	DST-C6
B26	Noon	6547	155.13	
B27	Noon	6553	155.27	
B28	Noon	6560	155.44	
B29	Noon	6558	155.39	
B30	Noon	6543	155.03	
B31	Noon	6540	154.96	
B32	Noon	6550	155.20	

Table F3. Superpave Gyratory Samples Asphalt Mix B (Cont.)

Sample	Interval	Weight (g)	Target height (mm)	Device- Shapes
B33	Noon	6547	155.13	DST-RV
B34	Noon	6555	155.32	
B35	Noon	6547	155.13	
B36	Noon	6553	155.27	
B37	Noon	6547	155.13	
B38	Noon	6553	155.27	
B39	Noon	6560	155.44	
B40	Noon	6558	155.39	
B41	Afternoon	6540	154.96	STNS-C6
B42	Afternoon	6548	155.15	
B43	Afternoon	6554	155.29	
B44	Afternoon	6565	155.55	
B45	Afternoon	6558	155.39	DST-C6
B46	Afternoon	6543	155.03	
B47	Afternoon	6560	155.44	
B48	Afternoon	6558	155.39	
B49	Afternoon	6540	154.96	
B50	Afternoon	6560	155.44	
B51	Afternoon	6558	155.39	
B52	Afternoon	6545	155.08	
B53	Noon	6548	155.15	STNS-C6
B54	Noon	6553	155.27	
B55	Noon	6560	155.44	
B56	Noon	6558	155.39	
B57	Morning	6553	155.27	STNS-C6
B58	Morning	6561	155.46	
B59	Morning	6550	155.20	
B60	Morning	6543	155.03	

Table F4. Volumetric Measurements of C6 Specimens- Asphalt Mix D

Sample	Spec.	Height Measurements (mm)						Weight (g)	Air Void (%)		
		H1	H2	H3	H4	Avg.	Diff.		Content	Avg.	Diff.
D01	S1	49.67	49.87	50.21	50.05	**49.95**	0.80	2128.8	6.52	**6.38**	0.27
	S2	49.00	49.15	49.34	49.11	**49.15**		2100.8	6.25		
D02	S1	49.00	49.81	50.05	49.97	**49.71**	0.34	2110.2	6.88	**6.89**	0.01
	S2	50.07	49.93	50.11	50.06	**50.04**		2124.1	6.90		
D03	S1	50.03	50.91	49.73	49.00	**49.92**	0.24	2135.1	6.18	**6.17**	0.03
	S2	51.00	50.08	49.98	49.55	**50.15**		2145.9	6.15		
D04	S1	49.45	49.52	50.05	50.20	**49.81**	0.12	2114.1	6.90	**6.87**	0.04
	S2	49.00	50.32	50.45	49.93	**49.93**		2120.2	6.85		
D05	S1	50.50	49.83	50.15	50.04	**50.13**	0.18	2126.3	6.97	**6.94**	0.05
	S2	49.76	50.08	50.31	49.64	**49.95**		2119.8	6.91		
D06	S1	50.17	50.21	50.05	50.00	**50.11**	0.10	2128.9	6.81	**6.73**	0.15
	S2	49.91	50.00	49.97	50.16	**50.01**		2128.2	6.66		
D07	S1	50.08	50.17	50.05	50.20	**50.13**	0.07	2135.9	6.54	**6.53**	0.02
	S2	50.10	50.15	50.06	49.91	**50.06**		2133.4	6.51		
D08	S1	51.10	50.07	50.06	51.00	**50.56**	0.30	2157.8	6.39	**6.63**	0.50
	S2	50.45	50.34	50.20	50.04	**50.26**		2133.6	6.88		
D17	S1	50.04	50.09	50.00	49.96	**50.02**	0.24	2126.6	6.75	**6.71**	0.08
	S2	49.70	49.82	49.63	49.97	**49.78**		2118	6.68		
D18	S1	50.35	50.33	50.74	50.81	**50.56**	0.86	2150.2	6.71	**6.82**	0.20
	S2	49.50	49.60	49.80	49.90	**49.70**		2109.1	6.92		
D19	S1	49.75	49.92	49.86	50.00	**49.88**	0.10	2118.2	6.86	**6.67**	0.38
	S2	49.90	50.07	50.05	49.91	**49.98**		2131.1	6.48		
D20	S1	49.96	49.84	50.09	50.06	**49.99**	0.13	2128.4	6.61	**6.71**	0.20
	S2	49.87	49.65	49.92	50.01	**49.86**		2118.5	6.81		
D21	S1	49.61	49.52	49.70	49.83	**49.67**	0.26	2112.8	6.69	**6.81**	0.24
	S2	49.89	49.72	50.05	50.02	**49.92**		2118.2	6.93		
D22	S1	50.02	49.95	49.91	49.88	**49.94**	0.06	2119.4	6.91	**6.86**	0.10
	S2	49.86	49.98	50.05	50.10	**50.00**		2124.1	6.82		
D23	S1	49.67	49.74	49.87	50.06	**49.84**	0.08	2113.7	6.97	**6.94**	0.05
	S2	49.75	49.97	49.98	49.95	**49.91**		2118.1	6.92		
D24	S1	49.82	49.88	49.56	49.95	**49.80**	0.19	2119.7	6.64	**6.81**	0.34
	S2	49.92	49.98	50.03	50.05	**50.00**		2120.2	6.98		
D49	S1	50.1	50.13	50.4	50.2	**50.21**	0.09	2148.5	6.14	**6.27**	0.26
	S2	50.34	50.37	50.28	50.21	**50.30**		2146.5	6.40		
D50	S1	50.39	50.32	50.37	50.28	**50.34**	0.20	2148.2	6.40	**6.29**	0.22
	S2	50.21	50.14	50.09	50.12	**50.14**		2144.7	6.18		

Table F4. Volumetric Measurements of C6 Specimens- Asphalt Mix D (Cont.)

Sample	Spec.	Height Measurements (mm)						Weight (g)	Air Void (%)		
		H1	H2	H3	H4	Avg.	Diff.		Content	Avg.	Diff.
D51	S1	50.23	50.47	50.08	50.36	**50.29**	0.06	2149.2	6.25	**6.38**	0.26
	S2	50.11	50.08	50.32	50.38	**50.22**		2140.5	6.52		
D52	S1	50.18	50.15	50.22	50.09	**50.16**	0.11	2141.4	6.36	**6.28**	0.17
	S2	50.23	50.32	50.4	50.15	**50.28**		2150.2	6.19		
D53	S1	50.33	50.42	50.13	50.25	**50.28**	0.07	2146.7	6.36	**6.29**	0.13
	S2	50.35	50.17	50.21	50.12	**50.21**		2146.8	6.22		
D54	S1	50.25	50.38	50.18	50.31	**50.28**	0.06	2145.5	6.41	**6.31**	0.20
	S2	50.29	50.12	50.27	50.18	**50.22**		2147.2	6.21		
D55	S1	50.21	50.16	50.19	50.17	**50.18**	0.06	2145.7	6.21	**6.18**	0.08
	S2	50.27	50.37	50.09	50.26	**50.25**		2150.2	6.14		
D56	S1	50.21	50.11	50.22	50.24	**50.20**	0.06	2140.5	6.47	**6.50**	0.07
	S2	50.24	50.28	50.18	50.33	**50.26**		2141.5	6.54		
D57	S1	50.21	50.6	50.2	50.04	**50.26**	0.07	2138.3	6.69	**6.54**	0.29
	S2	50.11	50.27	50.21	50.17	**50.19**		2141.9	6.39		
D58	S1	50.33	50.32	50.21	50.09	**50.24**	0.09	2147.2	6.25	**6.22**	0.05
	S2	50.11	50.52	50.47	50.22	**50.33**		2152.4	6.20		
D59	S1	50.35	50.06	50.23	50.1	**50.19**	0.03	2143.1	6.33	**6.38**	0.10
	S2	50.08	50.31	50.07	50.14	**50.15**		2139.4	6.43		
D60	S1	50.21	50.1	50.19	50.06	**50.14**	0.11	2139.6	6.40	**6.34**	0.13
	S2	50.05	50.11	50.6	50.23	**50.25**		2147.1	6.27		
D61	S1	50.31	50.42	50.01	50.51	**50.31**	0.27	2147.4	6.38	**6.49**	0.21
	S2	50.9	50.88	50.13	50.43	**50.59**		2154.1	6.60		
D62	S1	50.91	50.32	49.61	50.09	**50.23**	0.14	2136.6	6.71	**6.39**	0.62
	S2	50.27	50.01	49.91	50.18	**50.09**		2144.9	6.08		
D63	S1	50.02	50.31	50.91	50.2	**50.36**	0.09	2157.9	6.01	**6.08**	0.12
	S2	50.19	50.43	50.83	50.34	**50.45**		2158.8	6.14		
D64	S1	50.4	50.61	50.25	50.17	**50.36**	0.12	2158.2	6.00	**6.06**	0.14
	S2	50.17	50.73	50.45	50.57	**50.48**		2160.3	6.13		
D65	S1	50.9	50.77	50.54	50.98	**50.80**	0.28	2163.6	6.58	**6.71**	0.26
	S2	50.57	50.82	50.41	50.26	**50.52**		2145.5	6.84		
D66	S1	50.31	50.57	50.88	50.39	**50.54**	0.08	2153.2	6.55	**6.52**	0.06
	S2	50.71	50.28	50.54	50.93	**50.62**		2157.9	6.49		
D67	S1	50.34	50.44	50.42	50.34	**50.39**	0.17	2148.2	6.48	**6.53**	0.10
	S2	50.2	50.13	50.14	50.38	**50.21**		2138.6	6.58		
D68	S1	50.91	51.36	51.11	50.43	**50.95**	0.45	2178.2	6.23	**6.19**	0.09
	S2	50.37	50.33	50.71	50.6	**50.50**		2161.1	6.14		

Table F5. Volumetric Measurements of (Rectangular) Specimens-Asphalt Mix D

Sample	Spec.	Height (mm)						Length (mm)			Width (mm)			Weight (g)	Air Void (%)		
		H1	H2	H3	H4	Avg.	Diff.	L1	L2	Avg.	W1	W2	Avg.		Content	Avg.	Diff.
D09	S1	49.94	50.02	50.00	50.01	**49.99**	0.06	125.30	125.27	**125.29**	75.53	75.61	**75.57**	1153.1	5.57	**5.45**	0.25
	S2	49.93	49.84	49.97	49.98	**49.93**		125.41	125.45	**125.43**	75.32	75.52	**75.42**	1153.7	5.33		
D10	S1	50.01	50.02	49.95	50.00	**50.00**	0.04	125.51	125.53	**125.52**	75.12	75.32	**75.22**	1155.6	5.11	**5.13**	0.05
	S2	50.12	50.02	49.95	50.05	**50.04**		125.65	125.21	**125.43**	75.71	75.43	**75.57**	1160.5	5.16		
D11	S1	50.14	50.05	49.95	50.06	**50.05**	0.15	125.51	125.31	**125.41**	75.21	75.39	**75.30**	1156.9	5.13	**5.19**	0.13
	S2	49.91	49.98	49.65	50.06	**49.90**		125.15	125.17	**125.16**	75.15	75.43	**75.29**	1149.4	5.26		
D12	S1	50.09	50.04	49.72	49.82	**49.92**	0.07	125.23	125.25	**125.24**	75.43	75.21	**75.32**	1149.1	5.41	**5.35**	0.13
	S2	50.00	49.97	50.03	49.96	**49.99**		125.47	125.37	**125.42**	75.41	75.13	**75.27**	1153.3	5.28		
D13	S1	49.70	49.61	50.03	50.06	**49.85**	0.19	125.15	125.12	**125.14**	75.51	75.16	**75.34**	1148.2	5.30	**5.39**	0.18
	S2	50.02	50.10	50.04	49.99	**50.04**		125.21	125.15	**125.18**	75.32	75.43	**75.38**	1151.4	5.47		
D14	S1	50.10	50.06	50.09	50.04	**50.07**	0.26	125.09	125.41	**125.25**	75.10	75.65	**75.38**	1157.4	5.10	**5.42**	0.64
	S2	49.96	49.97	49.32	50.00	**49.81**		125.02	125.1	**125.06**	75.33	75.11	**75.22**	1139.6	5.74		
D15	S1	50.06	50.00	50.04	50.00	**50.03**	0.03	125.02	125.32	**125.17**	74.98	75.31	**75.15**	1146.5	5.56	**5.68**	0.25
	S2	49.96	49.99	50.00	50.02	**49.99**		125.05	125.31	**125.18**	75.21	75.15	**75.18**	1143.4	5.80		
D16	S1	49.98	49.78	50.02	50.13	**49.98**	0.09	124.97	125.76	**125.37**	75.75	75.00	**75.38**	1150	5.62	**5.69**	0.14
	S2	50.03	50.11	50.09	50.03	**50.07**		125.42	125.34	**125.38**	75.12	75.54	**75.33**	1149.7	5.76		

Table F5. Volumetric Measurements of (Rectangular) Specimens- Asphalt Mix D (Cont.)

Sample	Spec.	Height (mm)						Length (mm)			Width (mm)			Weight (g)	Air Void (%)		
		H1	H2	H3	H4	Avg.	Diff.	L1	L2	Avg.	W1	W2	Avg.		Content	Avg.	Diff.
D25	S1	50.70	50.40	50.00	50.60	**50.43**	0.20	125.50	125.40	**125.45**	75.10	74.90	**75.00**	1151.9	5.89	**5.85**	0.09
	S2	50.16	50.20	50.16	50.40	**50.23**		125.01	125.30	**125.16**	75.16	75.06	**75.11**	1147.5	5.81		
D26	S1	50.60	50.40	50.00	50.30	**50.33**	0.22	125.05	125.23	**125.14**	75.05	74.89	**74.97**	1153.2	5.33	**5.42**	0.19
	S2	50.05	50.12	50.09	50.15	**50.10**		125.08	124.91	**125.00**	75.21	75.03	**75.12**	1146.8	5.52		
D27	S1	50.40	50.40	50.20	50.60	**50.40**	0.32	125.24	124.98	**125.11**	75.05	75.03	**75.04**	1151.3	5.69	**5.63**	0.11
	S2	50.05	50.09	50.11	50.06	**50.08**		125.11	125.05	**125.08**	75.02	75.03	**75.03**	1144.8	5.58		
D28	S1	50.13	50.16	50.05	50.02	**50.09**	0.08	125.03	125.11	**125.07**	75.10	75.15	**75.13**	1143.9	5.79	**5.87**	0.15
	S2	50.08	50.32	50.04	50.25	**50.17**		125.02	125.17	**125.10**	75.33	75.13	**75.23**	1145.8	5.94		
D29	S1	50.06	50.00	50.04	50.10	**50.05**	0.02	125.05	125.12	**125.09**	74.98	75.31	**75.15**	1150.1	5.24	**5.42**	0.35
	S2	50.04	50.08	50.11	50.05	**50.07**		125.21	125.13	**125.17**	75.11	75.15	**75.13**	1146.8	5.60		
D30	S1	49.98	50.02	50.05	50.13	**50.05**	0.04	125.15	125.01	**125.08**	75.31	75.25	**75.28**	1145.4	5.79	**5.74**	0.10
	S2	49.94	50.06	50.00	50.01	**50.00**		125.05	125.11	**125.08**	75.15	75.04	**75.10**	1142.8	5.69		
D31	S1	50.06	50.11	50.07	50.10	**50.09**	0.06	124.97	125.13	**125.05**	75.12	75.34	**75.23**	1147.9	5.57	**5.43**	0.29
	S2	50.01	50.02	50.08	50.00	**50.03**		125.13	125.25	**125.19**	75.16	74.90	**75.03**	1148.3	5.28		
D32	S1	50.12	50.15	50.19	50.05	**50.13**	0.06	125.12	125.04	**125.08**	75.26	75.13	**75.20**	1150.9	5.38	**5.33**	0.11
	S2	49.87	50.05	50.13	50.20	**50.06**		125.32	125.40	**125.36**	74.78	75.04	**74.91**	1148.9	5.28		

Table F6. Volumetric Measurements of C4 Specimens, Asphalt Mix D

Sample	Spec.	Height Measurements (mm)						Weight (g)	Air Void (%)		
		H1	H2	H3	H4	Avg.	Diff.		Content	Avg.	Diff.
D33	S1	50.22	50.21	50.23	50.30	**50.24**	0.05	958.5	4.05	**3.99**	0.11
	S2	50.34	50.62	50.00	50.20	**50.29**		960.6	3.94		
D34	S1	50.12	50.22	50.61	50.60	**50.39**	0.04	960.4	4.14	**4.21**	0.14
	S2	50.62	50.31	50.41	50.37	**50.43**		959.8	4.28		
D35	S1	50.31	50.30	50.35	50.40	**50.34**	0.03	959.1	4.18	**4.36**	0.35
	S2	50.32	50.23	50.44	50.50	**50.37**		956.2	4.53		
D36	S1	50.05	50.10	50.21	50.15	**50.13**	0.25	955.3	4.16	**4.29**	0.26
	S2	50.39	50.57	50.32	50.24	**50.38**		957.5	4.42		
D37	S1	50.34	50.54	50.00	50.21	**50.27**	0.04	959.5	4.01	**3.95**	0.13
	S2	50.22	50.25	50.54	50.24	**50.31**		961.6	3.88		
D38	S1	50.56	50.37	50.41	50.43	**50.44**	0.13	963.4	3.95	**4.00**	0.11
	S2	50.12	50.32	50.35	50.45	**50.31**		959.8	4.06		
D39	S1	50.70	50.62	50.41	50.27	**50.50**	0.13	965.1	3.89	**4.13**	0.49
	S2	50.50	50.41	50.38	50.20	**50.37**		957.8	4.37		
D40	S1	50.12	50.07	50.35	50.21	**50.19**	0.20	955.9	4.21	**4.12**	0.18
	S2	50.40	50.34	50.31	50.50	**50.39**		961.5	4.03		

Table F7. Volumetric Measurements of C6 Specimens- Asphalt Mix C

Sample	Spec.	Height Measurements (mm)						Weight (g)	Air Void (%)		
		H1	H2	H3	H4	Avg.	Diff.		Content	Avg.	Diff.
C09	S1	50.12	50.21	50.22	50.32	**50.22**	0.02	2166.1	6.15	**6.22**	0.13
	S2	50.11	50.09	50.43	50.32	**50.24**		2164	6.28		
C10	S1	50.16	50.19	50.21	50.90	**50.37**	0.02	2170.1	6.25	**6.21**	0.09
	S2	50.33	50.38	50.40	50.28	**50.35**		2171.4	6.17		
C11	S1	50.26	50.37	50.47	50.39	**50.37**	0.05	2176	6.01	**6.00**	0.03
	S2	50.23	50.07	50.55	50.43	**50.32**		2174.5	5.98		
C12	S1	50.28	50.13	50.54	50.30	**50.31**	0.08	2176.3	5.89	**6.05**	0.32
	S2	50.21	50.23	50.28	50.21	**50.23**		2165.4	6.21		
C13	S1	50.16	50.19	50.21	50.90	**50.37**	0.03	2170.8	6.22	**6.18**	0.09
	S2	50.32	50.36	50.44	50.22	**50.34**		2171.7	6.13		
C14	S1	50.28	50.13	50.54	50.30	**50.31**	0.01	2176.2	5.89	**5.96**	0.13
	S2	50.23	50.09	50.55	50.41	**50.32**		2173.5	6.02		
C15	S1	50.18	50.23	50.54	50.30	**50.31**	0.04	2170.1	6.16	**6.17**	0.03
	S2	50.16	50.13	50.23	50.91	**50.36**		2171.4	6.18		
C16	S1	50.33	50.38	50.40	50.28	**50.35**	0.04	2175.6	5.98	**6.03**	0.10
	S2	50.21	50.53	50.50	50.32	**50.39**		2175.2	6.08		
C25	S1	50.31	50.22	50.41	50.20	**50.29**	0.05	2158.1	6.62	**6.37**	0.51
	S2	50.20	50.24	50.40	50.10	**50.24**		2167.7	6.12		
C26	S1	50.22	49.89	50.17	50.07	**50.09**	0.32	2153.6	6.45	**6.26**	0.38
	S2	50.50	50.35	50.45	50.32	**50.41**		2176	6.07		
C27	S1	50.50	49.76	49.83	50.51	**50.15**	0.20	2152.9	6.60	**6.38**	0.44
	S2	50.11	50.97	50.22	50.11	**50.35**		2171.7	6.16		
C28	S1	50.16	50.35	50.14	50.25	**50.23**	0.03	2160.2	6.42	**6.43**	0.02
	S2	50.41	50.56	50.03	50.00	**50.25**		2160.8	6.44		
C29	S1	50.27	50.54	50.30	50.06	**50.29**	0.09	2172.9	6.00	**6.14**	0.28
	S2	50.19	50.56	50.06	50.00	**50.20**		2162.5	6.28		
C30	S1	50.32	50.09	50.50	50.42	**50.33**	0.02	2169.8	6.21	**6.32**	0.22
	S2	50.80	50.07	50.00	50.54	**50.35**		2165.5	6.43		
C31	S1	50.27	50.55	50.07	50.00	**50.22**	0.30	2159.5	6.45	**6.26**	0.38
	S2	50.56	50.56	50.12	50.84	**50.52**		2181.1	6.07		
C32	S1	50.55	50.43	50.05	50.02	**50.26**	0.04	2170.5	6.05	**6.14**	0.19
	S2	50.16	50.40	50.25	50.08	**50.22**		2164.4	6.24		
C41	S1	50.32	50.12	50.13	50.11	**50.17**	0.19	2157.7	6.43	**6.51**	0.17
	S2	50.33	50.56	50.5	50.04	**50.36**		2161.9	6.60		
C42	S1	50.07	50.24	50.32	50.09	**50.18**	0.03	2170.3	5.90	**5.98**	0.17
	S2	50.12	50.17	50.53	50.02	**50.21**		2167.7	6.07		

Table F7. Volumetric Measurements of C6 Specimens- Asphalt Mix C (Cont.)

Sample	Spec.	Height Measurements (mm)						Weight (g)	Air Void (%)		
		H1	H2	H3	H4	Avg.	Diff.		Content	Avg.	Diff.
C43	S1	50.18	50.45	50.17	50.06	**50.22**	0.15	2162.8	6.29	**6.18**	0.23
	S2	50.19	50.52	50.29	50.45	**50.36**		2174.4	6.06		
C44	S1	50.54	50.17	50.17	50.42	**50.33**	0.00	2167.8	6.28	**6.16**	0.24
	S2	50.54	50.33	50.16	50.28	**50.33**		2173.4	6.04		
C45	S1	50.42	50.02	50.13	50.31	**50.22**	0.05	2158.7	6.48	**6.37**	0.22
	S2	50.53	50.26	50.15	50.14	**50.27**		2165.9	6.26		
C46	S1	50.13	50.56	50.18	50.26	**50.28**	0.11	2163.4	6.39	**6.26**	0.27
	S2	50.18	50.64	50.35	50.41	**50.40**		2174.5	6.12		
C47	S1	50.38	50.55	50.17	50.06	**50.29**	0.10	2174.5	5.92	**5.99**	0.13
	S2	50.29	50.42	50.19	50.65	**50.39**		2175.7	6.05		
C48	S1	50.34	50.27	50.27	50.52	**50.35**	0.08	2166.8	6.37	**6.26**	0.23
	S2	50.54	50.23	50.66	50.28	**50.43**		2175.4	6.14		
C49	S1	50.11	50.06	50.33	50.55	**50.26**	0.39	2163.4	6.35	**6.13**	0.44
	S2	50.92	50.67	50.56	50.47	**50.66**		2190.5	5.92		
C50	S1	50.33	50.56	50.08	50.16	**50.28**	0.24	2174.5	5.91	**5.96**	0.09
	S2	50.78	50.44	50.25	50.61	**50.52**		2182.7	6.00		
C51	S1	50.58	50.45	50.27	50.06	**50.34**	0.02	2162.8	6.52	**6.38**	0.29
	S2	50.19	50.52	50.19	50.55	**50.36**		2170.4	6.24		
C52	S1	50.44	50.37	50.07	50.42	**50.33**	0.25	2157.8	6.71	**6.46**	0.51
	S2	50.94	50.83	50.06	50.48	**50.58**		2180.4	6.21		
C53	S1	50.55	50.22	50.70	50.20	**50.42**	0.16	2179.2	5.96	**6.07**	0.22
	S2	50.51	50.13	50.32	50.08	**50.26**		2167.2	6.18		
C54	S1	50.57	50.63	50.50	50.73	**50.61**	0.39	2169.3	6.74	**6.59**	0.29
	S2	50.10	50.11	50.04	50.63	**50.22**		2159.4	6.45		
C55	S1	50.59	50.40	50.17	50.05	**50.30**	0.03	2170.2	6.13	**6.27**	0.28
	S2	50.10	50.37	50.37	50.50	**50.34**		2165.1	6.41		
C56	S1	50.44	50.37	50.59	50.60	**50.50**	0.09	2171.8	6.43	**6.29**	0.29
	S2	50.20	50.48	50.40	50.56	**50.41**		2174.6	6.14		
C57	S1	50.68	50.4	50.77	50.79	**50.66**	0.33	2196.9	5.65	**6.07**	0.84
	S2	50.22	50.57	50.23	50.29	**50.33**		2163.1	6.49		
C58	S1	50.4	50.48	49.82	50.4	**50.28**	0.23	2175.9	5.84	**6.14**	0.61
	S2	50.82	50.75	50.25	50.2	**50.51**		2171.7	6.45		
C59	S1	50.56	50.12	50.16	50.4	**50.31**	0.18	2163.1	6.45	**6.30**	0.32
	S2	50.31	50.75	50.27	50.64	**50.49**		2178.3	6.14		
C60	S1	50.22	50.5	50.78	50.62	**50.53**	0.10	2166.4	6.72	**6.72**	0.00
	S2	50.52	50.93	50.27	50	**50.43**		2162.1	6.72		

Table F8. Volumetric Measurements of (Rectangular) Specimens- Asphalt Mix C

Sample	Spec.	Height (mm)						Length (mm)			Width (mm)			Weight (g)	Air Void (%)		
		H1	H2	H3	H4	Avg.	Diff.	L1	L2	Avg.	W1	W2	Avg.		Content	Avg.	Diff.
C17	S1	50.32	49.98	50.05	50.13	**50.12**	0.07	126.21	125.80	**126.01**	75.59	75.33	**75.46**	1164.7	6.04	**5.96**	0.15
	S2	49.99	50.02	50.22	49.95	**50.05**		125.67	126.21	**125.94**	75.28	75.83	**75.56**	1165.7	5.88		
C18	S1	50.28	50.56	50.67	50.12	**50.41**	0.19	125.66	126.22	**125.94**	75.58	75.58	**75.58**	1173.9	5.94	**5.74**	0.39
	S2	50.17	50.27	50.12	50.32	**50.22**		126.11	125.23	**125.67**	75.80	75.01	**75.41**	1169.2	5.54		
C19	S1	50.66	50.67	50.31	50.52	**50.54**	0.36	125.82	126.25	**126.04**	75.63	75.69	**75.66**	1177.9	6.03	**5.88**	0.30
	S2	50.04	50.31	50.61	49.75	**50.18**		125.76	126.11	**125.94**	75.37	76.02	**75.70**	1172.8	5.73		
C20	S1	50.31	50.09	50.32	50.03	**50.19**	0.02	125.50	125.60	**125.55**	75.33	75.90	**75.62**	1164.3	6.05	**5.88**	0.34
	S2	50.04	50.29	50.25	50.10	**50.17**		126.21	125.18	**125.70**	75.01	75.83	**75.42**	1166.5	5.70		
C21	S1	50.07	49.88	50.37	50.07	**50.10**	0.29	125.57	125.86	**125.72**	75.30	76.14	**75.72**	1165.7	6.02	**5.95**	0.14
	S2	50.64	50.45	50.18	50.29	**50.39**		125.82	125.45	**125.64**	75.99	75.57	**75.78**	1174.4	5.88		
C22	S1	50.11	50.67	50.37	50.05	**50.30**	0.14	125.69	126.00	**125.85**	75.24	75.60	**75.42**	1167.3	5.99	**5.93**	0.12
	S2	50.05	50.28	50.29	50.00	**50.16**		125.43	125.97	**125.70**	75.64	75.54	**75.59**	1166.7	5.88		
C23	S1	50.10	50.24	50.80	50.76	**50.48**	0.24	125.80	125.90	**125.85**	75.14	75.44	**75.29**	1171.1	5.86	**5.79**	0.13
	S2	50.23	50.27	50.36	50.08	**50.24**		125.65	125.16	**125.41**	75.23	75.28	**75.26**	1162.5	5.73		
C24	S1	50.00	50.07	50.12	49.98	**50.04**	0.12	125.31	125.66	**125.49**	75.15	75.41	**75.28**	1155.6	6.02	**5.97**	0.09
	S2	50.13	50.23	50.27	50.00	**50.16**		126.09	125.7	**125.90**	75.61	75.31	**75.46**	1165.9	5.93		

Table F8. Volumetric Measurements of (Rectangular) Specimens- Asphalt Mix C (Cont.)

Sample	Spec.	Height (mm)						Length (mm)			Width (mm)			Weight (g)	Air Void (%)		
		H1	H2	H3	H4	Avg.	Diff.	L1	L2	Avg.	W1	W2	Avg.		Content	Avg.	Diff.
C33	S1	50.17	50.20	50.30	50.00	**50.17**	0.17	125.38	125.47	**125.43**	75.34	75.84	**75.59**	1164.00	5.91	**5.99**	0.16
	S2	50.29	50.52	50.40	50.14	**50.34**		125.50	126.35	**125.93**	75.82	75.30	**75.56**	1170.20	6.07		
C34	S1	50.15	50.04	50.23	50.28	**50.18**	0.33	125.12	125.94	**125.53**	75.38	75.20	**75.29**	1157.60	6.15	**5.97**	0.35
	S2	50.10	50.78	50.80	50.35	**50.51**		125.80	124.99	**125.40**	75.12	75.50	**75.31**	1168.70	5.80		
C35	S1	50.09	50.37	50.48	50.00	**50.24**	0.05	125.99	125.89	**125.94**	75.65	75.00	**75.33**	1165.80	5.95	**5.79**	0.31
	S2	50.21	50.25	50.38	50.32	**50.29**		125.74	125.75	**125.75**	75.23	76.01	**75.62**	1173.70	5.64		
C36	S1	50.11	50.54	50.56	50.66	**50.47**	0.16	125.54	125.24	**125.39**	75.47	75.89	**75.68**	1180.80	5.21	**5.36**	0.32
	S2	50.05	50.10	50.23	50.84	**50.31**		125.23	125.34	**125.29**	75.35	75.78	**75.57**	1170.30	5.52		
C37	S1	50.33	50.28	50.36	50.02	**50.25**	0.05	125.12	124.89	**125.01**	75.71	75.74	**75.73**	1166.60	5.70	**5.79**	0.17
	S2	50.13	50.54	50.06	50.48	**50.30**		125.12	125.20	**125.16**	76.11	75.46	**75.79**	1168.10	5.88		
C38	S1	50.89	50.31	50.80	50.00	**50.50**	0.17	125.23	125.04	**125.14**	75.47	75.6	**75.54**	1171.53	5.64	**5.87**	0.47
	S2	50.62	50.23	50.09	50.39	**50.33**		125.17	125.26	**125.22**	75.41	75.63	**75.52**	1162.40	6.10		
C39	S1	50.58	50.12	50.51	50.56	**50.44**	0.20	125.22	125.17	**125.20**	75.16	75.35	**75.26**	1170.20	5.33	**5.45**	0.24
	S2	50.75	50.33	50.95	50.55	**50.65**		125.54	125.27	**125.41**	75.32	75.65	**75.49**	1177.50	5.57		
C40	S1	50.20	50.34	50.00	50.74	**50.32**	0.10	125.73	125.43	**125.58**	75.35	75.91	**75.63**	1165.80	6.22	**5.92**	0.60
	S2	50.46	50.25	50.57	50.42	**50.43**		126.14	125.73	**125.94**	75.38	75.79	**75.59**	1178.30	5.62		

Table F9. Volumetric Measurements of C4 Specimens- Asphalt Mix C

Sample	Specimen	Height Measurements (mm)						Weight (g)	Air Void (%)		
		H1	H2	H3	H4	Avg.	Diff.		Content	Avg.	Diff.
C01	S1	50.11	50.21	50.02	50.30	**50.16**	0.12	964.1	4.12	**4.09**	0.05
	S2	50.06	50.00	50.10	50.00	**50.04**		962.3	4.07		
C02	S1	49.98	49.96	49.87	50.00	**49.95**	0.04	960.4	4.09	**4.12**	0.06
	S2	50.13	50.00	49.87	49.98	**50.00**		960.6	4.15		
C03	S1	49.76	50.05	50.00	49.92	**49.93**	0.03	960.1	4.08	**4.03**	0.09
	S2	49.88	49.95	49.96	50.06	**49.96**		961.6	3.99		
C04	S1	50.05	50.10	50.05	50.23	**50.11**	0.15	961.4	4.29	**4.19**	0.20
	S2	50.10	49.86	49.87	50.00	**49.96**		960.5	4.09		
C05	S1	50.13	50.00	49.87	49.98	**50.00**	0.04	960.5	4.16	**4.14**	0.04
	S2	49.98	50.15	50.07	49.92	**50.03**		961.6	4.12		
C06	S1	50.05	50.10	50.05	49.65	**49.96**	0.11	959.4	4.21	**4.20**	0.02
	S2	50.11	50.32	49.87	50.00	**50.08**		961.8	4.18		
C07	S1	50.06	50.00	50.10	50.12	**50.07**	0.12	960.1	4.34	**4.20**	0.29
	S2	49.98	49.96	49.87	50.00	**49.95**		960.8	4.05		
C08	S1	50.13	50.09	49.57	49.98	**49.94**	0.09	959.9	4.12	**4.08**	0.09
	S2	50.10	49.98	50.05	50.00	**50.03**		962.5	4.03		

Table F10. Volumetric Measurements of C6 Specimens- Asphalt Mix B

Sample	Spec.	Height Measurements (mm)						Weight (g)	Air Void (%)		
		H1	H2	H3	H4	Avg.	Diff.		Content	Avg.	Diff.
B09	S1	50.1	50.07	50.37	50.03	**50.14**	0.05	2167.6	5.77	**5.87**	0.22
	S2	50.20	50.12	50.27	50.17	**50.19**		2164.7	5.98		
B10	S1	50.25	50.19	50.20	50.22	**50.22**	0.18	2165.8	5.98	**6.25**	0.54
	S2	50.08	50.68	50.79	50.05	**50.40**		2161.3	6.52		
B11	S1	50.51	50.02	50.00	50.35	**50.22**	0.37	2169	5.85	**6.00**	0.30
	S2	50.18	50.65	50.89	50.65	**50.59**		2178.2	6.15		
B12	S1	50.00	49.61	49.91	50.24	**49.94**	0.34	2152.5	6.04	**6.02**	0.05
	S2	50.25	50.20	50.41	50.27	**50.28**		2168.5	5.99		
B13	S1	50.62	50.46	50.08	50.01	**50.29**	0.01	2156.3	6.54	**6.53**	0.01
	S2	50.17	50.65	50.33	50.00	**50.29**		2156.4	6.52		
B14	S1	50.62	50.25	50.59	50.01	**50.37**	0.03	2162.7	6.40	**6.14**	0.51
	S2	50.95	50.22	50.18	50.24	**50.40**		2175.8	5.89		
B15	S1	50.36	50.67	50.74	50.69	**50.62**	0.23	2181.6	6.04	**6.41**	0.74
	S2	50.57	50.55	51.30	50.95	**50.84**		2174.1	6.78		
B16	S1	50.87	50.46	50.32	50.44	**50.52**	0.15	2157.4	6.91	**6.69**	0.46
	S2	50.66	50.56	50.27	50.00	**50.37**		2161.6	6.46		
B25	S1	50.30	50.15	50.10	50.21	**50.19**	0.52	2163.1	6.05	**6.41**	0.72
	S2	50.39	50.82	50.92	50.73	**50.72**		2169	6.77		
B26	S1	50.40	50.10	50.32	50.85	**50.42**	0.04	2164.1	6.43	**6.32**	0.23
	S2	50.00	50.88	50.41	50.20	**50.37**		2167.5	6.20		
B27	S1	50.67	50.82	50.61	50.39	**50.62**	0.04	2175.1	6.34	**6.49**	0.30
	S2	50.43	50.45	50.80	50.64	**50.58**		2166.3	6.64		
B28	S1	50.31	50.57	50.83	50.84	**50.64**	0.15	2169.8	6.59	**6.33**	0.52
	S2	50.70	50.38	50.27	50.58	**50.48**		2175.3	6.07		
B29	S1	50.14	50.05	50.22	50.06	**50.12**	0.38	2153.5	6.33	**6.38**	0.10
	S2	50.43	50.35	50.46	50.73	**50.49**		2167.2	6.44		
B30	S1	50.80	50.26	50.00	50.62	**50.42**	0.00	2166.9	6.31	**6.24**	0.15
	S2	50.40	50.61	50.21	50.45	**50.42**		2170.3	6.16		
B31	S1	50.05	50.65	50.73	50.27	**50.43**	0.26	2165.8	6.37	**6.34**	0.06
	S2	50.67	50.83	50.85	50.38	**50.68**		2178.3	6.31		
B32	S1	50.44	50.27	50.20	50.25	**50.29**	0.07	2153.5	6.65	**6.34**	0.63
	S2	50.31	50.35	50.13	50.08	**50.22**		2164.9	6.02		
B41	T	50.39	50.56	50.25	50.15	**50.34**	0.08	2167.9	6.12	**6.15**	0.07
	B	50.26	50.36	50.41	50.63	**50.42**		2169.6	6.19		
B42	T	50.51	50.11	50.27	50.37	**50.32**	0.22	2172.4	5.88	**5.86**	0.05
	B	50.51	50.75	50.23	50.65	**50.54**		2183.1	5.83		

Table F10. Volumetric Measurements of C6 Specimens- Asphalt Mix B (Cont.)

Sample	Spec.	Height Measurements (mm)						Weight (g)	Air Void (%)		
		H1	H2	H3	H4	Avg.	Diff.		Content	Avg.	Diff.
B43	T	50.57	50.84	50.61	50.39	**50.60**	0.25	2172.4	6.42	**6.25**	0.34
	B	50.51	50.26	50.46	50.16	**50.35**		2169.3	6.08		
B44	T	50.46	50.01	50.12	50.56	**50.29**	0.16	2160.1	6.36	**6.20**	0.33
	B	50.25	50.54	50.38	50.61	**50.45**		2174.4	6.04		
B45	S1	50.00	50.00	50.89	50.29	**50.30**	0.23	2164.8	6.17	**6.27**	0.19
	S2	50.67	50.21	50.5	50.71	**50.52**		2170.3	6.36		
B46	S1	50.43	50.73	50.92	50.7	**50.70**	0.20	2173.5	6.54	**6.32**	0.44
	S2	50.31	50.85	50.56	50.27	**50.50**		2175.2	6.10		
B47	S1	50.38	50.20	50.51	50.38	**50.37**	0.04	2177.3	5.77	**5.94**	0.36
	S2	50.15	50.64	50.58	50.25	**50.41**		2170.7	6.12		
B48	S1	50.35	50.67	50.67	50.08	**50.44**	0.05	2162.7	6.54	**6.30**	0.47
	S2	50.26	50.58	50.27	50.87	**50.50**		2175.8	6.07		
B49	S1	50.53	50.63	50.77	50.95	**50.72**	0.15	2181.6	6.24	**6.28**	0.08
	S2	50.85	50.47	50.21	50.76	**50.57**		2173.5	6.31		
B50	S1	50.56	50.38	50.87	50.65	**50.62**	0.28	2175.2	6.32	**6.12**	0.39
	S2	50.43	50.25	50.36	50.31	**50.34**		2172.3	5.93		
B51	S1	50.31	50.88	50.74	50.54	**50.62**	0.02	2176.7	6.26	**6.58**	0.64
	S2	50.68	50.87	50.26	50.73	**50.64**		2162.7	6.89		
B52	S1	50.15	50.36	50.75	50.65	**50.48**	0.15	2174.5	6.09	**6.39**	0.60
	S2	50.48	50.66	50.83	50.54	**50.63**		2167.1	6.69		
B53	T	50.86	51.04	50.55	51.01	**50.87**	0.15	2190.4	6.13	**6.18**	0.10
	B	50.41	50.78	51.02	50.66	**50.72**		2181.7	6.23		
B54	T	51.12	50.36	50.99	50.86	**50.83**	0.08	2182.5	6.41	**6.31**	0.19
	B	50.82	51.03	50.74	51.05	**50.91**		2190.3	6.21		
B55	T	50.82	50.11	50.25	50.54	**50.43**	0.37	2165.9	6.38	**6.35**	0.06
	B	50.67	50.65	51.09	50.78	**50.80**		2183.1	6.32		
B56	T	50.87	50.97	51.05	50.75	**50.91**	0.16	2189.6	6.24	**6.14**	0.20
	B	50.32	50.89	51.01	50.79	**50.75**		2187.5	6.04		
B57	T	50.89	50.94	51.33	51.2	**51.09**	0.07	2189.6	6.58	**6.46**	0.24
	B	50.85	50.93	51.31	50.98	**51.02**		2192.1	6.34		
B58	T	50.85	50.89	51.17	51.5	**51.10**	0.17	2199.9	6.16	**6.19**	0.07
	B	51.02	51.06	50.76	50.91	**50.94**		2191.2	6.23		
B59	T	51	50.82	50.51	50.86	**50.80**	0.24	2186.5	6.17	**6.00**	0.35
	B	50.78	50.57	50.22	50.66	**50.56**		2184.2	5.82		
B60	T	50.36	50.87	50.82	51.05	**50.78**	0.08	2188.8	6.03	**5.95**	0.16
	B	51.03	50.87	50.96	50.54	**50.85**		2195.7	5.87		

Table F11. Volumetric Measurements of (Rectangular) Specimens- Asphalt Mix B

Sample	Spec.	Height (mm)						Length (mm)			Width (mm)			Weight (g)	Air Void (%)		
		H1	H2	H3	H4	Avg.	Diff.	L1	L2	Avg.	W1	W2	Avg.		Content	Avg.	Diff.
B17	S1	50.37	50.27	50.11	50.30	**50.26**	0.16	125.12	125.94	**125.53**	76.28	75.03	**75.66**	1162.2	6.21	**6.10**	0.22
	S2	50.56	50.34	50.30	50.51	**50.43**		125.30	125.09	**125.20**	75.58	75.03	**75.31**	1160.2	6.00		
B18	S1	50.14	50.31	50.71	50.20	**50.34**	0.12	125.99	125.89	**125.94**	75.80	74.15	**74.98**	1163.5	5.71	**5.98**	0.55
	S2	50.36	50.19	50.22	50.13	**50.23**		125.74	125.17	**125.46**	75.53	75.13	**75.33**	1155.1	6.26		
B19	S1	50.24	50.23	50.35	50.10	**50.23**	0.06	125.54	125.27	**125.41**	75.37	76.31	**75.84**	1164.6	6.09	**5.80**	0.60
	S2	50.17	50.08	50.27	50.17	**50.17**		125.23	125.43	**125.33**	75.33	75.15	**75.24**	1160.7	5.50		
B20	S1	50.64	50.29	50.18	50.29	**50.35**	0.25	125.12	125.73	**125.43**	75.11	75.25	**75.18**	1161.6	5.75	**5.63**	0.25
	S2	50.11	49.88	50.37	50.05	**50.10**		125.12	125.76	**125.44**	75.30	75.04	**75.17**	1158.9	5.51		
B21	S1	50.05	50.45	50.29	50.00	**50.20**	0.07	125.23	125.34	**125.29**	75.99	75.34	**75.67**	1163.7	5.80	**5.85**	0.10
	S2	50.04	50.67	50.25	50.10	**50.27**		125.05	125.26	**125.16**	75.24	75.60	**75.42**	1159.1	5.89		
B22	S1	50.07	50.60	50.37	50.07	**50.28**	0.11	125.21	125.17	**125.19**	75.64	75.54	**75.59**	1169.7	5.30	**5.59**	0.59
	S2	50.64	50.45	50.18	50.29	**50.39**		125.15	125.37	**125.26**	76.14	75.44	**75.79**	1168.7	5.89		
B23	S1	50.11	50.60	50.37	50.05	**50.28**	0.16	125.05	125.43	**125.24**	75.23	75.28	**75.26**	1157.7	5.90	**5.79**	0.21
	S2	50.07	49.88	50.37	50.17	**50.12**		124.97	125.73	**125.35**	74.25	75.41	**74.83**	1151.1	5.69		
B24	S1	50.64	50.46	50.11	50.59	**50.45**	0.15	125.13	125.76	**125.45**	75.15	75.00	**75.08**	1156.5	6.24	**5.97**	0.53
	S2	50.11	50.67	50.37	50.05	**50.30**		125.12	125.34	**125.23**	75.12	75.44	**75.28**	1160.7	5.71		

Table F11. Volumetric Measurements of (Rectangular) Specimens- Asphalt Mix B (Cont.)

Sample	Spec.	Height (mm)						Length (mm)			Width (mm)			Weight (g)	Air Void (%)		
		H1	H2	H3	H4	Avg.	Diff.	L1	L2	Avg.	W1	W2	Avg.		Content	Avg.	Diff.
B33	S1	50.18	50.65	50.89	50.65	**50.59**	0.40	125.30	126.40	**125.85**	75.80	75.67	**75.74**	1176.1	6.05	**5.81**	0.47
	S2	50.00	49.98	50.56	50.24	**50.20**		125.01	125.30	**125.16**	75.16	74.16	**74.66**	1149.7	5.58		
B34	S1	50.85	50.08	50.64	50.27	**50.46**	0.12	125.21	125.60	**125.41**	75.28	74.47	**74.88**	1157.7	5.88	**5.93**	0.11
	S2	50.64	50.29	50.11	50.33	**50.34**		125.12	124.91	**125.02**	75.21	75.03	**75.12**	1153.8	5.99		
B35	S1	50.39	49.84	50.07	50.62	**50.23**	0.14	125.24	124.98	**125.11**	75.05	75.13	**75.09**	1161.6	5.18	**5.47**	0.59
	S2	50.40	50.40	50.08	50.59	**50.37**		125.17	125.05	**125.11**	75.02	75.33	**75.18**	1158.9	5.76		
B36	S1	50.00	50.67	50.29	50.11	**50.27**	0.29	125.03	125.11	**125.07**	76.10	75.15	**75.63**	1160.2	6.00	**5.93**	0.13
	S2	50.67	50.60	50.87	50.07	**50.55**		125.02	125.37	**125.20**	75.33	75.13	**75.23**	1163.5	5.87		
B37	S1	50.43	50.73	50.67	50.09	**50.48**	0.02	126.05	125.42	**125.74**	75.98	75.31	**75.65**	1170.1	6.12	**5.80**	0.65
	S2	50.47	50.81	50.43	50.29	**50.50**		125.26	125.13	**125.20**	75.11	75.15	**75.13**	1165.6	5.47		
B38	S1	50.80	50.20	50.43	50.41	**50.46**	0.09	125.15	125.01	**125.08**	75.31	75.25	**75.28**	1163.9	5.64	**5.79**	0.31
	S2	50.40	50.39	50.08	50.61	**50.37**		125.05	125.11	**125.08**	75.25	75.04	**75.15**	1155.9	5.95		
B39	S1	50.05	50.22	50.29	50.80	**50.34**	0.02	124.97	125.13	**125.05**	75.12	76.04	**75.58**	1162.7	5.86	**5.56**	0.61
	S2	50.11	50.29	50.04	50.83	**50.32**		125.13	126.05	**125.59**	75.16	74.99	**75.08**	1166.9	5.25		
B40	S1	50.09	50.55	50.45	50.27	**50.34**	0.16	125.12	125.24	**125.18**	75.26	75.63	**75.45**	1161.9	5.86	**5.91**	0.10
	S2	50.14	50.97	50.67	50.22	**50.50**		126.32	125.26	**125.79**	75.78	75.24	**75.51**	1171.0	5.96		

Table F12. Volumetric Measurements of C4 Specimens- Asphalt Mix B

Sample	Spec.	Height Measurements (mm)						Weight (g)	Air Void (%)		
		H1	H2	H3	H4	Avg.	Diff.		Content	Avg.	Diff.
B01	S1	49.70	49.65	49.56	49.70	**49.65**	0.27	952.5	4.12	**4.21**	0.18
	S2	49.80	50.00	49.87	50.01	**49.92**		955.8	4.30		
B02	S1	49.80	49.70	50.10	49.99	**49.90**	0.13	956.1	4.23	**4.65**	0.84
	S2	49.91	50.06	50.11	50.05	**50.03**		950.3	5.07		
B03	S1	49.90	49.98	50.04	50.07	**50.00**	0.09	959.4	4.09	**4.18**	0.19
	S2	49.98	49.76	49.84	50.05	**49.91**		955.8	4.28		
B04	S1	50.11	49.99	49.76	50.10	**49.99**	0.04	951.9	4.83	**4.56**	0.54
	S2	49.98	49.94	49.85	50.04	**49.95**		956.6	4.28		
B05	S1	50.03	49.97	49.70	49.99	**49.92**	0.05	954.7	4.42	**4.42**	0.01
	S2	50.12	49.88	49.86	50.04	**49.98**		955.6	4.43		
B06	S1	50.06	49.99	50.10	49.92	**50.02**	0.07	960.6	4.01	**4.06**	0.10
	S2	49.97	49.95	50.08	49.77	**49.94**		958.2	4.11		
B07	S1	50.00	49.98	49.95	49.97	**49.98**	0.03	955.4	4.45	**4.27**	0.36
	S2	49.97	49.99	50.05	50.03	**50.01**		959.7	4.08		
B08	S1	49.99	50.10	50.09	49.98	**50.04**	0.25	959.1	4.20	**4.14**	0.12
	S2	50.03	49.84	49.22	50.07	**49.79**		955.5	4.08		

Appendix G: Tests results summaries (Raw data)

Table G1. Results of testing group (DST-C6-M) -Asphalt Mix D

150 mm Diameter SP- Type D (Morning)													
FSCH Tests @ 30 °C												RSCH Tests @ 50°C	
Sample	Frequency (Hz)	10	5	2	1	0.5	0.2	0.1	0.05	0.02	0.01		
D01	G* (Mpa)	779	566	380	266	203	130	91	70	43	27	Cycle	5,000
	Phase Angle (Degrees)	30.5	33.9	37.2	40	36.4	33.4	33	37.2	39.2	42.7	Permanent deformation (mm)	1.06
D02	G* (Mpa)	689	491	338	246	194	131	97	76	50	34	Cycle	5,000
	Phase Angle (Degrees)	29.7	33.4	36.3	38.5	35.1	31.8	31	34.6	34.9	37.4	Permanent deformation (mm)	0.85
D03	G* (Mpa)	777	571	389	275	213	138	99	77	48	31	Cycle	5,000
	Phase Angle (Degrees)	29.9	32.8	36.1	39	35.9	33.1	32.8	37.2	39	42.2	Permanent deformation (mm)	0.84
D04	G* (Mpa)	913	680	469	335	258	167	118	90	55	35	Cycle	5,000
	Phase Angle (Degrees)	25.6	30.2	34.4	37.7	35	32.4	32.5	37	38.7	41.6	Permanent deformation (mm)	1.17
D05	G* (Mpa)	783	567	387	277	219	145	106	85	54	36	Cycle	5,000
	Phase Angle (Degrees)	29.9	33.4	36.5	39.1	35.1	32.4	31.7	35.9	37.6	40.8	Permanent deformation (mm)	1.03
D06	G* (Mpa)	739	537	365	257	201	130	94	75	47	31	Cycle	5,000
	Phase Angle (Degrees)	29.7	33	36.5	39.5	36.3	33.2	32.4	36.7	38.4	41.5	Permanent deformation (mm)	1.12
D07	G* (Mpa)	783	556	371	260	200	128	90	70	43	27	Cycle	5,000
	Phase Angle (Degrees)	30.6	34.5	37.6	40.1	36.3	33.2	32.5	36.5	38.3	41.6	Permanent deformation (mm)	0.98
D08	G* (Mpa)	765	552	372	262	201	130	93	73	45	30	Cycle	5,000
	Phase Angle (Degrees)	31.7	35.2	38.2	40.7	38.1	34.2	32.7	36.3	37.8	41.1	Permanent deformation (mm)	0.80

Table G2. Results of testing group (DST-C6-N) - Asphalt Mix D

150 mm Diameter SP- Type D (Noon)													
FSCH Tests @ 30 °C												RSCH Tests @ 50°C	
Sample	Frequency (Hz)	10	5	2	1	0.5	0.2	0.1	0.05	0.02	0.01		
D17	G* (Mpa)	662.0	505.0	365.0	282.0	224.0	161.0	127.0	104.0	82.0	69.0	Cycle	5,000
	Phase Angle (Degrees)	29.2	31.1	33.5	34.7	33.0	26.6	25.9	30.9	29.9	30.6	Permanent deformation (mm)	0.965
D18	G* (Mpa)	605.0	457.0	332.0	260.0	209.0	151.0	120.0	97.0	75.0	63.0	Cycle	5,000
	Phase Angle (Degrees)	30.4	32.3	34.1	35.2	34.8	27.3	26.7	31.1	30.2	31.3	Permanent deformation (mm)	1.27
D19	G* (Mpa)	699.0	507.0	358.0	272.0	213.0	150.0	115.0	90.0	67.0	54.0	Cycle	5,000
	Phase Angle (Degrees)	29.8	32.4	34.4	35.7	35.9	28.1	27.3	31.4	30.3	31.2	Permanent deformation (mm)	1.245
D20	G* (Mpa)	660.0	485.0	361.0	288.0	237.0	177.0	143.0	119.0	96.0	83.0	Cycle	5,000
	Phase Angle (Degrees)	29.4	31.3	32.7	33.6	32.8	25.5	24.8	29.7	28.7	30.1	Permanent deformation (mm)	1.055
D21	G* (Mpa)	709.0	534.0	391.0	308.0	251.0	186.0	150.0	125.0	101.0	88.0	Cycle	5,000
	Phase Angle (Degrees)	30.4	32.3	33.7	34.5	32.9	25.6	24.7	29.4	28.6	29.9	Permanent deformation (mm)	1.09
D22	G* (Mpa)	784.0	595.0	433.0	339.0	273.0	200.0	160.0	130.0	103.0	88.0	Cycle	5,000
	Phase Angle (Degrees)	27.8	31.1	33.1	34.4	33.6	26.6	26.1	31.0	30.6	32.1	Permanent deformation (mm)	0.945
D23	G* (Mpa)	646.0	506.0	367.0	288.0	233.0	170.0	135.0	109.0	84.0	70.0	Cycle	5,000
	Phase Angle (Degrees)	28.9	30.3	32.6	34.0	34.2	26.3	26.0	30.8	30.7	32.0	Permanent deformation (mm)	1.25
D24	G* (Mpa)	729.0	556.0	410.0	320.0	258.0	188.0	148.0	117.0	90.0	74.0	Cycle	5,000
	Phase Angle (Degrees)	27.4	30.1	32.2	33.7	32.3	26.2	25.9	30.6	30.2	31.8	Permanent deformation (mm)	1.11

Table G3. Results of testing group (DST-C6-A) - Asphalt Mix D

150 mm Diameter SP- Type D (Afternoon)													
		FSCH Tests @ 30 °C										RSCH Tests @ 50°C	
Sample	Frequency (Hz)	10	5	2	1	0.5	0.2	0.1	0.05	0.02	0.01		
D49	G* (Mpa)	968	776	594	476	386	286	225	175	130	101	Cycle	5,000
	Phase Angle (Degrees)	23.62	25.53	27.78	29.52	27.6	23.02	23.48	29	29.92	32.54	Permanent deformation (mm)	0.89
D50	G* (Mpa)	965	780	600	483	392	290	227	178	133	106	Cycle	5,000
	Phase Angle (Degrees)	22.45	24.18	26.38	28.27	27.16	21.98	22.53	28.11	28.64	30.76	Permanent deformation (mm)	0.925
D51	G* (Mpa)	870	687	514	406	326	236	184	145	109	89	Cycle	5,000
	Phase Angle (Degrees)	26.5	28.4	30.4	31.91	30.97	25.15	25.11	30.33	30.39	32.11	Permanent deformation (mm)	0.95
D52	G* (Mpa)	860	679	511	407	332	246	196	157	120	99	Cycle	5,000
	Phase Angle (Degrees)	26.57	28.11	29.82	30.89	30.82	23.61	23.09	28.34	28.57	30.61	Permanent deformation (mm)	0.875
D53	G* (Mpa)	727	548	400	313	252	182	143	114	87	72	Cycle	5,000
	Phase Angle (Degrees)	29.16	31.22	32.85	34.16	34.28	26.7	26.07	30.67	30.41	32.18	Permanent deformation (mm)	0.935
D54	G* (Mpa)	870	686	524	420	348	263	212	172	135	112	Cycle	5,000
	Phase Angle (Degrees)	24.63	26.58	28.05	29.43	28	21.83	21.96	27.34	27.83	30.14	Permanent deformation (mm)	0.955
D55	G* (Mpa)	777	626	480	387	319	240	194	157	124	105	Cycle	5,000
	Phase Angle (Degrees)	24.93	27.49	29.42	30.8	28.62	23.2	23.11	27.99	28.08	30.01	Permanent deformation (mm)	0.965
D56	G* (Mpa)	934	746	566	455	371	276	220	177	137	114	Cycle	5,000
	Phase Angle (Degrees)	26.12	27.01	29.42	31.11	30.81	24.89	24.95	30.31	30.69	32.63	Permanent deformation (mm)	0.96

Table G4. Results of testing group (DST-C5-N) - Asphalt Mix D

99.06 mm Diameter SP- Type D (Noon)													
FSCH Tests @ 30 °C												RSCH Tests @ 50°C	
Sample	Frequency (Hz)	10	5	2	1	0.5	0.2	0.1	0.05	0.02	0.01		
D33	G* (Mpa)	1109	913	729	618	521	424	368	312	268	239	Cycle	5,000
	Phase Angle (Degrees)	23.02	24.47	25.95	26.75	25.54	18.86	18.57	24.33	24.35	26.25	Permanent deformation (mm)	0.895
D34	G* (Mpa)	1121	936	750	628	526	419	353	294	242	208	Cycle	5,000
	Phase Angle (Degrees)	21.71	23.08	24.56	25.8	24.57	18.16	18.31	23.83	24.18	26.55	Permanent deformation (mm)	0.82
D35	G* (Mpa)	1155	974	791	672	566	458	389	323	268	230	Cycle	5,000
	Phase Angle (Degrees)	20.82	22.04	23.35	24.28	21.42	16.7	16.7	22.87	23.13	25.62	Permanent deformation (mm)	0.775
D36	G* (Mpa)	1073	896	714	598	494	393	334	277	232	204	Cycle	5,000
	Phase Angle (Degrees)	21.46	23.02	24.91	25.93	24.47	18.75	18.73	24.8	24.71	26.58	Permanent deformation (mm)	1.09
D37	G* (Mpa)	1041	853	681	570	476	380	321	267	223	194	Cycle	5,000
	Phase Angle (Degrees)	22.33	23.98	25.27	26.43	25.97	19.23	19.43	25.24	25.59	27.82	Permanent deformation (mm)	0.98
D38	G* (Mpa)	1126	932	736	619	515	415	356	299	254	227	Cycle	5,000
	Phase Angle (Degrees)	24.01	24.83	26.27	26.79	25.7	18.9	18.49	24.35	24.22	26.05	Permanent deformation (mm)	0.91
D39	G* (Mpa)	1156	975	784	657	550	439	372	312	260	226	Cycle	5,000
	Phase Angle (Degrees)	20.55	22.23	23.94	25.05	22.67	16.97	16.76	22.64	22.44	24.53	Permanent deformation (mm)	1.115
D40	G* (Mpa)	1443	1182	959	810	682	552	475	396	335	290	Cycle	5,000
	Phase Angle (Degrees)	18.9	21.4	23.2	24.16	23.04	16.99	16.67	22.88	22.78	25.25	Permanent deformation (mm)	0.715

Table G5. Results of testing group (DST-RH-N) - Asphalt Mix D

Rectangular Horizontal, SP- Type D (Noon)													
FSCH Tests @ 30 °C												RSCH Tests @ 50°C	
Sample	Frequency (Hz)	10	5	2	1	0.5	0.2	0.1	0.05	0.02	0.01		
D09	G* (Mpa)	965	791	619	508	416	322	265	219	178	150	Cycle	5,000
	Phase Angle (Degrees)	22.76	24.42	26	27.1	24.35	18.98	18.49	23.97	23.56	25.31	Permanent deformation (mm)	1.24
D10	G* (Mpa)	972	764	593	481	396	307	254	213	177	154	Cycle	5,000
	Phase Angle (Degrees)	24.6	27.05	28.1	28.68	26.01	19.32	17.95	22.38	21.59	22.94	Permanent deformation (mm)	1.03
D11	G* (Mpa)	997	804	624	515	423	331	276	228	189	162	Cycle	5,000
	Phase Angle (Degrees)	24.97	26.28	28.19	29.14	26.27	21.42	21.15	26.51	26.34	28	Permanent deformation (mm)	1.02
D12	G* (Mpa)	887	703	535	442	365	289	247	210	180	163	Cycle	5,000
	Phase Angle (Degrees)	25.91	27.48	29.06	29.47	26.94	20.97	20.14	25.54	24.75	26.21	Permanent deformation (mm)	1.16
D13	G* (Mpa)	910	722	546	449	368	288	244	206	176	159	Cycle	5,000
	Phase Angle (Degrees)	26.65	28.25	29.63	30.16	28.76	21.7	20.78	26.11	25.38	26.7	Permanent deformation (mm)	0.84
D14	G* (Mpa)	1089	870	672	555	458	361	306	256	216	192	Cycle	5,000
	Phase Angle (Degrees)	25.44	26.76	28.22	28.89	26.78	20.64	20.08	25.48	24.84	26.5	Permanent deformation (mm)	0.82
D15	G* (Mpa)	929	741	571	471	387	305	258	218	186	167	Cycle	5,000
	Phase Angle (Degrees)	26.52	28.16	29.67	30.23	26.62	21.55	20.65	25.89	24.9	26.03	Permanent deformation (mm)	0.915
D16	G* (Mpa)	913	730	559	454	372	287	238	201	168	148	Cycle	5,000
	Phase Angle (Degrees)	25.67	27.52	28.63	29.24	25.99	19.66	18.4	23.27	22.08	23.31	Permanent deformation (mm)	1.085

Table G6. Results of testing group (DST-RV-N) - Asphalt Mix D

Rectangular Vertical, SP- Type D (Noon)													
FSCH Tests @ 30 °C												RSCH Tests @ 50°C	
Sample	Frequency (Hz)	10	5	2	1	0.5	0.2	0.1	0.05	0.02	0.01		
D25	G* (Mpa)	786	605	451	368	299	232	196	166	143	132	Cycle	5,000
	Phase Angle (Degrees)	28.93	30.7	32.22	32.72	30.89	24.01	22.71	27.66	26.65	27.92	Permanent deformation (mm)	0.83
D26	G* (Mpa)	848	681	527	437	362	290	250	214	185	168	Cycle	5,000
	Phase Angle (Degrees)	26.67	27.63	29.04	29.56	27.76	20.99	20.29	25.68	24.98	26.33	Permanent deformation (mm)	0.985
D27	G* (Mpa)	964	758	585	476	390	301	250	210	175	154	Cycle	5,000
	Phase Angle (Degrees)	25.09	27.73	28.93	29.98	27.54	21.16	20.32	25.11	24.53	26.03	Permanent deformation (mm)	1.1
D28	G* (Mpa)	733	571	426	346	280	222	190	164	145	132	Cycle	5,000
	Phase Angle (Degrees)	29.1	29.89	30.88	30.83	27.7	20.91	19.31	24.63	23.26	24.46	Permanent deformation (mm)	1.12
D29	G* (Mpa)	960	754	567	451	359	269	217	176	141	121	Cycle	5,000
	Phase Angle (Degrees)	25.97	27.6	29.4	30.39	28.41	22.44	21.86	27.41	26.81	28.19	Permanent deformation (mm)	1.07
D30	G* (Mpa)	887	700	536	439	360	284	241	205	176	158	Cycle	5,000
	Phase Angle (Degrees)	27.52	28.9	30.03	30.49	28.9	22.36	21.62	27.13	26.8	28.45	Permanent deformation (mm)	1.18
D31	G* (Mpa)	927	742	572	473	392	309	261	219	184	164	Cycle	5,000
	Phase Angle (Degrees)	25.37	27.41	28.87	29.5	26.96	21.4	20.94	26.24	25.98	27.77	Permanent deformation (mm)	0.765
D32	G* (Mpa)	910	735	572	473	393	309	262	220	184	162	Cycle	5,000
	Phase Angle (Degrees)	25.32	26.66	28.22	29.05	28.06	21.24	20.77	26.51	26.24	28.24	Permanent deformation (mm)	0.935

Table G7. Results of testing group (STNS-C6-M) - Asphalt Mix D

150mm Diameter, SP- Type D (Morning)														
FSNS Tests @ 30°C													RSNS Tests @ 50°C	
Sample	Spec.	Frequency (Hz)	10	5	2	1	0.5	0.2	0.1	0.05	0.02	0.01		
D61	S1	G* (Mpa)	542	433	378	337	297	258	227	199	172	154	Cycle	5,000
		Phase Angle (Degrees)	18.76	16.86	17.63	18.52	18.05	11.29	11.85	18.2	19.2	21.45	Permanent deformation (mm)	0.897
		Confining pressure (kPa)	113	113	113	113	113	113	113	113	113	113	Confining pressure (kPa)	113
	S2	G* (Mpa)	430	380	331	302	268	240	219	194	174	158	Cycle	5,000
		Phase Angle (Degrees)	12.71	13.26	14.5	14.89	17.61	8.84	9.52	17.54	19.58	23.05	Permanent deformation (mm)	1.172
		Confining pressure (kPa)	108.5	108.2	109.7	112.6	112	106.3	105	104.7	105.3	116.7	Confining pressure (kPa)	113
D62	S1	G* (Mpa)	548	443	398	363	327	293	267	239	218	203	Cycle	5,000
		Phase Angle (Degrees)	21.82	15.87	17.06	18.1	17.47	12.01	12.64	19.52	21.07	24.2	Permanent deformation (mm)	0.955
		Confining pressure (kPa)	111.5	109.1	106.1	104.9	112.9	104.7	107.3	105.4	111.2	109.3	Confining pressure (kPa)	113
	S2	G* (Mpa)	353	290	261	241	219	200	184	167	152	142	Cycle	5,000
		Phase Angle (Degrees)	15.91	12.09	13.61	14.59	16.18	7.1	7.66	14.76	16.43	19.55	Permanent deformation (mm)	1.00
		Confining pressure (kPa)	110.3	108.2	110	111.4	110.8	110.1	109.7	109	110.1	108.8	Confining pressure (kPa)	113
D63	S1	G* (Mpa)	305	272	235	209	186	164	148	133	119	108	Cycle	5,000
		Phase Angle (Degrees)	12.24	11.17	12.34	12.95	14.61	4.9	4.74	11.76	12.5	15.29	Permanent deformation (mm)	0.794
		Confining pressure (kPa)	108.9	109.6	111	109.4	108.9	108.4	114.8	111	115.7	104.8	Confining pressure (kPa)	113
	S2	G* (Mpa)	630	569	499	451	399	342	303	263	228	203	Cycle	5,000
		Phase Angle (Degrees)	18.48	14.77	15.34	16.12	15.01	9.82	10.65	17.42	18.83	21.48	Permanent deformation (mm)	1.016
		Confining pressure (kPa)	113	113	113	113	113	113	113	113	113	113	Confining pressure (kPa)	113
D64	S1	G* (Mpa)	487	444	392	357	318	277	250	219	191	171	Cycle	5,000
		Phase Angle (Degrees)	14.53	12.27	14.06	15.04	16.02	8.27	8.59	16.08	17.31	20.29	Permanent deformation (mm)	1.016
		Confining pressure (kPa)	111.1	110.2	108.6	111.9	112.1	108.9	108.3	109	109.6	110	Confining pressure (kPa)	113
	S2	G* (Mpa)	554	448	394	361	323	291	267	238	217	201	Cycle	5,000
		Phase Angle (Degrees)	22.32	15.88	17.39	18.22	17.87	12.79	13.6	21.17	23.37	26.76	Permanent deformation (mm)	1.081
		Confining pressure (kPa)	109.6	109.7	110.4	109.3	110.6	110	111.1	106.3	113.9	115.5	Confining pressure (kPa)	113

Table G8. Results of testing group (STNS-C6-N) - Asphalt Mix D

150mm Diameter, SP- Type D (Noon)														
FSNS Tests @ 30°C													RSNS Tests @ 50°C	
Sample	Spec.	Frequency (Hz)	10	5	2	1	0.5	0.2	0.1	0.05	0.02	0.01		
D57	S1	G* (Mpa)	660	610	552	502	448	385	344	301	266	240	Cycle	5,000
		Phase Angle (Degrees)	12.78	11.72	12.14	13.34	15.18	7.09	7.76	14.64	15.76	18.84	Permanent deformation (mm)	0.914
		Confining pressure (kPa)	109.9	112.1	106.6	114.4	113.1	105.1	111.3	110.9	115.5	114.1	Confining pressure (kPa)	113
	S2	G* (Mpa)	623	557	489	454	407	357	324	283	250	228	Cycle	5,000
		Phase Angle (Degrees)	13.36	12.02	13.37	13.46	16.02	8.47	9.09	17.4	19.96	23.54	Permanent deformation (mm)	0.904
		Confining pressure (kPa)	109.9	107.2	108.6	109.9	109.5	111.7	108.4	108.4	107.3	106.7	Confining pressure (kPa)	113
D58	S1	G* (Mpa)	546	424	378	358	327	300	278	252	232	219	Cycle	5,000
		Phase Angle (Degrees)	15.12	16.11	17.16	16.62	17.97	10.43	10.87	18.6	21.64	25.02	Permanent deformation (mm)	0.682
		Confining pressure (kPa)	109.4	108	110.4	109.3	108	111	111.6	114.2	114.9	102.6	Confining pressure (kPa)	113
	S2	G* (Mpa)	702	547	475	438	395	371	344	315	302	294	Cycle	5,000
		Phase Angle (Degrees)	19.45	21.05	21.2	21.69	23.77	17.71	18.55	26.31	29.44	34.03	Permanent deformation (mm)	0.639
		Confining pressure (kPa)	109	112	110.8	110.2	108.5	112	113.8	114	104.8	106.8	Confining pressure (kPa)	113
D59	S1	G* (Mpa)	708	609	547	501	446	397	360	317	288	268	Cycle	5,000
		Phase Angle (Degrees)	12.09	16.57	16.34	17	19.57	13.02	13.91	22.47	26.13	32.01	Permanent deformation (mm)	0.967
		Confining pressure (kPa)	111.7	109.5	109	108.3	108.3	111.8	109.9	109.1	111	110.1	Confining pressure (kPa)	113
	S2	G* (Mpa)	403	344	299	274	250	244	231	215	208	199	Cycle	5,000
		Phase Angle (Degrees)	18.42	17.51	17.82	18.22	19.81	12.92	14.24	22.11	24.74	28.23	Permanent deformation (mm)	0.807
		Confining pressure (kPa)	110.5	110.5	108.5	111.8	108.4	108.9	109.8	110.5	111.3	108.1	Confining pressure (kPa)	113
D60	S1	G* (Mpa)	717	621	554	498	444	382	337	296	255	227	Cycle	5,000
		Phase Angle (Degrees)	15.18	15.1	15.64	17	18.62	11.06	12.02	18.32	19.99	23.6	Permanent deformation (mm)	0.769
		Confining pressure (kPa)	109	110.3	109	110.8	110.9	110.4	109.8	110.4	111	108.6	Confining pressure (kPa)	113
	S2	G* (Mpa)	579	465	417	385	351	319	293	266	245	230	Cycle	5,000
		Phase Angle (Degrees)	17.34	16.86	16.97	17.34	18.22	11.26	11.47	18.3	20.71	23.92	Permanent deformation (mm)	0.588
		Confining pressure (kPa)	109.1	111	109.6	108.7	113.3	115.4	108	104.4	108.4	112	Confining pressure (kPa)	113

Table G9. Results of testing group (STNS-C6-A) - Asphalt Mix D

150mm Diameter, SP- Type D (Afternoon)														
FSNS Tests @ 30°C													RSNS Tests @ 50°C	
Sample	Spec.	Frequency (Hz)	10	5	2	1	0.5	0.2	0.1	0.05	0.02	0.01		
D65	S1	G* (Mpa)	469	395	357	328	295	260	236	208	183	166	Cycle	5,000
		Phase Angle (Degrees)	14.23	12.83	13.26	12.97	12.07	5.99	6.35	13.86	15.42	18.23	Permanent deformation (mm)	1.075
		Confining pressure (kPa)	110.6	109.1	110.5	109.5	109.4	109.1	109.6	108.2	110.9	109.6	Confining pressure (kPa)	113
	S2	G* (Mpa)	685	537	477	440	400	356	322	286	256	234	Cycle	5,000
		Phase Angle (Degrees)	20.72	18	18.77	18.97	14.52	12.17	12.59	19.84	21.56	24.42	Permanent deformation (mm)	0.773
		Confining pressure (kPa)	109.9	110	109.4	108.7	111.8	108.4	111.8	108.1	108.3	109.9	Confining pressure (kPa)	113
D66	S1	G* (Mpa)	481	457	416	382	346	302	272	238	207	185	Cycle	5,000
		Phase Angle (Degrees)	11.7	9.78	11.2	12.08	8.85	5.17	5.68	13.14	14.62	17.39	Permanent deformation (mm)	0.820
		Confining pressure (kPa)	111	111.4	111.2	109.6	110.5	108.4	110.8	110.8	109.5	109.2	Confining pressure (kPa)	113
	S2	G* (Mpa)	464	459	415	378	340	289	260	227	197	175	Cycle	5,000
		Phase Angle (Degrees)	9.65	10.06	11.14	11.64	8.15	4.27	4.64	12.02	13.44	16.34	Permanent deformation (mm)	0.817
		Confining pressure (kPa)	109	109.6	111.7	109.4	108.5	109.8	108.2	108.7	108.8	109.4	Confining pressure (kPa)	113
D67	S1	G* (Mpa)	478	436	393	367	334	290	261	231	203	185	Cycle	5,000
		Phase Angle (Degrees)	10.04	11.55	11.95	11.1	9.7	1.7	1.64	9.17	10.58	13.29	Permanent deformation (mm)	0.750
		Confining pressure (kPa)	109.6	108.3	110.7	109.5	111.5	111.9	111.2	109.3	109	110.7	Confining pressure (kPa)	113
	S2	G* (Mpa)	742	605	545	507	458	412	375	330	297	274	Cycle	5,000
		Phase Angle (Degrees)	21.01	18.4	18.87	19.07	20.03	12.03	13.24	20.99	23.76	27.4	Permanent deformation (mm)	0.617
		Confining pressure (kPa)	110.2	111.9	109.2	108.5	108.7	111.7	111.2	109.2	111.1	108.8	Confining pressure (kPa)	113
D68	S1	G* (Mpa)	793	662	589	541	488	435	390	347	310	284	Cycle	5,000
		Phase Angle (Degrees)	21.07	18.69	18.71	19.25	19.89	11.28	12.26	19.13	21.42	24.53	Permanent deformation (mm)	0.781
		Confining pressure (kPa)	111.1	107.7	108.2	111.8	109.7	111.7	108.9	111.6	110.6	108.4	Confining pressure (kPa)	113
	S2	G* (Mpa)	514	432	376	335	296	257	224	196	167	148	Cycle	5,000
		Phase Angle (Degrees)	18.44	16.11	17.35	18.61	18.89	10.85	11.28	17.23	18.4	20.27	Permanent deformation (mm)	0.756
		Confining pressure (kPa)	110.6	109.3	109.9	109.6	112.4	107.9	111.9	109.3	111.6	108.7	Confining pressure (kPa)	113

Table G10. Results of testing group (DST-C6-M) -Asphalt Mix C

150 mm Diameter, SP- Type C (Morning)													
FSCH Tests @ 30 °C												RSCH Tests @ 50°C	
Sample	Frequency (Hz)	10	5	2	1	0.5	0.2	0.1	0.05	0.02	0.01		
C09	G* (Mpa)	965	765	560	433	335	234	178	137	101	80	Cycle	5,000
	Phase Angle (Degrees)	25.65	28.04	31.01	33.1	32.08	26.4	26.02	31.23	30.25	31.28	Permanent deformation (mm)	0.951
C10	G* (Mpa)	1013	808	599	464	361	249	185	138	96	72	Cycle	5,000
	Phase Angle (Degrees)	26.41	28.63	31.24	33.44	32.67	27.8	28.13	33.06	32.58	33.44	Permanent deformation (mm)	0.976
C11	G* (Mpa)	935	731	545	428	345	252	199	160	124	102	Cycle	5,000
	Phase Angle (Degrees)	25.94	28.17	30.61	32.21	31.71	24.91	24.35	29.36	29.04	30.57	Permanent deformation (mm)	0.918
C12	G* (Mpa)	1085	860	642	506	402	290	224	173	126	97	Cycle	5,000
	Phase Angle (Degrees)	24.79	27.11	29.34	30.99	30.66	24.48	24.66	29.98	30.11	31.88	Permanent deformation (mm)	0.870
C13	G* (Mpa)	952	748	552	431	342	245	190	150	114	93	Cycle	5,000
	Phase Angle (Degrees)	25.65	28.37	30.66	32.23	32.7	25.83	25.1	29.66	28.88	30.14	Permanent deformation (mm)	0.816
C14	G* (Mpa)	945	761	584	471	383	283	225	181	140	116	Cycle	5,000
	Phase Angle (Degrees)	22.86	25.41	27.98	29.8	28.97	23.69	23.55	28.65	28.49	30.05	Permanent deformation (mm)	0.976
C15	G* (Mpa)	872	701	527	416	332	240	187	149	113	91	Cycle	5,000
	Phase Angle (Degrees)	22.83	26.01	28.74	30.66	31.16	24.38	23.9	29.06	28.77	30.33	Permanent deformation (mm)	0.886
C16	G* (Mpa)	995	790	579	449	351	248	191	149	112	89	Cycle	5,000
	Phase Angle (Degrees)	26.65	28.74	31.48	33.25	31.89	26.39	26.21	31.3	30.76	31.96	Permanent deformation (mm)	1.194

Table G11. Results of testing group (DST-C6-N) -Asphalt Mix C

150 mm Diameter, SP- Type C (Noon)													
FSCH Tests @ 30 °C												RSCH Tests @ 50°C	
Sample	Frequency (Hz)	10	5	2	1	0.5	0.2	0.1	0.05	0.02	0.01		
C25	G* (Mpa)	1167	964	742	598	485	358	280	216	159	123	Cycle	5,000
	Phase Angle (Degrees)	21.98	23.07	25.4	27.33	27.54	21.76	22.05	28	28.99	31.46	Permanent deformation (mm)	0.821
C26	G* (Mpa)	1063	879	695	571	471	356	284	225	170	135	Cycle	5,000
	Phase Angle (Degrees)	20.56	22.76	24.84	26.64	25.03	20.53	21.2	26.97	27.94	30.37	Permanent deformation (mm)	0.755
C27	G* (Mpa)	937	725	536	421	333	239	186	147	113	93	Cycle	5,000
	Phase Angle (Degrees)	26.55	28.62	31.26	32.95	32.55	26.98	25.94	30.32	29.77	30.86	Permanent deformation (mm)	0.791
C28	G* (Mpa)	1068	848	617	478	376	267	207	164	125	103	Cycle	5,000
	Phase Angle (Degrees)	26.74	28.89	31.27	32.87	31.92	25.85	25.19	30.17	29.33	30.47	Permanent deformation (mm)	0.900
C29	G* (Mpa)	943	750	563	443	351	251	195	153	115	91	Cycle	5,000
	Phase Angle (Degrees)	24.74	27.32	29.94	31.9	30.1	25.13	25	30.16	29.64	30.59	Permanent deformation (mm)	0.853
C30	G* (Mpa)	924	695	503	385	304	215	165	129	96	76	Cycle	5,000
	Phase Angle (Degrees)	27.46	30.27	32.66	34.02	33.48	26.38	25.68	30.56	30.38	31.9	Permanent deformation (mm)	0.969
C31	G* (Mpa)	1049	840	645	515	418	308	243	192	145	116	Cycle	5,000
	Phase Angle (Degrees)	24.37	26.39	28.58	30.23	28.93	23.4	23.57	28.65	29.16	31.13	Permanent deformation (mm)	1.322
C32	G* (Mpa)	1161	939	709	563	448	320	245	189	137	107	Cycle	5,000
	Phase Angle (Degrees)	23.35	25.12	27.89	29.84	28.92	23.85	24.18	29.62	29.7	31.39	Permanent deformation (mm)	0.826

Table G12. Results of testing group (DST-C6-A) -Asphalt Mix C

150 mm Diameter, SP- Type C (Afternoon)													
FSCH Tests @ 30 °C												RSCH Tests @ 50°C	
Sample	Frequency (Hz)	10	5	2	1	0.5	0.2	0.1	0.05	0.02	0.01		
C41	G* (Mpa)	997	785	573	444	346	243	186	146	109	88	Cycle	5,000
	Phase Angle (Degrees)	26.69	29.01	31.76	33.62	32.97	26.82	26.31	31.15	30.25	31.32	Permanent deformation (mm)	0.834
C42	G* (Mpa)	896	705	516	400	314	223	172	135	103	83	Cycle	5,000
	Phase Angle (Degrees)	26.27	28.36	30.95	32.5	31.34	25.38	24.87	30	29.13	30.27	Permanent deformation (mm)	1.026
C43	G* (Mpa)	915	747	569	451	362	263	204	162	121	97	Cycle	5,000
	Phase Angle (Degrees)	23.26	25.73	28.1	30.07	29.3	23.33	22.96	27.69	27.4	28.95	Permanent deformation (mm)	1.071
C44	G* (Mpa)	935	724	539	422	339	248	196	155	119	96	Cycle	5,000
	Phase Angle (Degrees)	25.36	28.1	30.25	31.64	30.13	23.94	23.68	28.83	28.82	30.8	Permanent deformation (mm)	1.305
C45	G* (Mpa)	1012	787	590	466	376	276	215	169	126	98	Cycle	5,000
	Phase Angle (Degrees)	23.02	25.94	28.06	29.56	30.82	23.02	22.57	28.11	28.55	30.94	Permanent deformation (mm)	1.068
C46	G* (Mpa)	924	750	573	457	368	267	208	163	122	97	Cycle	5,000
	Phase Angle (Degrees)	22.09	24.32	27.25	29.38	29.19	23.59	23.55	28.75	28.67	30.37	Permanent deformation (mm)	1.094
C47	G* (Mpa)	1074	874	670	538	433	316	245	188	137	106	Cycle	5,000
	Phase Angle (Degrees)	22.81	24.87	27.29	29.22	28.89	23.39	23.93	29.61	30.41	32.69	Permanent deformation (mm)	0.811
C48	G* (Mpa)	1151	968	767	634	525	400	320	254	192	152	Cycle	5,000
	Phase Angle (Degrees)	18.98	20.88	23.23	25.15	24.85	19.48	19.91	25.4	26.16	28.73	Permanent deformation (mm)	0.656

Table G13. Results of testing group (DST-C4-N) -Asphalt Mix C

99.06 mm Diameter, SP- Type C (Noon)													
FSCH Tests @ 30 °C												RSCH Tests @ 50°C	
Sample	Frequency (Hz)	10	5	2	1	0.5	0.2	0.1	0.05	0.02	0.01		
C01	G* (Mpa)	921	737	568	469	380	304	261	223	195	178	Cycle	5,000
	Phase Angle (Degrees)	25.36	26.99	28.49	28.9	29.92	20.44	19.38	25.07	24.08	25.17	Permanent deformation (mm)	0.697
C02	G* (Mpa)	1013	817	643	537	446	364	315	266	230	204	Cycle	5,000
	Phase Angle (Degrees)	24.26	25.01	26.25	26.77	25.15	18.71	18.42	24.54	24.42	26.68	Permanent deformation (mm)	0.729
C03	G* (Mpa)	1185	954	749	622	509	403	339	282	234	204	Cycle	5,000
	Phase Angle (Degrees)	23.3	25.19	26.69	27.33	27.12	19.28	18.53	24.11	23.43	24.83	Permanent deformation (mm)	0.7545
C04	G* (Mpa)	991	790	611	501	408	320	268	221	183	160	Cycle	5,000
	Phase Angle (Degrees)	24.11	25.56	27.07	27.68	25.93	19.79	19.36	25.19	24.88	26.58	Permanent deformation (mm)	0.859
C05	G* (Mpa)	1262	1091	859	701	574	441	354	280	218	177	Cycle	5,000
	Phase Angle (Degrees)	24.68	25.66	27.37	29.08	26.73	22.22	22.67	27.8	27.88	29.48	Permanent deformation (mm)	0.819
C06	G* (Mpa)	922	726	546	444	357	276	230	192	159	142	Cycle	5,000
	Phase Angle (Degrees)	27.52	28.91	30.63	31.25	28.7	22.48	21.57	26.72	25.66	26.57	Permanent deformation (mm)	0.820
C07	G* (Mpa)	879	699	529	431	346	267	221	182	150	132	Cycle	5,000
	Phase Angle (Degrees)	25.91	28.27	30.37	31.35	29.21	23.18	22.63	27.53	26.61	27.81	Permanent deformation (mm)	0.834
C08	G* (Mpa)	972	789	609	497	405	316	261	213	174	148	Cycle	5,000
	Phase Angle (Degrees)	24.85	26.54	28.25	29.28	25.88	21.36	21.15	26.53	26.28	28.09	Permanent deformation (mm)	1.04

Table G14. Results of testing group (DST-RH-N) -Asphalt Mix C

Rectangular Horizontal, SP- Type C (Noon)													
FSCH Tests @ 30 °C												RSCH Tests @ 50°C	
Sample	Frequency (Hz)	10	5	2	1	0.5	0.2	0.1	0.05	0.02	0.01		
C17	G* (Mpa)	917	714	535	434	349	271	228	193	166	150	Cycle	5,000
	Phase Angle (Degrees)	26.57	27.87	29.29	29.51	28.34	20.9	19.82	25.42	24.6	25.85	Permanent deformation (mm)	1.083
C18	G* (Mpa)	1151	882	663	535	430	328	270	223	182	158	Cycle	5,000
	Phase Angle (Degrees)	26.72	29.42	30.49	30.92	30.65	21.93	21.1	26.47	25.24	26.44	Permanent deformation (mm)	0.952
C19	G* (Mpa)	1116	912	710	588	479	370	305	250	203	176	Cycle	5,000
	Phase Angle (Degrees)	22.84	24.5	26.47	27.45	26.45	20.64	20.33	26.1	26.04	27.53	Permanent deformation (mm)	0.575
C20	G* (Mpa)	1144	953	759	626	517	401	330	270	216	182	Cycle	5,000
	Phase Angle (Degrees)	20.55	22.76	24.65	26.14	23.87	18.83	18.78	24.49	24.53	26.64	Permanent deformation (mm)	0.966
C21	G* (Mpa)	1158	930	730	602	498	393	329	272	224	193	Cycle	5,000
	Phase Angle (Degrees)	23.02	25.11	26.23	26.9	27.62	19.42	19.42	25.41	25.88	28.04	Permanent deformation (mm)	0.790
C22	G* (Mpa)	1239	1000	784	650	539	420	350	288	233	200	Cycle	5,000
	Phase Angle (Degrees)	23	24.84	26.48	27.48	26.48	20.21	20.27	26.3	26.56	28.38	Permanent deformation (mm)	0.866
C23	G* (Mpa)	1286	1065	854	717	597	470	395	328	271	236	Cycle	5,000
	Phase Angle (Degrees)	20.63	22.17	23.87	24.96	23.85	17.75	17.69	23.58	23.51	25.28	Permanent deformation (mm)	0.856
C24	G* (Mpa)	1161	968	769	633	514	393	322	258	203	169	Cycle	5,000
	Phase Angle (Degrees)	20.82	23.22	25	26.18	28.56	21.75	20.19	26.39	26.48	28.68	Permanent deformation (mm)	0.925

Table G15. Results of testing group (DST-RV-N) -Asphalt Mix C

Rectangular Vertical, SP- Type C (Noon)													
		FSCH Tests @ 30 °C										RSCH Tests @ 50°C	
Sample	Frequency (Hz)	10	5	2	1	0.5	0.2	0.1	0.05	0.02	0.01		
C33	G* (Mpa)	942	736	537	417	320	228	175	136	103	85	Cycle	5,000
	Phase Angle (Degrees)	27.78	29.55	31.77	32.91	31.52	25.05	24.06	28.51	26.85	27.28	Permanent deformation (mm)	1.371
C34	G* (Mpa)	1114	866	639	508	397	300	245	199	165	143	Cycle	5,000
	Phase Angle (Degrees)	27.2	29.11	30.89	31.46	31.93	23.82	22.2	27.63	26.72	28.05	Permanent deformation (mm)	1.040
C35	G* (Mpa)	1034	806	594	467	362	267	213	172	137	118	Cycle	5,000
	Phase Angle (Degrees)	26.22	29.37	30.98	31.7	32.16	23.8	21.16	25.56	24.29	25.11	Permanent deformation (mm)	1.107
C36	G* (Mpa)	1156	941	718	581	463	349	287	233	190	163	Cycle	5,000
	Phase Angle (Degrees)	22.94	25.02	27.06	27.97	29.23	21.58	20	25.82	25.15	26.61	Permanent deformation (mm)	0.871
C37	G* (Mpa)	1134	851	621	491	391	296	243	197	159	134	Cycle	5,000
	Phase Angle (Degrees)	30.25	31.13	32.29	32.66	34.46	24.49	23.95	29.33	28.88	30.24	Permanent deformation (mm)	0.895
C38	G* (Mpa)	1071	836	622	494	390	294	238	190	153	128	Cycle	5,000
	Phase Angle (Degrees)	28.18	29.31	30.92	31.65	30.68	23.95	23.45	28.89	28.64	30.1	Permanent deformation (mm)	0.841
C39	G* (Mpa)	1109	888	665	529	417	307	241	190	147	122	Cycle	5,000
	Phase Angle (Degrees)	26.46	27.49	29.91	31.44	30.76	24.68	24.38	29.38	28.44	29.24	Permanent deformation (mm)	0.865
C40	G* (Mpa)	1214	985	751	603	480	362	291	230	183	152	Cycle	5,000
	Phase Angle (Degrees)	22.22	24.27	26.8	28.21	27.11	21.38	21.12	26.81	26.28	28.23	Permanent deformation (mm)	1.013

Table G16. Results of testing group (STNS-C6-M) -Asphalt Mix C

150mm Diameter, SP- Type C (Morning)														
FSNS Tests @ 30°C													RSNS Tests @ 50°C	
Sample	Spec.	Frequency (Hz)	10	5	2	1	0.5	0.2	0.1	0.05	0.02	0.01		
C53	S1	G* (Mpa)	230	188	169	157	144	137	130	122	119	115	Cycle	5,000
		Phase Angle (Degrees)	15.24	13.41	14.22	14.85	16.13	7.88	8.48	15.51	17.28	19.78	Permanent deformation (mm)	0.705
		Confining pressure (kPa)	113	113	113	113	113	113	113	113	113	113	Confining pressure (kPa)	113
	S2	G* (Mpa)	565	475	431	394	358	324	296	266	242	221	Cycle	5,000
		Phase Angle (Degrees)	16.63	12.57	14.1	15.07	13.61	10.13	11.08	18.52	20.44	23.45	Permanent deformation (mm)	0.674
		Confining pressure (kPa)	110.9	110.2	110.3	108.1	111.1	112.2	109	108.5	111.4	109.6	Confining pressure (kPa)	113
C54	S1	G* (Mpa)	454	333	294	268	242	216	194	173	150	134	Cycle	5,000
		Phase Angle (Degrees)	13.56	11.85	12.78	13.65	14.07	5.73	5.86	12.82	13.29	15.54	Permanent deformation (mm)	0.714
		Confining pressure (kPa)	113	113	113	113	113	113	113	113	113	113	Confining pressure (kPa)	113
	S2	G* (Mpa)	648	526	474	440	395	358	328	292	268	247	Cycle	5,000
		Phase Angle (Degrees)	21.18	16.73	18.07	19.23	18.66	13.8	14.97	22.32	23.97	26.85	Permanent deformation (mm)	0.643
		Confining pressure (kPa)	109.9	111.3	111.6	112.2	108.3	108.7	109.9	110.3	108.6	110.4	Confining pressure (kPa)	113
C55	S1	G* (Mpa)	441	409	375	351	324	294	272	245	218	198	Cycle	5,000
		Phase Angle (Degrees)	7.6	6.95	8.21	8.48	10.37	1.22	1.37	8.86	10.33	13.56	Permanent deformation (mm)	0.610
		Confining pressure (kPa)	109.4	111	109.2	109.4	111.1	110.9	109	110	111.6	110.9	Confining pressure (kPa)	113
	S2	G* (Mpa)	316	288	264	247	229	217	200	181	161	145	Cycle	5,000
		Phase Angle (Degrees)	12.79	10.17	11.31	12.13	13	4.76	5.46	12.84	14.55	17.38	Permanent deformation (mm)	0.530
		Confining pressure (kPa)	113	113	113	113	113	113	113	113	113	113	Confining pressure (kPa)	113
C56	S1	G* (Mpa)	769	700	623	568	503	436	394	343	304	276	Cycle	5,000
		Phase Angle (Degrees)	18.23	13.58	15.15	16.41	15.75	11.16	11.82	20.24	23.26	27.15	Permanent deformation (mm)	0.707
		Confining pressure (kPa)	111	109.5	109.5	112.2	109.2	109.7	112.2	108.6	108.6	111	Confining pressure (kPa)	113
	S2	G* (Mpa)	579	534	487	452	414	371	339	303	268	248	Cycle	5,000
		Phase Angle (Degrees)	10.65	8.27	9.53	10.08	11.13	3.65	4.11	11.67	13.15	16.79	Permanent deformation (mm)	0.394
		Confining pressure (kPa)	111.4	109.5	109.7	110	111	109.4	109.3	111	108.7	108.6	Confining pressure (kPa)	113

Table G17. Results of testing group (STNS-C6-N) -Asphalt Mix C

150mm Diameter, SP- Type C (Noon)														
FSNS Tests @ 30°C													RSNS Tests @ 50°C	
Sample	Spec.	Frequency (Hz)	10	5	2	1	0.5	0.2	0.1	0.05	0.02	0.01		
C57	S1	G* (Mpa)	812	648	591	559	512	473	436	385	353	321	Cycle	5,000
		Phase Angle (Degrees)	17.5	15.57	16.93	17.8	16.31	11.35	11.93	19.69	20.16	22.36	Permanent deformation (mm)	0.557
		Confining pressure (kPa)	110.3	112.2	110.8	108.5	111	109.6	110.5	110.1	109.7	109.9	Confining pressure (kPa)	113
	S2	G* (Mpa)	486	426	384	350	316	278	248	219	188	167	Cycle	5,000
		Phase Angle (Degrees)	10.81	10.74	11.78	12.22	6.23	4.03	4.8	12.35	12.08	15.82	Permanent deformation (mm)	0.562
		Confining pressure (kPa)	113	113	113	113	113	113	113	113	113	113	Confining pressure (kPa)	113
C58	S1	G* (Mpa)	668	588	524	471	421	365	322	281	239	209	Cycle	5,000
		Phase Angle (Degrees)	14.5	11.56	13.25	14.62	9.54	8.7	9.54	16.66	17.72	20.01	Permanent deformation (mm)	0.513
		Confining pressure (kPa)	110.9	109.9	107.7	111.6	110.2	110.8	110.1	110.5	110.9	110.3	Confining pressure (kPa)	113
	S2	G* (Mpa)	1552	1272	1065	939	815	707	623	538	479	432	Cycle	5,000
		Phase Angle (Degrees)	23.43	20.32	22.7	24.13	19.01	18.23	18.62	25.69	26.73	28.89	Permanent deformation (mm)	0.492
		Confining pressure (kPa)	109.9	109.8	109.2	112	108.9	109.1	111.7	109.9	110.8	111	Confining pressure (kPa)	113
C59	S1	G* (Mpa)	761	641	574	530	478	424	377	332	281	244	Cycle	5,000
		Phase Angle (Degrees)	10.28	9.17	10.86	11.69	8.14	4.89	5.87	13.81	15.23	18.16	Permanent deformation (mm)	0.564
		Confining pressure (kPa)	109.9	110.4	111.1	109.5	110.3	112.2	107.9	108.4	109.1	111.1	Confining pressure (kPa)	113
	S2	G* (Mpa)	1409	1173	1020	906	805	682	599	515	444	394	Cycle	5,000
		Phase Angle (Degrees)	17.92	15.35	17.61	18.36	12.14	12.62	13.33	20.82	22.04	25.06	Permanent deformation (mm)	0.490
		Confining pressure (kPa)	113	113	113	113	113	113	113	113	113	113	Confining pressure (kPa)	113
C60	S1	G* (Mpa)	583	506	459	428	392	358	325	295	258	232	Cycle	5,000
		Phase Angle (Degrees)	11.24	9.96	11.17	11.87	9.58	4.22	4.76	12.29	13.48	16.11	Permanent deformation (mm)	0.434
		Confining pressure (kPa)	109.2	109.8	108.1	110.3	108	111.3	108.8	111	110.6	109.5	Confining pressure (kPa)	113
	S2	G* (Mpa)	1082	931	801	713	630	534	471	407	351	314	Cycle	5,000
		Phase Angle (Degrees)	16.64	13.95	16.15	17.01	10.71	11.05	12.29	19.94	22.54	25.53	Permanent deformation (mm)	0.593
		Confining pressure (kPa)	113	113	113	113	113	113	113	113	113	113	Confining pressure (kPa)	113

Table G18. Results of testing group (STNS-C6-A) -Asphalt Mix C

150mm Diameter, SP- Type C (Afternoon)														
		FSNS Tests @ 30°C											RSNS Tests @ 50°C	
Sample	Spec.	Frequency (Hz)	10	5	2	1	0.5	0.2	0.1	0.05	0.02	0.01		
C49	S1	G* (Mpa)	359	321	281	257	233	212	194	174	164	156	Cycle	5,000
		Phase Angle (Degrees)	20.56	14.96	16.12	17.04	17.13	11	11.79	18.77	20.97	24.22	Permanent deformation (mm)	0.718
		Confining pressure (kPa)	109.9	110.1	110.8	110.3	109.7	109.7	109.2	110.3	105.5	109.4	Confining pressure (kPa)	113
	S2	G* (Mpa)	922	680	608	569	518	471	426	376	338	318	Cycle	5,000
		Phase Angle (Degrees)	22.15	20.01	20.92	21.07	17.09	14.75	15.79	23.47	27.25	30.54	Permanent deformation (mm)	0.813
		Confining pressure (kPa)	109.3	108.8	109.6	110.4	109.5	107.7	108.1	112.9	117.1	104.8	Confining pressure (kPa)	113
C50	S1	G* (Mpa)	490	435	389	359	326	289	263	232	205	186	Cycle	5,000
		Phase Angle (Degrees)	12.94	11.14	12.79	13.32	12.66	6.48	6.9	14.56	15.99	19.18	Permanent deformation (mm)	0.670
		Confining pressure (kPa)	109	111.3	110	111	108.5	113.4	109.8	103.4	114.5	101	Confining pressure (kPa)	113
	S2	G* (Mpa)	986	704	638	607	558	524	483	435	418	397	Cycle	5,000
		Phase Angle (Degrees)	25.26	22.84	23.54	24.42	22.48	18.03	19.47	26.94	29.95	32.71	Permanent deformation (mm)	0.555
		Confining pressure (kPa)	110.6	108.5	112	110.9	110.8	109.8	110	110	110.4	109.7	Confining pressure (kPa)	113
C51	S1	G* (Mpa)	489	411	366	341	310	276	251	222	196	176	Cycle	5,000
		Phase Angle (Degrees)	13.85	9.82	11.94	12.79	13.69	6.42	7.01	14.97	16.63	20.04	Permanent deformation (mm)	0.763
		Confining pressure (kPa)	110.6	109.6	108.4	111.5	110.4	111.6	111.6	110.3	109.8	108.8	Confining pressure (kPa)	113
	S2	G* (Mpa)	742	530	476	439	390	354	327	293	281	269	Cycle	5,000
		Phase Angle (Degrees)	23.23	23.35	23.65	24.2	25.11	18.5	19.35	26.41	28.73	31.91	Permanent deformation (mm)	0.790
		Confining pressure (kPa)	110.3	109.7	110.8	108.4	109.2	109.5	110.4	110.5	108.9	108.6	Confining pressure (kPa)	113
C52	S1	G* (Mpa)	1113	843	756	704	627	548	495	434	404	378	Cycle	5,000
		Phase Angle (Degrees)	23.73	22.45	22.79	22.18	19.18	16.73	17.74	25.06	27.8	30.98	Permanent deformation (mm)	0.580
		Confining pressure (kPa)	110.5	107.6	108	110.8	110.9	111.9	111.6	108.4	111.9	114.5	Confining pressure (kPa)	113
	S2	G* (Mpa)	792	650	577	529	470	409	363	315	277	250	Cycle	5,000
		Phase Angle (Degrees)	20.89	18.02	19.37	19.96	17.59	13.82	14.86	21.99	23.49	26.66	Permanent deformation (mm)	0.581
		Confining pressure (kPa)	112.2	110	109.8	110.3	110	107.5	105.7	116.8	115.6	101.8	Confining pressure (kPa)	113

Table G19. Results of testing group (DST-C6-M) -Asphalt Mix B

150 mm Diameter, SP- Type B (Morning)													
FSCH Tests @ 30 °C												RSCH Tests @ 50°C	
Sample	Frequency (Hz)	10	5	2	1	0.5	0.2	0.1	0.05	0.02	0.01		
B09	G* (Mpa)	1092	856	649	512	413	301	233	180	132	101	Cycle	5,000
	Phase Angle (Degrees)	23.04	25.84	28.09	29.99	29.2	23.56	23.94	29.48	30.03	32.07	Permanent deformation (mm)	0.977
B10	G* (Mpa)	1141	894	670	527	416	297	227	174	127	100	Cycle	5,000
	Phase Angle (Degrees)	24.11	26.27	28.81	30.89	30.42	24.88	25.06	30.53	30.49	31.94	Permanent deformation (mm)	1.178
B11	G* (Mpa)	943	742	558	439	356	261	207	165	127	103	Cycle	5,000
	Phase Angle (Degrees)	24.51	27.18	29.64	31.32	30.7	24.19	24	29.3	29.31	31.1	Permanent deformation (mm)	1.152
B12	G* (Mpa)	1125	914	691	546	436	314	244	190	143	116	Cycle	5,000
	Phase Angle (Degrees)	22.87	25.04	27.92	29.97	29.25	24.02	24.03	29.36	29.24	30.59	Permanent deformation (mm)	0.690
B13	G* (Mpa)	1081	889	683	547	437	316	243	187	138	109	Cycle	5,000
	Phase Angle (Degrees)	22.34	24.33	27.12	29.4	28.9	24.12	24.61	30.14	30.3	31.92	Permanent deformation (mm)	0.929
B14	G* (Mpa)	1276	1023	786	625	505	373	290	224	164	124	Cycle	5,000
	Phase Angle (Degrees)	22.65	24.83	27.12	29.08	28.19	22.78	23.52	28.94	29.94	32.54	Permanent deformation (mm)	0.650
B15	G* (Mpa)	1105	900	690	551	443	322	249	193	143	112	Cycle	5,000
	Phase Angle (Degrees)	22.54	24.46	27.07	29.1	27.42	23.09	23.66	29.02	29.15	31.05	Permanent deformation (mm)	0.744
B16	G* (Mpa)	1031	828	620	488	386	275	210	161	118	92	Cycle	5,000
	Phase Angle (Degrees)	23.28	26.22	29.03	31.23	31.53	25.48	25.52	30.59	30.46	32.11	Permanent deformation (mm)	0.915

Table G20. Results of testing group (DST-C6-N) -Asphalt Mix B

150 mm Diameter, SP- Type B (Noon)													
FSCH Tests @ 30 °C												RSCH Tests @ 50°C	
Sample	Frequency (Hz)	10	5	2	1	0.5	0.2	0.1	0.05	0.02	0.01		
B25	G* (Mpa)	1091	880	664	524	416	298	229	176	129	100	Cycle	5,000
	Phase Angle (Degrees)	23.44	26.08	28.82	30.83	29.02	24.52	24.73	29.95	29.75	31.39	Permanent deformation (mm)	0.902
B26	G* (Mpa)	1171	977	766	624	512	386	308	246	188	152	Cycle	5,000
	Phase Angle (Degrees)	21.42	23.49	25.43	27.08	25.41	20.44	20.59	26.15	26.44	28.81	Permanent deformation (mm)	0.608
B27	G* (Mpa)	1065	872	660	527	422	307	241	189	143	115	Cycle	5,000
	Phase Angle (Degrees)	24.14	25.83	28.46	30.29	30.47	24.96	24.46	29.45	29.1	30.69	Permanent deformation (mm)	0.936
B28	G* (Mpa)	1015	822	614	480	378	269	205	158	117	92	Cycle	5,000
	Phase Angle (Degrees)	22.54	24.98	28.12	30.29	30.86	25.02	24.94	30.38	30.3	32.05	Permanent deformation (mm)	1.096
B29	G* (Mpa)	1017	818	606	476	374	267	206	159	117	93	Cycle	5,000
	Phase Angle (Degrees)	24.72	27.1	29.95	31.9	31.68	25.95	25.96	31.17	31.09	32.68	Permanent deformation (mm)	0.979
B30	G* (Mpa)	1052	877	671	536	429	313	244	189	142	113	Cycle	5,000
	Phase Angle (Degrees)	21.65	23.49	26.23	28.3	27.22	22.65	23.22	28.92	29.14	31.17	Permanent deformation (mm)	0.891
B31	G* (Mpa)	1056	858	639	500	391	275	209	158	116	90	Cycle	5,000
	Phase Angle (Degrees)	23.77	26.37	29.43	31.71	32.4	27.23	26.77	31.52	31.41	32.99	Permanent deformation (mm)	0.963
B32	G* (Mpa)	1146	931	713	573	460	335	259	198	143	108	Cycle	5,000
	Phase Angle (Degrees)	22.82	24.63	26.95	28.74	28.77	23.54	23.79	29.5	30.27	32.84	Permanent deformation (mm)	0.815

Table G21. Results of testing group (DST-C6-A) -Asphalt Mix B

150 mm Diameter, SP- Type B (Afternoon)													
FSCH Tests @ 30 °C												RSCH Tests @ 50°C	
Sample	Frequency (Hz)	10	5	2	1	0.5	0.2	0.1	0.05	0.02	0.01		
B45	G* (Mpa)	1009	801	594	464	364	258	198	153	114	90	Cycle	5,000
	Phase Angle (Degrees)	24.49	27.03	29.8	31.74	31.12	25.69	25.64	30.86	30.5	31.86	Permanent deformation (mm)	0.813
B46	G* (Mpa)	1259	1023	795	646	527	391	308	241	181	145	Cycle	5,000
	Phase Angle (Degrees)	21.58	23.73	25.77	27.69	25.8	21.93	22.69	28.45	28.98	31.24	Permanent deformation (mm)	0.680
B47	G* (Mpa)	1101	902	694	557	453	331	259	205	155	126	Cycle	5,000
	Phase Angle (Degrees)	23.35	24.98	27.32	29.26	28.49	23.36	23.38	28.79	28.86	30.66	Permanent deformation (mm)	0.828
B48	G* (Mpa)	1151	937	711	564	448	322	249	193	144	115	Cycle	5,000
	Phase Angle (Degrees)	23.14	25.02	27.65	29.73	29.05	24.1	24.28	29.7	29.52	30.94	Permanent deformation (mm)	0.722
B49	G* (Mpa)	1214	988	751	591	466	331	251	190	138	107	Cycle	5,000
	Phase Angle (Degrees)	22.47	24.7	27.62	29.76	28.8	24.29	24.73	30.14	30.31	31.9	Permanent deformation (mm)	0.731
B50	G* (Mpa)	1112	872	662	525	421	306	239	186	141	113	Cycle	5,000
	Phase Angle (Degrees)	24.9	27.4	29.56	31.37	30.37	24.58	24.48	29.46	29.21	30.86	Permanent deformation (mm)	0.732
B51	G* (Mpa)	1207	934	692	534	422	302	229	174	127	97	Cycle	5,000
	Phase Angle (Degrees)	24.73	26.75	29.25	31.19	30.62	24.76	24.78	30.27	30.43	32.25	Permanent deformation (mm)	1.211
B52	G* (Mpa)	1150	919	683	529	411	286	213	160	112	85	Cycle	5,000
	Phase Angle (Degrees)	23.74	26.24	28.95	31.2	30.04	25.5	25.97	31.41	31.6	32.96	Permanent deformation (mm)	0.872

Table G22. Results of testing group (DST-C4-N) -Asphalt Mix B

99.06 mm Diameter, SP- Type B (Noon)													
FSCH Tests @ 30 °C												RSCH Tests @ 50°C	
Sample	Frequency (Hz)	10	5	2	1	0.5	0.2	0.1	0.05	0.02	0.01		
B01	G* (Mpa)	1207	989	775	637	519	402	329	263	208	173	Cycle	5,000
	Phase Angle (Degrees)	21.86	24.04	26.29	27.6	24.48	20.84	21.09	26.86	26.98	28.77	Permanent deformation (mm)	0.948
B02	G* (Mpa)	1211	997	793	664	547	435	367	304	254	221	Cycle	5,000
	Phase Angle (Degrees)	21.59	23.89	25.55	26.45	25.26	18.91	18.68	24.59	23.96	25.66	Permanent deformation (mm)	0.966
B03	G* (Mpa)	1085	879	679	559	454	364	311	258	221	194	Cycle	5,000
	Phase Angle (Degrees)	23.93	25.58	27.52	28.23	25.72	20.22	19.61	25.61	25.3	27.2	Permanent deformation (mm)	1.032
B04	G* (Mpa)	1030	840	659	548	452	357	301	251	208	181	Cycle	5,000
	Phase Angle (Degrees)	22.98	24.64	26.23	27.02	24.17	19.02	18.57	24.25	23.97	25.63	Permanent deformation (mm)	0.969
B05	G* (Mpa)	1027	843	673	567	467	381	329	274	235	205	Cycle	5,000
	Phase Angle (Degrees)	25.5	26.33	27.25	27.57	30.23	20.87	20.86	27.1	27.61	29.73	Permanent deformation (mm)	1.100
B06	G* (Mpa)	1164	961	754	623	512	404	341	281	234	207	Cycle	5,000
	Phase Angle (Degrees)	22.13	24.26	26.07	26.78	25.87	19.15	18.64	24.52	24.08	25.77	Permanent deformation (mm)	0.879
B07	G* (Mpa)	1212	1007	790	654	534	412	340	276	221	192	Cycle	5,000
	Phase Angle (Degrees)	23.51	24.41	26.45	27.72	25.82	20.73	20.88	26.51	26.71	28.28	Permanent deformation (mm)	0.630
B08	G* (Mpa)	1082	894	703	588	486	384	322	263	213	180	Cycle	5,000
	Phase Angle (Degrees)	23.44	24.48	26.33	27.26	24.23	19.79	19.66	25.52	25.71	27.57	Permanent deformation (mm)	0.906

Table G23. Results of testing group (DST-RH-N) -Asphalt Mix B

Rectangular Horizontal, SP- Type B (Noon)													
FSCH Tests @ 30 °C												RSCH Tests @ 50°C	
Sample	Frequency (Hz)	10	5	2	1	0.5	0.2	0.1	0.05	0.02	0.01		
B17	G* (Mpa)	1331	1089	833	677	537	406	332	266	216	187	Cycle	5,000
	Phase Angle (Degrees)	23.02	24.83	27.12	28.25	27.13	21.48	20.9	26.86	26.2	27.59	Permanent deformation (mm)	0.908
B18	G* (Mpa)	1406	1172	914	750	606	459	370	294	231	191	Cycle	5,000
	Phase Angle (Degrees)	21.56	23.33	25.62	26.97	26.07	20.37	20.04	25.83	25.63	27.41	Permanent deformation (mm)	0.767
B19	G* (Mpa)	1283	1051	793	637	501	374	300	236	187	160	Cycle	5,000
	Phase Angle (Degrees)	23.49	24.08	26.55	27.83	27.75	22.38	22.31	28.44	28.06	29.09	Permanent deformation (mm)	0.828
B20	G* (Mpa)	1402	1155	906	740	598	455	364	283	217	172	Cycle	5,000
	Phase Angle (Degrees)	20.25	22.49	24.85	26.37	24.78	20.36	20.82	26.99	27.55	29.57	Permanent deformation (mm)	0.794
B21	G* (Mpa)	1200	953	732	590	476	361	293	235	188	158	Cycle	5,000
	Phase Angle (Degrees)	22.76	24.65	26.54	27.57	26.59	20.47	19.96	25.79	25.31	26.81	Permanent deformation (mm)	0.826
B22	G* (Mpa)	1332	1097	851	695	562	423	342	273	215	178	Cycle	5,000
	Phase Angle (Degrees)	22.74	24.54	26.89	28.3	27.31	22	21.87	27.7	27.51	29.18	Permanent deformation (mm)	0.938
B23	G* (Mpa)	1317	1108	871	719	587	451	366	289	226	187	Cycle	5,000
	Phase Angle (Degrees)	20.52	21.87	24.25	25.76	24.54	19.73	19.86	26.35	26.58	28.68	Permanent deformation (mm)	0.880
B24	G* (Mpa)	1273	1042	799	645	506	378	306	242	195	166	Cycle	5,000
	Phase Angle (Degrees)	23.67	25.82	27.96	28.85	29.83	23.02	21.68	27.56	26.89	28.34	Permanent deformation (mm)	0.926

Table G24. Results of testing group (DST-RV-N) -Asphalt Mix B

Rectangular Vertical, SP- Type B (Noon)													
FSCH Tests @ 30 °C												RSCH Tests @ 50°C	
Sample	Frequency (Hz)	10	5	2	1	0.5	0.2	0.1	0.05	0.02	0.01		
B33	G* (Mpa)	1229	1001	754	604	478	357	286	228	181	153	Cycle	5,000
	Phase Angle (Degrees)	23.5	25.08	27.75	29.1	27.08	22.01	21.64	26.94	26.16	27.34	Permanent deformation (mm)	0.733
B34	G* (Mpa)	1423	1160	899	731	584	443	359	288	231	198	Cycle	5,000
	Phase Angle (Degrees)	23.22	25.13	27.29	28.58	27.36	21.69	21.36	26.82	26.06	27.14	Permanent deformation (mm)	0.771
B35	G* (Mpa)	1234	988	755	610	492	377	307	246	191	155	Cycle	5,000
	Phase Angle (Degrees)	23.25	24.94	26.68	27.37	28.8	19.92	19.88	26.2	26.89	28.96	Permanent deformation (mm)	0.982
B36	G* (Mpa)	1457	1225	911	719	563	406	318	249	190	159	Cycle	5,000
	Phase Angle (Degrees)	22.72	23.31	26.24	27.72	27.87	21.49	21.4	27.15	26.77	27.54	Permanent deformation (mm)	0.488
B37	G* (Mpa)	1011	878	680	561	458	356	294	241	196	168	Cycle	5,000
	Phase Angle (Degrees)	25.78	23.38	24.89	25.74	24.87	18.55	18.19	24.21	23.77	25.4	Permanent deformation (mm)	0.824
B38	G* (Mpa)	1387	1094	851	698	565	440	367	297	247	209	Cycle	5,000
	Phase Angle (Degrees)	25.99	27.13	28.93	30.06	29.25	23.25	23.19	28.72	28.73	30.77	Permanent deformation (mm)	0.686
B39	G* (Mpa)	1356	1090	850	692	562	426	341	268	204	164	Cycle	5,000
	Phase Angle (Degrees)	23.9	25.45	27.39	29.13	27.85	22.9	23.56	29	29.14	30.69	Permanent deformation (mm)	0.443
B40	G* (Mpa)	1243	1022	784	634	506	376	301	239	186	154	Cycle	5,000
	Phase Angle (Degrees)	22.88	24.59	27.16	28.59	27.23	22.07	22.12	27.76	27.47	28.66	Permanent deformation (mm)	0.795

Table G25. Results of testing group (STNS-C6-M) -Asphalt Mix B

150mm Diameter, SP- Type B (Morning)														
FSNS Tests @ 30°C													RSNS Tests @ 50°C	
Sample	Spec.	Frequency (Hz)	10	5	2	1	0.5	0.2	0.1	0.05	0.02	0.01		
B57	T	G* (Mpa)	602	432	386	360	333	308	281	251	227	205	Cycle	5,000
		Phase Angle (Degrees)	18.05	14.81	15.93	16.1	12.92	10.07	10.56	18.05	19.88	22.71	Permanent deformation (mm)	0.735
		Confining pressure (kPa)	109.4	112	109.1	110.5	106.7	111	112.8	110.5	114.1	106	Confining pressure (kPa)	113
	B	G* (Mpa)	568	495	442	404	361	315	282	245	214	191	Cycle	5,000
		Phase Angle (Degrees)	17.46	12.82	14.11	14.87	12.34	10.32	10.87	18.74	20.55	23.97	Permanent deformation (mm)	0.852
		Confining pressure (kPa)	108.5	108.2	108.9	114.2	109.6	109.7	113.6	109.9	110.6	109.8	Confining pressure (kPa)	113
B58	T	G* (Mpa)	520	450	410	382	345	306	277	244	214	192	Cycle	5,000
		Phase Angle (Degrees)	14.25	10.8	11.26	11.75	8.26	5.62	5.9	14	15.57	18.76	Permanent deformation (mm)	0.766
		Confining pressure (kPa)	109.8	107.9	110.5	110.5	110.3	109.8	108.8	108.8	111.3	110.4	Confining pressure (kPa)	113
	B	G* (Mpa)	554	464	413	378	335	283	249	214	182	160	Cycle	5,000
		Phase Angle (Degrees)	12.22	12.08	12.87	12.3	9.53	4.61	4.97	12.23	13.45	15.76	Permanent deformation (mm)	1.002
		Confining pressure (kPa)	109.2	111.9	107.5	111.6	108.7	109.9	109.4	110.4	110.6	111.7	Confining pressure (kPa)	113
B59	T	G* (Mpa)	491	437	388	356	319	278	248	217	190	170	Cycle	5,000
		Phase Angle (Degrees)	13.54	11.65	13.27	14.55	11.71	8.32	8.95	16.33	17.64	19.87	Permanent deformation (mm)	0.794
		Confining pressure (kPa)	108.5	111.9	110.5	110.2	108.6	113.2	105.2	114	109.9	110.1	Confining pressure (kPa)	113
	B	G* (Mpa)	438	416	375	344	308	269	242	212	186	167	Cycle	5,000
		Phase Angle (Degrees)	9.72	8.86	10.72	11.98	11.76	5.94	6.4	14.41	15.85	19.08	Permanent deformation (mm)	0.823
		Confining pressure (kPa)	110.5	112.1	111.4	110.6	109	109.4	116.6	109.7	116	118.5	Confining pressure (kPa)	113
B60	T	G* (Mpa)	519	485	449	418	379	331	298	264	232	209	Cycle	5,000
		Phase Angle (Degrees)	10.41	8.29	10.05	11.44	9.29	5.94	6.91	15.07	16.7	19.93	Permanent deformation (mm)	0.626
		Confining pressure (kPa)	110.4	110.9	111.7	110.7	109	110.1	112.5	106.3	113.1	101.8	Confining pressure (kPa)	113
	B	G* (Mpa)	178	178	163	151	141	130	120	111	100	93	Cycle	5,000
		Phase Angle (Degrees)	12.7	9.46	10.39	10.91	9.05	3.11	3.48	10.87	12.16	14.93	Permanent deformation (mm)	0.688
		Confining pressure (kPa)	110.5	110.9	110.7	109.1	109.6	112.6	110.6	108.1	112.2	111.5	Confining pressure (kPa)	113

Table G26. Results of testing group (STNS-C6-N) -Asphalt Mix B

150mm Diameter, SP- Type B (Noon)														
FSNS Tests @ 30°C													RSNS Tests @ 50°C	
Sample	Spec.	Frequency (Hz)	10	5	2	1	0.5	0.2	0.1	0.05	0.02	0.01		
B53	T	G* (Mpa)	246	219	196	182	167	152	142	129	118	108	Cycle	5,000
		Phase Angle (Degrees)	10.81	9.72	10.63	11.27	13.04	3.86	4.22	12.08	13.55	16.5	Permanent deformation (mm)	0.994
		Confining pressure (kPa)	109.2	110.3	109.9	110.5	110.1	108.8	110.8	112.5	111	109.9	Confining pressure (kPa)	113
	B	G* (Mpa)	502	453	399	362	320	274	241	208	180	161	Cycle	5,000
		Phase Angle (Degrees)	14.71	12.22	13.95	15.38	17.81	8.92	9.59	16.61	17.46	20.15	Permanent deformation (mm)	0.727
		Confining pressure (kPa)	111.5	109.5	111.7	108.6	111.6	108.7	108.1	108.7	111.4	109.1	Confining pressure (kPa)	113
B54	T	G* (Mpa)	131	115	104	96	89	82	76	70	64	60	Cycle	5,000
		Phase Angle (Degrees)	13.19	11.67	11.93	12.39	12.99	3.83	3.97	10.29	11.33	13.87	Permanent deformation (mm)	1.031
		Confining pressure (kPa)	109.6	108.4	110.2	110.2	108.1	103.7	107.9	112.3	112.1	101.3	Confining pressure (kPa)	113
	B	G* (Mpa)	703	578	499	444	386	329	286	244	207	181	Cycle	5,000
		Phase Angle (Degrees)	19.85	14.6	15.63	16.66	16.92	10.5	10.97	18.61	20.01	22.77	Permanent deformation (mm)	0.973
		Confining pressure (kPa)	112.3	111.8	108.9	109.6	106.9	115.8	110.7	109.4	117.2	106	Confining pressure (kPa)	113
B55	T	G* (Mpa)	376	344	307	283	254	225	202	176	153	135	Cycle	5,000
		Phase Angle (Degrees)	11.59	9.05	10.43	10.91	11.49	4.72	5.33	13.73	15.57	18.97	Permanent deformation (mm)	1.595
		Confining pressure (kPa)	109.1	111.3	110.2	111	104.3	111.6	100.3	102.2	104.8	115.4	Confining pressure (kPa)	113
	B	G* (Mpa)	417	394	342	306	266	228	201	173	147	129	Cycle	5,000
		Phase Angle (Degrees)	11.92	10.21	11.99	12.75	11.96	6.07	6.27	14.25	15.39	18.32	Permanent deformation (mm)	1.418
		Confining pressure (kPa)	112	110.3	110.2	112.1	104.7	116.6	113.3	117.5	115.4	109.1	Confining pressure (kPa)	113
B56	T	G* (Mpa)	921	779	673	595	519	442	393	340	303	274	Cycle	5,000
		Phase Angle (Degrees)	22.95	19.41	19.85	20.15	15.21	13.91	14.3	21.47	22.82	25.25	Permanent deformation (mm)	0.905
		Confining pressure (kPa)	113	113	113	113	113	113	113	113	113	113	Confining pressure (kPa)	113
	B	G* (Mpa)	446	422	375	342	305	265	237	208	182	164	Cycle	5,000
		Phase Angle (Degrees)	11.94	9.68	11.24	12.18	12.38	6.09	6.61	14.35	16.03	19.25	Permanent deformation (mm)	1.106
		Confining pressure (kPa)	112.3	111.2	113	113.1	111.5	112.4	115.4	116.1	100.2	117.8	Confining pressure (kPa)	113

Table G27. Results of testing group (STNS-C6-A) -Asphalt Mix B

150mm Diameter, SP- Type B (Afternoon)														
FSNS Tests @ 30°C													RSNS Tests @ 50°C	
Sample	Spec.	Frequency (Hz)	10	5	2	1	0.5	0.2	0.1	0.05	0.02	0.01		
B41	T	G* (Mpa)	886	703	605	542	487	430	383	332	294	264	Cycle	5,000
		Phase Angle (Degrees)	19.32	17.83	19.73	20.45	14.36	13.44	13.86	21.47	22.82	25.34	Permanent deformation (mm)	0.845
		Confining pressure (kPa)	111.6	112	109.3	111.9	108.5	111.6	109.5	108.2	110.8	106.2	Confining pressure (kPa)	113
	B	G* (Mpa)	159	135	122	113	106	97	90	84	78	73	Cycle	5,000
		Phase Angle (Degrees)	13.52	12.66	12.92	13.45	14.17	5.07	5.24	11.44	12.45	15.01	Permanent deformation (mm)	0.656
		Confining pressure (kPa)	111.5	110.5	109.3	110.2	109.4	110.6	112.4	108.9	105.9	111.5	Confining pressure (kPa)	113
B42	T	G* (Mpa)	875	707	620	554	500	435	383	339	302	274	Cycle	5,000
		Phase Angle (Degrees)	17.23	15.94	17.4	18.67	11.67	11.79	12.81	19.47	20.45	23.5	Permanent deformation (mm)	0.664
		Confining pressure (kPa)	110.1	110.5	111.7	111.9	110.7	110.1	108.7	110.5	112.7	105.7	Confining pressure (kPa)	113
	B	G* (Mpa)	241	182	164	154	144	138	130	121	113	106	Cycle	5,000
		Phase Angle (Degrees)	16.07	13.82	14.3	14.56	15.65	6.7	6.98	13.91	15.36	18.02	Permanent deformation (mm)	0.567
		Confining pressure (kPa)	111	107.9	110.6	109.7	110.2	110.3	112.8	107.9	110.2	107.8	Confining pressure (kPa)	113
B43	T	G* (Mpa)	514	448	406	374	338	300	271	240	209	185	Cycle	5,000
		Phase Angle (Degrees)	11.6	9.9	11.3	12.07	8.34	4.93	5.39	13.44	14.88	17.85	Permanent deformation (mm)	0.851
		Confining pressure (kPa)	111.3	111	109.9	107.7	113.2	112.7	110.6	108.9	111	110.4	Confining pressure (kPa)	113
	B	G* (Mpa)	733	675	594	535	474	404	356	311	271	241	Cycle	5,000
		Phase Angle (Degrees)	14.33	12.76	15.1	16.61	10.81	10.53	11.58	18.5	20	22.78	Permanent deformation (mm)	0.416
		Confining pressure (kPa)	112	109.9	110.9	110.3	110.1	110.7	110.3	109	110.8	107.9	Confining pressure (kPa)	113
B44	T	G* (Mpa)	839	712	609	537	471	396	345	295	249	219	Cycle	5,000
		Phase Angle (Degrees)	16.19	14.31	16.55	17.65	11.92	10.78	11.33	18.16	18.51	20.78	Permanent deformation (mm)	0.645
		Confining pressure (kPa)	110.3	110.8	111.3	108.4	110.7	109.8	108.9	109.7	106.5	109.6	Confining pressure (kPa)	113
	B	G* (Mpa)	735	640	563	505	452	393	350	308	268	241	Cycle	5,000
		Phase Angle (Degrees)	14.79	13.39	15.4	16.4	12.11	10.02	10.53	17.57	18.84	21.5	Permanent deformation (mm)	0.677
		Confining pressure (kPa)	113	113	113	113	113	113	113	113	113	113	Confining pressure (kPa)	113